Spatial and temporal dynamics of alluvial cover in mixed bedrock-alluvial fluvial systems

MEL OLIVEIRA GUIRRO

Spatial and temporal dynamics of alluvial cover in mixed bedrock-alluvial fluvial systems

Mel Oliveira Guirro

Thesis submitted for the Degree of Doctor of Philosophy

Department of Geography

Durham University

United Kingdom

May 2025

Abstract

Mixed bedrock-alluvial rivers, characterised by spatially variable sediment cover over exposed bedrock, control landscape evolution and are important aquatic habitats. However, the mechanisms controlling alluvial cover variability remain poorly understood, particularly in post-glacial landscapes where glacial inheritance interacts with contemporary fluvial processes. This thesis investigates three objectives: (1) examining how channel and sediment properties correlate with alluvial cover, (2) identifying main drivers influencing alluvial cover at the network scale, and (3) exploring how sediment pulses influence cover dynamics. The study combines empirical analyses and numerical modelling within the River Carron catchment in the Scottish Highlands. Field survey across 92 reaches showed that channel slope and bankfull width were the strongest predictors of alluvial cover distribution. Post-glacial inheritance created high spatial variability in grain size and disrupted typical downstream patterns. Contemporary floods rework sediments in most reaches (88% during 50-year floods), though 12% remained immobile even during extreme events. To address network-scale alluvial cover dynamics, the NetworkSedimentTransporter model was modified to track alluvial cover changes across river networks. The modelling showed that controlling factors vary with sediment supply conditions. Under supply-limited conditions, channel slope primarily controlled spatial distribution. Under transport-limited conditions, sediment supply and grain size became more influential. Even at high sediment supply rates, complete alluviation was not achieved. Sediment pulse simulations demonstrated that pulse dynamics depend on pulse characteristics and pre-existing cover conditions. Pulses introduced at a bedrock site exhibited faster downstream transport, while pulses at an alluvial site showed greater local storage. These findings demonstrate that channel slope is the primary alluvial cover control, though its influence varies with sediment supply regime. This study provides important understanding for river management and habitat conservation.

Table of Contents

List of Tables

List of Figures

Declaration

I declare that the material contained in this thesis has not been previously submitted, in whole or in part, for a degree or other qualification at this or any other institution. All sources of information from the work of others have been acknowledge and referenced.

Statement of Copyright

The copyright of this thesis rests with the author. No quotation from it should be published without the author's prior written consent and information derived from it should be acknowledged.

Mel Oliveira Guirro

May 2025

Acknowledgements

1 Introduction

1.1 Context

Rivers shape landscapes, transport sediments and provide habitats around the world. Among the diverse fluvial systems, mixed bedrock-alluvial rivers are characterised by discontinuous sediment cover (alluvial cover) over bedrock in the channel bed or banks for at least part of their length (Montgomery & Buffington, 1997; Turowski et al., 2008). The spatial and temporal distribution of this alluvial cover influences river dynamics by the "tools and cover" effect: it can protect the underlying bedrock from erosion when deposited, or provide particles to act as tools for erosion when transported over exposed beds (Finnegan et al., 2007; Sklar & Dietrich, 2004). These processes drive landscape evolution by determining how channels incise bedrock and change their morphology on geological timescales (Whipple et al., 2013).

Alluvial cover distribution influences several aspects of fluvial system besides landscape evolution. Alluvial cover modifies sediment transport dynamics by providing particles and affecting flow characteristics near the river bed, such as changing shear stress distribution and sediment entrainment. Specifically, alluvial patches increase surface roughness and reduce flow velocities near the river bed, which decreases local transport capacity and promote sediment deposition, while exposed bedrock sections maintain higher flow velocities and transport rates (Ferguson et al., 2017b; Hodge et al., 2011; Inoue et al., 2014). These interactions shape river morphology, as channels adjusts their shape in response to changes in flow and sediment supply (Baynes et al., 2020; Chatanantavet & Parker, 2008; Papangelakis et al., 2021). For example, Baynes et al. (2020) demonstrated through field observation and experiments that increasing sediment supply leads to wider and steeper channels because sediment protects the bedrock from vertical erosion and promotes lateral erosion. Ecologically, stable alluvial cover provides ideal habitats for aquatic organisms, including spawning grounds for salmonoid fish (Buffington et al., 2004; Steiger et al., 2005; Wohl, 2015b). Therefore,

understanding alluvial cover dynamics is critical for predicting landscape evolution, managing river systems and protecting habitats.

Despite the importance of alluvial cover, there are knowledge gaps in our understanding of its distribution and dynamics. Several studies have analysed cover controls at the reach scale over short timescales (hours to months) (Chatanantavet & Parker, 2008; Hodge & Hoey, 2016; Johnson & Whipple, 2010), and other studies have modelled alluvial cover at the network scale in the context of long-term landscape evolution over geological timescales (thousands to millions of years) (Howard, 1994; Shobe et al., 2017; Whipple, 2002). However, our understanding of alluvial cover dynamics within an intermediate timescale (annual or decadal) at the network scale remain limited. This intermediate timescale is important because it allows us to understand the effects and morphological adjustments due to human interventions, flood events and sediment pulses that occur over years to decades. The relationships between alluvial cover and factors such as grain size, channel geometry and flow dynamics in these network systems over decades remain poorly understood, limiting our ability to predict and manage alluvial cover.

Post-glacial landscapes present a unique site for studying alluvial cover. These landscapes often exhibit irregular topography created by glacial erosion and have a combination of resistant bedrock and glacial deposits with varying erodibility (Ballantyne, 2002; Church and Ryder, 1972). Sediment supply in these landscapes has changed considerably since deglaciation, presenting initially very high supply from unconsolidated glacial deposits, followed by a general decline as sources moved downstream over millennia (Ballantyne, 2002; Church and Ryder, 1972). In addition, these landscapes were shaped by very high discharges during deglaciation due to glacial outburst floods and meltwater flows that where capable of mobilising very coarse sediments. Therefore, the contemporary fluvial morphologies may not be in equilibrium with modern discharge regimes. In addition, post-glacial rivers often present abrupt changes in channel morphology and alluvial thickness (Addy et al., 2011; Bergman et al., 2022; Brardinoni & Hassan, 2006; Jansen et al., 2010; Whitbread et al., 2015). These characteristics make post-glacial landscapes more complex to understand compared to

non-glaciated systems, but they are relevant sites for investigating alluvial cover controls under conditions of inherited topographic and changing sediment supply regimes.

This thesis investigates how grain-scale processes (sediment transport, deposition and erosion) produce network-scale patterns of alluvial cover in a post-glacial landscape – the River Carron catchment, Scotland. This research is conducted within the framework of the i-CONN project, a Marie Skłodowska-Curie Innovative Training Network funded by the European Commission under their H2020 programme. The i-CONN project involved scientists from diverse fields developing a unified framework for studying connectivity across complex systems. This thesis contributes to i-CONN's Work Package 2 by developing methods for analysing sediment connectivity and Work Package 3 by applying them to understand alluvial cover dynamics across scales in post-glacial landscapes. By integrating empirical analysis with numerical modelling, this research contributes both to theoretical understanding of sediment connectivity and its applications to river management.

1.2 Background

1.2.1 Mixed bedrock-alluvial rivers: Characteristics and importance

The definition of mixed bedrock-alluvial rivers is related to channels where bedrock constrains the position of the channel bed or banks, with variable alluvial cover overlying this bedrock substrate. Early classifications categorised rivers as either "bedrock" or "alluvial" based on dominant characteristics – whether the riverbed was at least partially exposed or fully covered by sediments (Montgomery & Buffington, 1997). More recent river classifications analysed the continuous variability that exists between purely exposed bedrock rivers and fully covered alluvial rivers (Meshkova & Carling, 2013; Turowski et al., 2008; Whitbread et al., 2015). Figure 1.1 shows this continuum of alluvial cover, with examples from the River Carron, showing bedrock, mixed, and alluvial reaches. Mixed bedrock-alluvial rivers can be identified as where: (1) the bedrock is exposed in parts of the channel beds or banks; (2) the channel morphology is affected by

the overall shape and topography of the underlying bedrock surface; and (3) sediment cover varies spatially throughout the reach (Meshkova & Carling, 2013; Turowski et al., 2008; Whipple, 2004). The extent of alluvial cover in these systems can be quantified as the fraction of bed area that is covered by sediment, ranging from zero in purely bedrock reaches to one in fully alluvial reaches (Chatanantavet & Parker, 2008; Sklar & Dietrich, 2004).
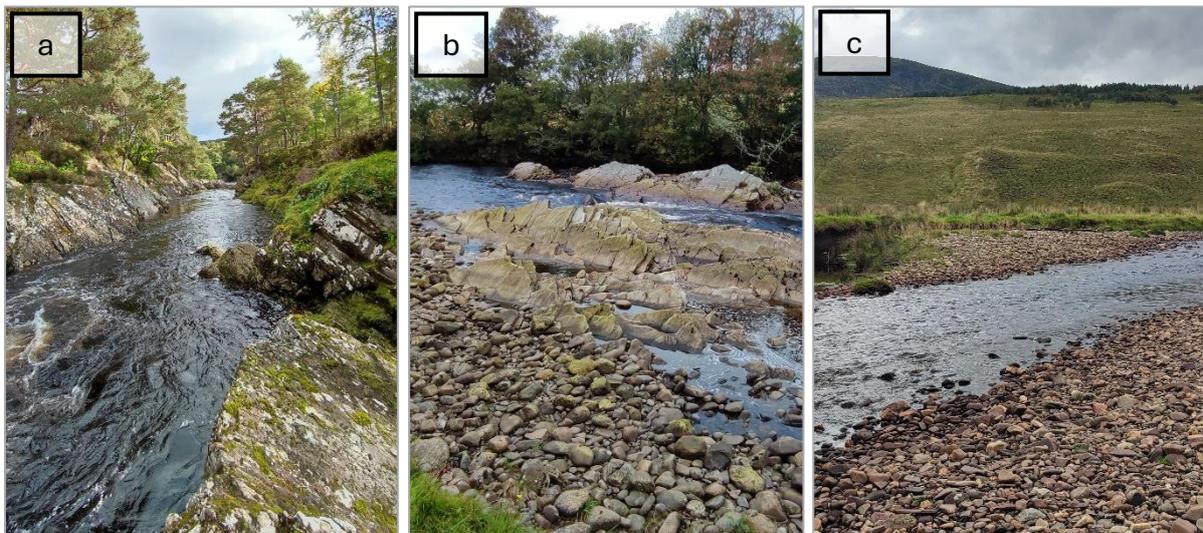
Figure 1.1: Examples of channel types in the River Carron, Scottish Highlands, with different alluvial coverage: a) bedrock reach in a gorge with exposed bedrock banks; b) mixed bedrock-alluvial reach with partial alluvial cover and bedrock exposure; and c) fully alluvial reach with complete sediment cover and no visible bedrock.

Mixed bedrock-alluvial rivers occur in diverse regions worldwide but are particularly common in mountainous areas. They frequently develop in upland regions with steep channel slopes and bedrock that is resistant to erosion (Montgomery et al., 1996), in post-glacial landscapes where irregular topography creates spatially variable channel slopes (Brardinoni & Hassan, 2006; Jansen et al., 2010), and in areas where sediment supply is limited relative to transport capacity (Whipple, 2004).

Rivers control landscape evolution, with mixed bedrock-alluvial rivers presenting unique patterns of evolution, as their rates and patterns of bedrock incision are controlled by the spatial and temporal exposure of bedrock and distribution of alluvial cover (Sklar &

Dietrich, 2004; Whipple, 2004). These rivers influence the development of longitudinal river profiles, knickpoint propagation, and the rate of landscape adjustment to tectonic and climatic forcing (Whipple, 2002; Whipple et al., 2013). In addition, mixed bedrock-alluvial rivers are particularly sensitive to anthropogenic interventions, such as dam construction and gravel extraction, due to their complex response to changes in flow and sediment regimes (Kondolf, 1997). Ecologically, the variability of alluvial cover creates diverse habitats, with alluvial patches providing optimal spawning grounds for salmonids (Buffington et al., 2004; Steiger et al., 2005; Wohl, 2015b). Understanding the controls on alluvial cover is necessary in order to predict river response to management decisions and to determine appropriate restoration measures (Wohl, 2015b).

Despite their importance, these rivers have received less research attention than purely alluvial rivers, particularly at the network scale. A challenge in the study of these channels is that the cover fraction is not static – it responds dynamically to changes in sediment supply and transport capacity (Johnson & Whipple, 2010; Turowski et al., 2013). Although we assume these channels are dynamic, we have limited information about the magnitude and timescales of alluvial cover variations due to the difficulty in measuring it in the field, particularly over longer timescales. This uncertainty about the dynamic nature of these systems makes predicting alluvial cover challenging, limiting our ability to model landscape evolution and river response to environmental changes.

1.2.2 Alluvial cover dynamics

Alluvial cover affects channel geometry, sediment transport and flow dynamics of mixed bedrock-alluvial rivers. The interactions between sediment transport, deposition and bedrock erosion create feedback mechanisms that affect both the short-term response of rivers to hydrological events and their long-term evolution.

1.2.2.1 Sediment supply and transport capacity balance

Sediment supply represents the volume and characteristics of material delivered to a river from upstream sources and lateral inputs. Transport capacity indicates the

maximum load of sediment that a flow can carry. The development and stability of alluvial cover is fundamentally controlled by the balance between these two factors, which is in turn controlled by discharge, channel geometry, and sediment characteristics (Johnson, 2014; Turowski et al., 2008). The ratio of sediment supply to transport capacity (Q_s/Q_t) provides a first-order predictor of alluvial cover extent (Chatanantavet & Parker, 2008; Sklar & Dietrich, 2004). When Q_s/Q_t is low, alluvial cover extent is low, limited to areas of reduced flow velocity or topographic lows (Hodge & Hoey, 2016). As the ratio Q_s/Q_t approaches 1, alluvial cover expands, potentially changing from bedrock to continuous alluvial reaches. This ratio can be used to classify rivers (Figure 1.2) (Montgomery & Buffington, 1997). Supply-limited (or detachment-limited) rivers occur when transport capacity exceeds sediment supply ($Q_s < Q_t$), leading to bedrock exposure. Transport-limited rivers occur where sediment supply exceeds transport capacity ($Q_s > Q_t$), leading to increased alluvial cover.
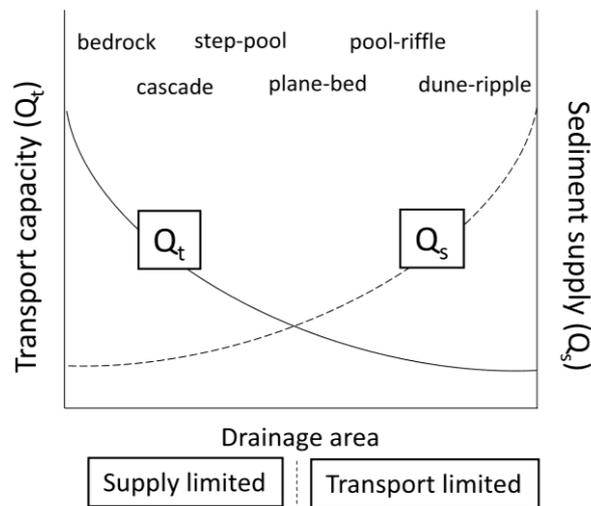
Figure 1.2: Conceptual model of channel morphology transitions along a river. Transport capacity (Q_t, solid line) typically decreases and sediment supply (Q_s, dashed line) increases with drainage area. This trend creates a transition from supply-limited conditions upstream (where bedrock, cascade and step-pool morphologies dominate) to transport-limited conditions downstream (where plane-bed, pool-riffle and dune-ripple morphologies dominate) (adapted from Montgomery & Buffington, 1997).

Transport capacity is controlled by the applied shear stress (τ) relative to the critical shear stress required for sediment entrainment (τ_c). Applied shear stress is determined by flow depth, channel slope and flow velocity, while critical shear stress depends on sediment properties such as grain size, shape, density and bed roughness conditions. Transport capacity is then determined using empirical relations that are functions of the dimensionless shear stress (τ/τ_c) or excess shear stress ($\tau - \tau_c$) (Wilcock & Crowe, 2003; Wong & Parker, 2006). Therefore, transport capacity varies with channel morphology, particularly with slope and width-to-depth ratio, as well as with discharge and sediment properties. When sediment supply is similar to transport capacity, small changes in discharge and shear stress can trigger changes in alluvial cover extent (Sklar & Dietrich, 2004). The spatial distribution of the balance between sediment supply and transport capacity varies throughout the river network, with upstream reaches typically having steeper slopes and greater transport capacity relative to supply compared to downstream reaches.

1.2.2.2 The tools and cover effect in bedrock erosion

Sediment in mixed-bedrock alluvial rivers has dual roles: it can act as tools that erode the bedrock ("tools effect"), but when abundant it forms deposits that protect the riverbed from incision ("cover effect"). Gilbert (1877) first hypothesized this "tools and cover effect", which has been supported by laboratory experiments and numerical models (Sklar & Dietrich, 1998; Sklar & Dietrich, 2001; Whipple & Tucker, 2002). These studies demonstrated a nonlinear relationship between sediment supply and erosion rate, with the Sklar & Dietrich (1998) model predicting maximum erosion occurring at an intermediate level of sediment supply, while Turowski et al. (2007) suggested maximum erosion occurs when sediment supply equals transport capacity. Erosion is minimised under two conditions: when no sediment is available to incise the bedrock, or when sediment supply is higher than transport capacity, although some erosion can still occur even under high sediment supply conditions (Sklar & Dietrich, 2004; Turowski et al., 2007). At higher slopes, both the maximum erosion rate and the optimum sediment supply for maximum erosion increase (Figure 1.3) (Sklar & Dietrich, 1998). This occurs

because steeper slopes generate higher shear stresses, which increase the transport capacity and allow more sediments to be transported before alluvial cover dominates, when further sediment supply decreases erosion rates.
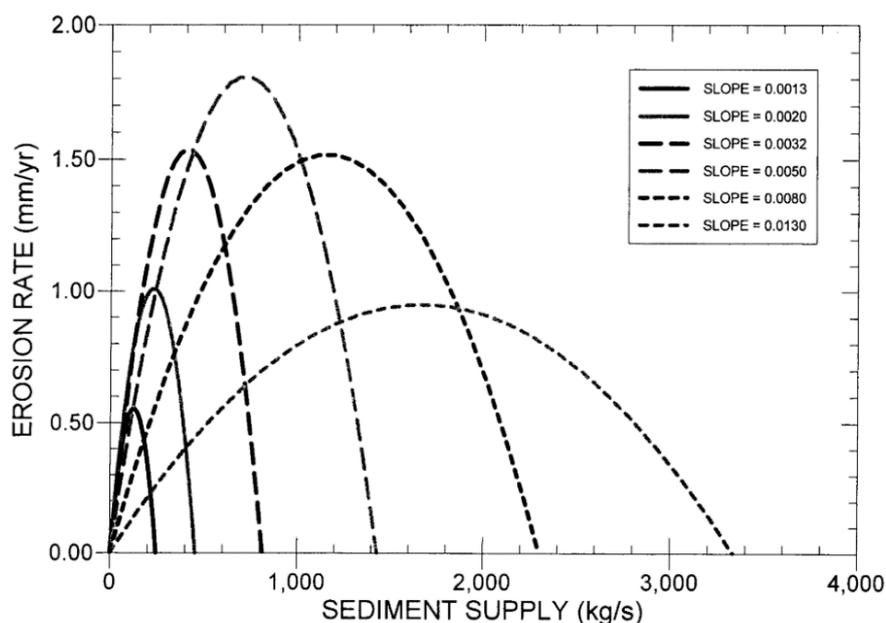
Figure 1.3: Relationship between sediment supply and bedrock erosion rate for different channel slopes, based on the numerical model proposed by Sklar & Dietrich (1998). For each slope, erosion rate initially increases with sediment supply (tools effect), reaches a maximum at an intermediate supply, and then decreases with further supply increases (cover effect).

1.2.2.3 Feedback mechanisms between alluvial cover and hydraulics

The interaction between alluvial cover and hydraulics creates feedback mechanisms that influence sediment transport at different spatial scales. At the grain scale, the presence of alluvial cover modifies surface roughness by creating irregular topography, which increases flow resistance and reduces flow velocities near the riverbed, thereby decreasing local shear stress and affecting sediment entrainment (Hodge et al., 2011; Inoue et al., 2014). Bedrock surfaces can have lower roughness than alluvial patches, resulting in higher critical entrainment thresholds in alluvial patches compared to bedrock reaches (Figure 1.4) (Ferguson et al., 2017b; Hodge et al., 2011). Bedrock reaches may have higher flow velocities and transport capacities for the same applied

shear stress compared to alluvial reaches, especially when the bedrock surface is smooth (Ferguson et al., 2017a).
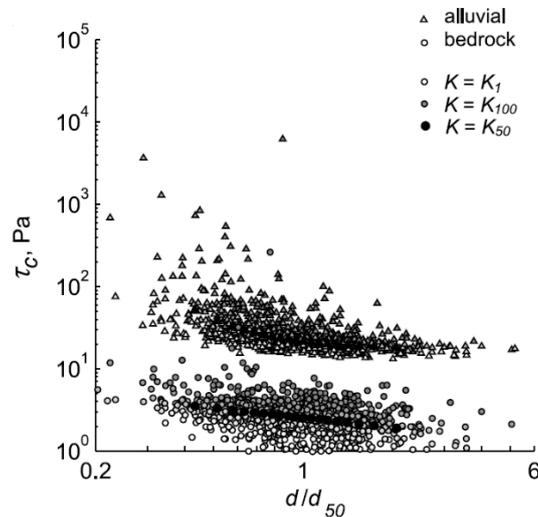
Figure 1.4: Critical entrainment shear stress (τc) for alluvial and bedrock channels as a function of relative grain size (d/d50) based on Monte Carlo simulations by Hodge et al., (2011). Critical shear stress in bedrock channels is approximately an order of magnitude lower than in alluvial channels with the same grain sizes – around 2.5 Pa in bedrock compared to 21.9 Pa in alluvial reaches. Different K values represent different underlying grain size distributions.

Sediment patches tend to initiate in topographic lows and areas with lower flow velocity (Hodge & Hoey, 2016). Once established, these patches create additional flow resistance that promote more deposition through a positive feedback mechanism (Johnson & Whipple, 2010). In addition, grain sheltering effects can promote additional deposition, as larger particles may protect smaller ones (Hodge et al., 2011).

At the reach scale, the spatial distribution of alluvial cover influences transport capacity. Greater alluvial cover generally increases flow resistance and reduces local transport capacity, promoting more deposition (Ferguson et al., 2017a). In contrast, areas with exposed bedrock maintain higher transport capacity, potentially inhibiting new cover formation (Hodge et al., 2011; Inoue et al., 2014). These feedbacks between hydraulic and alluvial cover can reinforce existing cover patterns. In an experiment conducted by Chatanantavet & Parker (2008), high-slope channels (> 0.015 m/m) presented "runaway

alluviation", a nonlinear response where increasing sediment supply had little effect on increasing alluvial cover until a threshold is reached, after which cover increased abruptly.

1.2.2.4 Channel morphology influence on alluvial cover

Channel morphology is a control on the development and stability of alluvial cover on river systems. Channel slope is a primary control on alluvial cover, with steeper slopes generally inhibiting alluvial cover due to increased shear stress and transport capacity (Ferguson et al., 2017b; Johnson & Whipple, 2010). Sklar & Dietrich (1998) found that mixed bedrock-alluvial rivers typically occur within a slope range of 0.001 to 0.1 m/m, with smaller drainage areas requiring higher slopes for bedrock exposure.

Channel width and depth also control alluvial cover patterns. Wider reaches typically have lower transport capacity per unit width because, for a given discharge, they have shallower flow depths, resulting in lower bed shear stress and reduced transport capacity, thereby promoting alluvial cover development (Johnson & Whipple, 2010; Turowski, 2018). In contrast, in narrower reaches the flow is deeper and hence shear stress is higher for the same discharge, maintaining exposed bedrock. Channel depth affects alluvial cover by influencing bed shear stress, with deeper flows generally producing higher shear stresses that increase sediment transport capacity and reduce alluvial cover.

The relationship between alluvial cover and channel geometry is demonstrated by comparing bedrock and alluvial reaches across different drainage areas (Figure 1.5) (Whitbread et al., 2015). Bedrock channels are typically narrower, deeper and steeper than alluvial channels for the same drainage area (Montgomery & Gran, 2001; Whitbread et al., 2015). However, these relationships can be different under certain conditions: when sediment flux is restricted, bedrock channels may become wider and shallower than alluvial channels (Buckley et al., 2024; Meshkova & Carling, 2013; Whitbread et al., 2015).
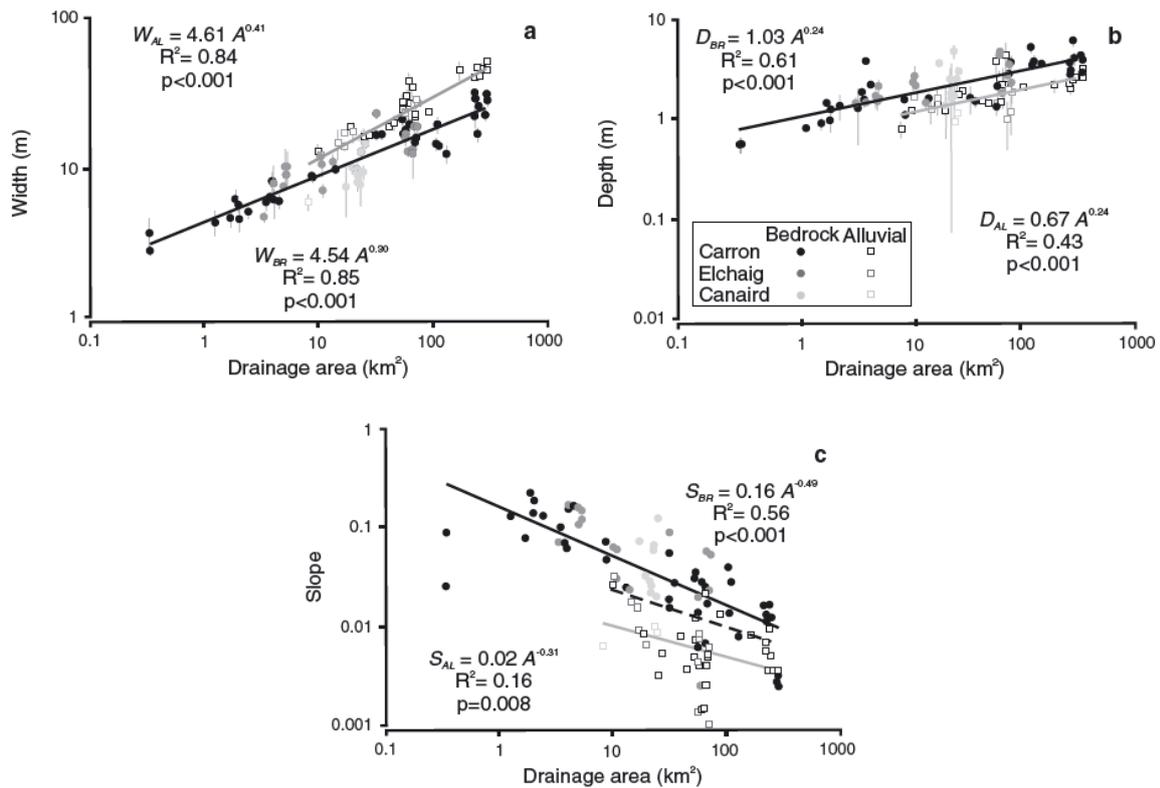
Figure 1.5: Relationships between drainage area and (a) Channel width, (b) depth, and (c) slope for bedrock and alluvial reaches from three rivers (Carron, Elchaig and Canaird) in the Scottish Highlands. Power-law regressions show different scaling relationships for bedrock (black) and alluvial (grey) reaches. In bedrock channels, slopes and depths are generally higher and widths are generally lower. The dashed line in (c) indicates the approximate critical slope threshold between predominantly bedrock and alluvial channels (adapted from Whitbread et al., 2015).

1.2.2.5 Sediment properties influence on alluvial cover

Grain size is another control on alluvial cover development and stability. For alluvial surfaces, grain size directly controls critical entrainment shear stress needed to initiate sediment transport. Coarser grains generally require higher shear stresses for entrainment, leading to more stable alluvial cover for a given flow (Hodge et al., 2011; Sklar & Dietrich, 2004). Grain size distribution also affects alluvial cover patterns, as mixed grain sizes tend to form less stable patches compared to uniform sediment sizes, though this effect may also be influenced by differences in grain shape between uniform and mixed sediments (Hodge & Hoey, 2016).

Sediment transport dynamics is different between bedrock and alluvial reaches: sediment in smooth bedrock sections tends to move quickly regardless of grain size, while transport in alluvial reaches is more grain size and shape dependent (Hodge et al., 2011). This difference in transport creates a pattern of sediment mobility and deposition, where particles tend to travel between existing sediment clusters and deposit at those clusters, creating a positive feedback mechanism that reinforces existing cover patterns.

1.2.2.6 Temporal dynamics and sediment pulses

Temporal variation of alluvial cover is controlled by fluctuations in discharge and sediment supply, which can occur due to episodic events, such as floods and landslides, that trigger sediment pulses. Flood events can modify alluvial cover patterns by eroding existing deposits or creating new ones (Cook et al., 2020; Turowski et al., 2013). The response of alluvial cover to flood events depends on the magnitude and sequence of floods, as well as the antecedent conditions of the channel. DeLisle & Yanites (2023) showed that extreme flood events might not always cause the greatest incision if they coincide with high sediment supply that increases alluvial cover.

Turowski et al. (2013) proposed a classification of channels based on their response to hydrological events: "flood-cleaning" (eroding during high flows and depositing during moderate flows) and "flood-depositing" (depositing during high flows and eroding during moderate flows). The behaviour depends on how sediment supply and transport capacity scale differently with discharge. In flood-cleaning channels, transport capacity increases faster than sediment supply during high flows, leading to erosion, while in flood-depositing channels, sediment supply increases relative to transport capacity during floods, promoting deposition. This classification demonstrates how the same hydrological event can have opposite effects on alluvial cover depending on channel characteristics and sediment supply.

Sediment pulses can be triggered by several mechanisms, including landslides, debris flow, extreme floods, dam removals and gravel augmentation (Benda & Dunne, 1997b; East et al., 2018; Gran & Czuba, 2017; Sklar et al., 2009; Vazquez-Tarrío et al., 2023). When introduced to a river, sediment pulses propagate downstream through some

combination of two mechanisms: translation (downstream movement as a coherent wave) and dispersion (spreading out in place). Most research on sediment pulse dynamics has focused on fully alluvial rivers, finding that dispersion is typically the dominant process (Cui et al., 2003; Lisle et al., 2001). However, translation may become more likely when the pulse material is finer than the existing bed material and under conditions of low Froude numbers (Sklar et al., 2009).

At the network scale, pulse propagation is complicated by factors such as tributary junctions, variations in channel geometry, and spatial patterns of transport capacity (Gran & Czuba, 2017). Another challenge is that the frequency and magnitude of sediment supply, transport and storage in river systems are stochastic and intermittent (Benda & Dunne, 1997b, 1997a). On larger spatial and temporal scales, such as in a catchment over decades, nonlinear interactions between hydraulics and sediment processes can result in disproportional response to a stimulus. For example, a moderate rainfall event might mobilise a larger amount of sediment from an old landslide deposit, delivering it to the river network. The stochastic nature of sediment inputs to rivers can generate unexpected patterns of disturbance and response, depending on the frequency and magnitude of events that deliver sediment to the river (Benda & Dunne, 1997a; Czuba & Foufoula-Georgiou, 2014). These sediment disturbances occur at multiple spatial and temporal scales (Figure 1.6). Small-scale, higher frequency events create fundamental variability in sediment dynamics, while large-scale, lower frequency perturbations control landscape form and reshape rivers.
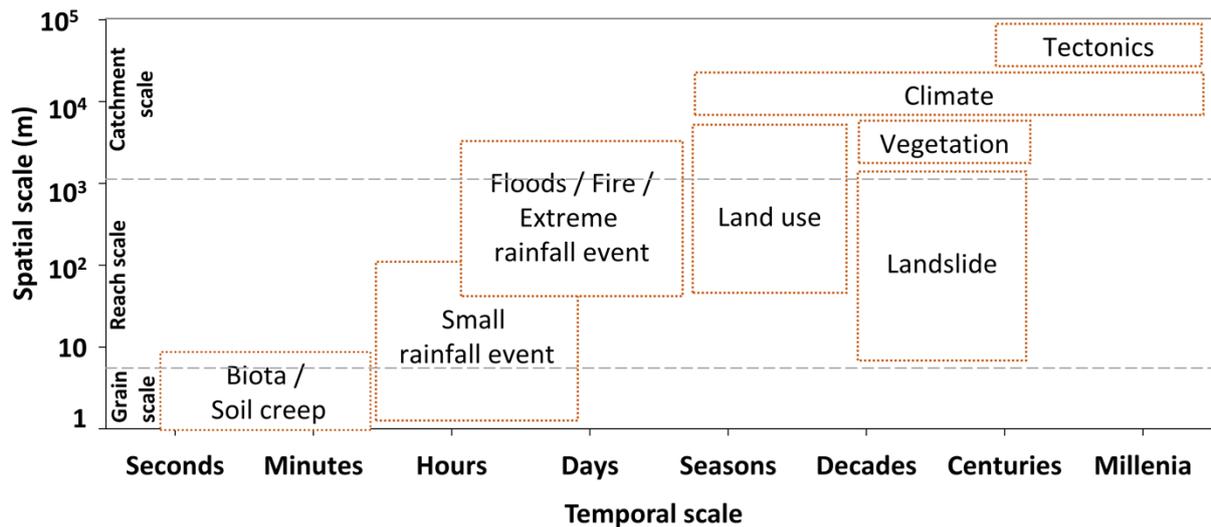
Figure 1.6: Spatial and temporal scales of disturbances affecting alluvial cover in mixed bedrock-alluvial rivers. The diagram illustrates how several natural and anthropogenic disturbances occur at different spatial scales (y-axis) and temporal frequencies (x-axis).

Fluvial systems tend to evolve toward morphological equilibrium under steady environmental conditions, readapting after pulse perturbations (Whipple, 2002). These perturbations produce feedbacks between channel morphology, hydraulics, and sediment processes across different spatial and temporal scales (Johnson & Whipple, 2010). At larger scales, such as river networks, sediment transport processes increase their complexity and interactions, leading to thresholds and feedbacks that remain poorly understood (Benda & Dunne, 1997a; Johnson & Whipple, 2010; Sklar & Dietrich, 2004).

1.2.2.7 Modelling alluvial cover dynamics

The mathematical representation of alluvial cover dynamics has evolved over the past decades, from simple conceptual models to more sophisticated numerical models. The first generation of models focused on quantifying the relationship between sediment supply, transport capacity and bedrock erosion. The tools and cover effect was first formalised mathematically by Sklar & Dietrich (1998, 2004), who proposed a model relating alluvial cover fraction linearly to the ratio of sediment supply to transport capacity. These early models provided understanding of how alluvial cover could control

bedrock incision, but they generally did not consider spatial alluvial cover patterns over channel beds.

More recent reach-scale models incorporated detailed physical processes to simulate the interactions between hydraulics, sediment transport and alluvial cover formation. These include models focusing on grain-bed interaction (Hodge & Hoey, 2012; Nelson & Seminara, 2011), detailed hydraulic simulations (Inoue et al., 2014; Johnson, 2014) and the effects of bed roughness on cover development (Jafarinik & Viparelli, 2020; Zhang et al., 2015). These detailed models provide understanding into physical processes that control alluvial cover dynamics but are generally limited to single reaches and shorter time scales (weeks to months).

The understanding that alluvial cover significantly influences landscape evolution has led to the development of models that incorporate cover effects into traditional landscape evolution models. An example is the SPACE model (Shobe et al., 2017), which tracks bedrock elevation, sediment thickness and erosion rates, allowing for transitions between detachment-limited and transport-limited behaviours. Another example is the Cidre model (Carretier et al., 2016), which integrates individual sediment particle tracking with landscape evolution to link flux-based models with field observations of sediment transport. These models advance our ability to simulate the evolution of topography and alluvial cover over geological timescales with simplified hydraulic representations.

Recently, network-scale models that simulate bedload sediment transport at intermediate temporal scales (years to centuries) have been developed. These include NetworkSedimentTransporter (Czuba, 2018; Pfeiffer et al., 2020), which uses a Lagrangian approach to track individual sediment parcels through river networks; D-CASCADE (Tangi et al., 2019), which simulates sediment cascades across multiple spatial scales; CAESAR-Lisflood (Coulthard et al., 2013), which combines hydraulic routing with sediment transport to simulate landform evolution; and EROS (Croissant et al., 2017; Davy & Lague, 2009), which uses a particle-based approach to simulate erosion and deposition dynamics with explicitly mass balance for streamflow. The spatial and

temporal scales of these models are suitable for addressing questions related to sediment connectivity, pulse propagation and patterns of alluvial cover.

The application of network-scale models to research and river management typically requires field data on hydraulic, channel and sediment properties. There are far fewer field datasets available for bedrock or mixed bedrock-alluvial rivers compared to fully alluvial rivers. The measurement of bedload and estimation of alluvial cover can be difficult due to methodological difficulties in assessing bedrock reaches, high flow variability and temporal fluctuations in cover patterns. Visual methods for estimating cover involve personal subjectivity and limitations due to water clarity. Recent advances in monitoring technologies include side-scan sonar, bathymetric LiDAR and terrestrial laser scanning (Buscombe et al., 2016; Gomez-Heras et al., 2019; Hodge & Hoey, 2016), but they can be costly or difficult to be implemented at large scales. Alluvial cover modelling will benefit from more datasets, allowing for calibration and validation of network-scale models for mixed bedrock-alluvial rivers.

1.2.3 Post-glacial landscapes and their fluvial systems

Many landscapes we observe today, particularly in high-latitude regions, were covered by ice sheets during the Last Glacial Maximum (LGM), approximately 26,000 to 20,000 years ago (Clark et al., 2009). During this period, ice sheets actively eroded the landscape, creating large quantities of glacial sediments and carving irregular topography, with deepened basins, hanging valleys and diverse sediment deposits such as moraines. By around 11,000 years ago, warming temperatures caused most ice sheets to disappear (Ballantyne, 2002). This deglaciation created post-glacial landscapes with unique conditions that influence river evolution.

Church & Ryder (1972) introduced the concept of the "paraglacial period", defined as a time of rapid geomorphic adjustment following deglaciation. During this period, large quantities of unconsolidated glacial sediments are reworked by fluvial and mass movement processes, with sediment supply typically following a declining trend as accessible sources are depleted (Ballantyne, 2002). The early paraglacial period is

characterized by high sediment supply relative to transport capacity, leading to aggradation and the formation of alluvial plains and terraces. As sediment inputs decrease over time, rivers begin to incise into these deposits, gradually exposing bedrock and creating terraces (Church & Ryder, 1972). However, this general tendency of declining sediment availability can be interrupted by episodic inputs from landslides, bank erosion, or extreme hydrological events that access previously stable deposits, temporarily increasing alluvial cover.

Post-glacial rivers inherit characteristics from glacial erosion and deposition, typically exhibiting irregular longitudinal profiles with abrupt changes in slope, ranging from steep bedrock steps and waterfalls to low-slope wetlands and lakes (Brardinoni & Hassan, 2006). In addition, they often contain a wide range of sediment sizes left from glacial deposits, from fine glaciolacustrine clays to large glacially transported boulders that may exceed the transport capacity of contemporary flows (Church & Ryder 1972). Unlike rivers in non-glaciated regions, rivers in post-glacial landscapes may not present the typical downstream fining pattern of grain sizes due to the inherited glacial deposits (Towers et al., 2024).

Post-glacial rivers often present a heterogeneous distribution of channel types, alternating between bedrock and fully alluvial reaches over relatively short distances (Addy et al., 2011; Bergman et al., 2022; Brardinoni & Hassan, 2006; Jansen et al., 2010; Whitbread et al., 2015). The high variability in channel slope creates abrupt transitions between transport-limited and supply-limited reaches, corresponding to transitions between bedrock and alluvial-dominated sections. These glacial inherited characteristics create a unique landscape for river adjustment, making the study of alluvial cover particularly complex in post-glacial landscapes compared to river systems in regions without glacial history.

1.2.4 Sediment connectivity and network-scale processes

Sediment connectivity describes the degree to which sediment can be transferred between different parts of the landscape, including both transfer between process domains (i.e., from hillslopes to fluvial systems) and within individual systems such as

river networks (Bracken et al., 2015; Wohl et al., 2019). In river networks, connectivity influences how effectively sediment moves through the system, affecting patterns of erosion, deposition and alluvial cover distribution.

Mixed bedrock-alluvial rivers refer to river systems that contain spatial variability in alluvial cover, which considers both individual reaches with partial alluvial cover and networks that alternate between predominately bedrock and alluvial reaches. Thus, these rivers may present a more complex sediment connectivity pattern than fully alluvial rivers. Bedrock reaches tend to increase connectivity by transporting sediment effectively, while alluvial reaches may reduce connectivity by temporarily storing sediment. These alluvial deposits create what Fryirs (2013) describes as "buffers" (structures that reduce sediment transfer) within the network. The spatial distribution of these buffers determines how efficiently sediment is transported through the river system.

Network-scale interactions between channel morphology, sediment transport and hydraulics create alluvial cover patterns that may not be predicted from reach-scale studies. These interactions can produce emergent behaviours and self-organising properties at a network-scale (Phillips, 2012; Werner, 1999). For example, sediment deposition in one reach can modify hydraulic conditions and sediment routing in downstream reaches, creating cascading effects that affect alluvial cover distribution throughout the network (Czuba & Foufoula-Georgiou, 2015). In addition, stochastic and intermittent sediment pulses from landslides and extreme floods can trigger non-linear responses at a network-scale, where small disturbances cause large changes in alluvial cover patterns (Benda & Dunne, 1997a). Understanding these network-scale dynamics requires coupling processes across different spatial and temporal scales, which is a challenge that connectivity analysis can help address (Bracken et al., 2015).

Recent network-scale models have improved our ability to analyse sediment connectivity patterns. The CASCADE model (Schmitt et al., 2016; Tangi et al., 2019) tracks individual sediment trajectories from source to sink, providing understanding into transport pathways and bottlenecks. Khan et al. (2021) used the CASCADE model to analyse connectivity in a mixed bedrock-alluvial system, identifying zones where

sediment moves efficiently versus areas where sediment movement is impeded by buffers such as floodplains. They demonstrated that sediment flux patterns correlate with different channel types, such as confined bedrock rivers and laterally unconfined alluvial rivers. Czuba & Foufoula-Georgiou (2015) developed a dynamic connectivity model that identifies sediment clusters and bottlenecks, finding that locations with high cluster persistence correlated with observed hotspots of channel lateral migration. Their approach showed that reaches with low transport capacity can create bottlenecks that decouple bed elevation changes from upstream sediment inputs (Czuba et al., 2017). These modelling approaches are valuable for investigating how reach-scale processes influence network-scale patterns of alluvial cover and sediment dynamics.

1.3 Study area: The River Carron catchment

The River Carron catchment (Figure 1.7), located in the northwest Scottish Highlands, has an area of 300 km^2 and is characterised by a mixed bedrock-alluvial river network. The climate in the catchment is temperate oceanic, typical of the Scottish Highlands. Analysis of CEH-GEAR gridded rainfall data for 2010-2019 shows mean annual precipitation of approximately 1,660 mm across the catchment, with spatial variation ranging from approximately 1,200 mm in the lower elevations to over 2,200 mm in the upland areas (Tanguy et al., 2021). This spatial variation in precipitation occurs due to orographic effects and influences discharge distribution throughout the network. Higher rainfall in steep headwater areas generates higher runoff and sediment mobilisation potential, while lower reaches have more sustained baseflow contributions. The River Carron is monitored by the Scottish Environmental Protection Agency (SEPA) at a stream gauge draining an area of 241 km^2, with a median discharge of 4.5 m^3/s (UKCEH, 2022). Table 1.1 summarises the main catchment characteristics.
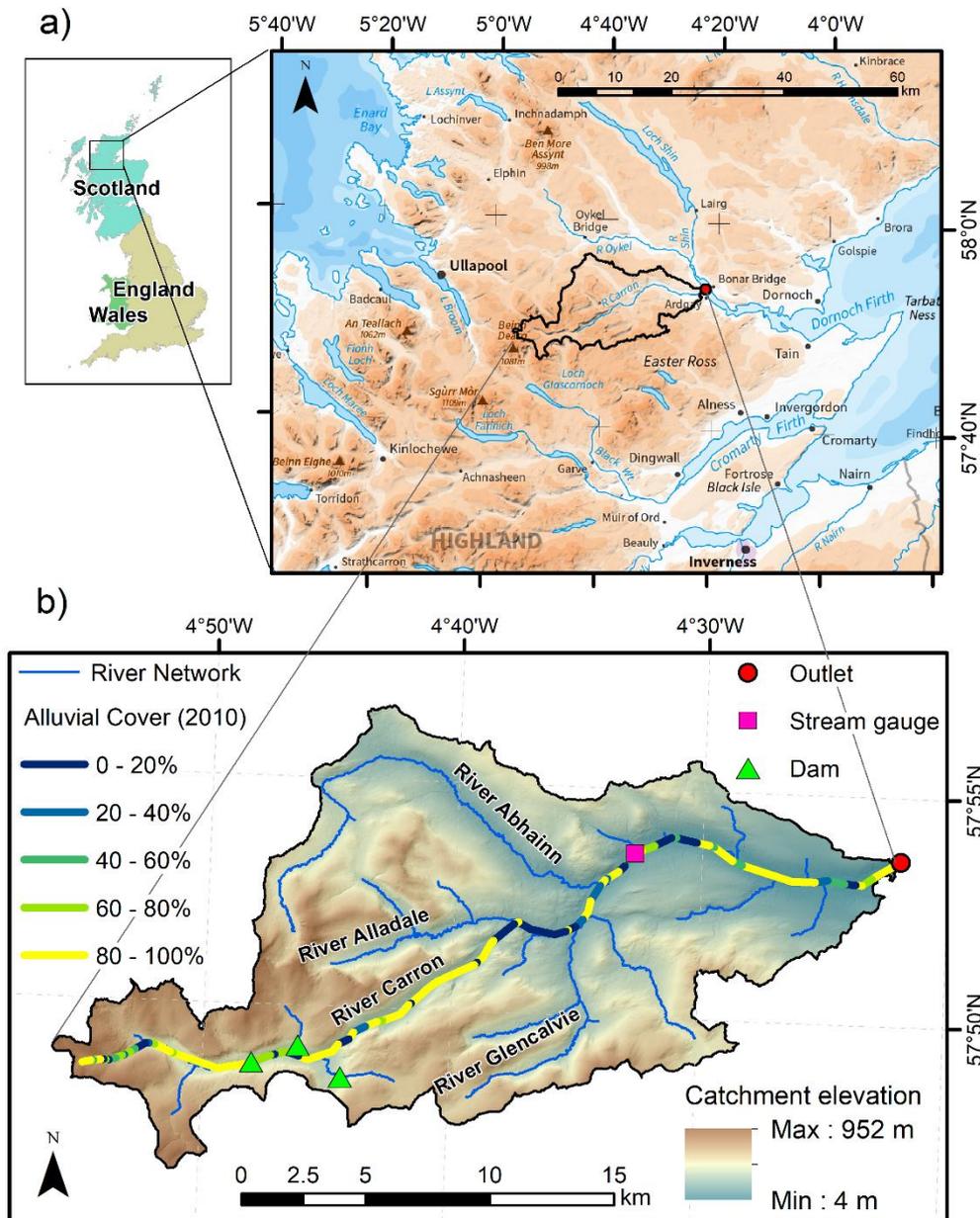
Figure 1.7: Location and characteristics of the River Carron catchment in the Scottish Highlands. a) Catchment location in the Scottish Highlands; b) River network with alluvial cover percentages from Whitbread (2015), catchment elevation, stream gauge, dam and outlet locations.

Table 1.1: Summary of River Carron catchment characteristics.

Characteristic	Value/Description	Source
Catchment area	300 km^2	Calculated using a Digital Elevation Model from OS Terrain 5 (Ordnance Survey, 2022)
Elevation range	4 – 953 m	
Main channel length	44 km	
Total river network length	138 km	
Channel slope range	0.001 – 0.184 m/m	Whitbread et al. (2015)
Bankfull width range	2.9 – 51.7 m	
Channel depth range	0.6 – 6.0 m	
Median discharge	4.5 m^3/s	Calculated using daily flow data from UKCEH (2022)
Dominant bedrock lithology	Psammite (73%), pelite (17%) and granite (10%)	British Geological Survey (2008)
Superficial deposits	Glacial (50%), organic (32%), mass movement (10%), fluvial (6%)	
Annual precipitation	1660 mm/year	Calculated with 2010-2019 data (Tanguy et al., 2021)

The catchment's geological history has been influenced by glaciation, with the most recent activity occurring during the Loch Lomond Readvance (Younger Dryas), which ended around 11,000 years ago (Bennett & Boulton, 1993; Small & Fabel, 2016). This glacial history created a varied topography, from steep slopes to flatter valley floors, which produced U-shaped valleys. Bedrock lithology is dominated by psammite (73% of catchment area) and pelite (17%), with granite (10%) primarily in the southeastern Glencalvie tributary (British Geological Survey, 2008). These metamorphic rocks have relatively low permeability, resulting in limited groundwater storage and rapid runoff responses to precipitation events. The rocks are predominantly fairly resistant to erosion, with glacial deposits overlying them (Table 1.1) (British Geological Survey, 2008). Land use is predominantly upland moorland, heath and bog (75%), with semi-natural grassland (10%), improved grassland (7%) used for sheep grazing concentrated in the lower elevations, and coniferous woodland (8%) (Rowland et al., 2025). The catchment

is sparsely populated, with three small dams in the uplands that affect 14% of the upstream drainage area.

Previous research on the River Carron by Whitbread et al. (2015) identified that bedrock reaches are generally narrower, deeper and steeper than alluvial reaches in the main channel. Whitbread (2015) provided data on alluvial cover fraction, channel width, channel slope and depth for the main channel. They divided the main channel into reaches with similar characteristics, including channel slope, width, depth and the degree of alluvial cover, and found that alluvial cover varied between 5% and 100% across these reaches.

The River Carron catchment was selected as the study area for this thesis for several reasons: (1) The river network presents a wide range of alluvial cover, from fully exposed bedrock to completely alluviated reaches distributed across the network, creating an ideal catchment to investigate controls on alluvial cover distribution; (2) Previous research by Whitbread (2015) and Whitbread et al. (2015) provided data on alluvial cover fraction, bankfull channel width, channel slope, and depth for the main channel, facilitating this study; (3) It is situated in a post-glacial landscape, which provides unique characteristics whose effects on alluvial cover distribution are not fully understood; (4) The catchment has little human intervention in the river system, allowing for the study of mainly natural processes. These characteristics make the River Carron catchment an ideal site for investigating the spatial and temporal variability of alluvial cover in a mixed bedrock-alluvial river system in a post-glacial landscape.

1.4 Research aim and objectives

The overarching aim of this thesis is to investigate the mechanisms driving the spatial and temporal variability of alluvial cover in mixed bedrock-alluvial river systems within upland post-glacial catchments, focusing on the correlations between channel morphology, sediment properties and hydrological dynamics. By combining empirical field investigations with numerical modelling, this thesis seeks to develop an understanding of alluvial cover controls across different spatial and temporal scales.

As discussed in the background section 1.2, alluvial cover dynamics in mixed bedrock-alluvial rivers are controlled by several factors across different spatial and temporal scales. A framework at different spatial scales (Figure 1.8) summarises these controls, describing how grain-scale processes influence reach-scale patterns, which in turn are affected by catchment-scale characteristics. This framework helps contextualise the current understanding of alluvial cover dynamics.
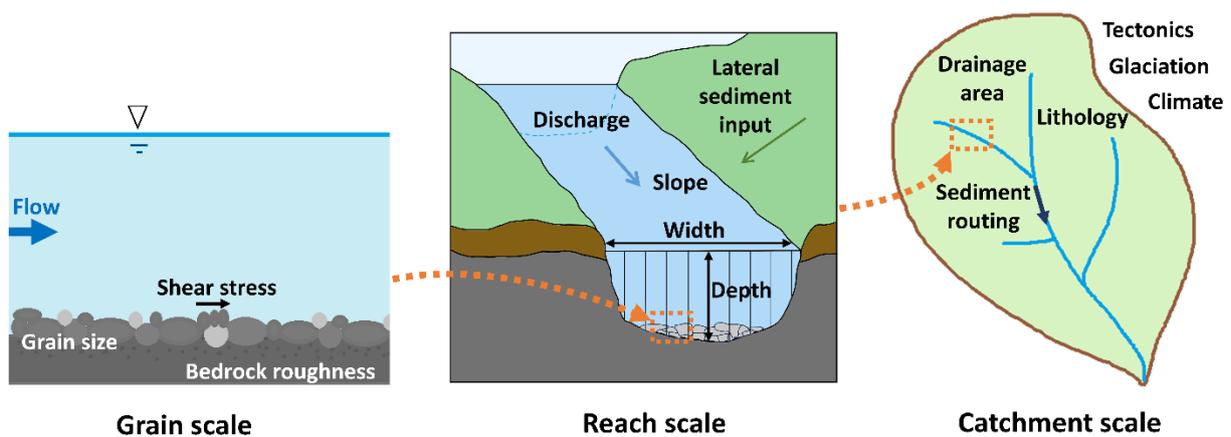
Figure 1.8: Controls on alluvial cover at different scales. The grain scale (left) illustrates how shear stress acts on individual sediment particles, with grain size and bedrock roughness affecting entrainment thresholds. At the reach scale (centre), channel geometry (width, depth, slope) and discharge determine transport capacity relative to sediment supply, controlling local patterns of alluvial cover. The catchment scale (right) shows larger control including drainage area, lithology, tectonics, climate and glaciation history that determine the landscape for river network and sediment routing. Orange dashed arrows indicate cross-scale interactions.

Despite the advances in understanding alluvial cover dynamics in mixed bedrock-alluvial rivers, several knowledge gaps remain that this thesis addresses through three specific objectives:

Objective 1: Examine how channel and sediment properties correlate with spatial patterns and temporal changes of alluvial cover in an upland post-glacial catchment.

Rationale: Although the influence of channel geometry on alluvial cover has been investigated in several landscapes (Massong & Montgomery, 2000; Montgomery & Gran, 2001; Whitbread et al., 2015), the role of grain size distribution in controlling

alluvial cover at a reach-scale is not well understood, particularly in post-glacial landscapes. Post-glacial rivers present a wide range of sediment sizes and topography inherited from glaciation (Church & Ryder, 1972), which may affect alluvial cover distribution. In addition, there is limited understanding of alluvial cover dynamics at intermediate temporal scales (years to decades). Most previous research has focused on either reach-scale studies over short timescales through flume experiments (Chatanantavet & Parker, 2008; Hodge & Hoey, 2016; Johnson & Whipple, 2010), short-term river responses to individual flood events (Cook et al., 2020; Turowski et al., 2013), or theoretical long-term landscape evolution (Howard, 1994; Whipple, 2002). This objective addresses these gaps by analysing the relationships between grain size, channel properties, hydrological variables and alluvial cover in the River Carron catchment, providing empirical temporal analysis of alluvial cover controls over a 12-year period.

Objective 2: Identify the main drivers influencing the extent, expansion and spatial distribution of alluvial cover in a river network.

Rationale: Studies have identified key controls on alluvial cover at reach scales (Chatanantavet & Parker, 2008; Hodge & Hoey, 2016; Johnson & Whipple, 2010), but our understanding of how these processes scale up to river networks remains limited. Network-scale interactions between channel geometry, sediment transport, and hydraulics may create alluvial cover patterns that cannot be predicted from reach-scale studies. River networks have more complex patterns of channel geometry, flow conditions and sediment supply that vary in space, potentially creating behaviours not observed by reach-scale studies. This objective addresses this gap by using a network-scale numerical modelling to investigate how different variables control alluvial cover distribution in river networks.

Objective 3: Explore how sediment pulses influence the pattern and dynamics of alluvial cover in mixed bedrock-alluvial river networks.

Rationale: Although studies have shown that sediment pulses can change river morphology and sediment transport processes (Benda & Dunne, 1997a; East et

al., 2018; Madej, 2001), our understanding of sediment pulse propagation in mixed bedrock-alluvial networks and their interaction with existing alluvial cover patterns is limited. Previous pulse studies have focused mainly on fully alluvial systems (Cui et al., 2003; Lisle et al., 2001), leaving questions about how pulses propagate and impact alluvial cover in mixed bedrock-alluvial networks. This objective investigates interactions between sediment pulses and alluvial cover dynamics at a network scale, examining how pulse characteristics and pre-existing alluvial cover patterns influence pulse transport and post-pulse alluvial cover patterns.

1.5 Thesis structure

This thesis is structured with a series of research chapters, with some designed as standalone manuscripts for publication in peer-review journals (chapters 2, 5 and 6) and others designed as traditional thesis chapters (chapters 2, 4 and 7). The chapters progress from empirical field investigations to model development and analyses using numerical simulations, addressing the three main research objectives outlined above. Due to the standalone manuscripts, some repetition of methodological descriptions, key equations and contextual figures occurs between chapters to ensure each function independently. A brief summary of the next chapters is provided below:

Chapter 2: Controls on spatial patterns of alluvial cover in a post-glacial landscape: evidence from the River Carron, Scotland

This chapter analyses spatial patterns in alluvial cover and their relationships with channel characteristics and grain size distribution in the River Carron catchment. Using field data collected from both the main channel and tributaries, it investigates how alluvial cover correlates with factors such as drainage area, channel slope, bankfull width, channel depth and grain size. The analysis also includes how flow regimes affect sediment mobilisation and current cover patterns. This chapter addresses Objective 1 on spatial correlations of alluvial cover.

Chapter 3: Temporal changes in alluvial cover in the River Carron over a 12-year period

This chapter extends the analysis of Chapter 2 by investigating temporal dynamics of alluvial cover over a 12-year period (2010-2022). It addresses methodological challenges in measuring temporal changes in alluvial cover and examines how these changes correlate with local channel morphology and recent hydrological events. By exploring temporal variations in alluvial cover using empirical data, this chapter addresses Objective 1.

Chapter 4: Development and modification of a network-scale sediment transport model for mixed bedrock-alluvial rivers

This chapter details the development and modification of the NetworkSedimentTransporter (NST) model to enable analysis of alluvial cover controls in mixed bedrock-alluvial systems. The modifications include a new function to calculate and track alluvial cover changes on bedrock surfaces, improvement of the sediment transport algorithm through networks with high slope variability and implementation of a flexible sediment input function to explore several different supply scenarios. This chapter is a methodological foundation for the analyses conducted in the next two chapters, allowing Objectives 2 and 3 to be addressed.

Chapter 5: Network-scale dynamics of alluvial cover in a mixed bedrock-alluvial river

Guirro, M. O., Hodge, R., Clubb, F., & Turnbull, L. (2025). Network-scale dynamics of alluvial cover in a mixed bedrock-alluvial river. Journal of Geophysical Research: Earth Surface, 130(3), e2024JF007968. https://doi.org/10.1029/2024JF007968

This chapter published at Journal of Geophysical Research investigates the principal controls on the spatial distribution of alluvial cover in mixed bedrock-alluvial networks in a steady-state using the modified NST model described in Chapter 4. It examines how changing sediment supply, flow depth, and grain size affect alluvial cover patterns at a network scale. This chapter also includes

connectivity analysis to evaluate cover transitions, fragmentation and expansion of alluvial reaches, directly addressing Objective 2 on alluvial cover controls and connectivity.

Chapter 6: Dynamics of sediment pulses and their interaction with alluvial cover in a mixed bedrock-alluvial river

This chapter explores the influence of sediment pulses on alluvial cover dynamics in mixed bedrock-alluvial river networks. It investigates how pre-existing alluvial cover affects the propagation of sediment pulses, how pulse characteristics (volume and introduction site) control pulse behaviour and how pulses change pre-existing alluvial cover patterns. This chapter directly addresses Objective 3.

Chapter 7: Research summary, implications and conclusions

The final chapter summarises the findings from the previous chapters, discussing their implications for understanding alluvial cover dynamics in mixed bedrock-alluvial river systems.

2 Controls on spatial patterns of alluvial cover in a post-glacial landscape: evidence from the River Carron, Scotland

2.1 Abstract

Mixed bedrock-alluvial rivers are common in post-glacial landscapes, where the distribution of alluvial cover influences channel evolution, sediment transport, and aquatic habitats. However, predicting alluvial cover patterns remains challenging, particularly due to the complex legacy of glaciation on channel morphology and sediment supply. This study investigates the controls on alluvial cover in the River Carron, Scotland, by analysing the relations between alluvial cover percentage and channel characteristics. We measured alluvial cover and grain-size distributions through field surveys and photo analysis complementing existing channel geometry data for a total of 92 reaches. Multiple regression analysis found that channel slope and bankfull depth were the strongest predictors of alluvial cover (p-value < 0.001 and R^2 = 0.45), while drainage area showed a significant relationship only when controlling for slope. We found high spatial variability in grain-size distribution both between and within reaches (Coefficient of Variation of median grain size up to 72% within reaches), reflecting the diverse sediment sources characteristic of post-glacial landscapes. Analysis of historical flow records revealed that contemporary floods actively rework these sediments, with 2-year floods capable of mobilizing median grain sizes in 63% of reaches, increasing to 88% during 50-year floods. Typical downstream patterns of channel morphology and sediment characteristics were disrupted by glacial inheritance, with both bedrock and alluvial channels occurring throughout the catchment regardless of drainage area, and no significant downstream fining of sediment or correlation between grain size and alluvial cover. Our findings demonstrate how post-glacial landscapes create distinct patterns in alluvial cover distribution and grain size as they adjust to deglaciation.

2.2 Introduction

Alluvial cover, the layer of sedimentary material overlying bedrock in river channels, influences various aspects of fluvial systems. River channels can be classified based on the extent of this cover: bedrock channels have exposed bedrock in their bed or banks for at least part of their length, though they may contain patches of alluvial cover – often classed as mixed bedrock-alluvial - while fully alluvial channels have a continuous cover of sediment that completely masks the underlying bedrock (Montgomery & Buffington, 1997; Turowski et al., 2008). This sediment layer has a dual effect on the underlying bedrock: it can protect the bed from erosion when stable and it can provide sediment particles that act as tools for erosion when mobilised, controlling the long-term evolution of river channels (Finnegan et al., 2007; Sklar & Dietrich, 2004). These processes are fundamental in driving landscape evolution, as they determine how river channels cut through bedrock and develop their long-term morphology (Whipple et al., 2013). Alluvial cover also modifies sediment-transport processes by providing mobile particles and altering flow dynamics near the bed, which affects shear stress and sediment entrainment (Hodge et al., 2011; Inoue et al., 2014; Johnson & Whipple, 2010). Consequently, alluvial cover influences channel morphology, as its presence allows the channel to adjust its shape in response to changes in flow and sediment supply (Baynes et al., 2020; Chatanantavet & Parker, 2008; Papangelakis et al., 2021; Turowski et al., 2013). In addition, stable alluvial cover provides essential habitats for aquatic organisms, such as spawning grounds for salmonid fish (Buffington et al., 2004; Steiger et al., 2005; Wohl, 2017).

Despite the importance of alluvial cover for predicting landscape evolution and protecting aquatic systems, predicting its dynamics in mixed bedrock-alluvial rivers is complex. The distribution of alluvial cover in these systems is influenced by an interaction of geomorphic and hydrologic factors. Discharge and sediment supply are primary controls: alluvial cover forms when sediment supply exceeds the channel's transport capacity, which typically occurs during periods of lower discharge or higher sediment input (Chatanantavet & Parker, 2008; Ferguson et al., 2017b; Inoue et al., 2014; Johnson, 2014). Temporal variations in these parameters lead to changes in alluvial cover

over time (Cook et al., 2020; DeLisle & Yanites, 2023; Turowski et al., 2013). The grain-size distribution of sediments also affects the formation and stability of alluvial deposits. Larger grains generally promote more extensive and stable alluvial cover as they typically require higher flows for mobilisation, though this size-selective mobility can be reduced when grains move over smooth bedrock surfaces (Ferguson et al., 2017b; Hodge et al., 2011). Flume experiments have demonstrated how sediments preferentially deposit in areas of low slope and high bed roughness, while subsequent particle clustering promotes the stability and expansion of these initial deposits (Chatanantavet & Parker, 2008; Hodge & Hoey, 2016; Johnson & Whipple, 2010).

Empirical analysis of field data to identify alluvial cover controls has found that channel geometry also influences alluvial cover formation, as steeper and narrower channels typically inhibit cover development due to higher shear stresses that promote sediment transport rather than deposition (Massong & Montgomery, 2000; Montgomery & Gran, 2001; Whitbread et al., 2015). Bedrock channels are commonly found in these high-energy environments, but they can also be wider and found in low slope regions (Buckley et al., 2024; Jafarinik & Viparelli, 2020). Lithology further contributes to the complexity of alluvial cover dynamics, as more resistant rock types reduce sediment availability through decreased erosion rates of both the channel and hillslopes, limiting alluvial cover formation (Buckley et al., 2024; Massong & Montgomery, 2000). The complex interactions among these factors, along with their temporal and spatial variability, challenge the prediction and understanding of alluvial cover dynamics.

Post-glacial landscapes present a unique context for studying alluvial cover dynamics. During glaciation, ice erodes the landscape irregularly, creating a wide range of slopes – from very steep to flatter sections (Ballantyne, 2002). During and following deglaciation, exposed glacial erosional features, meltwater discharge, extensive sediment deposition, and enhanced paraglacial sediment supply from over-steepened and unstable hillslopes leads to a complex pattern of resistant bedrock and more easily erodible glacial deposits. The fluvial system develops by reworking these sediments, such as glacial till, glaciofluvial, and glaciolacustrine deposits, which contain a wide range of grain sizes from clay to large boulders (Church & Ryder, 1972). Therefore, these landscapes often exhibit mixed bedrock-alluvial channels, with abrupt changes in channel morphology

and alluvial cover thickness over relatively short distances (e.g., Addy et al., 2011; Bergman et al., 2022; Brardinoni & Hassan, 2006; Jansen et al., 2010; Whitbread et al., 2015). The presence of coarse glacially-derived sediments that exceed the transport capacity of modern channels may create persistent alluvial cover patches, further complicating the complex relations between cover, grain size and channel geometry observed in fluvial systems (Towers et al., 2024). Therefore, predicting and managing alluvial cover dynamics in post-glacial catchments can be more complex than in non-glaciated catchments due to the additional influences of glaciation on sediment sources and channel morphology.

Despite advancements in understanding the factors that control alluvial cover, knowledge gaps remain, particularly how alluvial cover correlates with factors such as grain size and channel geometry in post-glacial systems. In post-glacial landscapes, two contrasting scenarios may exist: if alluvial cover is primarily inherited from glaciation, we would expect weak correlations between cover patterns and current channel characteristics; however, if the system has reworked glacial sediments towards a steady state (e.g. Ballantyne, 2002), we might observe typical scaling relations similar to those in unglaciated catchments (Massong & Montgomery, 2000; Montgomery & Gran, 2001; Rice & Church, 1998). Whitbread et al. (2015) investigated some of these relations in the River Carron, a post-glacial river in the Scottish Highlands, finding typical correlations between channel geometry and alluvial cover in the main channel. However, questions remain about the role of grain size in these relations and how sediment mobility has evolved since deglaciation.

This study expands upon Whitbread et al. (2015) through three main contributions: (1) expansion from the main channel only to the river network including tributaries, (2) introduction of grain size analysis and sediment mobility assessment using historical flow records dating back to the 1970s, and (3) employment of continuous alluvial cover analysis (0-100%) rather than binary channel classification. We collect new field data from tributaries and more data from the main channel, and analyse them to determine the relations between the percentage of alluvial cover and other channel variables. Our approach includes analysis of grain size mobility using historical hydrological records to assess contemporary sediment transport potential, indicating post-glacial river

adjustment processes. This expanded framework enables us to address a new set of research questions:

1) How do different geomorphic and hydrologic variables (e.g., drainage area, channel slope, bankfull width, channel depth, and grain size) control the distribution of alluvial cover in a post-glacial catchment?

2) How does the variability of grain size within and between reaches influence the relation between grain size and alluvial cover in this post-glacial catchment?

3) To what extent has the historical flow regime been capable of mobilising the observed grain-size distribution, and how might this influence current alluvial cover pattern?

2.3 Description of study area

The Carron catchment, located in northwest Scotland (Figure 2.1a), covers an area of 300 km^2. This mixed bedrock-alluvial river system was selected as our study site due to the availability of data on alluvial cover fraction, bankfull channel width, channel slope and depth (Whitbread, 2015; Whitbread et al., 2015). The main channel of the Carron is 44 km long, with the entire river network extending to about 138 km. The catchment's elevation ranges from 952 m to 4 m at the outlet. The predominant bedrock lithologies are psammite (metamorphosed sandstone) and pelite (metamorphosed mudstone). In the southeast, particularly in the tributary Glencalvie, granite is also prevalent (Figure 2.1b). The catchment is sparsely populated, with agricultural activity in the lowlands. A dam in the upper main channel, and small weirs constructed around 1950 in two minor upper tributaries, may reduce downstream flow, but they are unlikely to significantly impact the processes analysed in this study as they capture water from a small proportion (14%) of the drainage area.

The Carron catchment's geological history is marked by glaciation, with the most recent glacial activity occurring during the Loch Lomond Readvance (Younger Dryas), ending approximately 11 ka ago (Bennett & Boulton, 1993; Small & Fabel, 2016). Glacial erosion created diverse topography, ranging from steep slopes to flatter valley floors, with typical

U-shaped valley morphology. The subsequent fluvial processes that reworked the glacial deposits have resulted in mixed bedrock-alluvial channels, with the bedrock reaches generally being narrower, deeper and steeper than the alluvial reaches (Whitbread, 2015).

The catchment's superficial geology is mainly composed of glacial (50% of catchment area) and organic (32%) deposits, with fluvial deposits (6%) along the rivers and some paleo-landslide deposits (10%) concentrated at the bottom of steep hillslopes (Figure 2.1c). Sediment supply to the rivers primarily comes from alluvial deposits near the channels, such as raised alluvial terraces and debris fans associated with tributary streams. Flat alluvial plains with fine sand and peat provide organic sediments, particularly in the northern tributary, the River Abhainn.

Hydrological data for the River Carron is monitored by the Scottish Environmental Protection Agency (SEPA) at one stream gauge, which drains an area of 241 km^2 (location in Figure 2.1a). The median discharge at this gauge is 4.5 m^3/s, with a bankfull discharge of 243 m^3/s occurring on average every 6 years. Using SEPA gauging records from ~1960 to 2009, Whitbread et al. (2015) developed regional power law relationships between discharge (Q) and drainage area (A) to estimate discharge at ungauged sites within the catchment. The flow data used in this study were obtained from the UK National River Flow Archive (UKCEH, 2022).
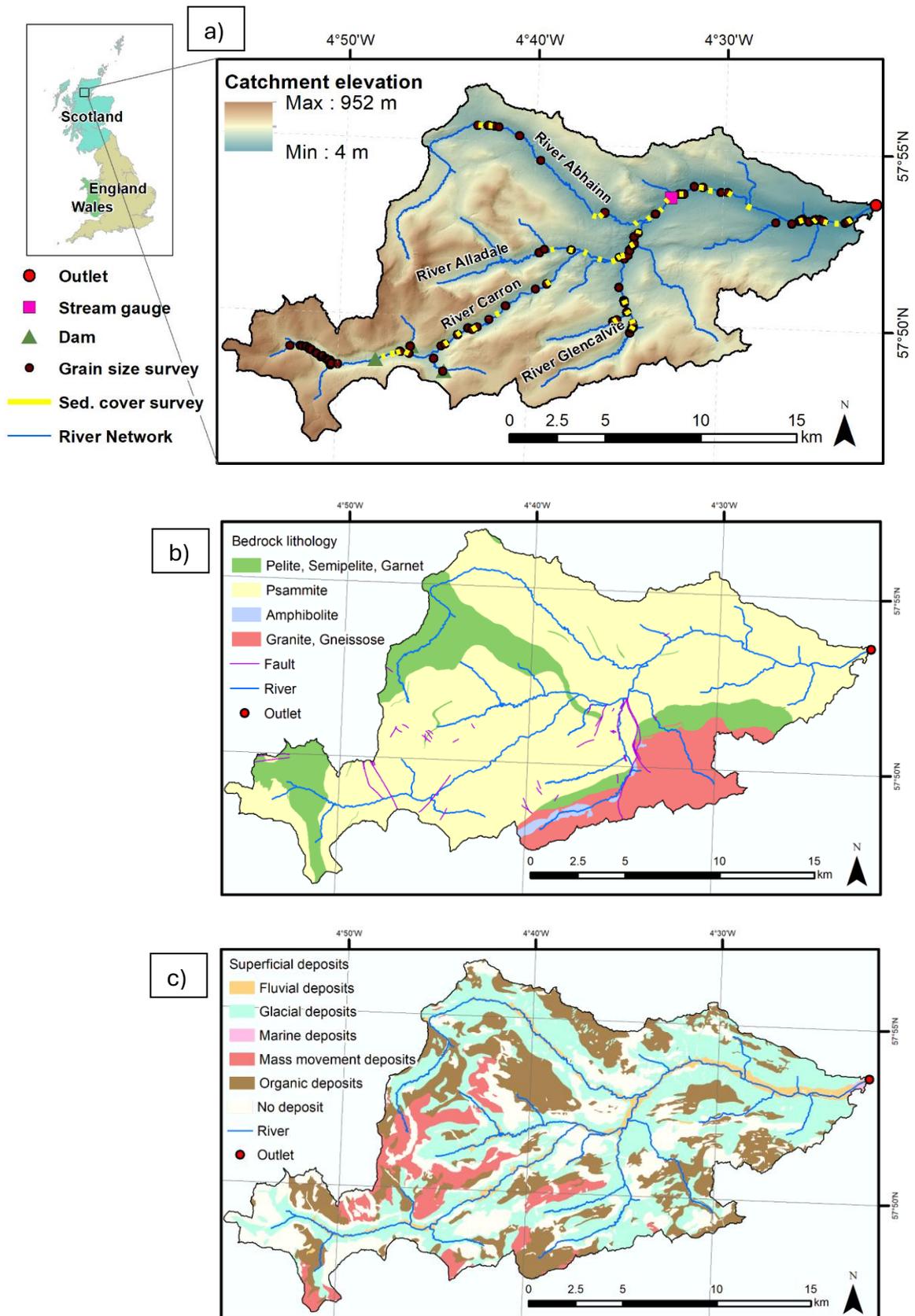
Figure 2.1: Carron catchment characteristics: a) Location and elevation of Carron Catchment, with locations of stream gauge, dams in the upper channels, grain size

sampling and alluvial cover estimation from 2022; b) Bedrock lithology of the Carron Catchment (data source: British Geological Survey, 2008); c) Superficial deposits of the Carron Catchment (data source: British Geological Survey, 2008).

2.4 Methods

This study consisted of collecting field data on alluvial cover and channel geometry from the River Carron and analysing them statistically to understand what controls the spatial distribution of alluvial cover in mixed bedrock-alluvial channels in post-glacial landscapes.

2.4.1 Data sources, field data collection and processing

The main source of existing data used for the Carron catchment is Whitbread (2015), which provides channel geometry (bankfull width and depth), channel slope, drainage area and alluvial cover percentage for reaches in the main River Carron. This dataset was collected between 2009 and 2011 and provides data for reaches, i.e., channel segments with similar channel morphology, with lengths from 100 m to 2 km. However, this dataset lacks grain size measurements and is limited to the main channel.

To extend the analysis to tributaries, a 5-m resolution Digital Elevation Model (DEM) sourced from the OS Terrain 5 (Ordnance Survey, 2022) was used to calculate the channel slope of 100 m long reaches in each tributary. Additionally, high resolution (25 cm) vertical aerial imagery from the EDINA Aerial Digimap Service (Getmapping, 2023) was used to estimate the width of tributaries at cross sections where field measurements were collected. We used a power-law scaling relation provided by Whitbread et al. (2015) that relates drainage area and bankfull channel depth data from the main channel to estimate depth of tributaries. This scaling relation accounts for 61% of the spatial variation in bankfull channel depth of the main river (Whitbread et al., 2015). Although the scaling relation depth-drainage area is not directly validated in the tributaries due to focus on grain size measurements and time constraints, it represents the best available estimate of channel

depth given that it was derived from the same catchment under similar geological and climatic conditions.

To address the lack of grain size data and extend the alluvial cover data to tributaries, fieldwork was conducted between 19th to 23rd September 2022, during which the discharge in the River Carron was around its median (4.5 m^3/s). A comprehensive photo survey was conducted to estimate grain size, capturing 1437 images of gravel bars, riverbeds and sediment sources. Grain size and alluvial cover data were collected across 43 reaches of the river network, including 29 in the main channel covering headwaters, mid and lower sections of the River Carron, and 14 in its main tributaries (Alladale, Glencalvie and Abhainn rivers) and six other minor tributaries (Figure 2.1a). The upstream areas of some tributaries were not covered due to accessibility issues.

In each reach the percentage alluvial cover was estimated visually at 11 transects: one at the midpoint, five upstream, and five downstream of the midpoint, spaced approximately 20 meters apart, covering a reach length of 200 meters. The average percentage of alluvial cover for each reach was calculated. Visual estimations were associated with varying levels of uncertainty due to challenges in observing the riverbed through peat-rich water. Uncertainty levels were categorized as follows: "high" for cases where more than 70% of the riverbed was obscured, "medium" for 50% to 70% obscured, and "low" when less than 50% of the riverbed was obscured.

The grain-size Distribution (GSD) of 98 gravel bars in the 43 reaches was determined using PebbleCounts, a grain-sizing tool for photo surveys (Purinton and Bookhagen, 2019) (Figure 2.2). A total of 274 high-resolution photographs were analysed, with each photo calibrated using a reference object to determine the resolution (mm/pixel). Most gravel bars were represented by three photos to capture variations within each bar. The automatic mode of PebbleCounts, which uses an edge detection algorithm to identify individual grains and automatically measure their dimensions without manual selection, was employed to estimate the GSD. The algorithm measured the lengths of the larger and intermediate axes of each grain visible in the photos. We used the grain area to define each grain's contribution to the size distribution. The grain size was calculated by considering each grain as an ellipse using the measured axes. The GSD percentiles (D_5,

D_{16}, D_{25}, D_{50}, D_{75}, D_{86}, and D_{95}) of each gravel bar and reach was then estimated based on the cumulative grain size area plotted against the intermediate axis lengths, where D_{50} represents the grain size at which 50% of the total measured area is composed of smaller grains.

Uncertainties in the automatic GSD estimation were addressed by comparing the automatic mode of PebbleCounts with manual grain size estimation for 100 grains in 14 randomly selected photos, covering 6% of the total photos. It was found that the automatic mode tended to underestimate the D_{50} by approximately 3 mm (3% error relative to the average D_{50} of 100 mm found in the catchment), which was considered minor for this study. Automatic grain selection was less effective at identifying grains underwater and that were not well-rounded or had surface irregularities, such as moss or rock stripes. Of the initial 274 photos, 36 were discarded due to poor selection by the automatic mode. The small number and diverse characteristics of discarded photos suggest low impact on the overall grain size distribution. The effect of fine material such as sand, undetected by PebbleCounts due to its threshold of 20 times the photo resolution (approximately 0.75 cm in our survey), was assessed. Approximately 26% of the photos contained fine material below this threshold. A subset of six photos was selected to estimate the impact of fine material on the GSD. The analysis revealed that incorporating fine material would increase the grain-size distribution area by an average of 4.2%, reducing the D_{50} by 2 mm when extrapolated across all relevant photos. Given the low presence of fine material in most channels in the Carron catchment, its impact on the overall GSD was considered negligible for this study.
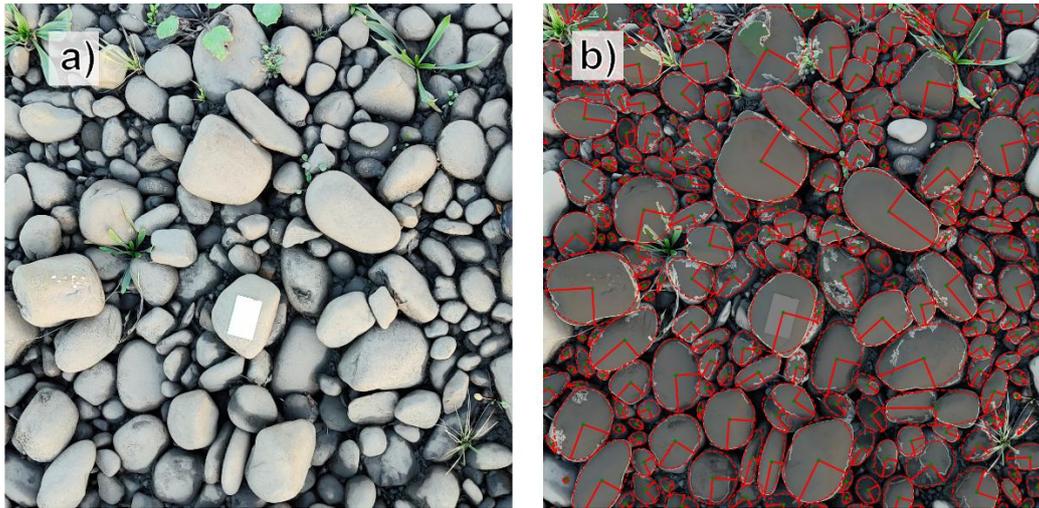
Figure 2.2: Example of grain size measurement using PebbleCounts (Purinton and Bookhagen, 2019). a) Original photograph of a gravel bar with a white reference object for scale. b) Output from PebbleCounts showing automatic identification of individual grains (red outlines) and their measured axes, used to calculate the grain-size distribution. The software measures both the larger and intermediate axes of each identified grain to estimate grain size based on the grain area.

Hydrological data (daily and peak flow data) used in this study is from the 3002 - Carron at Sgodachail gauging station run by the Scottish Environment Protection Agency since January 1973. These data were used to analyse the flow regime and estimate flood magnitudes for sediment mobility calculations, as described in section 2.4.3.

2.4.2 Statistical analysis of alluvial cover and channel morphology

We performed a series of statistical analysis using reach-level data from two sources. For the main channel, we used Whitbread's (2015) data from 2010 on alluvial cover percentage, drainage area, channel slope, bankfull width, and bankfull depth in 78 reaches, complemented with our grain size measurements from 2022 in 29 of these reaches. For the tributaries, we used our estimations of alluvial cover percentage, drainage area, channel slope, bankfull width, and grain size from 2022 in 14 reaches. The variation in the data availability across the total 92 reaches surveyed influenced the number of reaches that could be included in different analyses. Due to the skewed distribution of channel slope—characterized by many low-slope reaches and a few steep

ones—a log transformation was applied to normalise slope, generating a more robust statistical analysis.

The first analysis explored the relations between various geomorphic variables and alluvial cover in the Carron catchment. Simple linear regressions were conducted for each variable independently to assess their individual correlations with alluvial cover, using Whitbread's 2010 alluvial cover data for the main channel and our 2022 data for the tributaries. Next, multiple linear regression was performed to evaluate how the variables interact collectively to explain variations in alluvial cover. Although drainage area was included in the simple linear regression, it was excluded from the multiple regression analysis because it typically acts as a proxy for channel width and depth in river systems, which could create issues of multicollinearity. The predictor variables (channel slope, bankfull width, bankfull depth, and grain size) were standardized to have a mean of zero and a standard deviation of one. This standardization ensured that all variables were on comparable scales, facilitating the interpretation of regression coefficients. This analysis identifies the combined effect of all variables on the alluvial cover. To refine the model, stepwise regression was employed (Agostinelli, 2002). This method systematically added variables based on their statistical significance, resulting in a model that included only the most significant predictors of alluvial cover. Next, K-fold cross-validation (k=5) was conducted to assess the stability and predictive power of the regression models (Rodriguez et al., 2010). This method involved randomly dividing the data into five subsets, training the model on four subsets, and validating it on the remaining subset. The process was repeated five times and the results were averaged to estimate the model's performance using two metrics: R-squared (R^2) and Mean Squared Error (MSE). Finally, Principal Component Analysis (PCA) was used with all variables, including drainage area, to identify the primary channel parameters influencing alluvial cover and to determine whether the characteristics of bedrock and alluvial reaches differ significantly. This analysis reduced the dimensionality of the data and highlighted the most influential variables.

We also explored the relation between grain size and the percentage of alluvial cover by conducting analyses at multiple spatial scales. We started by investigating the spatial variability of grain sizes by comparing grain-size distributions among different channels

in the catchment. To quantify within-reach variability, we analysed the distribution of grain sizes among gravel bars within each reach. We calculated the coefficient of variation (CV) of D_{50} for reaches with at least two gravel bar measurements, where CV is the standard deviation divided by the mean, expressed as a percentage. This metric allowed comparison of grain-size variability within reaches while accounting for differences in mean grain size. We then tested for correlation between within-reach grain size variability (CV) and alluvial cover using Pearson's correlation coefficient (r).

2.4.3 Grain size mobility analysis

We analysed the hydraulic conditions required for sediment entrainment to assess the potential mobility of the measured grain sizes across the catchment. This analysis involved several steps to estimate flow depths and resulting shear stresses during flood events of different magnitudes.

First, we conducted a flood frequency analysis using the log-normal distribution fitted to annual maximum flows from the Carron at Sgodachail gauging station (1973-2022). This analysis resulted in discharge estimates for flood events with return periods of 2, 5, 10, 25, 50 and 100 years. The 50-year flood (307.5 m^3/s) is close to the highest recorded flow in the catchment (307.1 m^3/s, measured on 26 October 2006). To estimate discharges at ungauged locations throughout the catchment, we used a drainage-area ratio method (Equation 2.1).

$$Q_2 = Q_1(A_2/A_1)^{1.0} \qquad \text{(Equation 2.1)}$$

where Q_2 is the discharge at the ungauged location (m^3/s), Q_1 is the discharge at the gauge (m^3/s), A_2 is the drainage area of the ungauged location (km^2), and A_1 is the drainage area of the gauge (km^2). We used an exponent of 1.0 due to lack of regional studies on scaling discharge in Scottish rivers.

For each reach and flood magnitude, we calculated flow depths (H) using Manning's equation (Equation 2.2).

$$Q = \frac{1}{n}\, W\, H \left(\frac{W\, H}{(W + 2H)} \right)^{2/3} S^{1/2} \qquad \text{(Equation 2.2)}$$

where Q is discharge (m³/s), n is Manning's roughness coefficient (dimensionless, set to 0.04 for natural channels with moderate irregularity; Arcement & Schneider, 1989), W is channel width (m), H is flow depth (m), and S is channel slope (m/m). We solved this equation iteratively to determine flow depth (H).

Using the calculated flow depths, we calculated boundary shear stress (τ_b) at the bed (Equation 2.3).

$$\tau_b = \rho\, g\, H\, S \qquad \text{(Equation 2.3)}$$

where τ_b is boundary shear stress (N/m²), ρ is water density (kg/m³), g is gravitational acceleration (m/s²), H is flow depth (m), and S is channel slope (m/m).

We then compared the boundary shear stress with the critical shear stress (τ_c) required to mobilise the median grain size (D_{50}) in each reach, determined using Shield's criterion (Equation 2.4).

$$\tau_c = \theta\, (\rho_s - \rho)\, g\, D_{50} \qquad \text{(Equation 2.4)}$$

where τ_c is critical shear stress (N/m2), θ is Shield's parameter (dimensionless, set to 0.045 for gravel-bed channels), ρ_s is sediment density (kg/m³), ρ is water density (kg/m³), g is gravitational acceleration (m/s²), and D_{50} is the median grain size (m).

The ratio of boundary to critical shear stress (excess shear stress, τ_b/τ_c) was used to identify reaches where D_{50} particles could potentially be mobilised during floods of different magnitudes, with values greater than 1 indicating potential for mobilisation. We repeated this analysis for D_{84} to assess the mobility of coarser fractions. This grain size mobility analysis allowed us to investigate how historical flood events may have reworked the alluvial cover in recent decades.

2.5 Results

2.5.1 Correlations between channel characteristics and alluvial cover

The initial simple linear regressions between each channel variable and alluvial cover showed significant correlations for channel slope (p-value < 0.001), bankfull width (p-value = 0.001), bankfull depth (p-value = 0.006), and width-to-depth ratio (p-value < 0.001) (Figure 2.3). The data is scattered, with low R-squared values found in all linear regressions – the highest R-squared found was with width-to-depth ratio (R^2 = 0.3). The lack of a significant correlation between the alluvial cover and drainage area indicates that bedrock and alluvial channels are distributed throughout the catchment. The relation with grain size (D_{50}) was not statistically significant (p-value > 0.05) (Figure 2.3e), and additional analysis with coarser grain size percentiles (D_{84} and D_{95}) also showed no significant correlations with alluvial cover (p-value > 0.05). This result indicates that grain size alone does not appear to control alluvial cover distribution in this post-glacial setting. Overall, channels with higher alluvial cover were typically characterized by lower slopes, greater width, and shallower depth in the Carron catchment.
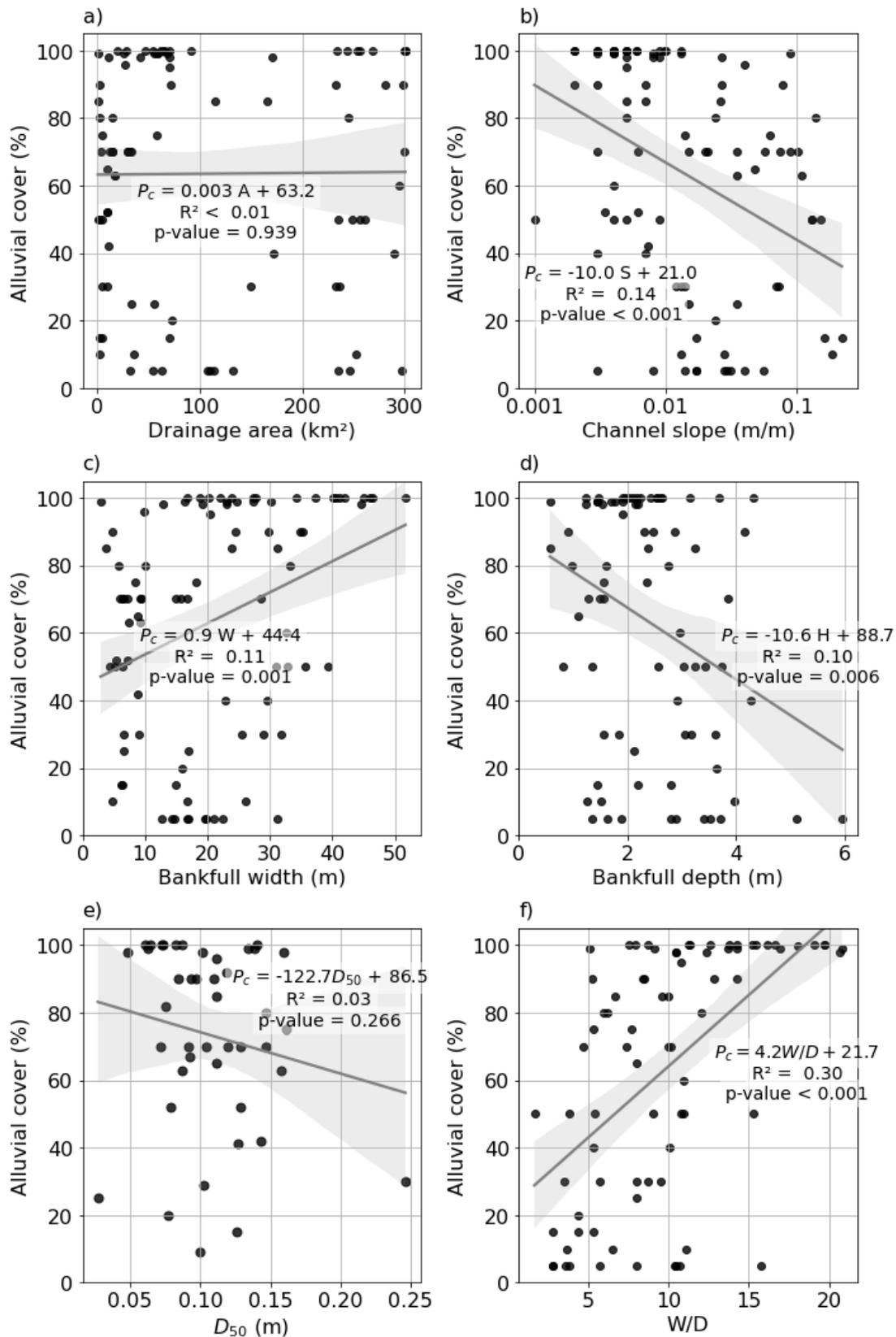
Figure 2.3: Simple linear regressions between the percentage of alluvial cover (P_c) and a) drainage area (A); b) channel slope (S); c) bankfull width (W); d) bankfull depth (H); e) grain size (D_{50}); and f) width-to-depth ratio (W/D) for the sampled reaches in the Carron

catchment. The shaded areas around the regression lines represent the 95% confidence intervals.

Multiple linear regression was conducted with all variables (channel slope, bankfull width, bankfull depth, and grain size) to explain the percentage of alluvial cover (Table 2.1). Due to limited grain size data availability, this complete model could only include 29 reaches with data for all variables, while the dataset for geometry variables contained 78 reaches. The linear regression model with all variables produced a higher R-squared value (R^2 = 0.54) than the single regressions and a p-value of the F-statistic of < 0.001, with channel slope and bankfull depth being the only variables showing a significant correlation with alluvial cover (p-value < 0.05). Stepwise regression also identified channel slope and depth as the most significant predictors of alluvial cover. A subsequent multiple linear regression with only these variables found a lower R-squared value (R^2 = 0.45) but maintained statistical significance (p-value < 0.001) (Table 2.1), with the advantage of utilising the full 78-reach dataset. Figure 2.4 illustrates the relation between measured alluvial cover and predicted alluvial cover with the multiple regression model with all variables.

Table 2.1: Multiple linear regression results for the models with all variables and selected variables (channel slope and depth). The variables were standardised; thus, the coefficients are directly comparable, and the constant coefficient indicate the predicted value of alluvial cover when all variables are at their mean values. The p-values highlighted in red indicate significant variables (p-value < 0.05).

Variable	Complete model: Regression with all variables			Reduced model: Regression with slope and depth		
	Coefficient	Std. error	p-value	Coefficient	Std. error	p-value
Constant	68.90	4.56	<0.001	63.22	3.11	<0.001
Channel slope	-25.06	7.94	0.004	-23.14	3.35	<0.001
Bankfull width	2.61	7.26	0.722	-	-	-
Bankfull depth	-15.53	5.16	0.006	-19.85	3.35	<0.001
Grain size (D_{50})	-0.89	4.95	0.858	-	-	-
R-squared	**0.543**			**0.447**		
Adj. R-squared	**0.467**			**0.432**		
F-statistic	**7.14**		**<0.001**	**30.30**		**<0.001**
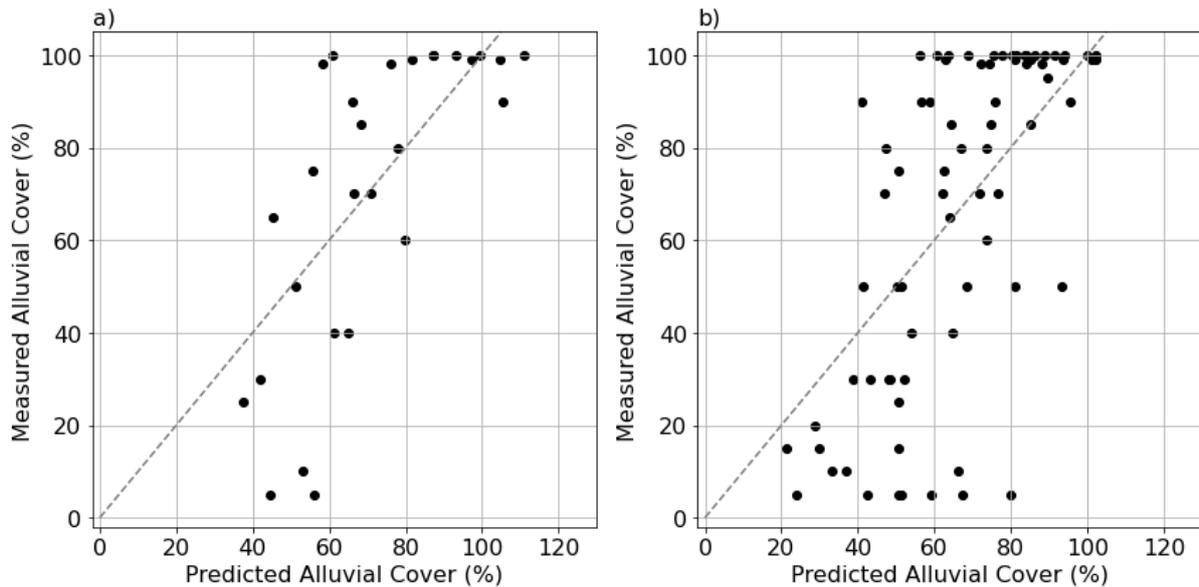
Figure 2.4: Predicted vs. measured alluvial cover of reaches for the multiple linear regression model with a) all variables (n = 29 reaches with complete data for all variables); and b) only channel slope and depth (n = 78 reaches). Details of the regression models are in Table 2.1. The dashed line represents a 1:1 fit, where predicted values would exactly match the measured values.

K-fold cross-validation was performed to evaluate the stability and predictive power of the regression models. Both models showed similar moderate predictive power. The model incorporating all variables achieved an R-squared of 0.39 and a Root Mean Squared Error (RMSE) of 23 percentage points, while the reduced model (using only channel slope and depth) had an R-squared of 0.38 and RMSE of 28 percentage points. These results indicate that the predictions typically deviate from observed values by about ±23-28 percentage points, indicating that the models capture some key controls on alluvial cover, but other factors likely influence its distribution. Importantly, the reduced model could include 78 reaches that had channel slope and depth data, compared to only 29 reaches in the complete model due to limited grain size data availability. This larger sample size makes the reduced model more representative of the catchment's characteristics.

Principal Component Analysis (PCA) was conducted using all variables, i.e., drainage area, channel slope, bankfull width, bankfull depth, and grain size (Figure 2.5). The first two principal components (PC1 and PC2) explained 77% of the variability in the dataset,

with PC1 alone accounting for 57%. PC1 was mainly associated with drainage area, channel slope, width, and depth, indicating that these channel geometry variables are correlated with each other (Table 2.2). PC2 was mainly driven by grain size (D_{50}), suggesting that grain size distribution in this post-glacial landscape varies independently from channel geometry. Neither component showed strong correlation with alluvial cover (R^2 = 0.10 and p = 0.091 for PC1; R^2 = 0.006 and p = 0.689 for PC2), suggesting that the relations between channel characteristics and alluvial cover are complex and likely influenced by multiple interacting factors.

Table 2.2: PCA loadings for the Carron catchment for the two principal components (PC1 and PC2).

	PC1	PC2
Drainage area	0.52	0.17
Channel slope	0.51	0.10
Bankfull width	0.48	0.29
Bankfull depth	0.45	0.01
Grain size (D_{50})	0.19	0.93
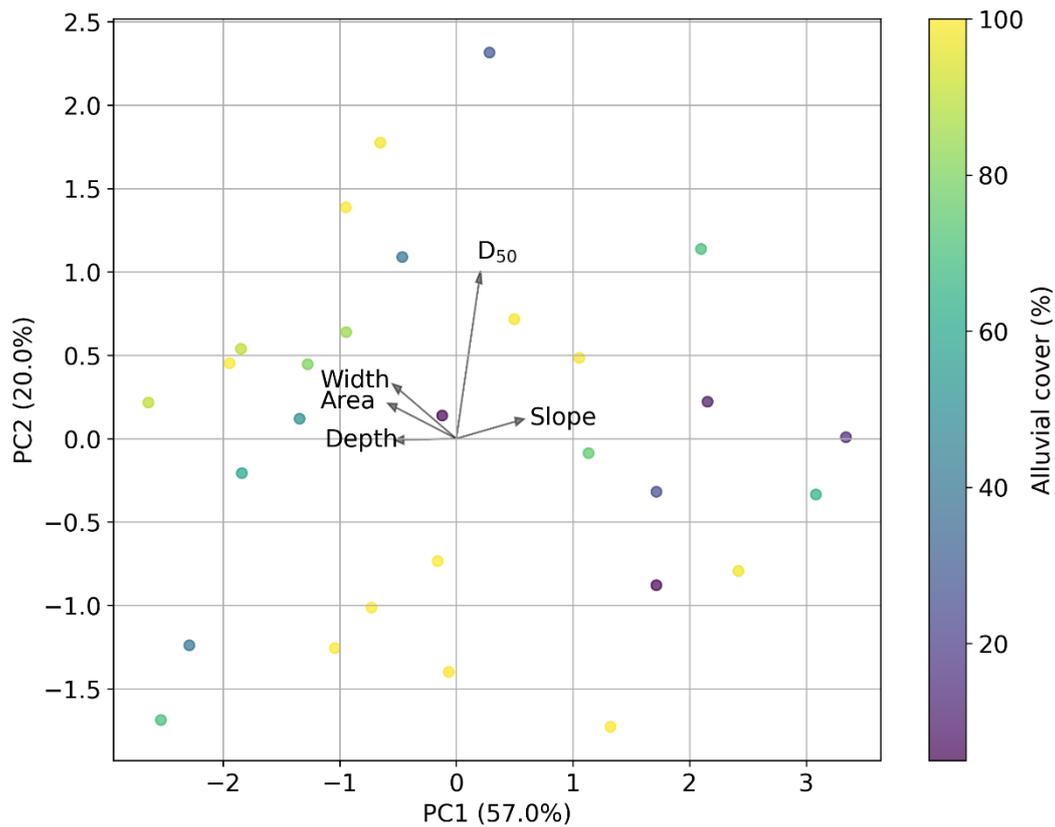
Figure 2.5: PCA biplot for the Carron catchment, showing the first two principal components (PC1 and PC2), which explain 57% and 20% of the variance, respectively. The vectors represent the loadings of the geomorphic and hydrologic variables (drainage area, channel slope, grain size (D_{50}), bankfull width and bankfull depth) on these components. The coloured points correspond to the sampled sites, with colours indicating the percentage of alluvial cover.

2.5.2 Grain size variability within and between reaches

Given that linear regressions between grain size (D_{50}) on a reach scale and alluvial cover showed no significant correlation (p-value = 0.525 in Figure 2.3e), we further explored the variability of grain size within reaches and its correlation with alluvial cover. Analysis of grain-size distributions showed considerable spatial variability both between and within reaches. The median grain size found in the Carron catchment was 0.10 m, but the grain size distribution changed considerably among different channels (Table 2.3 and Figure 2.6). The River Glencalvie and minor tributaries presented the largest median D_{50}s of 0.110 and 0.113 m respectively. In contrast, the River Alladale showed finer grain sizes,

with a median D_{50} of 0.041 m. In addition, many sand bars were found in River Abhainn which were not included in the grain size analysis of this study.

Table 2.3: Average grain size percentiles of the main channel and tributaries of the Carron catchment. Values represent reach-averaged grain sizes based on measurements from multiple gravel bars (n indicates the number of gravel bar samples).

Tributary	D5 (m)	D16 (m)	D25 (m)	D50 (m)	D75 (m)	D84 (m)	D95 (m)	n
Abhainn	0.020	0.041	0.054	0.096	0.177	0.217	0.264	7
Alladale	0.014	0.021	0.027	0.041	0.058	0.068	0.094	2
Carron	0.020	0.039	0.053	0.094	0.150	0.178	0.236	64
Glencalvie	0.023	0.046	0.062	0.110	0.184	0.219	0.267	14
Minor tributaries	0.021	0.045	0.063	0.113	0.177	0.202	0.268	11
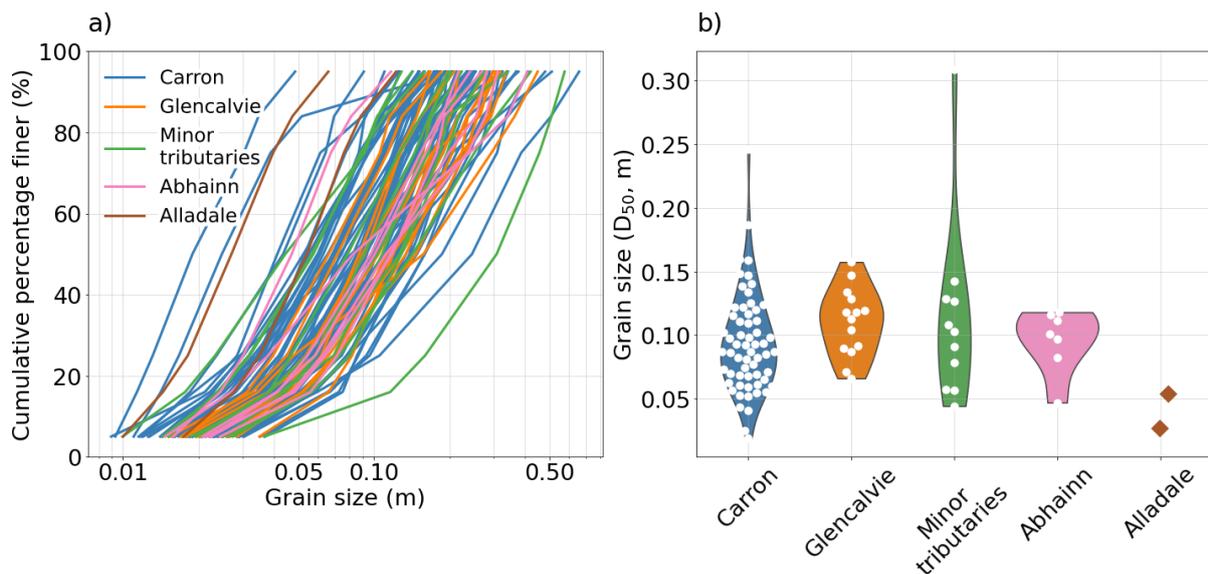
Figure 2.6: a) Grain Size Distribution curves for 98 gravel bars, with colours representing different subcatchments; b) Violin plots showing the distribution of median grain size (D_{50}) of gravel bars in each subcatchment – the River Alladale had only two gravel bar samples which are shown as points.

Analysis of within-reach grain-size variability showed differences in the grain size of bars within the same reach. The coefficient of variation (CV) of D_{50} within reaches ranged from 1% to 72%, with a mean of 34.8%. This high variability is shown in the box plots of Figure

2.7a, which show the distribution of grain sizes measured at different gravel bars within each reach. Some reaches exhibited relatively uniform grain sizes (CV < 10%), while others showed considerable heterogeneity (CV > 50%). This within-reach variability showed no significant correlation with alluvial cover (p-value = 0.625), indicating that local grain size sorting processes operate independently of reach-scale sediment cover. The longitudinal profile shows that alluvial cover correlates with slope, with steeper sections exhibiting lower cover and flatter sections greater sediment accumulation (Figure 2.7b). However, both median grain size and its variability remain similar across reaches regardless of their alluvial cover percentage.
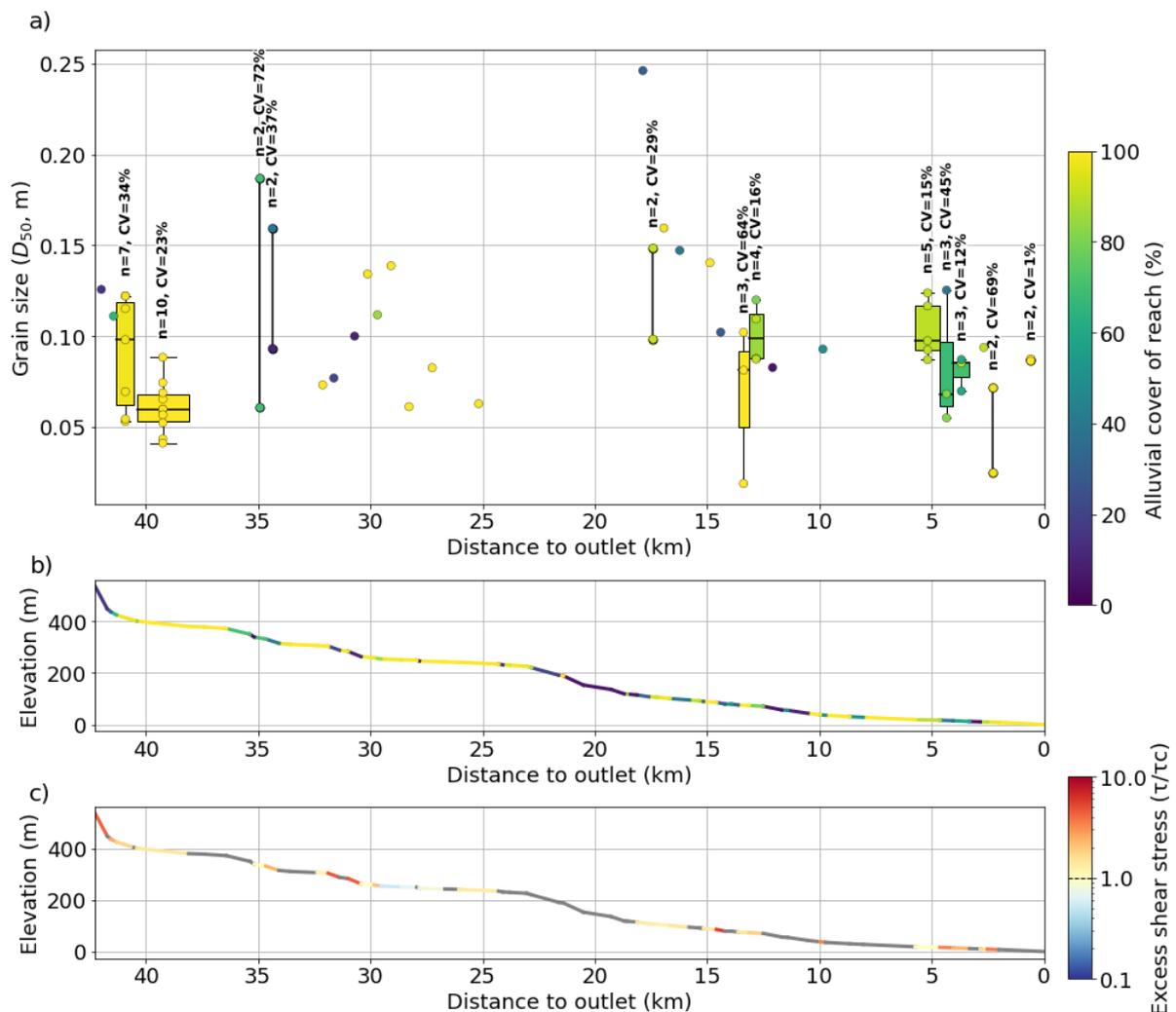
Figure 2.7: Longitudinal patterns of grain size, alluvial cover and excess shear stress along the main River Carron. a) Grain size (D_{50}) distribution in reaches with grain size measurements. Individual points represent reaches with data from a single gravel bar.

Where two bars were measured in a reach, points are connected by a vertical line. Box plots are shown for reaches with three or more bars, where box boundaries indicate the 25th and 75th percentiles and whiskers show the 5th and 95th percentiles for gravel bars within each reach. Numbers above each reach (n) indicate the number of gravel bars measured and CV indicates the coefficient of variability of each reach with at least two gravel bars. Points and boxes are coloured according to the percentage of alluvial cover in the reach. b) River profile coloured by the percentage of alluvial cover in each reach, showing transitions from reaches with high alluvial cover (yellow) to low cover (purple). c) River profile coloured by excess shear stress (τ/τ_c) during a 50-year flood, where values greater than 1.0 (yellow and red colours) indicate potential mobility of the median grain size (D_{50}) in that reach, while values less than 1.0 (blue colours) indicate conditions below the threshold for grain mobility. Grey segments indicate reaches where excess shear stress could not be calculated due to missing grain size data.

2.5.3 Grain size mobility

The highest flow recorded in the catchment since 1973 was 307 m^3/s, measured on 26 October 2006, representing a flood with a return period of 49.3 years (approximately a 50-year flood) (Figure 2.8a). Analysis of excess shear stress during floods of different magnitudes shows widespread potential for sediment mobility throughout the catchment (Figure 2.8c). During 2-year floods, 63% of reaches show potential for D_{50} mobility ($\tau/\tau_c > 1$), increasing to 88% during 50-year floods. The mobility of D_{84} shows a similar pattern but with lower percentages, ranging from 39% during 2-year floods to 53% during 50-year floods. The percentage of mobile reaches plateaus for both grain sizes at higher floods, with no additional reaches becoming mobile between 50- and 100-year floods (Figure 2.8c). This plateau occurs mainly because flow depth increases is less relevant at higher flows. Between 2-year and 5-year floods, mean flow depth increases by 13.7% (from 1.17 to 1.33 m), but this increase drops to just 4.3% (from 1.61 to 1.68 m) between 50-year and 10-year floods (Figure 2.8b). The reaches that remain with immobile grains even during extreme floods are characterized by very low channel slopes, with a median slope of 0.006 m/m, compared to 0.028 m/m for mobile reaches (Figure 2.8d).
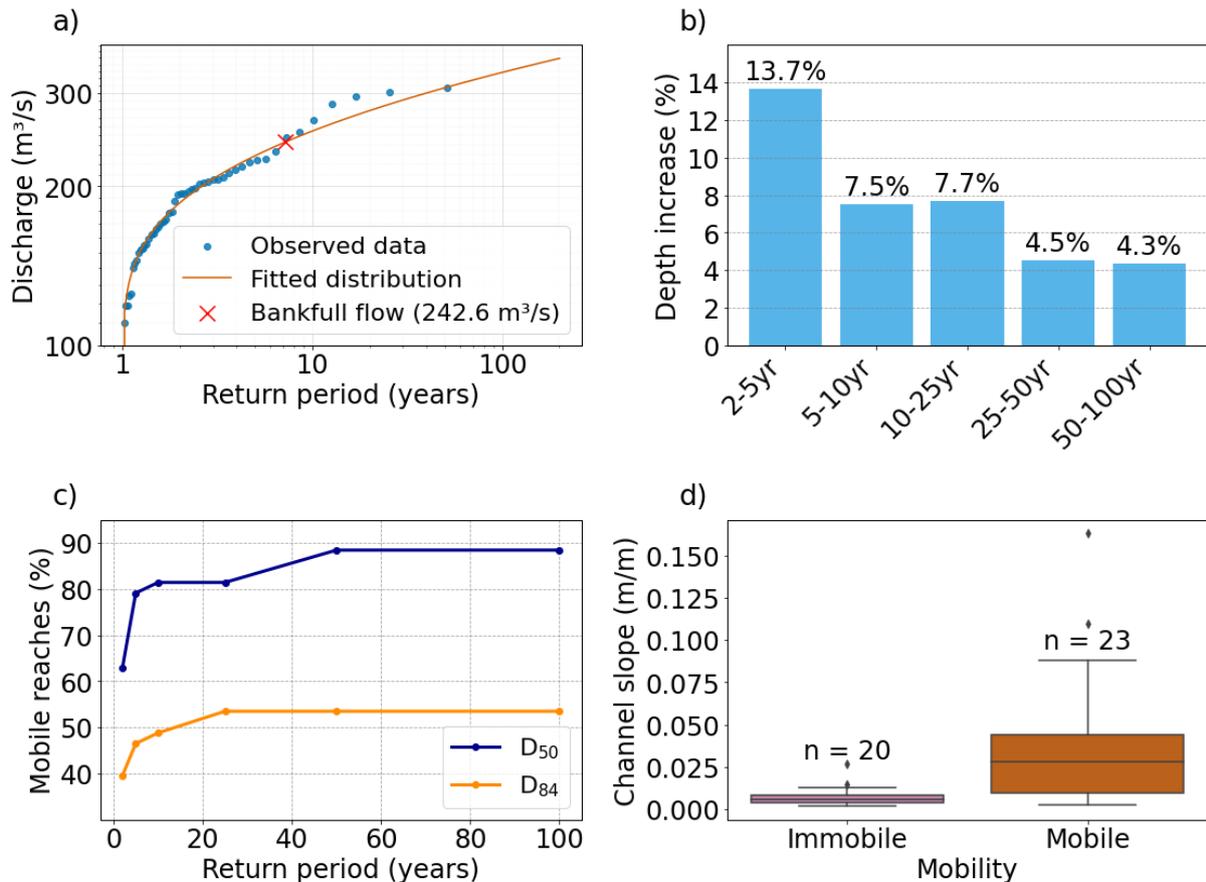
Figure 2.8: Flood characteristics and sediment mobility analysis in the Carron catchment. a) Flood frequency analysis showing observed peak flows at the gauge station, fitted log-normal distribution and bankfull flow (242.6 m^3/s); b) Percentage increase in mean flow depth of all reaches between successive flood return periods; c) Percentage of reaches with mobile grain sizes (D_{50} and D_{84}) at different flood return periods. d) Channel slope distribution in mobile versus immobile reaches for D_{84} during the 100-year flood, "n" indicates de number of reaches in each category.

The spatial distribution of excess shear stress during the 50-year flood in the main channel (Figure 2.7c) shows considerable variability along the river profile. High excess shear stress values ($\tau/\tau_c > 1$) occur throughout the catchment, especially in steeper sections, which typically have low alluvial cover. However, some relatively low slope reaches also show high excess shear stress due to deeper flows during floods and smaller median grain sizes requiring less force for mobilisation. These channel characteristics compensate for the low slope, creating sufficient shear stress for sediment mobilisation.

Comparison of excess shear stress patterns between 2-year and 50-year floods (Figures 2.9b and 2.9c) shows that while the magnitude of shear stress increases with flood size, the spatial patterns remain similar. Reaches with drainage areas less than 50 km^2 show the greatest variability in excess shear stress, with values ranging from 0.2 to above 10. This hydraulic variability directly influences alluvial cover distribution, as shown by the significant negative correlation between excess shear stress (τ/τ_c) for D_{50} during 2-year floods and the percentage of alluvial cover (R^2 = 0.22, p-value = 0.002; Figure 2.9d). This relation demonstrates that reaches with higher excess shear stress during frequent flood events tend to maintain lower alluvial cover.
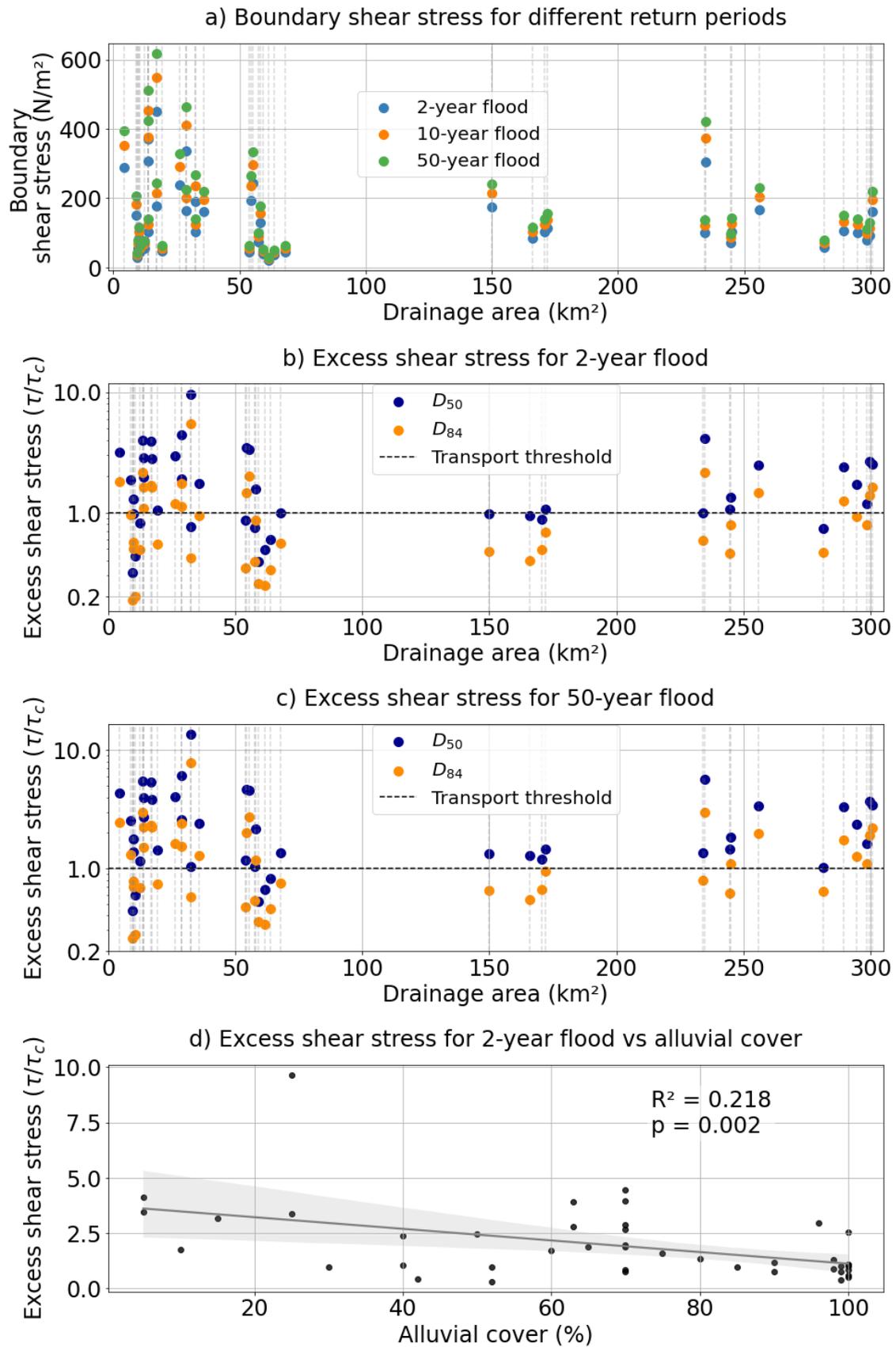
Figure 2.9: Shear stress analysis in the Carron catchment. a) Boundary shear stress (τ) calculated for floods with different return periods (2-, 10- and 50-year floods) plotted

again drainage area of each reach. b) Excess shear stress (τ/τ_c) for D_{50} and D_{84} during a 2-year flood. Values above 1 (dashed line) indicate potential grain mobility. c) Excess shear stress (τ/τ_c) for D_{50} and D_{84} during a 50-year flood, showing increased mobility potential compared to the 2-year flood. d) Correlation between alluvial cover percentage and excess shear stress (τ/τ_c) for D_{50} during a 2-year flood. The regression line indicates the linear relationship, with R^2 and p-value indicating the strength and significance of the correlation.

2.6 Discussion

2.6.1 Controls on alluvial cover distribution in post-glacial landscapes

Our study analyses alluvial cover as a continuous variable (1-100%) rather than using traditional discrete classifications (bedrock and alluvial channels). Using this continuous approach, channel slope and bankfull depth emerged as the strongest predictors of alluvial cover in the Carron catchment, collectively explaining 45% of the variance in alluvial cover distribution (Table 2.1). This finding complements the result found by Whitbread et al. (2015) that bedrock channels are typically narrower and deeper than alluvial channels by quantifying the gradual transition between channel types in a continuous range of alluvial cover values.

The negative correlation between alluvial cover and both slope and depth (Table 2.1) can be explained by fundamental hydraulics. Steeper channels have higher stream power, which increases sediment transport capacity and reduces deposition (Massong & Montgomery, 2000). Similarly, for a given drainage area, narrower channels develop deeper flows that maintain higher shear stress even during moderate flows, inhibiting sediment accumulation (Ferguson et al., 2017b; Hodge et al., 2011). This hydraulic constraint is demonstrated in the multivariate analysis (Table 2.1), where both slope and depth appear significant predictors of alluvial cover, while width alone showed weaker correlation.

The moderate R-squared value of our model (R^2 = 0.45; Table 2.1) indicates that other factors not included in our analysis, such as sediment supply, bedrock roughness and lithology, influence the alluvial cover distribution. In the Carron catchment, drainage area

alone showed no significant correlation with the percentage of alluvial cover (p-value > 0.05; 2.3a), as both bedrock and alluvial channels exist at any position in the catchment. Previous research demonstrated strong correlations ($R^2 > 0.7$) between channel geometry (width, depth) and drainage area in both bedrock and alluvial channels (Montgomery & Gran, 2001), a finding that also applies to the Carron catchment (Whitbread et al., 2015). However, the distribution of alluvial cover does not follow this predictable scaling with drainage area in our post-glacial setting. This lack of correlation between alluvial cover and drainage area is likely affected by the irregular distribution of sediment sources inherited from glaciation (Brardinoni & Hassan, 2007). Although glacial deposits dominate the overall catchment area (50%, Figure 2.1c), the river surroundings (within a 10 m buffer of the river channel) are mainly covered by fluvial deposits (71%), with glacial deposits covering 21% of this riparian zone. This pattern suggests reworking of glacial material by fluvial processes since deglaciation, transferring glacial materials from the wider catchment to the channel network, which reworks them into fluvial deposits. The presence of mass movement deposits (10% of catchment area, Figure 2.1c) on steeper slopes in upstream areas further contributes to the irregular sediment supply patterns. This spatial variability of sediment sources, with discrete sediment inputs from glacial deposits, raised terraces, and debris fans, creates a complex pattern of alluvial cover. In addition, the variable glacial erosion along the river profile can interfere to the correlation between alluvial cover and drainage area, since glacial erosion can create steep bedrock reaches independent of catchment position.

Our findings broadly align with previous studies that used binary classification of alluvial cover to analyse channel morphology. These studies consistently found that bedrock channels have steeper slopes and are generally deeper than alluvial channels for a given drainage area (Addy et al., 2011; Massong & Montgomery, 2000; Montgomery & Gran, 2001; Whipple, 2004; Whitbread et al., 2015; Wohl & David, 2008). However, our results extended these studies by quantifying the gradual transition between channel types. Instead of discrete transitions, we observe gradual changes in alluvial cover that correlate with channel geometry. This continuous analysis provides several advantages over binary classification: it enables the quantification of subtle variations in the analysis of cover controls and facilitates the detection of temporal changes in cover. Such detailed

understanding is particularly valuable in post-glacial landscapes, where complex patterns of glacial erosion and deposition create highly variable channel conditions that may not be fully captured by discrete classifications.

2.6.2 Grain size patterns: glacial inheritance versus contemporary reworking

Our analysis found considerable spatial variability in grain size both between and within reaches, with within-reach coefficients of variation in D_{50} up to 72% (Figure 2.7a). This high variability originates from the diverse sediment sources characteristic in the Carron's post-glacial landscape, composed by glacial, organic, fluvial and mass movements or different sizes (Figure 2.1c). The weak correlation between grain size and alluvial cover (p-value > 0.05; Figure 2.3e) suggests that local patterns of glacial deposition affect the typical downstream fining patterns observed in fluvial systems (Rice & Church, 1998; Towers et al., 2024). This high variability in grain size indicates that the glacial inheritance affects the complex patterns of alluvial cover distribution and downstream fining in the Carron catchment.

However, our analysis of excess shear stress indicates that contemporary flows actively rework these inherited sediment patterns. Even relatively frequent floods (2-year return period) can mobilise D_{50} in 63% of reaches and D_{84} in 40% of reaches, while large floods (≥ 50-year return period) can potentially mobilise D_{50} in 88% of reaches and D_{84} in 54% of reaches (Figure 2.8a). The significant negative correlation between excess shear stress during 2-year-floods and alluvial cover percentage (Figure 2.9d) further supports this active reworking, suggesting that contemporary hydraulic conditions directly influence sediment distribution patterns. According to threshold theory, rivers typically mobilise D_{50} during annual floods (Phillips et al., 2022). The finding that 37% of reaches in the Carron show no D_{50} mobility during 2-year floods and 12% remain immobile even during 50-year floods, suggests that some reaches are considerably immobile. This pattern of substantial but variable sediment mobility is particularly significant in the Carron's post-glacial landscape, where abrupt transitions between bedrock and alluvial reaches create conditions favourable for enhanced sediment mobilisation. Baynes et al. (2023) demonstrated that channel steepness is the main control on sediment production during

extreme events, with these morphological transitions acting as hotspots for sediment mobilisation. These transitions enhance mobility primarily through abrupt changes in channel slope, where flow accelerates as it moves from low slope alluvial sections to steeper bedrock reaches, or where sediment rapidly deposits as flow decelerates when moving from steep bedrock to low slope alluvial sections (Baynes et al., 2023). In addition, bedrock and alluvial sections typically have different critical shear stress thresholds for sediment entrainment (Ferguson et al., 2017b; Hodge et al., 2011), creating zones where relative mobility changes abruptly at transition points.

Beyond these transition zones, we found that the spatial variability in grain size mobility is particularly pronounced in upstream reaches (drainage area < 50 km^2), where excess shear stress varies by more than an order of magnitude (Figure 2.9). This higher variability in upstream reaches reflects the irregular valley profiles created by glacial erosion, combined with proximity to diverse local sediment sources and greater variations in channel slope - characteristics typical of post-glacial headwater channels (Brardinoni & Hassan, 2006). The observed plateau in the proportion of mobile reaches at higher flood magnitudes (no increase between 50- and 100-year floods; Figure 2.8a) indicates that some reaches maintain low excess shear stress values regardless of discharge. These immobile reaches present low channel slopes (median 0.006 m/m compared to 0.028 m/m in mobile reaches, Figure 2.8b). This difference in slope represents a hydraulic threshold that 100-year floods cannot overcome, suggesting a pattern of partial adjustment where some low slope reaches retain characteristics inherited from glaciation while steeper reaches have been more extensively reworked by fluvial processes.

The spatial variability in grain-size distribution across different tributaries further demonstrates the interaction between inherited and active processes. The southern tributary (Glencalvie), underlain by granite, appears to have coarser sediments (D_{50} = 0.11 m; Table 2.3) than the main channel (D_{50} = 0.094 m), though this difference is not statistically significant (ANOVA, p-value = 0.14). The main channel is dominated by metamorphosed sandstones, siltstones and mudstones. In contrast, the northern tributary (Abhainn), presents extensive sand deposits derived from glaciofluvial deposits and peat accumulation in the flatter, northern sections of the catchment (Figure 2.1). The

presence of these fine sediments, combined with the coarse glacial deposits in other areas, demonstrates the broad range of grain sizes typically found in post-glacial landscapes. Other studies have also shown similar lithology controls on channel morphology and sediment characteristics in bedrock-alluvial rivers, with more resistant rocks (igneous-metamorphic) leading to coarser grain sizes and narrower and steeper channels (Buckley et al., 2024; Jansen et al., 2010; Whitbread, 2015).

This combination of high mobility potential during moderate floods and spatially variable grain size patterns suggests that the Carron represents an intermediate stage of post-glacial adjustment. Ballantyne (2002) conceptualised this as part of the paraglacial cycle, where landscapes initially have high sediment supply and substantial adjustment immediately following deglaciation, but gradually exhaust this paraglacial sediment supply as materials are reworked through the system. In the Carron, we observed evidence of this transition: contemporary floods actively redistribute sediments in most reaches (88% for D_{50} during 50-year floods), but 12% of reaches remain immobile even during extreme events, corresponding to reaches with very low slope, which suggests two constraints in channel evolution: both sediment availability and stream power influence adjustment processes. The decreased discharge since deglaciation likely contributed to limited mobility in low-slope reaches, while the irregular distribution of sediment sources created the observed spatial variability in grain sizes. The resulting channel characteristics reflect both inherited glacial conditions and ongoing fluvial modification, with the system gradually returning into previous steady-state conditions before glaciation. This understanding of partial adjustment is important for predicting future channel evolution in post-glacial landscapes.

2.6.3 Implications for river management and future research implications

Our results demonstrate how glacial legacy adds complexity to relations predicting channel morphology, with implications extending beyond our study area to other post-glacial regions worldwide. The combined effect of glacial history and ongoing fluvial processes challenges traditional river management strategies, which often assume uniform and predictable channel responses. River management approaches in post-

glacial landscapes should account for fundamental controls on channel processes and the inherited spatial heterogeneity in slope and sediment supply, particularly when considering how these landscapes might respond to ongoing climate change. Our finding that increased flood magnitudes (from 2-year to 50-year events) mobilise D_{50} in an additional 25% of reaches suggests that if climate change increases flood magnitude and frequency as projected (Chan et al., 2018; Slater et al., 2021), this landscape could undergo rejuvenation. This process means that the greater erosion and sediment transport would accelerate the transition from glacial toward fluvial dominated channel forms, potentially increasing bedrock exposure in some reaches. However, the 12% of reaches that remain immobile even during extreme events would likely maintain their current characteristics, creating an increasingly heterogeneous pattern of erosion and sediment cover distribution. This complex effect on channel morphology particularly affects habitat management, as the presence or absence of alluvial cover influences both flow dynamics and ecological conditions (Steiger et al., 2005; Wohl, 2015b). For example, the patchy distribution of alluvial cover influences the availability and quality of spawning grounds for salmonid fish, which requires specific substrate conditions for reproduction (Buffington et al., 2004). The high within-reach variability in grain size and alluvial cover observed in post-glacial landscapes creates more diverse habitat conditions than standard habitat models assume, complicating habitat assessment and management in these environments.

Several knowledge gaps remain for further consideration. More frequent monitoring of alluvial cover would help better understand the timescales of cover change and its relationship to flow and channel conditions, which will be explored in Chapter 3 through analysis of temporal changes in Carron catchment. Side-scan sonar surveys and bathymetric LiDAR (Light Detection And Ranging) could provide a more detailed and frequent estimation of the percentage of alluvial cover (Buscombe et al., 2016; Gomez-Heras et al., 2019). In addition, the role of sediment supply in controlling alluvial cover remains poorly quantified, particularly in post-glacial landscapes where sediment sources are spatially heterogeneous. Future research could focus on quantifying sediment inputs from different sources (e.g., glacial deposits, bank erosion and tributary inputs) and their relative importance in maintaining alluvial cover. The high within-reach

variability in grain size observed in our study influences local sediment mobility, possibly contributing to a more complex and heterogeneous pattern of sediment mobility within a reach (Buechel et al., 2022). The interaction between grain size heterogeneity and bedrock roughness in controlling sediment transport and storage contributes to the complex relationship observed between grain size and alluvial cover. Understanding these local-scale processes will support the development of more accurate models of channel evolution in post-glacial landscapes.

2.7 Conclusion

This study analysed the controls on alluvial cover distribution in the post-glacial River Carron catchment using a continuous measurement analysis of alluvial cover (0-100%) instead of traditional binary classification (alluvial or bedrock channel). This approach allows us to analyse subtle variations in cover through detailed statistical analysis, providing information into the gradual transition between channel types. Our key findings are:

1. Channel slope and bankfull depth were the strongest predictors of alluvial cover through multiple regression analysis (p-value < 0.001 and R^2 = 0.45), with steeper and deeper channels exhibiting lower sediment cover due to their high transport capacity.

2. Grain-size distributions showed high spatial variability both between tributaries and within individual reaches (Coefficient of Variation of D_{50} up to 72% within reaches), reflecting the complex sediment sorting patterns in post-glacial landscapes. This high variability appears to be driven by the heterogeneous distribution of superficial deposits, with glacial materials dominating the overall catchment (50%) but fluvial deposits dominating riparian zones (71%).

3. Analysis of excess shear stress revealed widespread potential for sediment mobility, with even 2-year floods capable of mobilising D_{50} in 63% of reaches, increasing to 88% during 50-year floods. However, an important portion of reaches (12%) remained immobile even during extreme floods, mainly in areas

with low channel slopes (median 0.006 m/m compared to 0.028 m/m in mobile reaches).

4. Traditional downstream patterns were disturbed by glacial inheritance, with both bedrock and alluvial channels occurring throughout the catchment regardless of drainage area. This spatial complexity is an effect of the Carron being in an intermediate stage of paraglacial adjustment, where contemporary fluvial processes have been actively reworking glacial deposits.

These findings contribute to our understanding of how post-glacial landscapes influence fluvial dynamics. Future research should focus on obtaining higher temporal resolution data on cover changes and quantifying the relative importance of different sediment sources in maintaining alluvial cover. In addition, analysing how these partially adjusted systems respond to increasing flood magnitudes under different climate change scenarios would be valuable for river management. Sediment transport simulations with numerical models could isolate the effect of each parameter in the riverbed cover under different spatial and temporal scales, which it is not possible with the empirical analysis of field data. Such knowledge would improve our ability to predict channel response to environmental changes in post-glacial landscapes.

3 Temporal changes in alluvial cover in the River Carron over a 12-year period

3.1 Abstract

Understanding temporal changes in alluvial cover is essential for predicting river evolution and managing aquatic habitats in mixed bedrock-alluvial rivers, yet empirical studies documenting these changes remain rare, particularly over decadal timescales. This study investigates temporal dynamics of alluvial cover in the River Carron, Scotland, by comparing measurements from 2010 (Whitbread, 2015) and 2022 across 29 reaches over a 12-year period. We examine how these changes correlate with channel characteristics and hydrological conditions. Results show a widespread increase in alluvial cover, with 83% of reaches exhibiting increased sediment cover and an average rise of 18 percentage points. No statistically significant relationships were found between cover change and channel characteristics (drainage area, slope, width, depth, grain size), suggesting that multiple interacting factors and other variables control temporal changes in alluvial cover. Hydrological analysis showed that the period between surveys experienced relatively stable flow conditions with only one bankfull exceedance event in 2014, followed by years of moderate flows that may have facilitated gradual sediment accumulation. The study discusses methodological challenges in measuring temporal cover changes, including water visibility limitations, observer bias and differences in survey protocols, emphasising the need for standardised approaches and more frequent future monitoring.

3.2 Introduction

Understanding temporal changes in alluvial cover is important for predicting evolution and managing aquatic habitats in mixed bedrock-alluvial rivers (Buffington et al., 2004;

Turowski et al., 2013; Wohl, 2015b). Rivers can respond differently to flood events in terms of sediment dynamics. Turowski et al. (2013) proposed a classification where rivers can be "flood-cleaning" (eroding during high flows and depositing during moderate flows) or "flood-depositing" (depositing during high flows and eroding during moderate flows). These contrasting behaviours depend on the balance between flow and sediment supply during flood events. In flood-cleaning rivers, transport capacity exceeds sediment supply during high flows and leads to erosion, while in flood-depositing rivers, high sediment supply overcomes transport capacity during floods, resulting in deposition (Turowski et al., 2013). This classification helps understand how rivers respond to hydrological events across different timescales based on their sediment supply regime.

Studies of temporal changes in alluvial cover have mainly focused on the short-term response to individual flood events. During floods, alluvial cover may be removed in some locations and deposited in others, depending on local hydraulic conditions and upstream sediment supply (Turowski et al., 2013). Cook et al. (2020) demonstrated how flood events can lead to both erosion and deposition in different channel segments, showing that the response to floods can vary spatially within the same river. These spatial variations are caused by local differences in channel geometry and bedrock roughness (Cook et al., 2020; Hodge et al., 2011; Hodge & Hoey, 2016). Narrower and steeper reaches typically experience higher shear stresses during floods, promoting erosion, while wider and lower-gradient reaches may reduce flow velocity, promoting deposition (Ferguson et al., 2017a; Papangelakis et al., 2021). Additionally, local variations in bedrock roughness can promote sediment entrainment or deposition, with higher bedrock roughness typically promoting sediment deposition and smoother bedrock surfaces sediment entrainment (Chatanantavet & Parker, 2008; Hodge et al., 2011; Johnson & Whipple, 2010). These interactions can create feedback mechanisms where erosion processes modify bedrock roughness, which in turn affects sediment deposition patterns, leading to variations in alluvial cover.

While short-term changes in alluvial cover have been studied through flume experiments lasting minutes to hours (Hodge & Hoey, 2016; Johnson & Whipple, 2010), field surveys of individual flood events (Cook et al., 2020), and numerical modelling simulating equilibrium over several hours (Chatanantavet & Parker, 2008; Inoue et al., 2014), there

is a research gap in empirical studies documenting these changes over decadal periods. This gap exists primarily by challenges in maintaining consistent measurement over log timeframes. However, such longer-term datasets are critical for understanding landscape evolution and for validating numerical models beyond laboratory timescales.

This knowledge gap is pronounced in post-glacial landscapes, where sediment dynamics are shaped by historical glacial conditions and ongoing paraglacial adjustments (Ballantyne, 2002). In post-glacial landscapes like the Carron catchment, these dynamics are particularly complex due to the irregular distribution of sediment sources left by glaciation (Figure 2.1c from Chapter 2) and the varying capacity of modern flows to rework these deposits, as discussed in Chapter 2. In the Carron catchment, although glacial deposits dominate the overall catchment area (50%), the river surroundings (10 m buffer) are mainly covered by fluvial deposits (71%), suggesting reworking of glacial material by fluvial processes since deglaciation.

Chapter 2 analysed the spatial patterns of alluvial cover and its relation with channel characteristics in the River Carron using data collected by Whitbread (2015) in 2010 and grain size data collected in 2022. This chapter extends the spatial analysis of Chapter 2 by investigating temporal changes in alluvial cover over a 12-year period (2010-2022). Documenting and analysing temporal dynamics present methodological challenges, particularly in systems where underwater visibility is limited, as in the River Carron. By addressing these challenges and discussing approaches to compare measurements taken under different conditions, this chapter contributes to future monitoring and provides empirical data on temporal cover, allowing the following questions to be addressed:

1. How does alluvial cover change over time in a post-glacial mixed bedrock-alluvial river?

2. To what extent does the temporal variability in alluvial cover correlate with changes in local channel morphology or recent hydrological events?

The chapter first presents the methodological challenges associated with measuring temporal changes in alluvial cover. Then, it examines the observed changes between 2010 and 2022, analysing their relations with channel characteristics and hydrological

conditions. Finally, it discusses the implications of these changes for understanding post-glacial river evolution and future monitoring approaches.

3.3 Methods

3.3.1 Field survey methods and assessment of uncertainty

This study compares alluvial cover data collected at two time periods (2010 and 2022) in the River Carron. The initial dataset was collected by Whitbread (2015) during low flow conditions between October 2009 and April 2011, covering 78 reaches along the main channel. In each reach, bed cover was surveyed at 10 m intervals by visually estimating the proportion of bedrock exposure in a 2 m wide swath across the channel, which included both bed and banks. The overall fraction of bed cover for each reach was calculated as the average cover along its length.

The 2022 survey, conducted in September 2022 during median flow conditions (4.5 m^3/s), focused on 29 reaches that were previously classified as bedrock or mixed bedrock-alluvial by Whitbread (2015). At each reach, alluvial cover was estimated at 11 transects spaced about 20 m apart, covering a 200 m stretch centred on the midpoint of Whitbread's original reaches. The 2022 survey employed a modified sampling strategy (11 transects at 20 m spacing over 200 m reaches) compared to the 2010 survey (10 m intervals over the entire main channel) due to practical constraints of the fieldwork timeframe and a focus on the most dynamic mixed bedrock-alluvial reaches. The 2022 survey assessed measurement uncertainty due to visibility limitations (Figure 3.1). Uncertainty levels were categorised based on the percentage of riverbed obscured by water: high uncertainty where more than 70% was obscured, medium for 50-70% obscurity, and low for less than 50% obscurity. For example, if 50% of the riverbed was visible and entirely covered by sediments, the transect would be recorded as 100% alluvial cover with medium uncertainty. Photographic documentation shows similar flow and visibility conditions between the 2010 and 2022 surveys, though the earlier survey did not explicitly record uncertainty levels (Figure 3.2).

Figure 3.1: Examples of different visibility conditions affecting uncertainty in alluvial cover measurements during the 2022 survey. a) Clear visibility of riverbed showing 100% alluvial cover with low uncertainty (<50% obscured). b) Mixed bedrock-alluvial reach with partial water coverage showing 30% alluvial cover and low uncertainty, even though around 30% of the transect is obscured. c) Deep pool in a bedrock reach with high uncertainty (>70% obscured), estimated 10% alluvial cover in visible areas. d) Alluvial reach with medium uncertainty (50-70% obscured) showing 100% cover in visible sections.

Figure 3.2: Comparison of River Carron reaches photographed in 2010 (left, from Whitbread, 2012) and 2022 (right). a) A mixed bedrock-alluvial reach showing similar visibility conditions and flow levels between surveys. Note the consistent position of the gravel bar and exposed bedrock. b) A mixed bedrock-alluvial reach characterized by abrasion with plucking erosion features, demonstrating stable channel morphology and comparable flow conditions. c) An alluvial reach at Deanich showing an in-filled loch, illustrating similar meandering patterns and channel positions over the 12 years.

3.3.2 Alluvial change analysis

Temporal changes in alluvial cover were measured by calculating the difference in percentage points between the 2022 and 2010 measurements. These changes were analysed in relation to channel characteristics and hydrological conditions. Channel characteristics were derived from several sources: channel slope, bankfull width and depth measurements from Whitbread (2015) (assuming these bankfull dimensions remained stable between 2010 and 2022); drainage area obtained from a 5-m resolution DEM (Ordnance Survey, 2022); and grain-size distributions calculated from 2022 field photographs analysed using PebbleCounts software (Purinton and Bookhagen, 2019). The potential for sediment mobility was assessed using excess shear stress calculations for floods with different return periods (2, 5, 10, 25, 50 and 100-year floods). Detailed information on all these channel characteristic data can be found in Chapter 2. Linear regression analysis was employed to evaluate relations between alluvial cover change and channel characteristics, utilising p-values and Pearson correlation (r) values to determine significance and correlations. All analyses included visual representation of the uncertainty classifications from the 2022 survey (with 3 reaches in high uncertainty, 20 in medium uncertainty, and 4 in low uncertainty categories) to aid in qualitative evaluation of confidence in observed relations. Rather than excluding data points based on uncertainty levels, we retained all data in the statistical analyses and visually distinguished them, allowing readers to assess whether patterns were consistent across different uncertainty levels.

Hydrological analysis used discharge data from the SEPA gauging station "Carron at Sgodachail", which has been operating since 1973, providing daily mean flows and peak flow records above 100 m^3/s. At the gauging station, a rating curve ($Q = 14.98\ H^{2.53}$) was developed using stage and discharge data from SEPA. The bankfull stage of 3.01 m at this site (Whitbread, 2015) corresponds to a discharge of 242.62 m^3/s. Flood frequency analysis estimated that this bankfull discharge has a return period of approximately 7 years (see Chapter 2 for methodological details on flood frequency analysis). To understand how hydrological conditions might influence alluvial cover change, flow statistics were analysed across three time periods: the entire record (1973-2022),

periods of 7 years preceding each survey (corresponding to the bankfull return period), and the period between surveys (2010-2022). Key hydrological metrics calculated for each period included mean daily flow, median daily flow, maximum peak flow, and frequency of flows exceeding bankfull discharge (> 242.62 m^3/s). These flow statistics were used to assess whether the observed changes in alluvial cover might be related to differences in flow conditions between the survey periods, particularly the occurrence of the flood events capable of mobilising the measured D_{50} and D_{84}. To further compare flow conditions between periods, flow duration curves for the three periods analysed were generated. These curves show the percentage of time that flows of different magnitudes were equalled or exceeded. These analyses are used to determine whether temporal changes in alluvial cover correspond to periods of higher or lower potential sediment mobility.

3.4 Results

3.4.1 Changes in alluvial cover 2010-2022

A comparison of alluvial cover measurements between 2010 and 2022 showed a general trend of increased sediment cover within the River Carron (Figures 3.3 and 3.4). Out of the 29 surveyed reaches, 24 showed an increase in alluvial cover, with an average rise of 18 percentage points. The magnitude of change varied considerably: the largest increase was 49 percentage points (from 30% to 79%), and the largest decrease was 16 percentage points (from 25% to 9%). Changes were observed across all uncertainty categories. The spatial distribution of these changes (Figure 3.4 and 3.5a) shows that increases in alluvial cover occurred throughout the main channel, with larger increases generally observed in the middle and lower reaches.
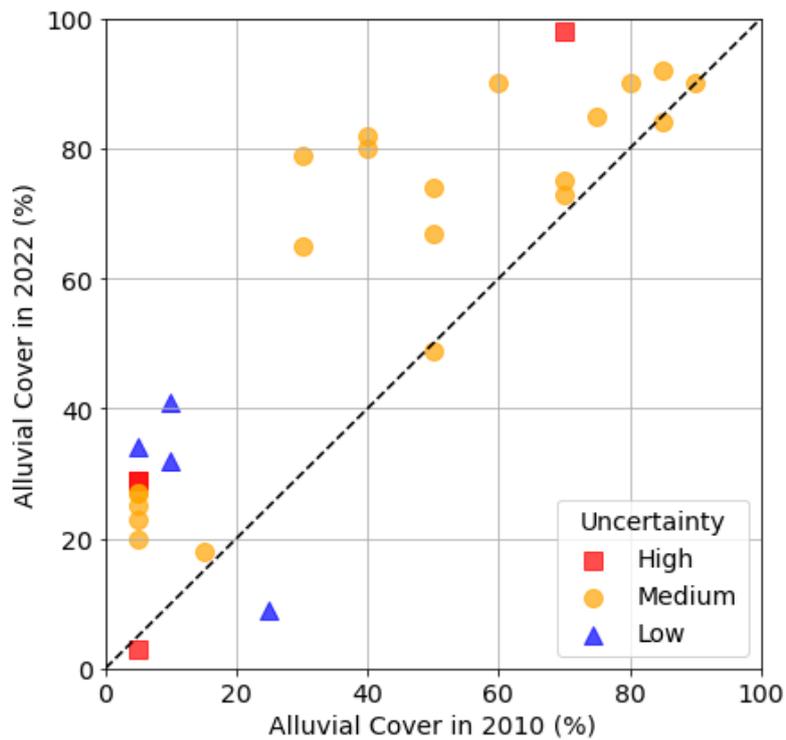
Figure 3.3: Comparison of alluvial cover between 2010 and 2022 across different reaches in the Carron catchment. The black dashed line represents the 1:1 line, where points along this line indicate no change in alluvial cover during the period. Each point represents an individual reach and is coloured according to measurement uncertainty in 2022: red squares for high uncertainty, orange circles for medium, and blue triangles for low uncertainty.
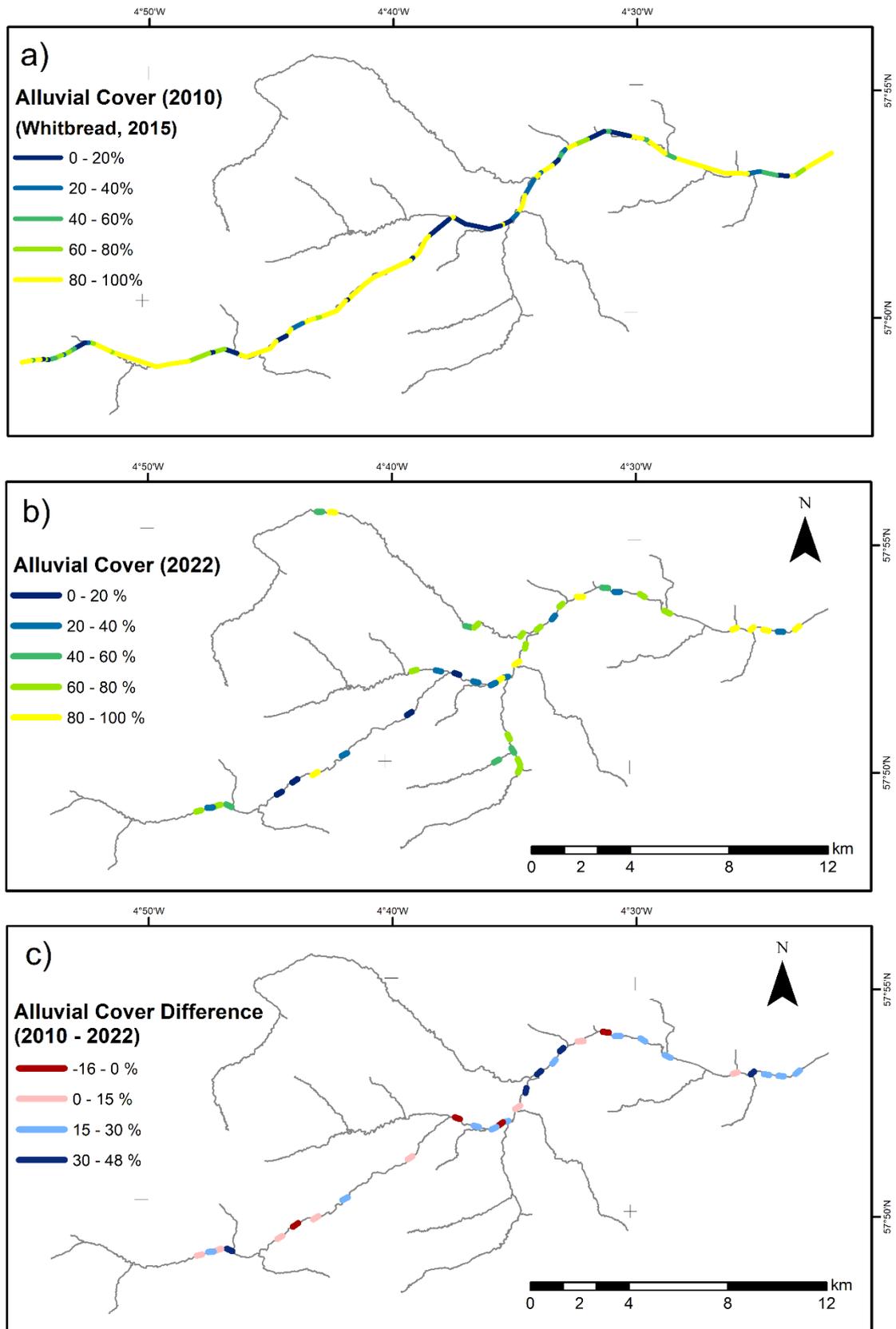
Figure 3.4: Spatial distribution of alluvial cover in the Carron Catchment: a) alluvial cover percentages recorded in 2010 (Whitbread, 2015); b) Alluvial cover percentages recorded

in 2022; c) Change in alluvial cover between surveys (2010 – 2022), with positive values indicating increases and negative values indicating decreases in cover. Note that the 2022 measurements were only collected in reaches previously classified as bedrock or mixed bedrock-alluvial, while the 2010 data include all reach types from the main channel.

Analysis of the relations between cover change and channel characteristics showed no statistically significant correlations (p-value > 0.05 for all variables; Figure 3.5). However, the drainage area demonstrated a near-significant positive relationship (r = 0.36, p-value = 0.055), suggesting that reaches with larger drainage areas tended to show greater increases in alluvial cover. The correlations for all other channel variables were considerably weaker. The potential for grain size mobility, indicated by excess shear stress during 50-year floods, showed no correlation with changes in alluvial cover (r =0.05, p-value = 0.861; Figure 3.5f). This result suggests that reaches with a higher potential for sediment mobility did not consistently show either more or less alluvial cover than reaches with lower mobility potential.
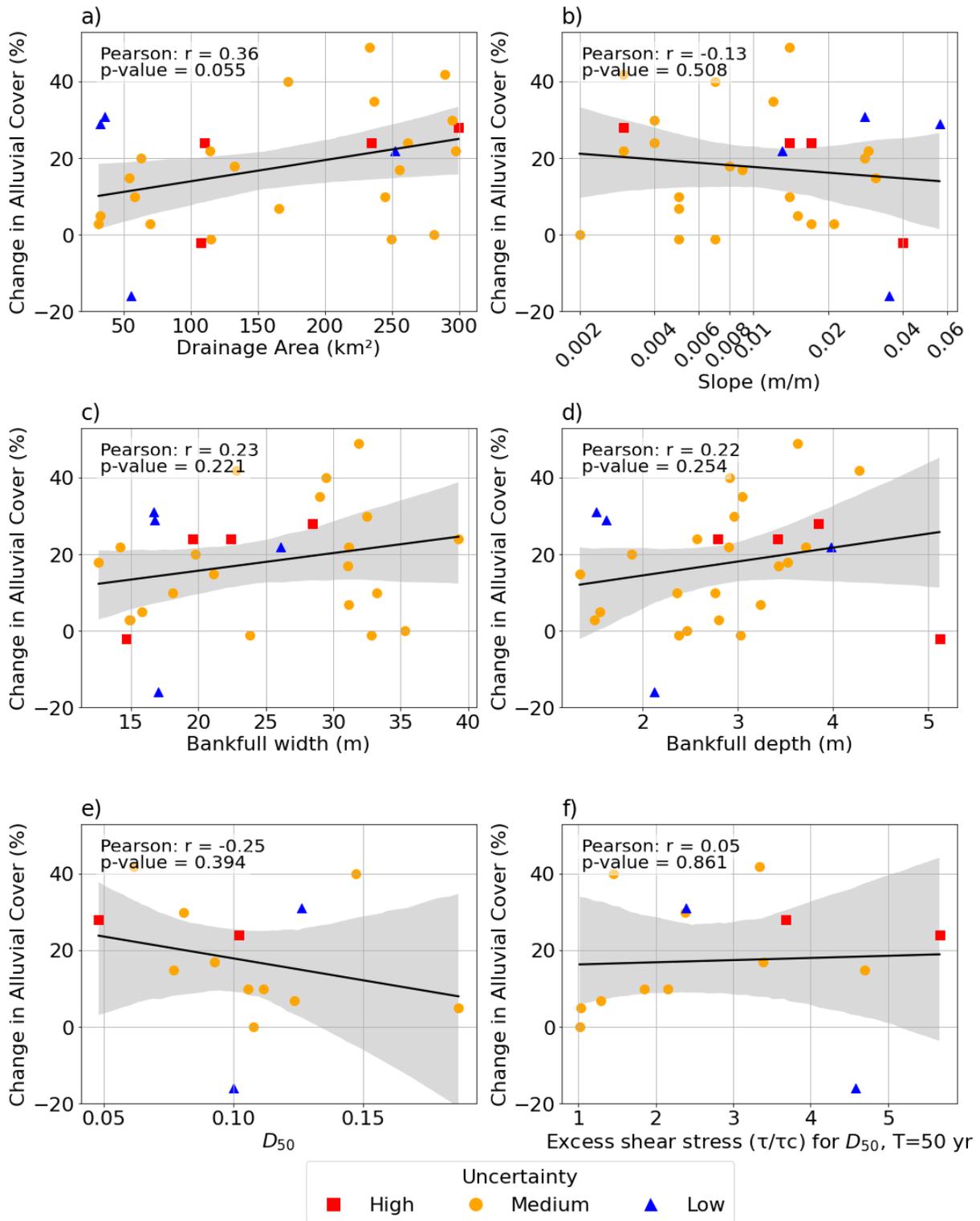
Figure 3.5: Relationships between changes in alluvial cover (2022-2010) and geomorphological variables: a) drainage area; b) channel slope; c) bankfull width; d) bankfull depth; e) median grain size (D_{50}); and f) excess shear stress (τ/τ_c) for D_{50} during a 50-year flood. Each point represents an individual reach and is coloured according to measurement uncertainty in 2022: red squares for high uncertainty, orange circles for medium, and blue triangles for low uncertainty. Shaded areas in grey around the

regression lines represent 95% confidence intervals. Note that analyses involving grain size (panels e and f) include fewer reaches (n = 14) due to limited grain size measurements, compared to other variables (n = 29).

3.4.2 Hydrological conditions

Analysis of flow records from 1973 to 2022 shows relatively stable long-term flow patterns in the River Carron, with some variations between analysis periods (Table 3.1 and Figure 3.6). The mean daily flow remained consistent across periods (approximately 9.1-9.5 m^3/s), with the highest mean daily flow recorded in the seven years prior to 2010 (2003-2010, referred as "pre-2010" period) at 9.50 m^3/s. Median flows also show stability, ranging from 4.45 to 4.66 m^3/s. However, the frequency of bankfull exceedance events (>242.62 m^3/s) varied between periods. The entire 49-year record contained 8 bankfull exceedance events, but their occurrence was not uniform. Only one bankfull exceedance event occurred during the period between surveys (2010-2022), which was in August 2014. The highest recorded peak flow in the catchment (307.11 m^3/s) occurred during the pre-2010 period (2003-2010), while the seven years prior to 2002 (2015-2022, referred to as "pre-2022" period) had no bankfull exceedance events and a lower maximum peak of 208.23 m^3/s. These trends suggest that the period between surveys (2010-2022) experienced fewer extreme events compared to the pre-2010 period, which may have influenced the observed changes in alluvial cover distribution. The low frequency of bankfull exceedance events between the surveys may have created conditions favourable for sediment accumulation in some reaches. The close overlap of the flow duration curves (Figure 3.6b) confirms the overall stability in flow patterns. However, subtle differences are visible for medium-high flows (exceedance probability <25%), with the pre-2010 period showing slightly higher discharges than other periods. The bankfull discharge (242.62 m^3/s) is exceeded less than 0.5% of the time across all periods.

Table 3.1: Summary of flow characteristics for different analysis periods in the River Carron.

Metric	Entire Record (1973-2022)	Between Surveys (2010-2022)	Pre-2010 (7yr)	Pre-2022 (7yr)
Mean daily flow (m^3/s)	9.10	9.08	9.50	9.19
Median daily flow (m^3/s)	4.54	4.54	4.45	4.66
Maximum peak flow (m^3/s)	307.11	302.21	307.11	208.23
Bankfull exceedance events (> 243 m^3/s)	8	1	2	0
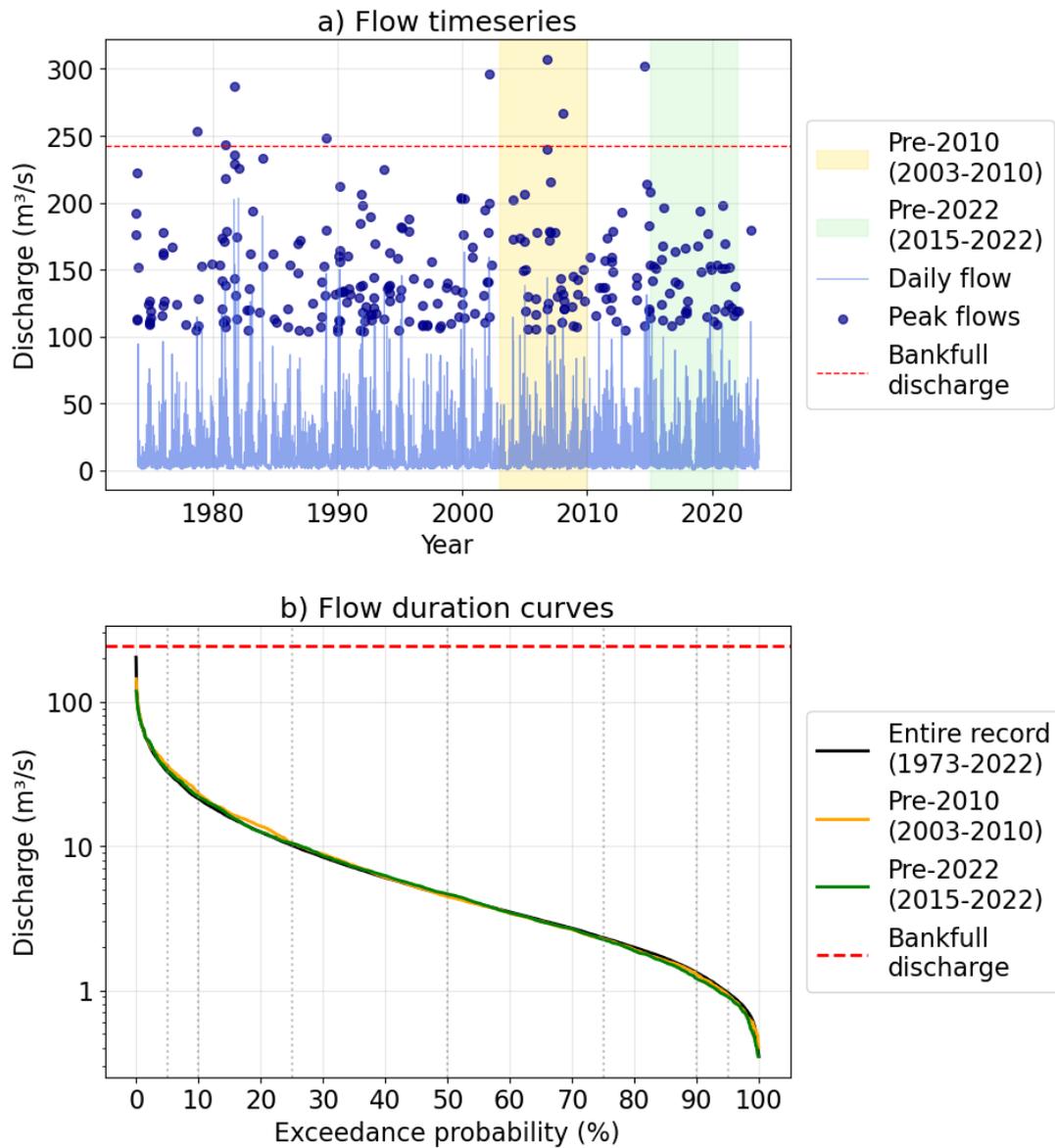
Figure 3.6: a) Time series of mean daily flows and peak flows in the River Carron from 1973 to 2022. The light blue line shows mean daily discharge and dark blue dots indicate peak flows above 100 m^3/s. Yellow and green shaded areas highlight the 7-year periods preceding the 2010 and 2022 alluvial cover surveys, respectively. b) Flow duration curves for different time periods in the River Carron. The curves show the percentage of time that flows of given discharges were equalled or exceeded. The red dashed lines represent bankfull discharge (242.62 m^3/s).

3.5 Discussion

3.5.1 Interpretation of changes

The observed increase in alluvial cover across most surveyed reaches (24 out of 29) between 2010 and 2022, with an average increase of 18 percentage points, suggests a general shift in sediment storage within the River Carron (Figure 3.3). This tendency toward increased alluvial cover can be interpreted through both hydrological conditions and spatial patterns of change.

The hydrological analysis shows that the period between surveys (2010-2022) had relatively stable flow conditions with fewer extreme events compared to the pre-2010 period (Table 3.1 and Figure 3.6), particularly in the years following the 2014 bankfull event. With only two temporal snapshots of alluvial cover (2010 and 2022) and no measurements immediately before and after flood events, we cannot classify Carron's behaviour as either flood-cleaning or flood-depositing within Turowski et al.'s (2013) classification. However, the lower frequency of extreme events after 2014 may have created favourable conditions for sediment accumulation. Without frequent large floods to mobilise and redistribute sediments, moderate flows may have gradually transported material from upstream sources, leading to incremental increases in alluvial cover. This pattern of sediment accumulation during periods of moderate flow has been observed in other mixed bedrock-alluvial rivers (Turowski et al., 2013; Cook et al., 2020).

The spatial pattern of change (Figure 3.4) and the near-significant positive correlation between drainage area and cover change (r = 0.36, p-value = 0.055; Figure 3.5a) suggest that lower reaches accumulated more sediments than upper reaches. This pattern of larger drainage areas presenting greater increases in alluvial cover could be due to the cumulative effects of sediment transport and storage during moderate flow conditions. Reaches with larger drainage areas typically have wider channels, creating opportunities for sediment storage through features such as lateral bars and margins. To investigate whether this pattern was also related to downstream changes in sediment mobility, the relation between excess shear stress ratios and drainage area was analysed. We found no significant correlation (r = -0.13, p = 0.403), indicating that sediment mobility does not

consistently decrease downstream, which suggests that position in the drainage network alone does not determine grain mobility. Instead, local channel characteristics, such as width variations that tend to occur in reaches with larger drainage area, likely exert a stronger control in sediment dynamics. Cook et al. (2020) demonstrated how such width variations influence sediment storage patterns, with wider sections generally storing more sediment during moderate flows. Although the width variations in the Carron are on a smaller scale (5 to 52 meters) compared to those in Cook et al.'s (2020) study (20 to several hundred meters), the principle that wider channels can provide more opportunities for sediment storage may still apply. In addition, reaches with larger drainage areas receive inputs from several tributaries, potentially increasing sediment supply during the period of lower flood frequency.

The temporal changes observed between 2010-2022 elaborate on the spatial patterns identified in Chapter 2, which found that channel slope and bankfull depth were the strongest predictors of alluvial cover distribution. However, these variables showed no significant correlation with temporal change (Figure 3.5). This suggests that the channel characteristics that control the spatial distribution of alluvial cover do not predict how cover changes over time. The near-significant correlation with drainage area may indicate that temporal changes are more influenced by network position and cumulative sediment dynamics than by local channel geometry. This complexity may be due to the post-glacial landscape, where glacial legacy creates diverse channel morphologies and sediment sources that can influence contemporary channel evolution (Ballantyne, 2002; Brardinoni & Hassan, 2006). The relatively high bankfull return period (approximately 7 years) observed at the gauge station, compared to typical 1-2 years in many alluvial systems (Williams, 1978), may demonstrate this post-glacial influence. The high banks and wide channel at the gauge site may reflect a river system still adjusting to deglaciation, where channel dimensions were initially shaped by larger glacial and paraglacial processes rather than being in equilibrium with current flow regimes. In this context, the reduced frequency of bankfull flows during the study period could have allowed gradual erosion of glacial deposits and river banks to contribute sediment to the channel network without large events evacuating this material downstream, contributing to the observed increased in alluvial cover throughout much of the catchment.

It is important to note that the observed changes in alluvial cover occurred over a 12-year period, which, while relatively short in the context of post-glacial landscape evolution, represents a temporal scale rarely captured in previous studies. The tendency of increasing alluvial cover may be a temporary phase rather than a long-term trend. Future extreme events could reverse these changes, particularly given that the analysis in Chapter 2 showed that 50-year floods can mobilise D_{50} grain sizes in 88% of reaches. The reaches most susceptible to cover removal during extreme events would be those with higher excess shear stress ratios. However, the response might vary spatially – reaches with larger drainage areas that showed the greatest increase in cover might be more resistant to complete cover stripping due to their wider channels, potentially maintaining some cover even during extreme events. This spatial variability in potential response demonstrates the dynamics of sediment storage in mixed bedrock-alluvial rivers.

3.5.2 Methodological challenges

The comparison of alluvial cover measurements between 2010 and 2022 showed several methodological challenges and offer perspective for future monitoring surveys. Differences in methodology between surveys affected the comparability of results and promote important considerations for temporal studies of alluvial cover.

A fundamental difference between the surveys was the reach length and sampling strategy, as described in section 3.3.1. The 2010 survey assessed bed cover at 10 m intervals along reaches of 100 m to 2 km length (Whitbread, 2015), while the 2022 survey used 11 transects at 20 m spacing over 200 m reaches. This difference in spatial coverage could affect the representativeness of measurements, particularly in reaches with higher spatial variability in cover. Both surveys relied primarily on visual estimation of alluvial cover, but were conducted by different people, which introduced observer bias. Whitbread's methodology included probing the riverbed with poles where safe when visibility was limited, providing additional verification of bed cover that was not included in the 2022 visual survey.

The proportion of the bed covered by water was noted as the main source of uncertainty in the 2022 survey. The classification of uncertainty levels (high, medium and low) based on the percentage of visible riverbed provides important context for interpreting the results. For example, Figure 3.3 shows that measurements with high uncertainty can appear at both extremes of alluvial cover values (both bedrock and alluvial reaches). The consistent pattern of increased cover across all uncertainty categories supports the overall trend, though different assumptions may have been made about unseen areas between surveys. Alternative survey methods could reduce this uncertainty in future surveys. Drone surveys are potentially more efficient than walking surveys but would still be limited by water clarity – the same constraint as visual surveys. Side-scan sonar and bathymetric LiDAR (Buscombe et al., 2016; Dietrich, 2017; Gomez-Heras et al., 2019) can provide detailed bed mapping, but have some limitations – sonar requires boat access and sufficient water depth, while LiDAR is costly and still requires water clarity for light penetration. These advanced technologies might be more useful at key reaches where higher precision is needed or uncertainty is high, rather than for surveying over larger spatial extents as done in the Carron.

The lack of correlation between changes in alluvial cover and excess shear stress (Figure 3.5f) complements Chapter 2's finding that contemporary floods can mobilise D_{50} in 88% of reaches during 50-year events and even 2-year floods can mobilise sediments in 63% of reaches. This temporal analysis indicates that despite the high potential for sediment mobility during floods, the overall alluvial cover in most reaches increased over the 12-year period, suggesting that sediment supply generally exceeded transport capacity across the catchment. The widespread increase in alluvial cover observed in this study, particularly following the period of moderate flows after 2014, indicates how the upstream supply and local transport conditions control cover changes. However, methodological limitations in the sediment mobility calculations may also have contributed to the lack of correlation between grain size mobility and cover change (Figure 3.5f). The use of drainage area scaling relationships to estimate discharge at ungauged locations provides understanding of broad patterns of potential mobility across the catchment but does not capture the local hydraulic conditions that control actual sediment transport. This simplified approach ignores local variations in flow depth

and grain-grain interaction that could affect sediment dynamics. Therefore, while our excess shear stress calculations provide a general potential for sediment mobility across the catchment, they may not be precise enough to predict specific locations of alluvial cover change.

For future alluvial cover monitoring, we recommend some methodological improvements. The fundamental challenge remains visibility through water particularly in peatland rivers like the Carron. Approaches such as probing the riverbed with poles where safe can provide verification of visual estimates. Additionally, standardising reach lengths and sampling protocols would ensure comparability between surveys and implementing regular monitoring, especially before and after flood events. Future studies should include monitoring of sediment sources and supply in addition to channel cover and combine several measurement techniques to reduce uncertainty. The systematic documentation of measurement uncertainty is valuable and should be maintained to assess confidence in results. While our understanding of the Carron's temporal dynamics is limited by data availability and quality, these limitations helped identify priorities for future monitoring of mixed bedrock-alluvial rivers. The suggested approaches to estimate alluvial cover could be standardised and adopted more widely in geomorphological surveys where direct measurement is challenging in order to fill the gap in understanding temporal change of alluvial cover.

Another potential source of uncertainty in the hydrological analysis is water management in the catchment, including both dams and possible water abstraction. Three small dams were observed in the upper catchment, likely constructed around the 1950s (before the available hydrological data). These structures could alter flow patterns by attenuating peak flows and changing the timing of water release downstream, but their influence would likely be consistent throughout most of the river network. Additionally, any water extraction for agricultural or other uses would further influence flow regimes, particularly during low flow conditions. However, without detailed records of dam operations and extraction volumes over time, it is difficult to quantify their effect on observed flow patterns and sediment dynamics. This factor should be considered when interpreting relations between hydrological conditions and alluvial cover changes.

3.5.3 Implications for river evolution and management

The observed changes in alluvial cover in the River Carron advance our understanding of both post-glacial landscape evolution and river management approaches. The general increase in alluvial cover between 2010 and 2022 reflects the river's response to recent hydrological conditions, particularly the period of moderate flows following the 2014 flood, combined with the glacial legacy effects. The temporal change observed is particularly relevant due to projected climate change in Scotland. Climate models predict increased winter rainfall and more frequent intense precipitation events (Chan et al., 2018; Slater et al., 2021), which could affect sediment dynamics in the Carron. The response to future extreme events may be intensified by the post-glacial landscape configuration, as observed in other deglaciated catchments where flood events can trigger substantial channel changes through the reworking of glacial sediments (Reid et al., 2022). Increased winter rainfall might accelerate sediment accumulation during moderate flows, but more frequent extreme events could periodically strip this cover, creating more dynamic cycles of sediment storage and removal than currently observed.

Gravel-bed rivers and their floodplains support diverse habitat and species interactions (Hauer et al., 2016). The ecological consequences of changing alluvial cover are significant in Scottish rivers, which are important habitats for salmonid fish. Stable alluvial cover creates spawning grounds for salmonids (Buffington et al., 2004), but excessive sediment accumulation, particularly of fine sediment that can block pores in the gravel, can reduce flow connectivity and habitat quality. These effects may be stronger in lower reaches, where our study suggested greater cover increases. From a management perspective, these findings demonstrate the need to consider both glacial context and future climate scenarios. Management approaches should be specific for different sites: reaches showing the greatest increase in cover might require more active monitoring for potential flood risk and ecological benefits, with particular attention to changes in sediment-size distribution that might affect habitat suitability.

3.6 Conclusion

This chapter investigated temporal changes in alluvial cover in the River Carron by comparing measurements from 2010 and 2022 in 29 reaches. Alluvial cover data from two different methodologies were compared: the 2010 survey assessed bed cover at 10 m intervals along reaches of varying length (100 m to 2 km), while the 2022 survey used 11 transects at 20 m spacing over 200 m reaches. The analysis combined field surveys of alluvial cover with hydrological data to understand how cover patterns changed over this 12-year period and their relationships with channel characteristics and flow conditions. Through comparing these surveys and documenting their limitations, particularly regarding underwater visibility and reach length differences, the key findings were:

1. Widespread increase in alluvial cover between 2010 and 2022, with 24 out of 29 reaches showing increased cover and an average rise of 18 percentage points.

2. No statistically significant relations between cover change and channel characteristics (drainage area, slope, width, depth and grain size), indicating that the interactions of several factors may control temporal changes in alluvial cover.

3. Complex response to flow conditions, with one extreme flood in 2014 followed by years of moderate flows, potentially facilitating sediment accumulation, particularly in downstream reaches.

The comparison of different survey approaches showed important methodological considerations for monitoring alluvial cover change. Visual estimation of cover can estimate temporal dynamics, but its reliability is dependent on water visibility conditions. Alternative methods such as side-scan sonar or bathymetric LiDAR could reduce these uncertainties but present limitations in terms of cost and accessibility.

Future alluvial cover monitoring would benefit from standardised protocols and regular surveys, especially around extreme flood events. In addition, combining several measurement techniques, maintaining consistent reach lengths between surveys and documenting uncertainty levels are essential for robust temporal analysis. Longer-term monitoring with improved methodologies will be essential to better understand how alluvial cover patterns may evolve with changing climate conditions and continued post-glacial adjustment.

4 Development and modification of a network-scale sediment transport model for mixed bedrock-alluvial rivers

4.1 Introduction

Understanding the controls on alluvial cover in mixed bedrock-alluvial rivers is critical for predicting landscape evolution, managing river systems and protecting aquatic habitats. Previous chapters of this thesis (Chapters 2 and 3) investigated these controls through empirical analysis of field data from the River Carron, Scotland. These chapters explored spatial patterns in alluvial cover distribution, but they showed challenges in understanding the temporal dynamics of cover changes. This limitation derives from the scarcity of long-term monitoring data on alluvial cover, making it difficult to empirically analyse how cover patterns evolve over time and respond to varying environmental conditions.

Numerical modelling offers an effective alternative approach for investigating alluvial cover dynamics. Models can overcome the limitations of field studies by allowing systematic investigation of individual parameters, simulating longer time periods than typically available in monitoring data, and simulating extreme events rarely observed in nature. In addition, numerical models can provide continuous spatial and temporal coverage, unlike discrete field measurements, facilitating the investigation of process interactions that may be difficult to observe in the field.

The choice of a model depends on the processes to be studied and the spatial and temporal scales of interest. Numerical models that address sediment transport and alluvial cover can have a large range of scales and processes. At the smaller scale, reach-scale models focus on grain processes and local cover dynamics. Examples include models focusing on grain-bed interactions and sediment patches (Hodge & Hoey, 2012; Nelson & Seminara, 2011), reach-scale sediment transport (Turowski, 2018) and detailed

hydraulic simulations (Inoue et al., 2014; Johnson, 2014). Recent advances include models that account for bed roughness effects on alluvial cover development (Jafarinik & Viparelli, 2020) and feedbacks between cover and hydraulics (Cho & Nelson, 2024a; Zhang et al., 2015).

At the largest scales, landscape evolution models (LEMs) function at catchment scales over geological time periods. Models like SPACE (Shobe et al., 2017), Fastscape (Yuan et al., 2019) and EROS (Davy & Lague, 2009) simulate long-term development of river networks through the interaction of erosion, sediment transport and deposition. These models can capture broad patterns of channel evolution, but most tend to simplify alluvial cover dynamics due to their large spatial and temporal scales.

Between these extreme scales, there is an intermediate one: the network scale over decadal time periods. This scale is particularly relevant for river management and understanding the river network response to environmental change. Examples of bedload transport models that operate at this intermediate scale are NetworkSedimentTransporter (Pfeiffer et al., 2020), D-Cascade (Tangi et al., 2019) and CAESAR-Lisflood (Coulthard et al., 2013). These models have been used to simulate network-scale processes such as sediment cascades (Murphy et al., 2019; Schmitt et al., 2016), fluvial connectivity related to reservoir sediment trapping (Schmitt et al., 2018), sediment pulse propagation in gravel-bed rivers (Ahammad et al., 2021) and landscape response to extreme flood events (Coulthard et al., 2013).

Considering the research objectives of this thesis – to investigate mechanisms driving spatial and temporal variability of alluvial cover in mixed bedrock-alluvial cover – the NetworkSedimentTransporter (NST) model was selected as it a suitable model for our analysis. NST simulates bedload transport processes at network spatial scales over a decadal temporal scales, which are the scales analysed in this thesis. An advantage of NST is its Lagrangian approach, which allows for tracking of individual sediment parcels through the network, making it possible to monitor the exact movement and deposition patterns needed for alluvial cover analysis. In addition, NST is built on Landlab, an open-source Python library code with a modular structure that makes it suitable for necessary modifications.

Applying NST to analyse alluvial cover controls in mixed bedrock-alluvial systems requires important modifications. The original model was developed for alluvial systems and lacks specific functions for bedrock exposure analysis. Additionally, its sediment transport algorithm assumes constant velocity within a timestep, which can create unrealistic sediment movements in networks with variable channel slopes. This chapter details these modifications that have three main objectives:

1. To develop new functionality for calculating and tracking alluvial cover over bedrock surfaces.
2. To enhance the model's sediment transport algorithm for improved representation of parcel movement through networks with high slope variability.
3. To implement a flexible sediment input function for exploring various supply scenarios.

These modifications will allow the investigation of spatial and temporal changes in alluvial cover patterns and their controlling factors, complementing the empirical analyses presented in previous chapters (Chapters 2 and 3) and providing a foundation for the analyses presented in subsequent chapters (Chapters 5 and 6).

4.2 The NetworkSedimentTransporter model

The NetworkSedimentTransporter (NST) (Pfeiffer et al., 2020) simulates bedload sediment transport in river networks using a Lagrangian approach, i.e., by tracking the movement of individual sediment parcels along the river network. Each parcel represents a group of sediments with similar characteristics, allowing the model to calculate the sediment deposit thickness and its spatial distribution over bedrock beds. The model simulates mixed grain sizes by assigning different characteristics to different parcels. The 1D river network is structured through nodes (channel junctions or endpoints) connected by links (river segments) (Figure 4.1). Links contain channel properties, including reach length, width, flow depth and slope, while nodes contain topographic and bedrock elevation data.
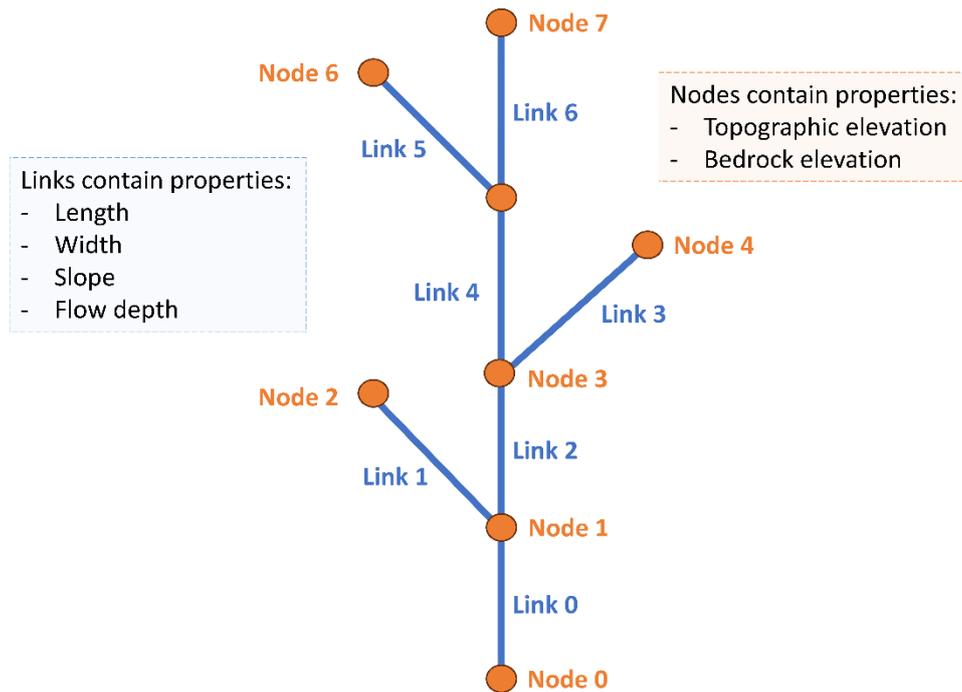
Figure 4.1: Conception representation of a river network in the NST model. The network consists of nodes (orange circles) representing channel junctions or endpoints and links (blue lines) representing river segments. Nodes store elevation data and links contain channel properties.

NST is initialised through a sequence of operations (Figure 4.2). First, the river network is defined using nodes and links. Channel and topographic properties are assigned to these elements, defining the physical structure in which sediments will move. Then, the network is populated with sediment parcels, each with defined properties such as location, density, grain size and volume. Flow directions are determined based on elevation differences between nodes – ensuring sediments move from higher to lower nodes. After initialisation, NST computes sediment transport through a series of timesteps. At every timestep, the model executes the following sequence of physically-based calculations:

1. Active layer: Determines which sediment parcels are available for transport by calculating active layer thickness using the Wong and Parker equation (Wong et al., 2007) (Equation 4.1).

$$L_a = 0.515 \, D_{50} \, [3.09 \, (\tau^* - 0.0549)^{0.56}] \qquad \text{(Equation 4.1)}$$

2. where L_a is active layer thickness (m), D_{50} is median grain size (m) and τ^* is dimensionless shear stress calculated as $\tau^* = \tau\,[(\rho_s - \rho)\,g\,D_{50}]$, where τ is bed shear stress (N/m^2), ρ_s is sediment density (kg/m^3), ρ is fluid density (kg/m^3) and g is gravitational acceleration (m/s^2). The active layer capacity (volume) for each link is calculated as the product of active layer thickness, channel width and reach length. Parcels within each link are then sorted by arrival time (most recent first) and their volumes are cumulatively summed. Parcels whose cumulative volume falls within the active layer capacity are classified as active (mobile), while those exceeding this capacity are classified as inactive (in storage) Elevation adjustment: Updates node elevations based on the volume of stored (inactive) sediment (Equation 4.2).

$$z = \frac{z_{br} + V_s}{[(1 - \varphi)\,A]} \qquad \text{(Equation 4.2)}$$

where z is surface elevation (m), z_{br} is bedrock elevation (m), V_s is stored sediment volume (m^3), ϕ is bed porosity (set as 0.3) and A is channel bed area (m^2).

3. Slope updating: Updates channel slopes based on the newly adjusted node elevations (Equation 4.3).

$$S = \frac{(z_{up} - z_{down})}{l} \qquad \text{(Equation 4.3)}$$

where S is channel slope (m/m), z_{up} and z_{down} are upstream and downstream node elevations (m), and l is link length (m).

4. Transport calculation: Computes velocities for active parcels using the Wilcock and Crowe transport equation (2003). The dimensionless transport rate (W^*) for each parcel is calculated as Equations 4.4.

$$W^* = 0.002 \left(\frac{\tau}{\tau_r}\right)^{7.5} \quad \text{for } \tau/\tau_r < 1.35 \qquad \text{(Equation 4.4a)}$$

$$W^* = 14 \left(\frac{\tau}{\tau_r}\right)^{7.5} \qquad \text{for } \tau/\tau_r \geq 1.35 \qquad \text{(Equation 4.4b)}$$

where τ_r is the reference shear stress (N/m^2) defined by the Wilcock and Crowe (2003) formulation. This reference shear stress depends on the mean active grain size, the sand fraction of the bed surface and accounts for the hiding effects of mixed grain sizes. Individual parcel velocities are then computed (Equation 4.5)

$$u_p = \frac{\left(W^* \, \tau^{1.5} \, F_p\right)}{\left(\rho^{1.5} \, g \, R \, L_a\right)}$$

(Equation 4.5)

where u_p is parcel velocity (m/s), F_p is the volumetric proportion of an individual parcel relative to the total volume of all active within that link, and R is the ratio of sediment to fluid density calculated as $R = (\rho_s - \rho)/\rho$.

5. Parcel movement: Updates the location of active parcels based on their calculated velocities and the timestep duration, moving parcels downstream through the network until they come to rest or exit the system.

The model repeats this sequence each timestep, repeatedly updating parcel positions and channel morphology throughout the simulation. More details regarding the model calculations can be found in Czuba et al. (2017).
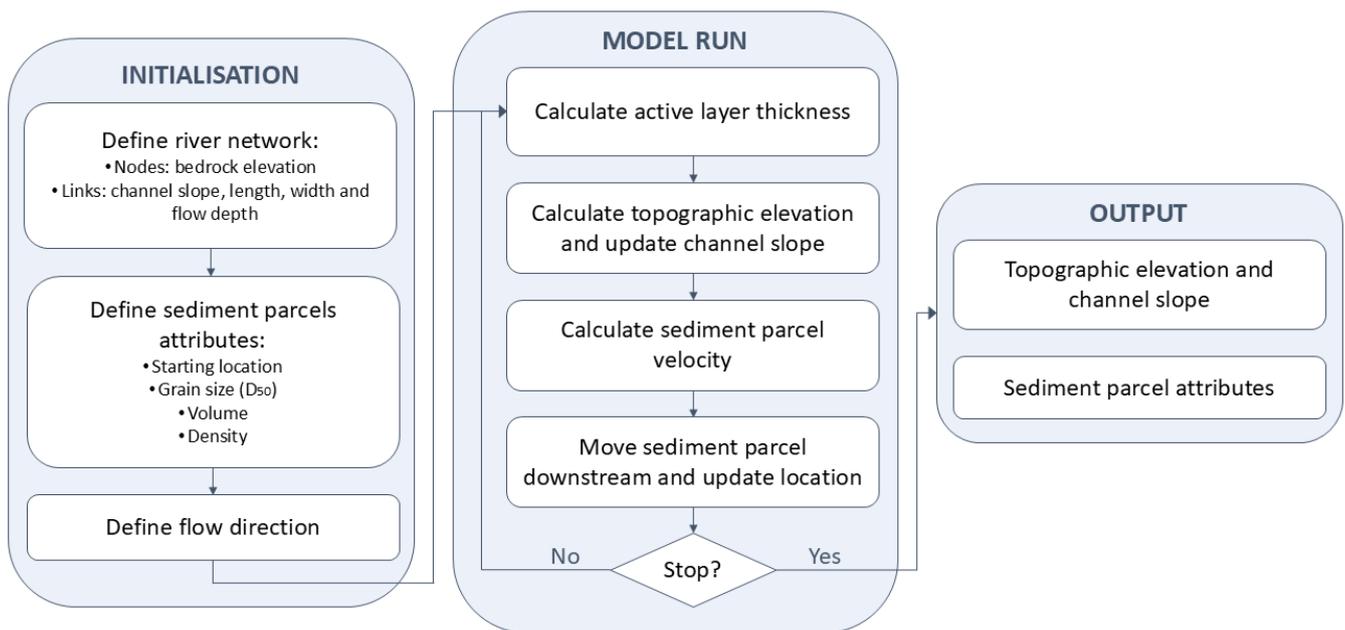
Figure 4.2: Workflow diagram of the NetworkSedimentTransporter model showing the three main sections: (1) Initialisation, with the definition of network structure, sediment characteristics and flow conditions; (2) Model run sequence showing the iterative calculations performed per timestep; and (3) Output data produced by the model.

The model has several assumptions and simplifications that influence its operation. Regarding hydrodynamic assumptions, it assumes steady flow conditions for each

timestep, with flow depth determined individually at each link without enforcing flow continuity between reaches. Flow depth remains constant within each reach throughout the simulation, regardless of changes in sediment volume or channel morphology. Regarding channel geometry assumptions, channel geometry is fixed as rectangle cross sections, without considering width adjustments, bank erosion or deposition. Channel width and depth are specified as input parameters and remain constant throughout the simulation, even as sediment accumulate or erodes. In relation to sediment transport assumptions, calculations focus on bed load transport, with suspended sediment not modelled. The model assumes identical transport mechanisms for both bedrock and alluvial reaches, using the same critical shear stress formulation regardless of bed substrate type. In addition, the underlying bedrock surface elevation remains fixed and non-erodible throughout the simulation. Bedrock roughness and topographic variability at sub-reach scales are not represented. These simplifications make the model computationally efficient but simplify the processes and should be considered when interpreting the results.

NST has been applied to several fluvial geomorphology problems, for example, investigating sediment pulses in gravel-bed rivers (Ahammad et al., 2021) and analysing post-wildfire sediment cascades (Murphy et al., 2019). However, it has not been applied to mixed bedrock-alluvial systems, as its original model lacks specific functionality for tracking and analysing alluvial cover dynamics. This gap motivates the modification presented in the next section of this chapter.

4.3 Model modifications

This section details the implementation of three key modifications to the NetworkSedimentTransport model that enable it to simulate cover dynamics in mixed bedrock-alluvial networks with high channel slope variability.

4.3.1 Alluvial cover calculation

The original NetworkSedimentTransporter tracks sediment volumes throughout the network, but it lacks specific functionality for quantifying and analysing alluvial cover over bedrock. Developing a specific function to convert sediment volumes into alluvial cover fractions requires consideration of channel morphology and grain characteristics. This function allows spatial and temporal analysis of bedrock exposure versus sediment cover in a river network.

The cover fraction represents the proportion of the channel bed covered by sediment and can be calculated as the ratio of sediment volume to potential bed volume. It can be expressed mathematically by Equation 4.6.

$$p_c = \frac{V_l}{l_l \; W_l \, D_l \; (1-\varphi)}$$
(Equation 4.6)

where p_c is the alluvial cover fraction in link l; V_l is the volume of sediment parcels in link l (m³); l_l is the link length (m); W_l is the link width (m); D_l is the average median grain size of sediment parcels in link l; and ϕ is the bed porosity, for which the default value is set as 0.3.

This formulation allows for varying degrees of sediment accumulation, from partial cover to multiple layers of deposits (Table 4.1). A cover fraction of 0 indicates exposed bedrock, values between 0 and 1 represent partial cover and values greater than 1 indicate multiple layers of sediment accumulation. For example, a cover fraction of 2 indicates enough sediment to create two layers of median grain size depth.

Table 4.1: Interpretation of alluvial cover fraction in river cross-sections. Cover fraction ranges from 0 (bare bedrock) to values greater than 1 (multiple sediment layers). Blue represents water, light grey circles represent sediment grains, and hatched grey represents bedrock. Channel type classifications are based on the amount of sediment cover.

Cover fraction	Physical meaning	Channel type	Cross-section
0.0	No sediment cover	Bedrock	
0.5	Partial cover	Mixed	
1.0	Single layer cover	Alluvial	
2.0	Two complete sediment layers	Alluvial	
3.0	Three complete sediment layers	Alluvial	
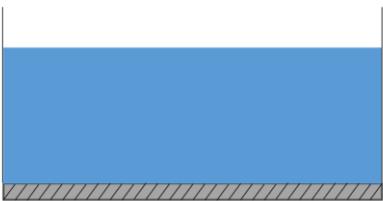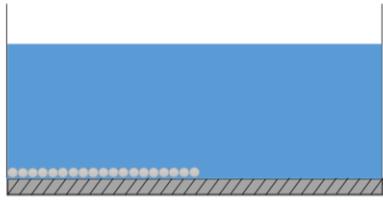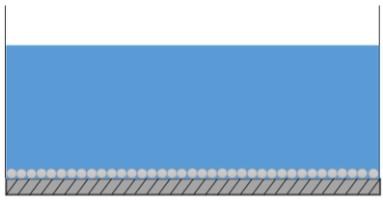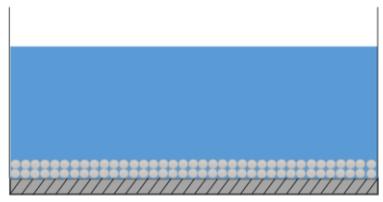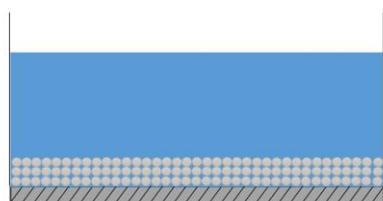
The alluvial cover calculation is based on several assumptions. The model assumes sediment is uniformly distributed within each link across the channel width and length, with grain size distribution within each link represented by the mean of the median grain

sizes (D_{50}) from all parcels in the link. Bed porosity is treated as constant regardless of sediment depth. In addition, channel width and depth are constant within each link, without accounting for the existence and type of banks. The model also does not represent the small-scale topographic variability of bedrock surfaces, such as bedrock roughness or depressions. These assumptions simplify the reality of sediment distribution in natural channels, but they provide a tractable approach for quantifying cover at the network scale.

This modification is an important first step towards adapting NST to analyse alluvial cover in mixed bedrock-alluvial river networks. Future developments should incorporate different sediment transport dynamics for bedrock and alluvial reaches, as the critical shear stress required for grain entrainment is lower on smooth bedrock surfaces than on rough alluvial beds (Hodge et al., 2011). This modification would better represent how sediment mobility changes as reaches change between bedrock and alluvial states.

The complete code for calculating the alluvial cover fraction is available in Appendix A1.1.

4.3.2 Downstream sediment movement

The original NetworkSedimentTransporter has limitations in representing sediment transport through adjacent links of varying slopes. The parcel velocity is calculated only once per timestep, based on the parcel's initial location. This velocity is then used to calculate the total travel distance for that timestep, regardless of the different channel conditions a parcel might find along this path. This approach leads to unrealistic sediment movement, particularly in networks with significant slope variations. For example, a parcel starting in a steep reach could be assigned a high velocity and, within a single timestep, travel through multiple downstream reaches or even exit the network, even if downstream reaches had much lower slopes that would realistically slow parcel movement (Figure 4.3a).
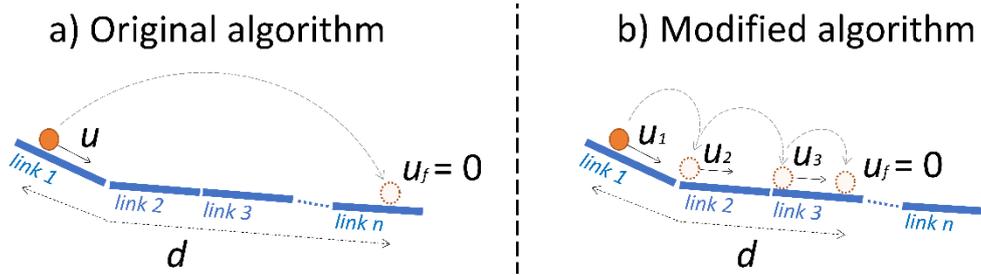
Figure 4.3: Comparison of sediment movement between original and modified algorithms. In the original algorithm, parcels maintain a constant velocity (u) and can skip multiple links, while the modified algorithm updates velocities (u_1, u_2, u_3) at each link the parcel travels through. The variable d represents the total distance travelled by the parcel during a timestep and $u_f = 0$ indicated the final parcel state when it comes to rest.

To address this limitation, the sediment transport algorithm was modified to dynamically update parcel velocities as parcels move through the network (Figure 4.3b). The advanced algorithm tracks parcel movement using time rather than distance, calculating the time required to traverse each link based on local channel conditions (Figure 4.4). For each link moving downstream, the algorithm:

1. Calculates the time required to exit the current link (t_l) (Equation 4.7).

$$t_l = \frac{d_l}{u_l}$$ (Equation 4.7)

   where d_l is the remaining distance in the current link and u_l is the velocity calculated using local channel conditions.

2. Updates the remaining travel time (t_{left}) (Equation 4.8).

$$t_{left} = dt - t_l$$ (Equation 4.8)

   Where dt is the timestep length and t_l is the time required to exit the current link.

3. Recalculates parcel velocity for the next link using the Wilcock and Crowe equation (2003) (Equation 4.5).

The modified algorithm also implements dynamic transport capacity in each link by tracking parcels moving through it. As parcels travel multiple links within a timestep, the algorithm monitors and updates the available transport capacity of each link (Figure 4.4). When parcels enter a new link, they use part of that link's capacity based on their volume. If a link's remaining capacity is insufficient for additional incoming parcels, those parcels

have their remaining travel time set to zero, stopping their movement for that timestep. Contrarily, when parcels leave a link, its capacity is restored by the volume of the parcels that have left. This dynamic tracking prevents unrealistic sediment flux through reaches, better representing the physical constraints on sediment movement through the network.
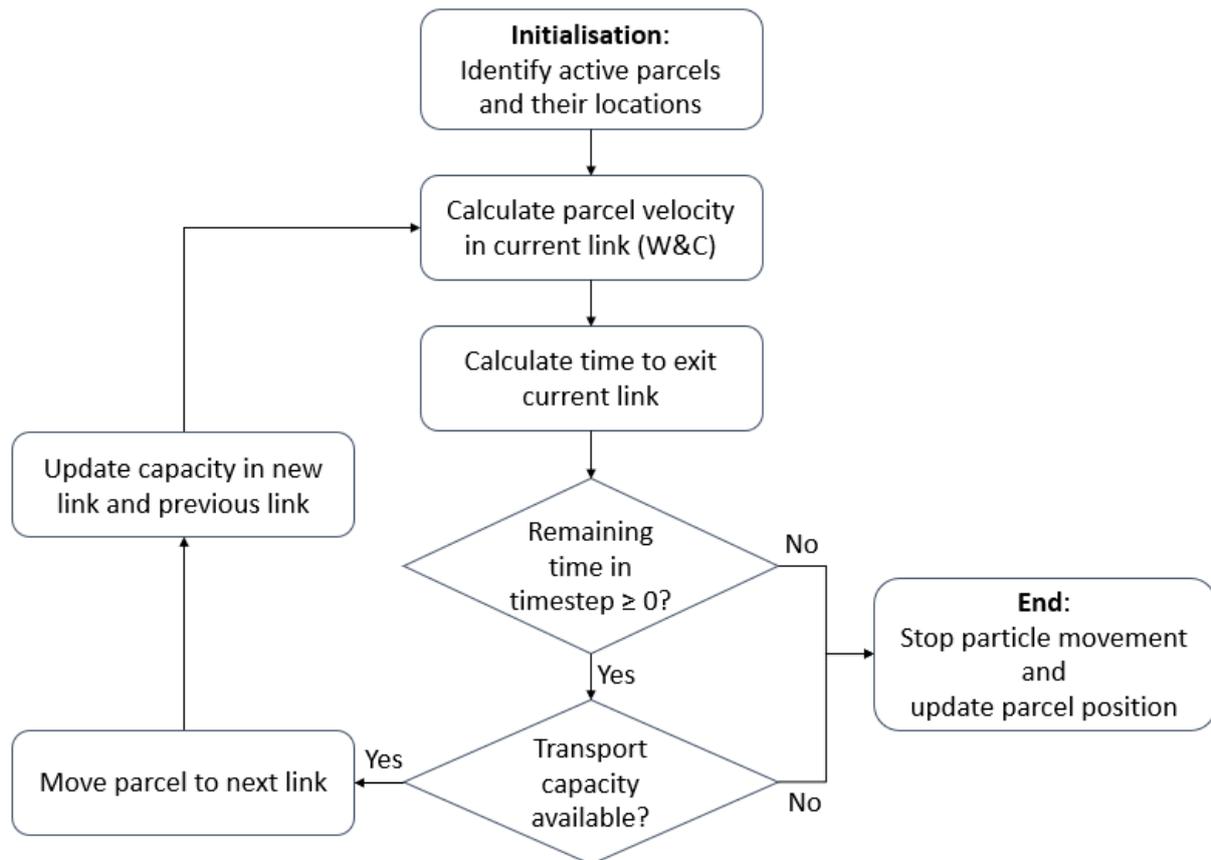
Figure 4.4: Workflow diagram of the modified sediment transport algorithm. Parcel velocity is calculated using the Wilcock and Crowe (W&C) equation (2003). Time check compares the remaining time in the timestep against zero, where the remaining time is the timestep length minus the time required for the parcel to exit the current link. The "Transport capacity available?" decision diamond evaluates whether the downstream link that the parcel would move into has sufficient remaining transport capacity to accommodate the parcel.

This advancement in the sediment transport algorithm better represents the physical constraints on sediment movement through the network. The complete code for the modified function that moves parcels downstream is provided in Appendix A1.2.

4.3.3 Sediment input function

To allow flexible sediment input scenarios, a new function to add sediment parcels at specified locations and specified times during the model execution was created. During the course of this research, similar functionality was independently developed and incorporated into the official NetworkSedimentTransporter as the SedimentPulserAtLinks class, demonstrating the need for studying dynamic sediment inputs in river networks. However, in this study, we used our own algorithm to add sediments into the river network.

Our implementation provides a function that allows the addition of sediment parcels to any link in the network at any timestep. Each new parcel is assigned properties including volume, density and grain size (Table 4.2). The grain-size distribution can follow either a uniform or lognormal distribution based on the median diameter (D_{50}) defined by the user. Consistent with how NST initially distributes parcels, the longitudinal position of each new parcel within its link is randomly defined between the upstream and downstream ends of the link. Each new parcel is initially set as active (available for transport) with an arrival time slightly greater than zero to ensure integration with the model's timestep calculations. The parcels are added directly to the model's DataRecord object, which maintains the history of all parcel properties throughout the simulation.

Table 4.2: Parameters required by the function to add sediment input.

Parameter	Description
Parcels	NST's DataRecord object that stores parcels information
Receiver link	Link IDs where parcels will be added
Parcels per link	Number of parcels to be added per link
Volume of parcel	Parcel volume (m^3)
Median diameter	Median grain size (D_{50}) (m)
Density	Sediment density (default: 2650 kg/m^3)
Abrasion rate	Mass loss per unit distance travelled (set to zero in this work)
Time	Timestep at which parcels will be added

The official NST implementation (SedimentPulserAtLinks) offers more functionality compared to our version, including more control over pulse timing and parameter variations. However, our simpler implementation adequately serves the needs of this study, allowing the investigation of several sediment supply scenarios presented in Chapters 5 and 6. The complete code of the function to add sediment parcels used in this study is provided in Appendix A1.3.

4.4 Model testing and verification

The model modifications were tested using an artificial river network to verify the new functionalities. The artificial network is composed of 7 links and 8 nodes (Figure 4.5). The initialisation parameters of the river network and parcel properties are described in Table 4.3. Three separate simulations were conducted to test each modification:

1. Cover calculation test: Using slopes from 0.0005 to 0.0065 m/m and starting with 100 parcels per reach with log-normal grain size distribution (D_{50} = 0.05 m) to test cover development patterns. This initial configuration resulted in cover fractions ranging from 104% to 133% across the reaches.

2. Sediment movement test: using slightly higher slopes (0.001 to 0.0065 m/m) and only one parcel per reach to clearly track individual parcel movements and verify velocity updates at link transitions.

3. Sediment input test: Same characteristics as the cover calculation test but adding 30 new parcels per timestep at all upstream links (IDs: 1,3,5 and 6) to verify the effect of continuous sediment supply.
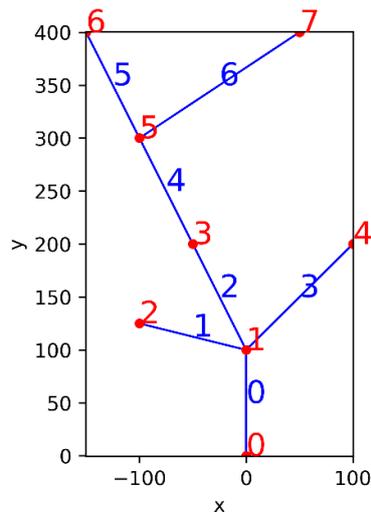
Figure 4.5: Structure of the artificial river network used to test the model modifications. Link IDs are indicated in blue and node IDs in red. The outlet is at node 0.

Table 4.3: Network configuration and initialisation parameters for testing scenarios.

Parameter	Cover test	Movement test	Input test
Link length	200 m	200 m	200 m
Link width	1 m	1 m	1 m
Flow depth	3 m	3 m	3 m
Link slopes	0.0005 – 0.0065 m/m	0.001 – 0.0065 m/m	0.0005 – 0.0065 m/m
Initial parcels per link	100	1	100
Grain size	Log-normal (D_{50} = 0.05 m)	Uniform (0.05 m)	Log-normal (D_{50} = 0.05 m)
Parcel volume	0.1 m^3	0.1 m^3	0.1 m^3
Simulation duration	9 timesteps	9 timesteps	9 timesteps
Added parcels	None	None	30 per timestep in links 1,3,5,6

Results demonstrate that the modified code successfully handles all new functionalities. The alluvial cover calculation tracks sediment accumulation patterns, showing expected behaviour where steeper upstream reaches (links 1,3,5 and 6) present exposed bedrock while flatter downstream reaches accumulated sediments (Figure 4.6). Link 0, at the network outlet, accumulated up to three layers of sediment cover (cover fraction = 3), consistent with its position and slope.

a)

b)
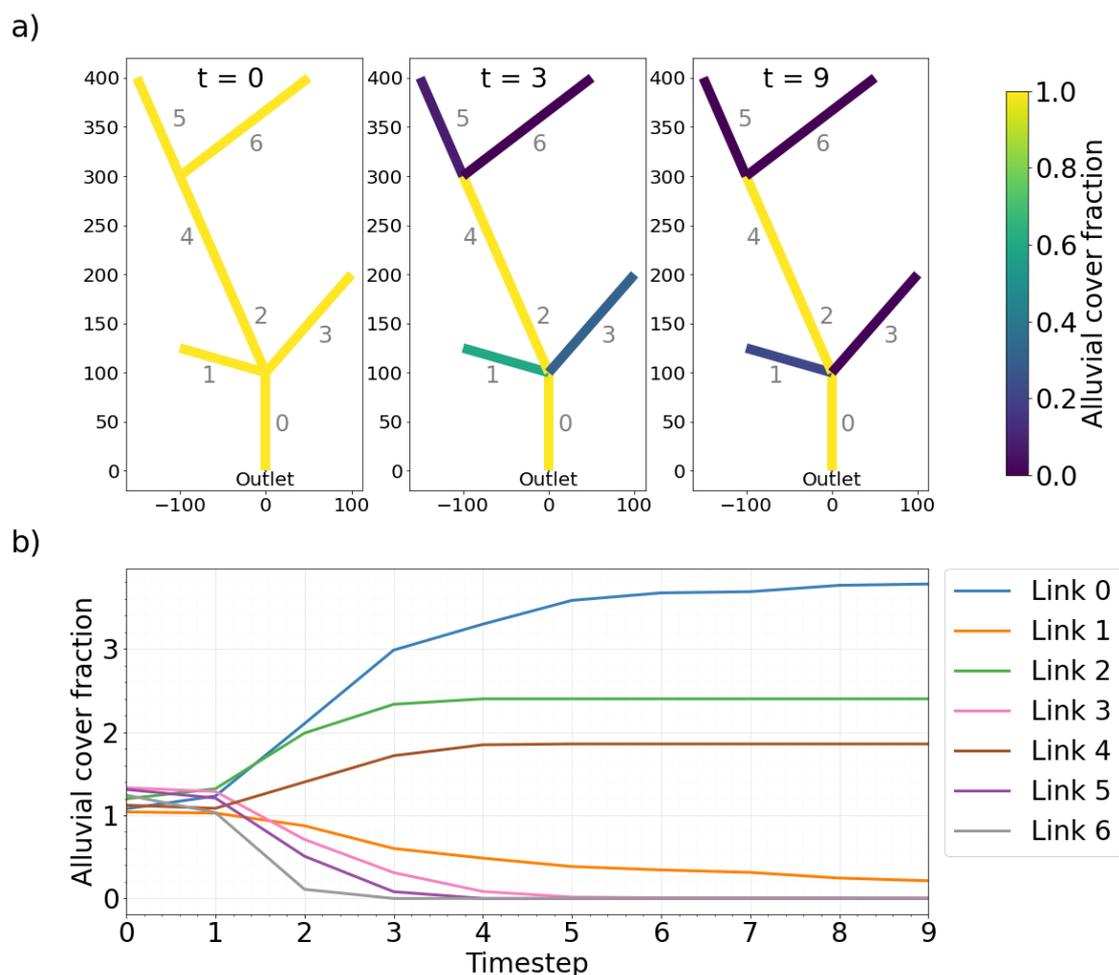
Figure 4.6: Example of the result of the alluvial cover fraction calculation. a) River network visualisation at three timesteps (t = 0, 3 and 9) showing the spatial distribution of alluvial cover fraction. Numbers in grey indicate the Link ID. b) Temporal evolution of alluvial cover fraction for each link along the simulation period.

The test of the modified algorithm that moves parcels downstream showed improvements in parcel movement representation (Figure 4.7). In the original algorithm, parcels starting in steep reaches (P1 and P2) exited the network within a single timestep, as they had enough velocity to move a distance longer than the path to the network outlet (Figures 4.7a and 4.7c). In contrast, the modified algorithm updated parcel velocities when they moved into the next link, allowing parcels to slow down when entering lower channel slopes and preventing the parcels from leaving the network within one timestep. In the modified algorithm, all parcels remained in the network and moved downstream gradually, providing a more realistic parcel movement (Figure 4.7b and 4.7c).
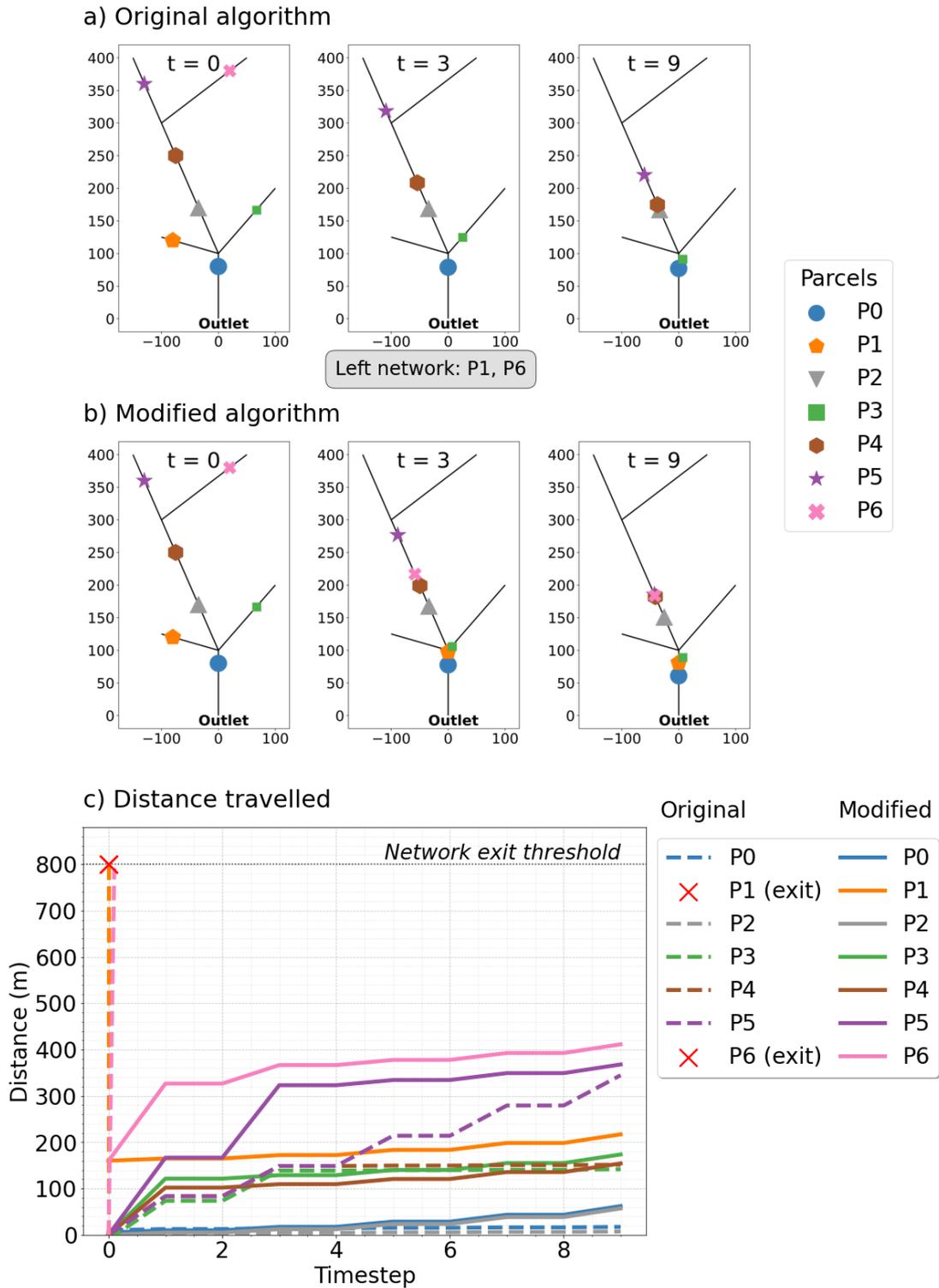
Figure 4.7: Comparison of sediment parcel movement between original and modified NST models. a) Parcel positions at three timesteps (t = 0, 3 and 9) in the original algorithm. Parcels P1 and P6 in steep reaches exit the network within one timestep. b) Parcel positions at the same timesteps in the modified algorithm. All parcels remained in the network and moved downstream gradually. c) Distance travelled by parcels over

time, showing the difference between original (dashed lines) and modified (solid lines) algorithms. Red X marks indicate parcels exiting the network (distances > 800 m). The horizontal dotted line at 800 m represents the network exit threshold (maximum possible travel distance within the network).

The new sediment input function was tested by adding 30 sediment parcels per timestep at upstream links (1, 3, 5 and 6) at all timesteps. When sediment input was simulated, total sediment volume increased throughout the network, with accumulation in both upstream and downstream reaches (Figure 4.8). Without sediment input, upstream reaches (Links 1, 3, 5 and 6) quickly decrease their initial sediment as parcels move downstream, with the upstream reaches approaching zero volume by timestep four (Figure 4.8c). With continuous sediment input, these same reaches maintain higher sediment volumes throughout the simulation or reduce the sediment volume gradually (Figure 4.8d). The simulation with sediment input creates a more realistic representation of sediment retention in upstream reaches and transport throughout the network.
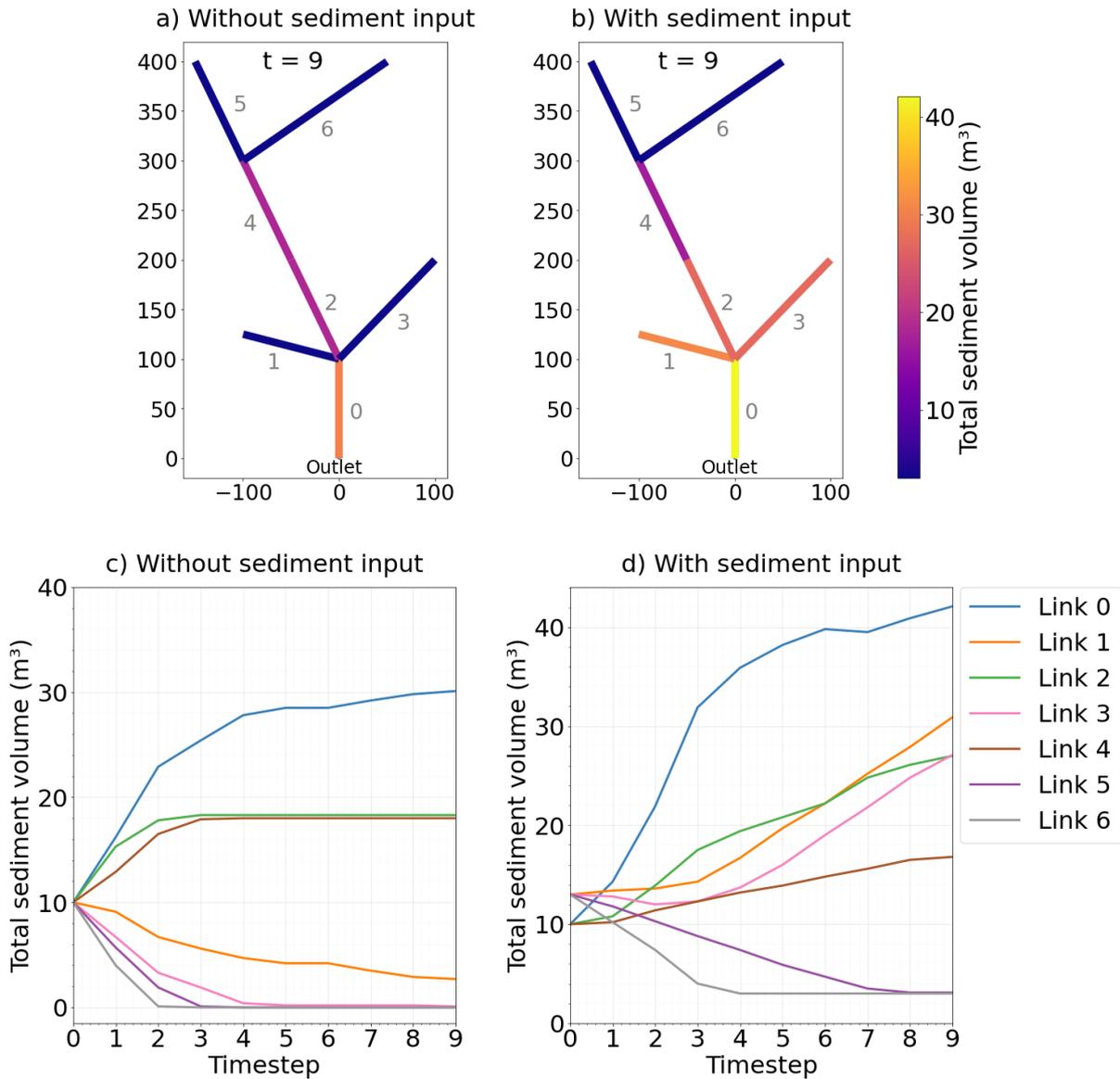
Figure 4.8: Comparison of sediment volume accumulation with and without continuous sediment input. a-b) Network visualisation at timestep t = 9 showing the spatial distribution of total sediment volume (m³): a) without sediment input; b) with sediment input at upstream links. Link IDs are shown in grey. c-d) Temporal evolution of sediment volume over 9 timesteps: c) without sediment input; d) with sediment input.

These test results confirm that all three modifications function as intended and improve the model's capacity to simulate alluvial cover dynamics in mixed bedrock-alluvial networks.

4.5 Summary

This chapter presented the development and implementation of three modifications to the NST model to improve the investigation of alluvial cover dynamics in mixed bedrock-alluvial river networks. These modifications address specific limitations in the original model and improve its capacity for analysing spatial and temporal patterns of alluvial cover.

The first modification – the alluvial cover calculation function – transforms sediment volume data into cover fraction, by quantifying the degree to which the riverbed of a reach is covered with sediment. The second modification improves the algorithm that moves parcels downstream by updating parcel velocities at each reach they move through in the network. This improvement creates more realistic sediment transport rates, particularly when parcels move from high slope to low slope reaches. The third modification provides a sediment input function, allowing for simulations with different sediment supply scenarios, which is necessary for investigating how spatial and temporal variations in sediment input influence alluvial cover in river networks. The three modifications were tested and proven to work as intended.

These modifications allow for alluvial cover studies on a river network scale and will be used when applying NST in the analyses presented in the next chapters. Chapter 5 uses the modified model to investigate steady-state patterns of alluvial cover and identify primary controls in its spatial distribution, while Chapter 6 uses the modified model to simulate sediment pulses, examining how temporal variations in sediment supply influence cover dynamics. Although the modified model provides advancements to study alluvial cover dynamics at the network scale, it has simplifications, such as constant channel geometry and not differentiating between bedrock and alluvial reaches' sediment transport mechanisms. These simplifications should be considered when interpreting the results from the model in the next chapters.

The model advances presented in this chapter also benefit the broader discipline of fluvial geomorphology by providing tools for investigating the interactions between channel properties, sediment dynamics and alluvial cover on a river network scale. This modified model can be used for exploring how river networks respond to different

environmental conditions and human impacts, with applications in river management, habitat management, and landscape evolution modelling.

5 Network-scale dynamics of alluvial cover in a mixed bedrock-alluvial river

5.1 Abstract

Limited understanding of how sediment cover varies spatially in mixed bedrock-alluvial river networks inhibits our comprehension of erosion processes in these systems. This study investigates the complex interactions between channel and sediment properties that control the extent, spatial distribution, and connectivity of alluvial cover in mixed bedrock-alluvial river networks. Employing a combination of field data, sediment transport modelling, and connectivity analysis, this study aims to understand the key drivers influencing sediment cover patterns at the network scale. Sediment transport simulations using the NetworkSedimentTransporter model explored how varying initial fluvial and channel parameters affect the steady-state alluvial cover across the River Carron network in the Scottish Highlands. The results demonstrate that increased initial sediment cover, increased sediment supply, and larger grains increased the extent and connectivity of alluvial sections, whereas deeper flow reduced them. In supply-limited conditions, the spatial distribution of alluvial cover is most sensitive to slope, while in transport-limited conditions, sediment supply and grain size become more critical. Even at high sediment supply rates, not all reaches achieved full alluviation, suggesting inherent limitations in sediment distribution. Additionally, channel slope was the most significant factor controlling the directional growth of alluvial sections. These findings

contribute to the limited research on the controls of alluvial cover at the network scale, thereby improving our understanding of landscape evolution, river management, and habitat conservation of mixed bedrock-alluvial rivers.

Key points

- Model effectively simulated broad network-scale alluvial cover patterns.
- Slope is a primary control on alluvial cover distribution and expansion, particularly in supply-limited conditions.
- Alluvial cover extent is highly responsive to sediment supply and discharge, especially in supply-limited conditions.

Plain Language Summary

Rivers can have their bedrock exposed, be covered by sediment, or a mix of both. Understanding how sediment cover changes across river networks is important for predicting erosion, managing rivers, and protecting habitats. This study used a computer model to simulate sediment movement in the River Carron network in Scotland. We explored how factors such as initial sediment cover, water depth, sediment supply, and grain size affect sediment distribution. We found that more initial sediment, higher sediment supply, and larger grains increased sediment cover, while deeper water reduced it. Even with high sediment supply, exposed bedrock persisted in some areas. Slope was the main factor controlling where sediment accumulated, especially when sediment supply was low. However, sediment supply became more important in controlling where sediment accumulated when supply was high. Our study highlights the complex interaction of factors shaping river landscapes and provides insights for better river management and conservation strategies.

5.2 Introduction

River channels can be predominantly alluvial, characterised by sediment deposits covering the riverbed and banks, or bedrock, where exposed rock is present in the channel bed or banks. Bedrock rivers control landscape evolution because river incision into bedrock sets the hillslope base level (Whipple et al., 2013). Some river systems comprise a combination of bedrock exposure and sediment-covered patches, termed mixed bedrock-alluvial river systems. In this context, alluvial cover refers to areas covered in sediment regardless of the underlying bedrock's elevation. While continuous long bedrock channels are relatively rare, mixed bedrock-alluvial river systems are relatively common worldwide (Whipple et al., 2013). The alluvial cover of river channels is the result of complex interactions between hydraulics and sediment transport processes. These interactions play a crucial role in the evolution of rivers, influencing ecosystems, river engineering, and shaping the terrestrial features around them.

Fluvial discharge and sediment supply play major roles in controlling alluvial cover. A higher discharge increases the shear stress and sediment transport rate (Ferguson et al., 2017a). However, large rainfall events can trigger a larger sediment supply, leading to greater potential for alluvial cover development or bedrock incision (Cook et al., 2020; DeLisle & Yanites, 2023; Turowski et al., 2013). When sediment supply is low, increasing it can lead to more frequent impacts of grains on the bed, increasing erosion. However, as sediment supply continues to increase, it eventually forms continuous alluvial cover, protecting the underlying bedrock from erosion. These processes are known as the "tools and cover" effect and the balance between them is critical in determining whether a reach will incise or develop alluvial cover (Sklar & Dietrich, 2004; Turowski et al., 2007).

Understanding these complex interactions is important because transitions between bedrock and alluvial reaches impact the location of bedrock incision within the channel, and affects sediment connectivity, i.e. the degree to which sediment can move through the system without being retained in transient storage zones (Fryirs, 2013). These factors can alter patterns of alluvial erosion and deposition across the river network. The extent of alluvial cover is typically predicted based on the relative sediment flux, which is the sediment supply rate relative to the bed load transport capacity (Chatanantavet & Parker,

2008; Inoue et al., 2014; Johnson, 2014; Sklar & Dietrich, 2004). However, flume and field experiments have shown that several stable cover fractions can form for a given sediment supply-to-transport capacity ratio depending on bed roughness, antecedent alluvial cover, channel geometry, and entrainment probability (Chatanantavet & Parker, 2008; Hodge et al., 2011). Discharge and sediment supply are extrinsic parameters influenced by regional climate, tectonics, and hillslope processes including landslides. These controls exhibit complex interactions across diverse spatial and temporal scales, challenging the prediction of the spatial patterns and evolution of bedrock and alluvial reaches.

Channel geometry, including slope, width, and depth, influences alluvial cover by affecting flow dynamics and sediment transport. Steeper slopes and narrower channels generally increase shear stress and promote sediment transport. Bedrock channels are typically expected to be narrower, deeper, and steeper than alluvial channels for a given drainage area (Montgomery & Gran, 2001; Whitbread et al., 2015). However, when sediment flux is restricted, bedrock channels may be wider and shallower than alluvial channels (Buckley et al., 2024; Meshkova & Carling, 2013; Whitbread et al., 2015) and may be found in low-slope reaches (Jafarinik & Viparelli, 2020). The transport capacity of a channel, which is influenced by its geometry, fluctuates with changes in discharge (Sklar & Dietrich, 1998). This dynamic relationship creates a feedback loop between form and function: channel morphology affects sediment transport, while sediment dynamics shape the channel through processes of bedrock erosion and sediment deposition (Baynes et al., 2020; Johnson & Whipple, 2010; Turowski, 2018). Consequently, channel morphology and sediment transport are interlinked. However, a comprehensive understanding of this feedback is still lacking, particularly in mixed bedrock-alluvial reaches.

The presence of sediment cover in mixed bedrock-alluvial channels affects transport processes, with the fraction of sediment cover affecting grain entrainment, transport, and deposition. Previous work has shown that sediment particles tend to travel between sediment patches and deposit in those patches, creating a positive feedback mechanism (Ferguson et al., 2017b; Hodge et al., 2011). Grain characteristics, such as grain size and shape, also influence alluvial cover in mixed bedrock and alluvial systems. In bedrock

reaches, sediment can be transported across bedrock patches independently of grain size due to smoother bed surfaces and fewer particle-particle interactions. Transport in alluvial channels is more size-selective due to rough bed surface and complex particle interactions such as grain hiding, which also increases critical shear stress (Hodge et al., 2011). However, exceptionally large particles, such as glacial erratics, may not be transported easily in bedrock reaches (Whitbread et al., 2015). In bedrock channels, sediment patches tend to initially cluster in lower-slope areas and near other larger grains; i.e., the riverbed morphology and large grains influence the formation of sediment patches, which in turn can affect subsequent development of channel morphology (Goode & Wohl, 2010; Hodge & Hoey, 2016).

Despite extensive research on individual bedrock-alluvial reaches, our understanding of sediment transport dynamics and controls on alluvial cover at the network scale remains limited. Most previous studies have explored alluvial cover controls in single reaches at shorter timescales, typically months, without considering larger spatial and temporal scales. These studies include flume experiments (Chatanantavet & Parker, 2008; Hodge & Hoey, 2016; Johnson & Whipple, 2010; Papangelakis et al., 2021), field analysis (Ferguson et al., 2017b; Finnegan et al., 2017; Hodge et al., 2011; Inoue et al., 2014; Rennie et al., 2018; Turowski et al., 2008), or modelling (Jafarinik & Viparelli, 2020; Johnson, 2014; Lague et al., 2005; Turowski, 2018). To address this gap in understanding, it is essential to examine the feedback mechanisms between discharge, sediment supply, channel geometry and grain characteristics and their effects on alluvial cover dynamics at both reach and network scales.

Sediment connectivity within river networks is a critical concept that determines the transport efficiency and depositional patterns of sediments, influencing both small and large-scale processes (Bracken et al., 2015; Schmitt et al., 2016). Within this context, alluvial patches act as these transient storage zones, by increasing the residence time of sediments and reducing their availability for downstream transport (Czuba & Foufoula-Georgiou, 2015). In contrast, bedrock reaches tend to facilitate faster sediment transport, enhancing connectivity by minimising sediment retention. Therefore, the distribution and characteristics of bedrock and alluvial reaches within a river network are expected to directly influence the temporal and spatial dynamics of bedload sediment

connectivity. Furthermore, the direction of the alluvial patch expansion, whether upstream or downstream, is expected to vary in response to environmental conditions, such as sediment supply, flow dynamics, channel geometry, and sediment characteristics. By understanding sediment connectivity, we can explore how feedback mechanisms between channel form and sediment transport processes operate across different scales, providing insights into how small-scale processes affect large-scale patterns.

Recent sediment transport models, such as CASCADE (Schmitt et al., 2016; Tangi et al., 2019) and NetworkSedimentTransporter (Czuba, 2018; Pfeiffer et al., 2020), reproduce sediment transport processes at a network scale, providing a comprehensive understanding of sediment connectivity and transfer within river systems. These models track bed load sediment particles in the river system, depending on the hydraulics, grain characteristics, and channel morphology of reaches. Studies have used these models to analyse the effect of sediment pulses in river networks (Ahammad et al., 2021; Czuba & Foufoula-Georgiou, 2014; Gran & Czuba, 2017), hotspots for fluvial geomorphic change (Czuba & Foufoula-Georgiou, 2015), spatiotemporal changes in bed sediment thickness (Czuba et al., 2017), dam effects on sediment transport dynamics (Schmitt et al., 2018), wildfire sediment cascades (Murphy et al., 2019) and to discriminate between multi- and single-channel patterns (Bizzi et al., 2021). However, none of these studies have explored patterns of alluvial cover in a mixed bedrock-alluvial river network, despite the importance of sediment cover for landscape evolution (Whipple, 2002), river management (Toone et al., 2014), and habitat conservation.

This study aims to clarify the complex interactions among primary controls on alluvial cover within mixed bedrock-alluvial river networks by employing a combination of field data from the River Carron in the Scottish Highlands, network scale modelling using NetworkSedimentTransporter, and connectivity analysis. We use field data to parameterise the model and evaluate its performance. We create several scenarios to assess how changing sediment supply, flow depth, and grain size affect the alluvial cover patterns at the network scale. Finally, we conduct a connectivity analysis to evaluate cover transitions, fragmentation, and expansion of alluvial reaches.

5.3 Study Area

We focus on the River Carron in the northwest of the Scottish Highlands (Figure 5), a mixed bedrock-alluvial river system with available data on alluvial cover fraction, bankfull channel width, channel slope, channel depth, and discharge (Whitbread, 2015; Whitbread et al., 2015). The catchment area is 300 km². The total river network is approximately 138 km long while the main River Carron is 44 km. Bedrock reaches are generally narrower, deeper, and steeper than alluvial reaches in this system (Whitbread et al., 2015).
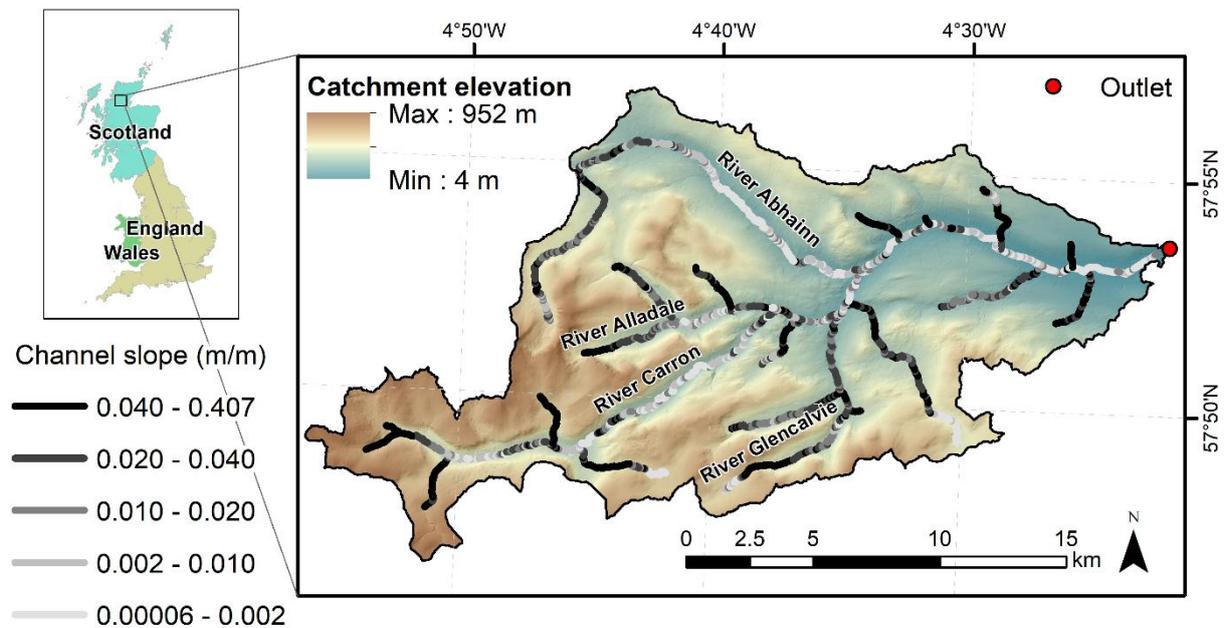
Figure 5.1: Elevation map of the Carron catchment and channel slope of the river network (white = low slope; black = high slope). The inset map shows the location of the Carron catchment in the Scottish Highlands.

The Carron catchment has a history of glaciation, with the most recent glacial activity occurring during the Last Glacial Period, ending approximately 11 ka ago (Ballantyne, 2008). The bedrock lithologies in this region exhibit moderate to high resistance to erosion. They are mainly composed of metamorphosed sandstone (psammite and

pelite), with granite in the southeast region (British Geological Survey, 2008). The superficial deposits in the catchment are mainly of glacial origin, including till and glaciofluvial sediments. However, there are localised regions covered by organic peat near the rivers and mass movement deposits near the toes of hillslopes. The main sources of sediment supply to the rivers are alluvial deposits situated in proximity to the channels, including raised alluvial terraces and debris fans associated with tributary streams, and infrequent landslides in the catchment.

5.4 Methods

We used a combination of field data collection (Section 5.4.1), sediment transport modelling (Section 5.4.2), and connectivity analysis (Section 5.4.3) to investigate controls on the spatial distribution of sediment cover, using the River Carron as a representative river network. Field data was used to approximate input parameters for the sediment transport model, which we used to explore how varying initial sediment cover, discharge, sediment supply, and grain size affected steady-state sediment cover across the network. Model outputs were compared with field data and analysed using statistical and connectivity metrics.

5.4.1 Data sources and field data collection

Channel morphology data collected by Whitbread (2015) in 2010-2011 provides measurements of sediment cover percentage, channel width, and depth for the River Carron's main channel. Further field data on grain size and sediment cover percentage were collected in September 2022 for the main channel and eight other tributaries. Grain size distributions were determined by analysing at least three photos from each of 91 gravel bars using the automated mode of PebbleCounts (Purinton & Bookhagen, 2019). The median grain size (D_{50}) across all bars was used as the default model grain size. It was found that the automatic mode of PebbleCounts decreased D_{50} by 3 mm compared to manual analysis. However, this uncertainty in the D_{50} was considered acceptable for this

study, and therefore the automatic mode was used. Sediment cover percentage was estimated in 41 reaches, each with a length of approximately 200 m. The average alluvial cover was visually estimated along 11 transects spaced every 20 m for each reach. In total, sediment cover data were collected for approximately 8 km of the channel. The sediment cover data from Whitbread (2015) and the percentage of alluvial cover collected in 2022 were used to evaluate the performance of the alluvial cover fraction resulting from the sediment transport modelling. The detailed dataset collected in 2022, including site locations, grain size (D_{50} and D_{84}), and sediment cover data, is available in Guirro et al., 2025b.

5.4.2 Sediment transport simulations

Network scale sediment transport simulations were conducted to analyse how varying initial sediment cover, discharge, sediment supply, and grain size affect the extent and spatial distribution of alluvial cover in a river network at steady state. The NetworkSedimentTransporter model (Pfeiffer et al., 2020) is a physically based model that simulates the transport and evolution of sediment parcels through a river network over time. Sediment parcels are individual units representing a group of particles with identical characteristics, such as grain size. The model tracks the movement of these parcels. Key outputs are changes in parcel locations, bed elevation, and bed slope over time. This capability facilitates the analysis of bedload sediment connectivity within the river network.

To set up the NetworkSedimentTransporter model, the river network, represented as a grid of links (river segments) and nodes (initial and end points of river segments), was constructed using the LSDTopoTools topographic analysis software package (Mudd et al., 2023) and a 5-m resolution Digital Elevation Model (DEM) sourced from the OS Terrain 5 (Ordnance Survey, 2022). A minimum drainage area threshold of 2.5 km^2 was defined to create the river network. A link length of approximately 100 m was used, as this length captures the shortest bedrock reach observed in the field by Whitbread (2015). The river network was manually adjusted at the outlet based on aerial imagery due to poorly constrained channel locations in the low-slope DEM region. Other node and link

parameters required by NetworkSedimentTransporter, such as node elevations, link lengths, and drainage areas, were also defined using the DEM and LSDTopoTools (Mudd et al., 2023). Link widths and depths were derived from power-law scaling relations based on drainage area and bankfull data from the River Carron (Whitbread et al., 2015), accounting for 86% of the spatial variation in channel width and 61% of the variation in channel depth.

The NetworkSedimentTransporter model was implemented using the open-source code (available on Github: github.com/landlab/landlab). We modified the original model to better represent the transport dynamics and to estimate the spatial distribution of alluvial cover. Four key adaptations were implemented.

The first adaptation was the determination of the percentage of the alluvial cover of each river segment. The alluvial cover develops on a non-erodible bed, with the elevation defined by the topographic elevation from the DEM. Sediment parcels with a volume of 1 m^3 were added on top of the non-erodible bed. On average, 194 parcels were required to achieve 100% coverage of one-grain diameter deep at each river segment. A fully alluvial reach can be 100% covered or more, creating layers of alluvial cover. The alluvial cover percentage (p_c) for a given river segment or link (l) was calculated using Equation 5.1.

$$p_c = \frac{V_l}{l_l \cdot W_l \cdot D_l \cdot (1-\varphi)} \times 100 \qquad \text{(Equation 5.1)}$$

where p_c is the alluvial cover percentage in link l; V_l is the volume of sediment parcels in link l (m^3); l_l is the link length (m); W_l is the link width (m); D_l is the average median grain size of sediment parcels in link l; and φ is the bed porosity, which was set as 0.3. This equation does not consider the spatial distribution of alluvial cover within a reach and the effect of bed roughness on alluvial cover.

The second modification of the model was the creation of a function to add sediment parcels into the system at each timestep. This function allows the choice of the location (river segment) to which parcels are added. In the simulations, parcels were added at the second-most upstream links in all tributaries. The most upstream link was not chosen because the upstream node elevation is fixed, preventing the links from adjusting their slope and transporting sediments. Adding sediments to the second-most upstream link

allowed the slope to adjust freely and transport sediments to downstream links. To avoid boundary effects, the two most upstream links of each tributary were excluded from further analysis.

The third modification was that a minimum transport capacity in low slope links was set to prevent bottleneck issues and ensure that the simulations could achieve a steady state in a reasonable time, i.e., in less than 2 weeks of CPU time. It was enforced that links with slopes lower than 0.002 m/m, which represent 20% of the river network, would have more than 100% cover and a transport capacity at least equal to the sediment input. This modification kept the sediment cover realistic and did not break the sediment connectivity in the system due to artificial bottlenecks. A similar approach of setting a minimum transport capacity to prevent bottleneck issues was taken by Czuba et al. (2017) and Gran & Czuba (2017).

Finally, the downstream sediment parcel movement function was modified to update the parcel velocity and transport capacity for each link traversed by a parcel. Without this modification, grains originating in steep links would maintain their high velocities even when transiting through flatter downstream links, and so traverse unrealistically long distances within a single timestep. The updated approach recalculates velocity for each link, reflecting varying hydraulic conditions, and reassesses transport capacity as parcels exit a link. These improvements prevent sediment parcels from unrealistically skipping across links, thereby improving the connectivity analysis and representation of sediment dynamics in river networks. However, the sediment transport processes are the same regardless of whether the reach is bedrock or alluvial.

The model operates by iterating through timesteps, moving parcels downstream and adjusting bed topography. The timestep length was defined as one day for the simulations. The model dynamics for each timestep is as follows:

1. Add sediment parcels into the second-most upstream link or each tributary.
2. Define active and inactive sediment parcels based on grain size and flow conditions, according to Wong et al. (2007). Active parcels determine the active layer thickness, from which parcels will be entrained.

3. Calculate the reach slope based on bed topography, which considers both bedrock topography and alluvial depth.

4. Move active parcels downstream according to the parcel velocities calculated using the Wilcock & Crowe (2003) sediment transport equation. This equation relates the dimensionless transport rate of each parcel to the ratio of bed shear stress, calculated by slope-depth product, to reference shear stress. The reference shear stress represents the critical shear stress required to initiate motion for the parcel grain size, adjusted by the effects of the median grain size of the bed surface. In our implementation, we calculated reference shear stress using a constant dimensionless reference Shield stress of 0.036. This value was achieved by setting the Wilcock-Crowe sand fraction parameter to zero, a simplification justified by our field observations showing low sand presence (Appendix A2).

5. Update parcel location of active parcels, which will change bed elevation and reach slope in the next timestep.

6. Calculate the alluvial cover percentage of each reach (Equation 5.1).

Further details on the model dynamics and model derivation can be found in Czuba (2018) and Czuba et al. (2017).

An initial exploration assessed model sensitivity to initial sediment cover, analysing its effect on the final percentage of alluvial cover of reaches at steady state. The initial sediment cover was varied from 1% to 1000% (average depths of 0.01 to 10 times D_{50}, forming up to ten layers of alluvial cover). After the sensitivity analysis, simulations were performed until steady state to investigate how parameters (initial sediment cover, flow depth, sediment input, grain size) impacted the percentage of alluvial cover on the network scale (Table 5.1). Parameters were varied individually from default values, which were initially approximated using field data for realistic scenarios, although not aiming to reproduce exact field conditions. A reach was considered to be in a steady state if the alluvial cover varied by less than 10% in 100 timesteps. Some reaches displayed regular periodic fluctuations in the sediment cover. These links are in a dynamic equilibrium but were not included in the previous steady state definition of cover changing by less than 10% in 100 timesteps. Therefore, the system was considered to be in a steady state when

the number of reaches in steady state remained constant for 100 timesteps. On average, 78% of the reaches achieved this condition in each run. To contextualize our NetworkSedimentTransport model results at steady state, we also developed a zero-order model based on transport capacity for comparison. This simpler model assumes full alluviation when a reach's transport capacity exceeds the sediment supply. Details of this comparison are provided in Appendix A5.

Table 5.1: Parameter values used in the simulations. The default values are common to all simulations apart from when the impact of that parameter is being investigated. The specific values evaluated for the initial sediment cover, flow depth, sediment supply, and grain size were modified separately for different simulations.

Parameter	Default value rationale	Default value	Values simulated
Initial sediment cover	200% due to the sensitivity analysis	194 parcels/reach on average	1%, 10%, 25%, 50%, 75%, 90%, 100%, 200%, 500%
Flow depth	Bankfull depth (H_b)	1.8 m on average	0.25 H_b, 0.5 H_b, 0.75 H_b, H_b, 1.25 H_b, 1.5 H_b, 1.75 H_b, 2 H_b
Sediment supply	Average transport capacity (Q_t) across all reaches	60 parcels/tributary	0 Q_t, 0.02 Q_t, 0.1 Q_t, 0.2 Q_t, 0.4 Q_t, 0.8 Q_t, Q_t, 1.25 Q_t, 1.7 Q_t, 2.5 Q_t, 3.3 Q_t
Grain size	Median grain size (D_{50}) measured in the field	0.10 m	0.3 D_{50}, 0.5 D_{50}, 0.7 D_{50}, D_{50}, 1.3 D_{50}, 1.5 D_{50}, 1.7 D_{50}

The default initial sediment cover for the simulations of 200%, i.e., cover depth is twice D_{50}, was chosen based on the sensitivity analysis results comparing the final percentage of alluvial cover across multiple model runs with varying initial sediment covers. Simulations starting with initial sediment covers of 200% or more found similar final alluvial cover percentages, indicating stability. In contrast, simulations with initial sediment cover below 200% showed substantial variability in the final percentage of

alluvial cover, demonstrating sensitivity to the initial conditions. We therefore include initial sediment cover in our analysis.

The default value of flow depth was set to bankfull depth, as D_{50} is expected to be mobile at bankfull conditions. Bankfull depth for each reach was estimated according to the power law channel geometry scaling relations to drainage provided by Whitbread (2015) for the River Carron. The model does not enforce flow continuity between links, because depth is specified independently per link without verifying the consistency of inflows and outflows. The model focuses on tracking sediment transport and bed topography evolution rather than full hydrodynamic routing (Czuba et al., 2017).

The default value of sediment supply was set to match the average transport capacity of the system, which is a critical threshold for sediment cover dynamics. This average transport capacity was calculated by taking the mean of the transport capacities of all reaches in the network during the first timestep, using the Wilcock and Crowe equation as implemented in the model. This calculation considered only the initial bedrock topography, not accounting for potential changes in slope due to sediment deposition. A range of simulations with low sediment supply (less than transport capacity) and high sediment supply (greater than transport capacity) were then tested (Table 5.1). Sediments were added at the top of all tributaries, instead of from hillslopes, representing sediments coming from upstream reaches and so focussing on simulating river network sediment dynamics. The number of sediment parcels input per timestep was constant across all tributaries reflecting that they all have the same upstream catchment area. Here, we use the terms "supply-limited" and "transport-limited" to describe network-scale conditions, rather than individual reach states. When the network sediment supply is less than the average transport capacity, we consider the network "supply-limited", although individual reaches may still be transport-limited. Conversely, when sediment supply exceeds average transport capacity, we consider the network "transport-limited", although some reaches may remain supply-limited. This approach allowed us to analyse how the network-scale alluvial cover adjust as overall sediment supply changes relative to the network's average transport capacity.

The default value of the grain size was equal to the D_{50} measured in the field, which was 0.1 m. Simulations were performed with a uniform grain size distribution. The parcel volume was set as 1 m³. No abrasion rate was defined, i.e., sediments did not lose size or volume when transported. The sediment density was 2650 kg/m³, and the starting location of parcels in each link was randomly defined, which is the only random parameter in the model. Four runs of the default simulation, varying only the random starting location of parcels, verified that this randomness can alter the total alluvial length in the network by ± 2%.

Alluvial cover results from all simulations were compared with field observations to assess the plausibility of the model outputs given the network's topology, rather than to precisely replicate field conditions. For the River Carron, data from Whitbread (2015) were used, while field data collected in 2022 were used for the tributaries. This comparison aimed to verify the model's ability to capture the general patterns of alluvial cover distribution within the river network. The Percentage Bias (PBIAS) was calculated to quantify the difference between the average simulated and average observed alluvial cover across the river network. The Root Mean Square Error (RMSE) and the Mean Absolute Error (MAE) quantified the error of the model's accuracy in a reach-by-reach analysis.

5.4.3 Analysis of controls on the alluvial cover: extension, spatial distribution, and connectivity of the alluvial cover

For each simulation, we assessed how the extent and spatial distribution of alluvial cover varied to investigate the impact of initial sediment cover, flow depth, sediment supply, and grain size. Reaches were classified based on the percentage of alluvial cover at steady state: <10% cover as bedrock, 10% to 99% cover as mixed, and >99% cover as alluvial. The <10% threshold for classifying reaches as bedrock was chosen to account for occasional transient sediment accumulation in bedrock reaches, ensuring reaches with temporary cover were not misclassified as mixed.

The sequence of different reach types was examined by analysing the order and transition of different riverbed categories along the river network. This involved mapping the transitions between bedrock, mixed, and alluvial reaches to understand the spatial progression of sediment cover types. By studying the frequency of these transitions, we aimed to identify patterns and factors that control the distribution and connectivity of sediment cover within the river system.

Sub-networks of each riverbed category (bedrock, mixed, alluvial) were created by selecting only reaches of the corresponding type from the overall river network. Within each sub-network, adjacent reaches of the same category were linked to form continuous sections using the weakly connected components algorithm from NetworkX (Hagberg et al., 2008; Available on Github: github.com/networkx/networkx). This algorithm identifies clusters of connected sections within the same category, allowing us to measure the total length of connected sections of the same category, and the number of these sections. This analysis provided insights into how varying channel and sediment properties influence the continuity and fragmentation of alluvial, bedrock and mixed reaches.

5.5 Results

5.5.1 Comparison of simulation results with field observation

The final alluvial cover from all simulations was compared with field observations (Figure 5.2). On a network scale, the simulation using the default parameter values specified in Section 5.4.2 (Figure 5.2b) exhibited the closest agreement to the field observation (Figure 5.2a), overestimating the total average amount of observed cover by an average of 1% (PBIAS = -1%). In contrast, the simulation with no sediment supply (Figure 5.2c) showed the poorest match with the field data (Figure 5.2a), underestimating the observed alluvial cover by an average of 40% (PBIAS = 40%). However, point-by-point comparisons revealed substantial local variance between simulations and the field data. Both the best-performing and worst-performing simulations showed a wide spread of errors at

specific locations (Figures 5.2d and 5.2e). For the best-performing simulation, the RMSE was 0.48, and the MAE was 0.36. This result indicates that while the model accurately captured the average network-scale alluvial cover, its accuracy at predicting cover at discrete locations was limited. Despite these location-specific discrepancies, the model adequately represented the overall pattern of alluvial cover on the network and is thus suitable for investigating the processes controlling alluvial cover on a network scale.

In general, the simulations that closely matched the field observations had high values of initial sediment cover (> 200%) and intermediate values of flow depths (1 to 1.5 bankfull depth), sediment supply (0.75 to 1.25 transport capacity), and grain size (0.75 to 1 times field D_{50}) (Figure 5.2f). Among these, sediment supply was the most influential parameter affecting model performance, with the no-supply simulation performing the worst compared to the field data.
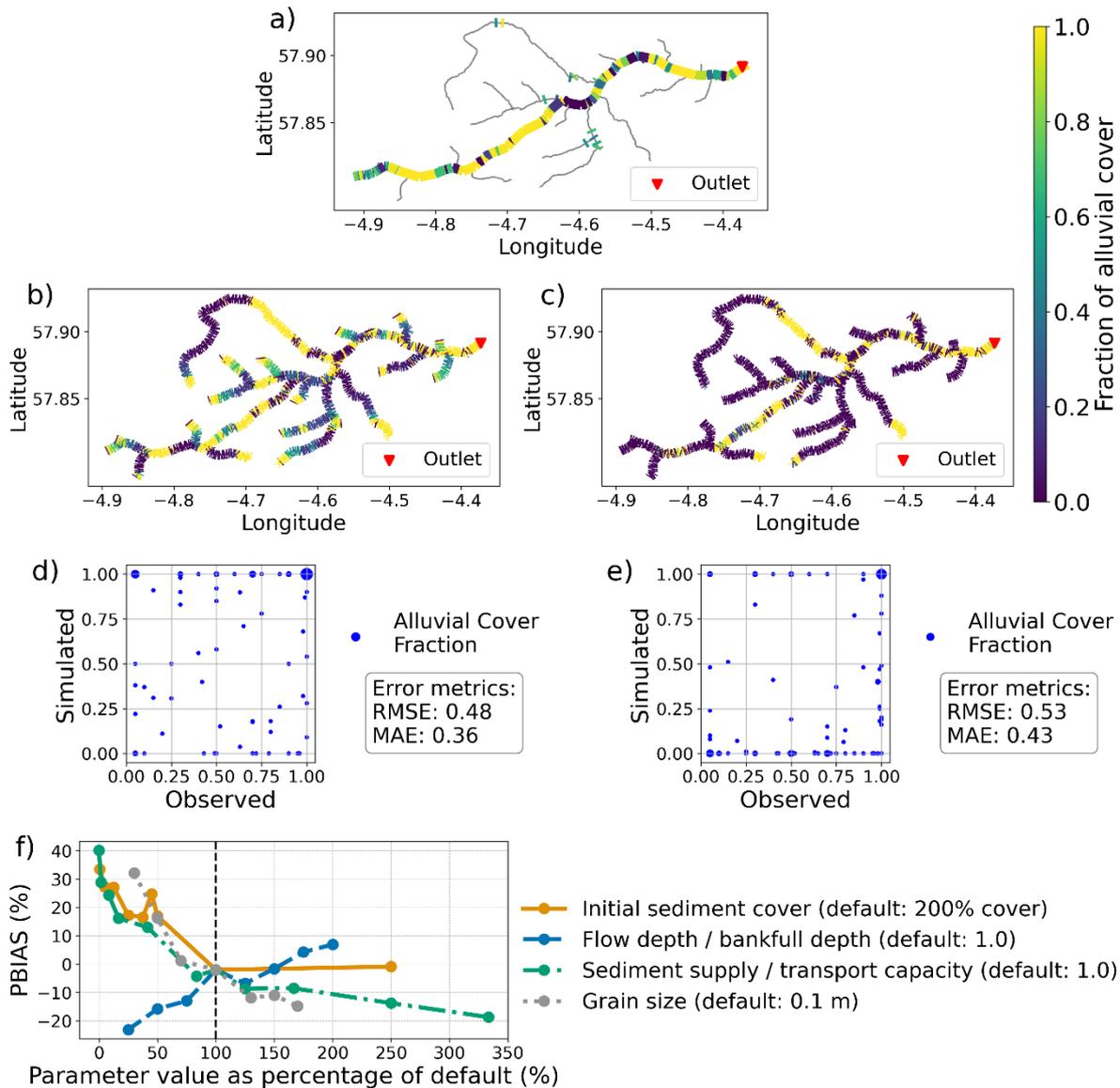
Figure 5.2: Comparison of model results and field observations. Spatial distribution of the alluvial cover fraction: a) Observed in the River Carron (data from Whitbread, 2015, for the main channel, and fieldwork conducted in 2022 for tributaries); b) Best-performing simulation, with default parameter values specified in Section 5.4.2 and PBIAS = -1%; c) Worst-performing simulation, with no sediment supply and PBIAS = 40%. Scatter plots of observed and simulated alluvial cover fraction for (d) best-performing and (e) worst-performing simulation. The size of the blue points indicates the number of reaches at each location, with larger points representing more reaches. The smallest point represents one reach, while the largest point represents eleven reaches. The root mean square error (RMSE) and the mean absolute error (MAE) quantify the error in the model's accuracy; f) Percentage bias (PBIAS) fit between the average simulated alluvial cover fraction and the average observed field data for all simulations. A value of 100% on the x-axis indicates the parameter's default value, as detailed in the legend and Table 5.1. Values below or above 100% represent reductions or increases from this reference value, representing different simulations.

5.5.2 Controls on the alluvial cover

The percentage of alluvial cover in the river network at steady state increased with higher initial sediment cover, sediment supply, and grain size (Figures 5.3a, 5.3c, 5.3d and 5.4), but decreased with increased flow depth (Figures 5.3b and 5.4). The proportion of alluvial reaches was most sensitive to flow depth, particularly when depth was less than bankfull (Figure 5.4). The influence of flow depth exhibited a threshold behaviour, with the greatest variations in sediment cover occurring when flow depth was less than bankfull depth (Figures 5.3b and 5.4). Beyond this threshold, additional increases in flow depth resulted in marginal changes in alluvial cover, highlighting the system's reduced sensitivity to excess flow depth. Grain size also demonstrated a threshold behaviour (Figure 5.4). Below a critical size (around the median size of 0.1 m found in Carron catchment), smaller grain sizes severely limited the alluvial cover, as they were easily transported downstream. Above this threshold, increases in grain size had minor effect on further alluvial cover formation.

The overall increase in alluvial reaches with increasing sediment supply was gradual (Figure 5.4). However, the development of bedrock reaches (cover < 10%) and mixed reaches (cover between 10 and 99%) showed a threshold behaviour (Figure 5.3c). Simulations with low sediment supply, particularly below the river network's average transport capacity, resulted mostly in reaches with either 100% or 0% cover, inhibiting mixed reaches. As sediment supply increased towards the system's transport capacity, mixed reaches became more common. Beyond this threshold, further increases in sediment supply had minor impact on the formation of bedrock, mixed and alluvial reaches (Figure 5.3c).
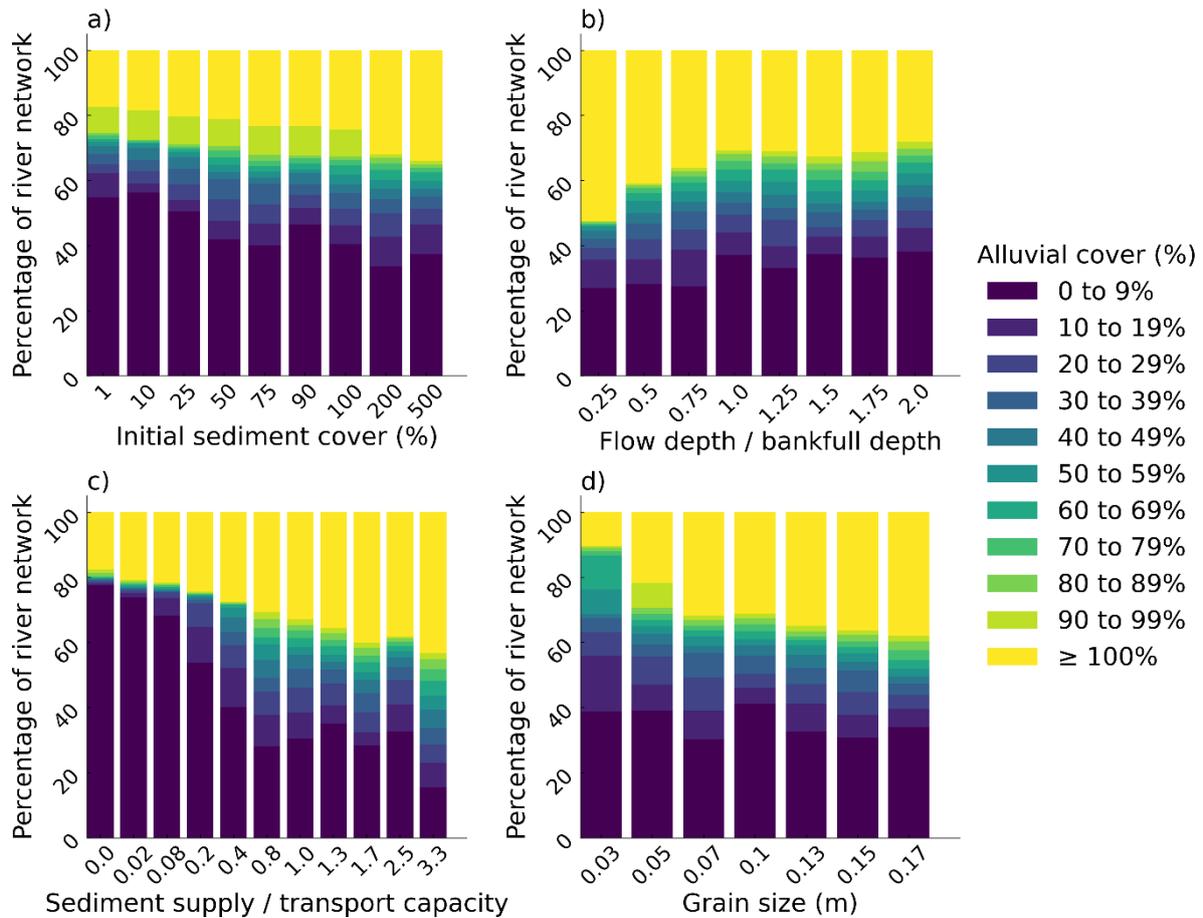
Figure 5.3: Influence of parameter values on alluvial cover in a steady-state river network. The analysed parameters include: a) initial sediment cover (e.g., 100% indicates a completely covered riverbed and 500% indicates a sediment depth equivalent to five times D_{50}); b) flow depth relative to bankfull depth; c) sediment supply in relation to the river network's average transport capacity; and d) uniform grain size. Each bar represents a simulation outcome. All other parameters were maintained at default values. Note: The x-axis is unscaled.
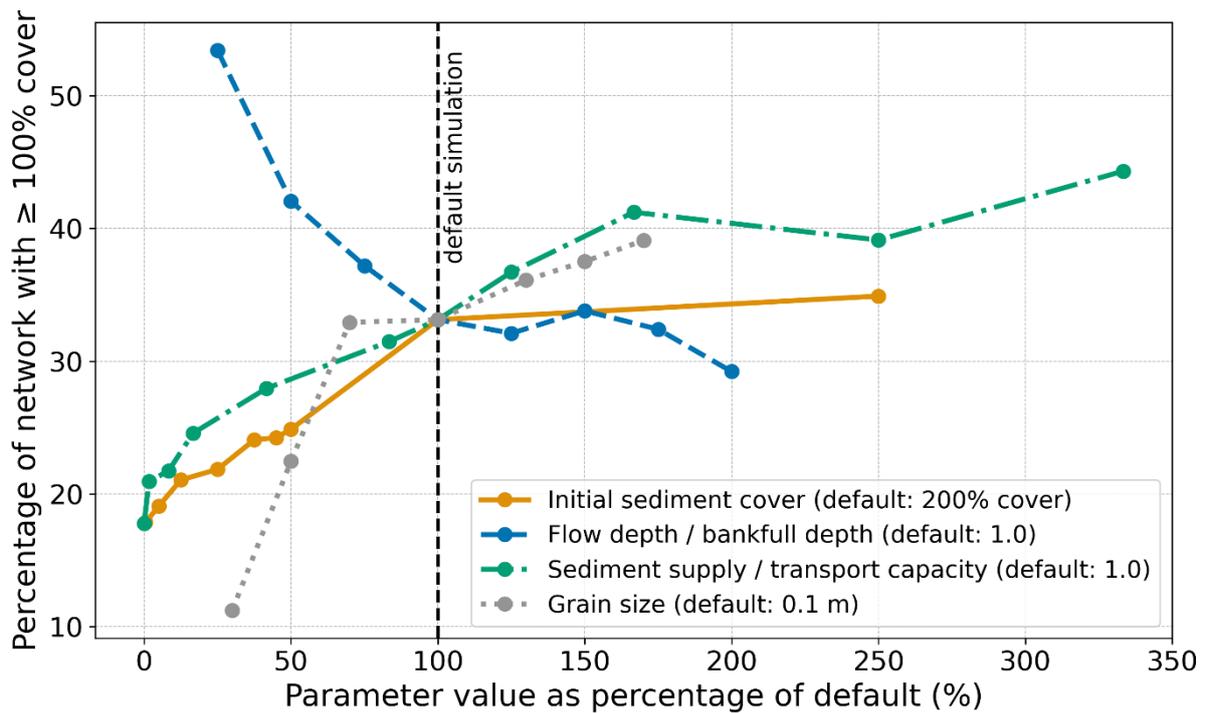
Figure 5.4: Sensitivity analysis of parameters influencing the percentage of network reaches with ≥ 100% alluvial cover. A value of 100% on the x-axis indicates the parameter's default value, as detailed in the legend and Table 5.1 and highlighted by the dashed vertical line. Values below or above 100% represent reductions or increases from this reference. Differences up to 2% in the percentage of network with ≥ 100% cover are in the range affected by the randomness of the model as discussed in section 5.4.2.

In addition to the total amount of sediment cover, analysing its spatial distribution across the network is also important for understanding river system dynamics. Spatial variations in alluvial cover under distinct channel and sediment simulations revealed that higher initial sediment cover and supply, along with larger grain sizes and reduced flow depth, tended to increase the number of alluvial sections (Figure 5.5 and Appendix A3), which provides videos demonstrating the variation in steady state sediment cover across the range of all parameter values). The threshold parameter value at which each river segment transitioned from a non-alluvial state in one run to an alluvial state in another run (defined as > 99% cover) was identified (Figure 5.6). Under extreme scenarios, such as minimum initial sediment cover, no sediment supply, smallest grain size, and highest flow depth, some alluvial reaches were still formed (Figure 5.6). As parameter values changed to favour sediment deposition, new alluvial segments generally connected to

existing alluvial reaches, leading to the elongation of continuous alluvial sections rather than the formation of additional small, fragmented sections. This indicates that the growth in the total length of alluvial cover primarily occurs through the expansion of existing alluvial sections.
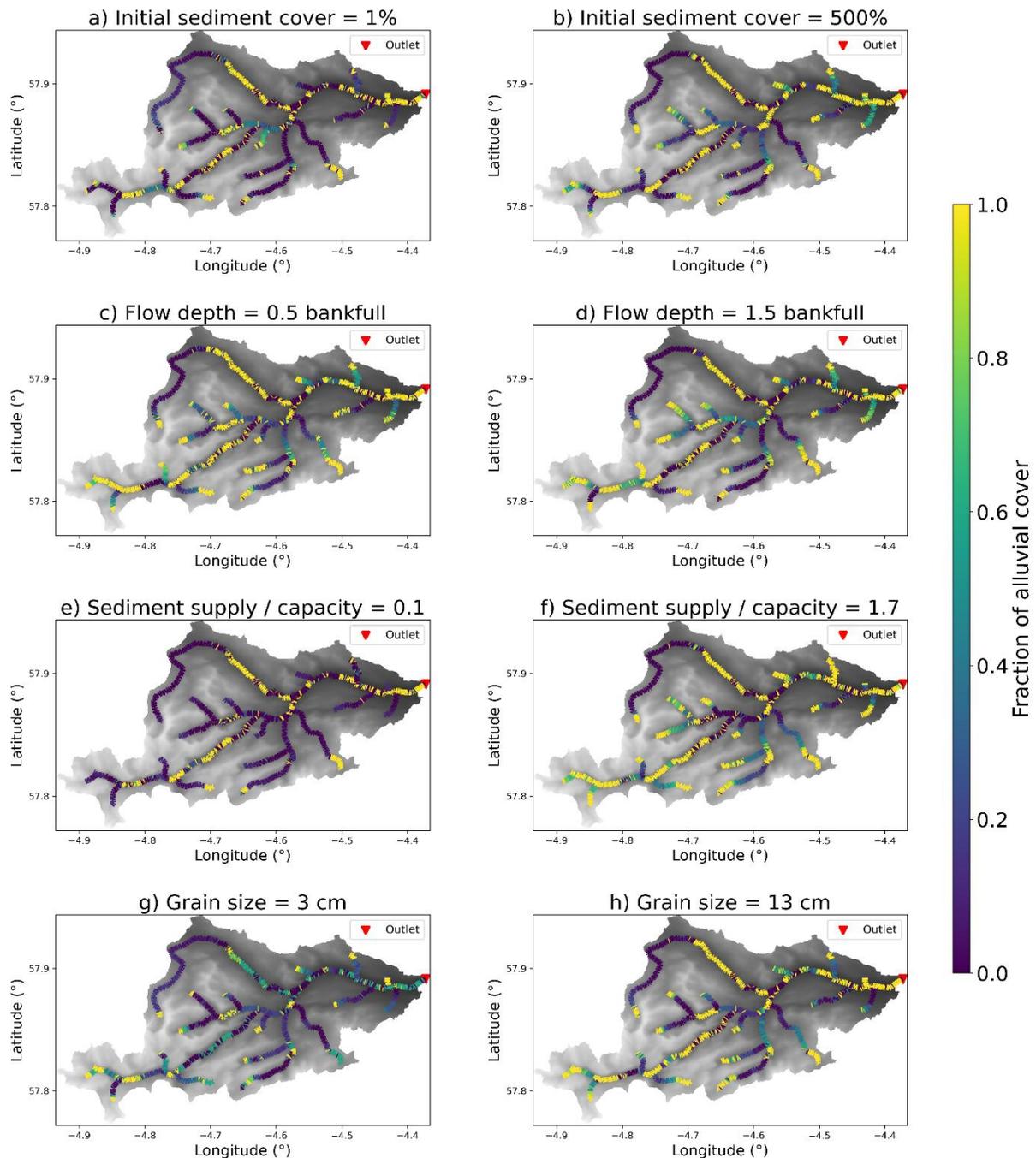
Figure 5.5: Spatial variations of the cover fraction at steady state. Each figure indicates different parameter values: a) low initial sediment cover (1%) versus b) high initial

sediment cover (500%, equivalent to five layers); c) reduced flow depth (0.5 bankfull) versus d) increased flow depth (1.5 bankfull); e) limited sediment supply (0.1 of transport capacity) versus f) high sediment supply (1.7 of transport capacity); and g) small grain size (0.03 m) versus h) large grain size (0.13 m). Elevation ranges from 4 m (in black) to 952 m (in white). Additional simulation results for all parameter values are presented in Appendix A3.
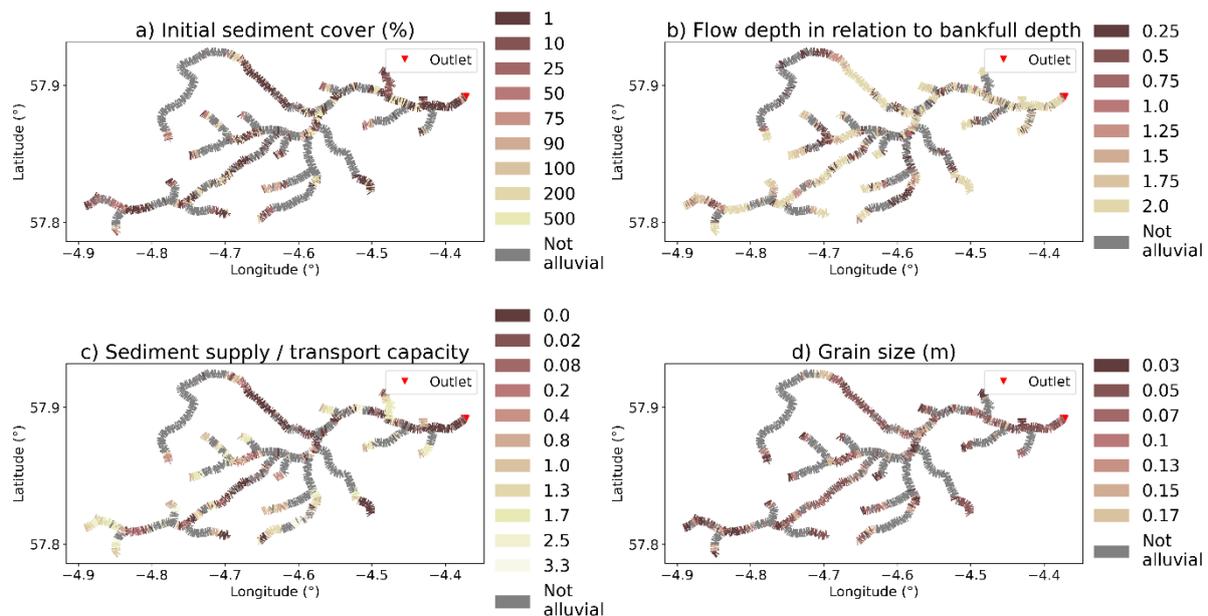
Figure 5.6: Threshold values of parameters required to achieve full alluviation (> 99% cover) in each river segment, demonstrating how different reaches become fully alluvial at different parameter values. Each panel shows the threshold value for a different parameter: a) initial sediment cover (%); b) flow depth relative to bankfull depth; c) sediment supply relative to transport capacity; and d) grain size (m). The colour of each river segment indicates the minimum parameter value at which that segment becomes fully alluvial. For example, in (a), dark brown segments become fully alluvial at just 1% initial cover, while lighter colours require higher initial cover to become fully alluvial. River segments labelled as "Not alluvial" (in grey) never achieved full alluviation under any simulated parameter value, indicating persistent bedrock exposure.

To assess the controls on alluvial cover formation, we consider the slopes of reaches that developed alluvial cover in each simulation. The slopes of alluvial reaches (cover fraction > 99%) were generally higher with decreased flow depth, increased sediment supply, larger grain size, and higher initial sediment cover (Figure 5.7). Threshold behaviour was again observed, with lower sensitivity of alluvial reaches to slopes at flow depths exceeding bankfull and at sediment supplies exceeding transport capacity. The

occurrence of steep alluvial reaches in the 0.03 m grain size simulation was due to the small number of alluvial reaches, which were primarily formed in the tributary heads due to their proximity to the sediment supply source.
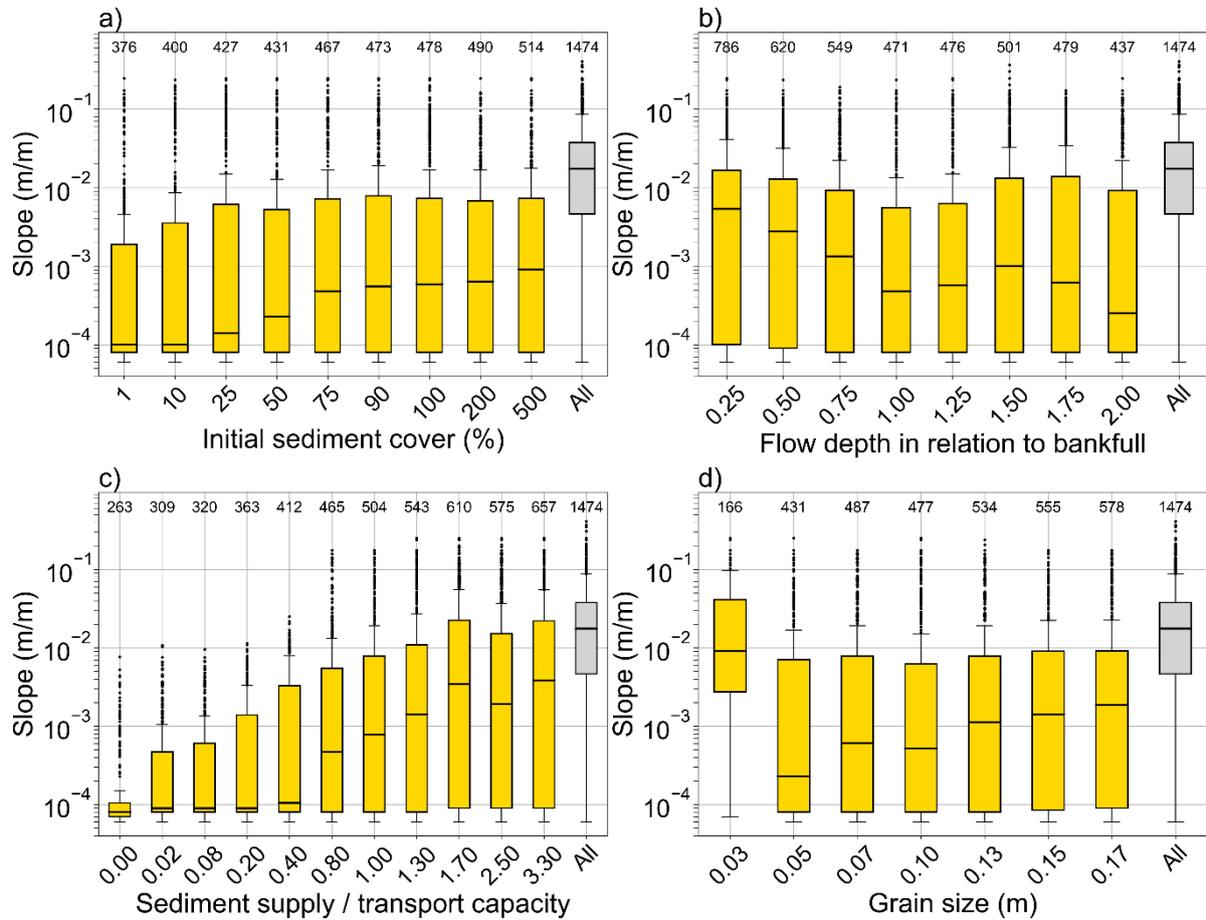
Figure 5.7: Channel slopes of all alluvial reaches (i.e., cover fraction > 99%) for each simulation in steady state, when varying the parameters: a) initial sediment cover; b) flow depth relative to bankfull depth; c) sediment supply relative to transport capacity; and d) grain size. Each box plot represents a simulation initiated with the respective parameter value. All other parameter values were maintained at default values. The grey bar refers to the initial slope of all reaches in the network, which is independent of the simulation. The numbers at the top of each boxplot indicate the number of alluvial reaches.

Figure 5.8 complements Figure 5.7 by presenting the distribution of slopes of reaches that became alluvial (i.e., cover fraction > 99%) compared to the simulation with the

previous parameter value. The transition to an alluvial state occurred across a range of slopes, revealing distinct patterns between the different parameters (Figure 5.8). As sediment supply increased up to the transport capacity threshold, steeper reaches achieved alluvial cover (Figure 5.8c). However, beyond this threshold, additional sediment supply did not result in steeper reaches becoming alluvial, indicating that slope did not control the formation of new alluvial reaches once the transport capacity was exceeded. The relation between flow depth and the slope of reaches achieving alluvial cover showed a complex pattern (Figure 5.8b). When starting from bankfull flow depth, decreasing flow depth facilitated the achievement of steady-state alluvial cover on steeper reaches (Figures 5.7b and 5.8b). However, this trend was not consistent at higher flow depths. For initial sediment cover values above 1%, there is a general trend of reaches with lower slopes attaining alluvial cover as initial sediment cover increases (Figure 5.8a). However, this relationship is not strictly monotonic, with some fluctuations observed, particularly between 75% and 100% initial cover. For grain size values above 0.03 m, increasing the grain size increased the slope of the additional alluvial reaches (Figure 5.8d). The patterns for initial sediment cover, flow depth, and grain size (Figures 5.8a, 5.8b, and 5.8d) were less pronounced compared to the clearer trend observed for sediment supply (Figure 5.8c).
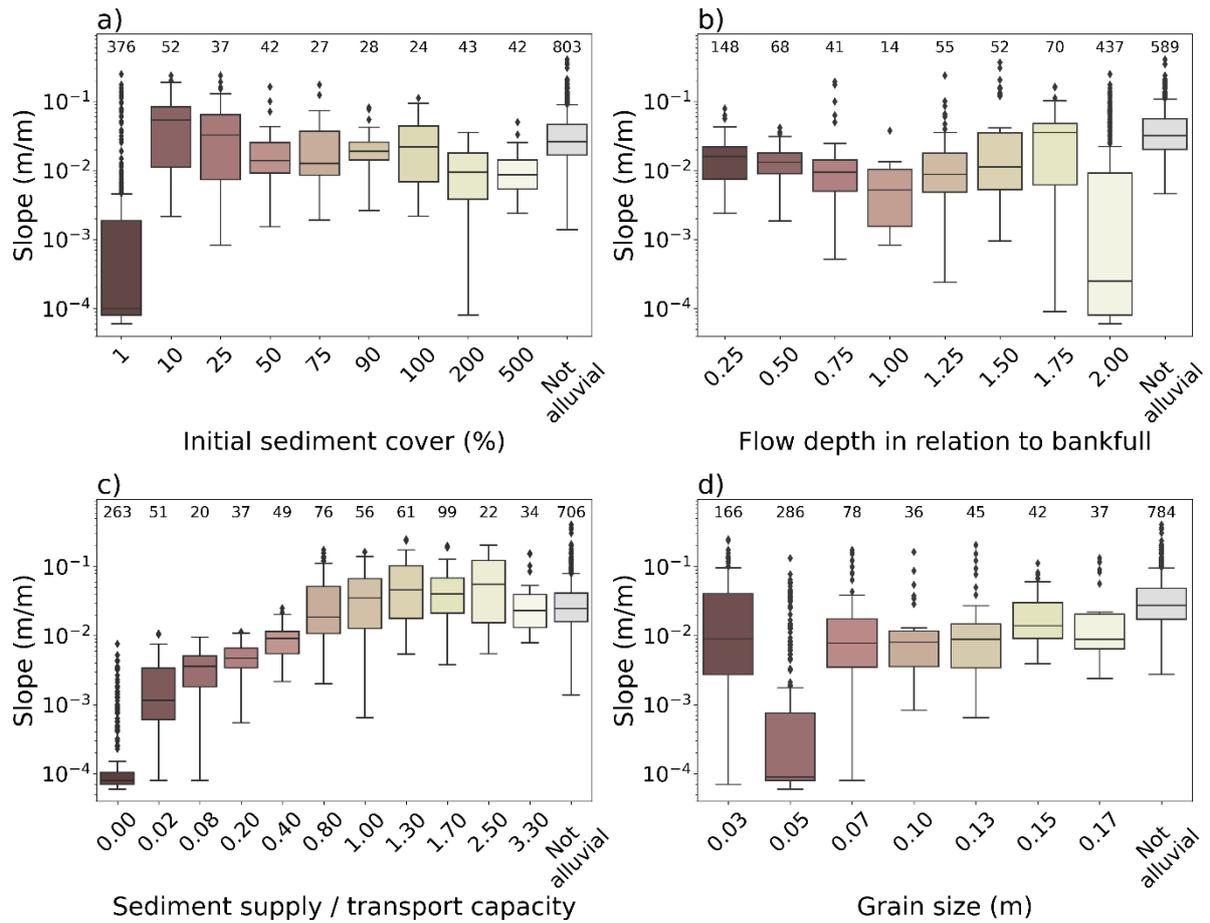
Figure 5.8: Box plot of channel slopes for newly formed alluvial reaches (i.e., cover fraction > 99%) at steady state under varying parameters: a) initial sediment cover; b) flow depth relative to bankfull depth; c) sediment supply relative to transport capacity; and d) grain size. Each box plot represents the slopes of new alluvial reaches formed in the specific simulation compared with the previous simulation with lower parameter values. The simulations with 1% initial sediment cover, 2 times bankfull flow depth, no sediment supply, or 0.03 m grain size represent extreme conditions where fewest river segments achieved alluvial cover. The numbers at the top of each box plot indicate the number of new alluvial reaches formed in that specific simulation. The colour of each box indicates the threshold value of the parameter required for that reach to become alluvial: darker colours represent lower threshold values (i.e., reach that become alluvial more easily), while lighter colours represent higher thresold values. The "Not alluvial" box (in grey) shows the slopes of the reaches that never achieved an alluvial state across all simulations.

The results show that channel slope is a determining factor in the formation of alluvial reaches (Figures 5.7 and 5.8). In general, decreasing flow depth and increasing initial sediment cover, sediment supply, and grain size caused increasingly steeper reaches to

become alluvial. The slope played a critical role in controlling the locations of alluvial cover formation, especially when the sediment supply was below the river network's average transport capacity. For instance, with a sediment supply of 0.4 times the transport capacity, the median slope of alluvial reaches was around 0.0001 m/m, while at 0.8 times the transport capacity, the median slope increased to around 0.0005 m/m (Figure 5.7c). These findings demonstrate that steeper gradients can support greater sediment deposition when sediment supply is increased up to the transport capacity of the river. However, beyond the transport capacity threshold, other factors have a major influence on alluviation, as evidenced by the lack of further increase in the slope of alluvial reaches with additional sediment supply (Figure 5.8c).

5.5.3 Connectivity of reach cover types

An important aspect of the spatial pattern of sediment cover is whether alluvial reaches are adjacent to other alluvial reaches or are more likely to alternate with bedrock sections. Analysis of the transition probabilities between adjacent upstream and downstream reaches showed that reaches were most likely to maintain their cover type between sequential 100 m reaches in each simulation (Figure 5.9). The probability of transitioning from bedrock to bedrock, mixed to mixed, or alluvial to alluvial reaches was around 80%, while the probability of transitioning between different cover types was generally lower than 20% (Figure 5.9). This low probability of transition between different reach types means that the total length of most alluvial, mixed, or bedrock sections was longer than 100 m. Transitions to another cover category were more common in simulations with low initial sediment cover, flow depth, sediment supply, and grain size. Specifically, low initial sediment supply and grain size values increased transitions from alluvial to mixed bedrock-alluvial reaches (AL to BR-AL), hindering the formation of long continuous alluvial sections (Figures 5.9a and 5.9d). Similarly, low flow depth and sediment supply values increased transitions from mixed bedrock-alluvial to bedrock reaches (BR-AL to BR), limiting the development of extensive mixed bedrock-alluvial sections (Figures 5.9b and 5.9c). Direct transitions from alluvial to bedrock reaches or

vice versa (AL to BR or BR to AL) were less common. The transition matrix for the default simulation is shown in Table 5.2.
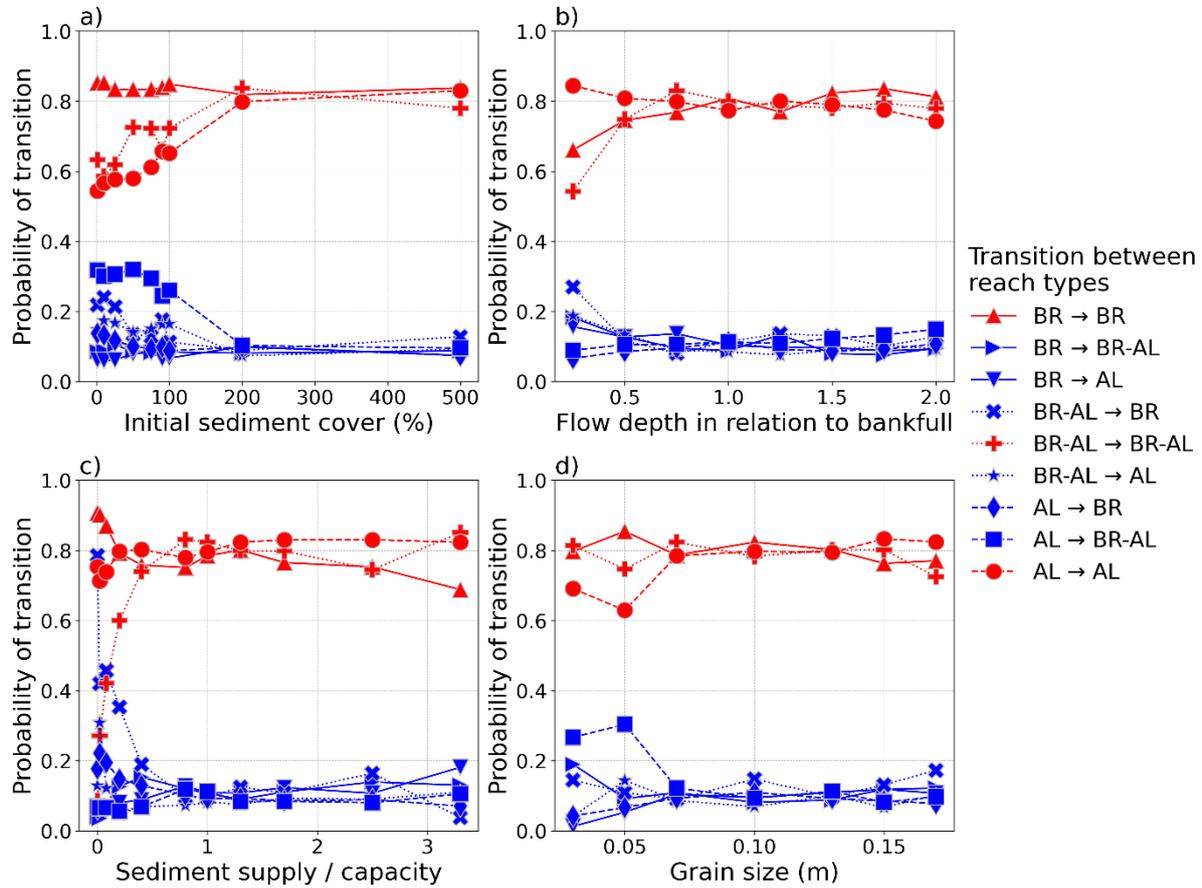
Figure 5.9: Probability of transition of cover categories between adjacent reaches of 100 m for each simulation that varied the parameters: a) initial sediment cover; b) flow depth relative to bankfull depth; c) sediment supply relative to transport capacity; and d) grain size. In the legend: "BR" denotes bedrock reaches with < 10% cover; "BR-AL" represents mixed bedrock-alluvial reaches with 10%-99% cover; "AL" denotes alluvial reaches with > 99% cover. The colours demonstrate the continuity between the same cover (in red) and the change to another cover type (in blue).

Table 5.2: Probability of transition matrix of cover type from one reach to the next reach downstream for the default simulation. This matrix shows the probability of transitioning from one cover type (rows) to another (columns) in adjacent downstream reaches. "AL" stands for alluvial, "BR-AL" for mixed bedrock-alluvial, and "BR" for bedrock reaches. The "n" column indicates the number of reaches each type in the network.

From/to	BR	BR-AL	AL		n
BR	0.82	0.08	0.10		498
BR-AL	0.09	0.84	0.07		505
AL	0.10	0.10	0.80		511

The analysis of continuous cover section length and fragmentation across different cover types (bedrock, mixed, and alluvial) provides insights into the persistence and spatial organization of these sections within the river network (Figure 5.10). As initial sediment cover and sediment supply increased, the fragmentation of alluvial and mixed sections decreased, resulting in longer average lengths (Figures 5.10b and 5.10d). However, increasing sediment availability had contrasting effects on bedrock sections: initial sediment cover had minimal impact on average length (Figure 5.10b), while increased sediment supply significantly reduced bedrock section length, from 1 to 0.2 km on average (Figure 5.10d). Greater flow depths reduced the fragmentation of bedrock and mixed sections by increasing their length, while increasing the fragmentation of alluvial sections (Figure 5.10c). Grain size had minor effects on section characteristics compared to other parameters, with alluvial sections slightly lengthening with larger grains while bedrock and mixed sections maintained relatively constant lengths (Figure 5.10e). These findings indicate that sediment availability and flow conditions are the main controls on the connectivity of cover sections, particularly the promotion of long bedrock sections under low sediment supply conditions. A similar connectivity analysis comparing the main River Carron field data to simulation results is presented in Appendix A4, providing further information into the model's performance in replicating observed cover patterns. This analysis shows that the model generally produced connectivity trends observed in the field, but it tended to produce shorter and more sections for all cover types compared to field observations.
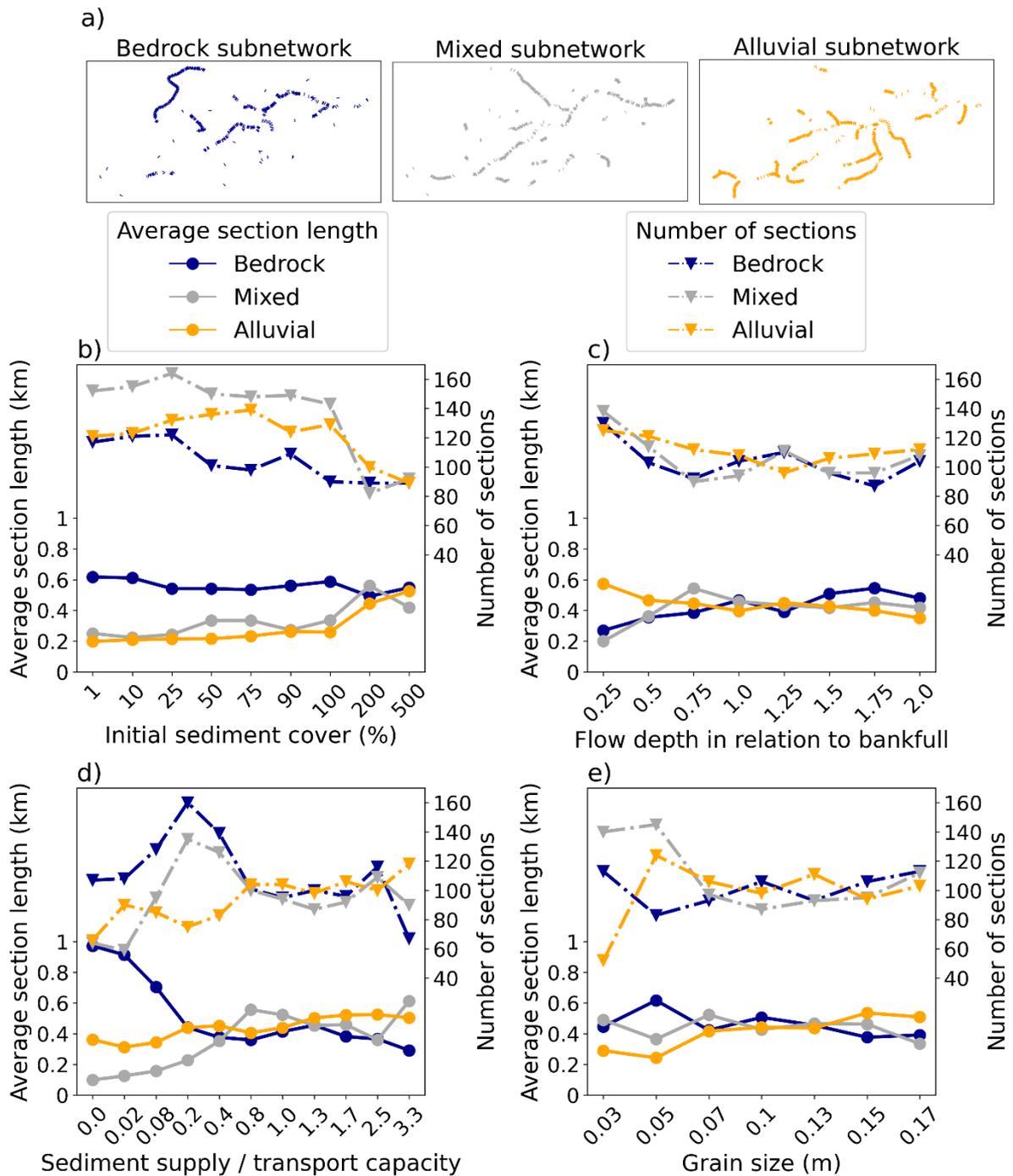
Figure 5.10: Length and fragmentation of cover sections. a) Examples of subnetworks for each cover category (bedrock, mixed, or alluvial) from the default simulation. Variation in average section length and number of sections of each cover category under different simulations that varied the following parameters: b) initial sediment cover; c) flow depth relative to bankfull depth; d) sediment supply relative to transport capacity; and e) grain size.

The slope of the river profile and the sediment supply location control the direction of the alluvial extension between model runs (Figure 5.11). Alluvial sections predominantly expanded in the direction of increasing slope, producing downstream expansion in reaches with convex profiles (as highlighted by the dashed boxes in Figure 5.11) and upstream expansion in reaches with concave profiles (as highlighted by the dotted boxes in Figure 5.11). River segments characterised by uniform slope and no concavity displayed a tendency towards fragmented alluvial formation without a distinct direction in alluvial expansion. The longitudinal profiles further revealed that the sediment supply location in the most upstream reach of each tributary produced an elongation of alluvial sections in the downstream direction near headwater nodes. In the simulations tested, this upstream sediment supply location affected alluviation up to 2 km downstream when there was a high sediment supply.
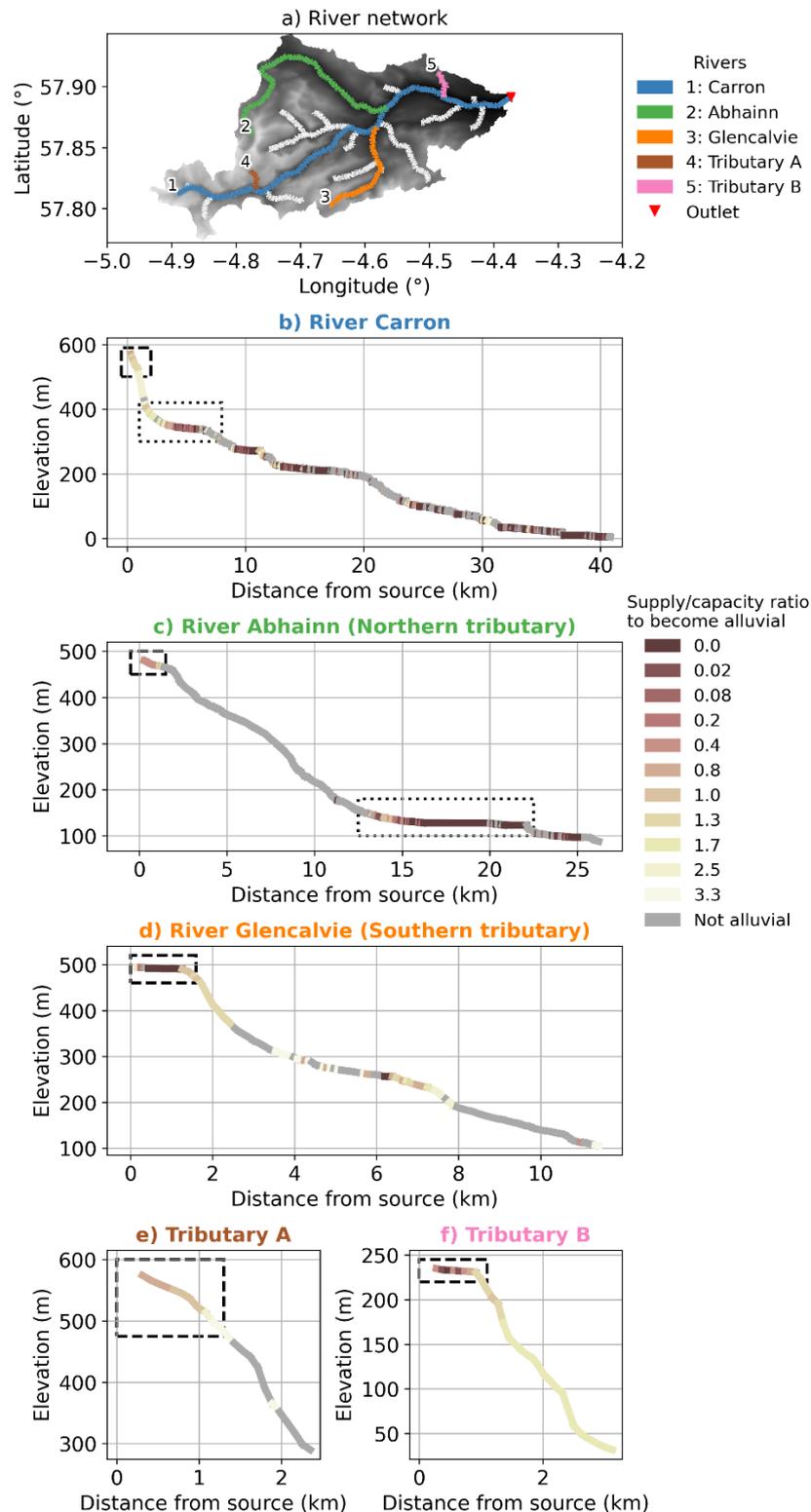
Figure 5.11: Longitudinal river profiles showing the sediment supply to transport capacity ratio required for reaches to become alluvial. A) Location of the river profiles analysed. River profiles of: b) main river Carron; c) northern tributary Abhainn; d) southern tributary Glencalvie; e) small tributary A; and f) small tributary B. Colours indicate the minimum supply/capacity ratio at which each reach becomes fully alluvial (>99% cover), with

darker colours representing reaches that become alluvial at lower supply/capacity rations and lighter colours require higher rations. Gray indicates reaches that never become fully alluvial in our simulations. Dashed boxes indicate areas where alluvial cover extends downstream as sediment supply increases and dotted boxes indicate indicate upstream alluvial expansion as sediment supply increases. Note that the downstream expansions near headwater nodes were influenced by the proximity of the sediment supply location.

5.6 Discussion

5.6.1 Spatial distribution and extent of alluvial cover

Our network-scale modelling reveals complex interactions between channel slope, discharge, and sediment supply that control the spatial distribution and extent of alluvial cover in mixed bedrock-alluvial river systems. These interactions can be understood through the concepts of transport-limited and supply-limited conditions, providing insights beyond previous reach-scale studies. We found that channel slope primarily controlled the spatial distribution of alluvial cover, especially when the network was under supply-limited conditions (Figures 5.6, 5.7 and 5.8). Reaches with lower bedrock slopes were more likely to achieve alluvial cover, while steeper bedrock reaches remained sediment starved. This finding extends previous reach-scale studies that also indicated preferential sediment deposition in topographic lows (Chatanantavet & Parker, 2008; Hodge & Hoey, 2016; Johnson & Whipple, 2010). Our network-scale approach demonstrates how these processes influence alluvial cover patterns across a full range of slope variations within an entire river network. We found that even under simulations with very low sediment availability, reaches with slopes of 0.0001 m/m or lower consistently tended to become alluvial (Figure 5.7). While reach-scale studies have shown that alluvial cover depends primarily on the local supply-to-capacity ratio (Chatanantavet & Parker, 2008), our network-scale perspective demonstrates how sediment redistribution across the network can maintain alluvial cover in low-slope reaches even when overall sediment supply is low.

While slope controlled the spatial distribution of alluvial cover, particularly in supply-limited conditions, the overall extent of alluvial cover was highly sensitive to changes in

sediment supply and discharge. As sediment supply increased within supply-limited conditions, reaches with greater bedrock slopes became progressively covered, indicating that sediment supply controlled the extent of alluvial cover, while bedrock slope controlled its spatial distribution. These observations align with reach-scale flume experiments that reported a positive correlation between sediment flux and alluvial cover extent (Chatanantavet & Parker, 2008; Johnson & Whipple, 2010; Papangelakis et al., 2021). However, our network-scale approach found a critical transition: in transport-limited conditions, where sediment availability exceeded the network's transport capacity, the underlying bedrock slope exerted less influence on the spatial distribution of alluvial cover. Increasing sediment supply above the network's transport capacity led to the formation of new alluvial cover in reaches with similar underlying bedrock slopes to existing alluvial reaches, rather than alluvial cover developing on steeper bedrock slopes. This shift signifies a move towards a system in which sediment cover dynamics are controlled more by sediment availability than by the underlying bed topography. Understanding this transition from slope-controlled to sediment supply-controlled dynamics can improve predictions of landscape evolution in mixed bedrock-alluvial river networks (e.g., Lague, 2010; Shobe et al., 2017; Zhang et al., 2015) by incorporating the spatial variability and process interactions observed at the network scale.

Additionally, in transport-limited conditions, the overall extent of alluvial cover became less sensitive to changes in sediment supply and discharge. Our simulations revealed a threshold behaviour in the influence of flow depth on alluvial cover extent (Figure 5.4). The effect of sediment supply was more complex: while the overall increase in alluvial cover with sediment supply was gradual (Figure 5.4), there was a threshold behaviour in its influence on the extent of bedrock and mixed reaches (Figure 5.3c). In supply-limited conditions, alluvial cover was highly sensitive to changes in flow depth, while the formation of bedrock and mixed reaches was primarily controlled by sediment supply. However, in transport-limited conditions, further increases in flow depth and sediment supply resulted in marginal changes in alluvial cover extent, suggesting the river's sediment transport had approached maximum efficiency. This non-linear response indicates two distinct regimes: a supply-limited space where the extent of bedrock and alluvial reaches are highly sensitive to changes in controlling parameters, and a

transport-limited space where sensitivity is decreased. These findings indicate that both the magnitude of channel parameters and the regime in which variation occurs affect alluvial and bedrock distributions.

Even at sediment supply rates exceeding three times the average network's transport capacity, our results show that a fully alluviated bed did not develop across the network. This finding contradicts reach scale analyses (e.g., Chatanantavet & Parker, 2008; Cho & Nelson, 2024b) that achieved full alluviation under high sediment supply. In our network-scale model, individual reaches can remain supply-limited even when overall sediment supply exceeds the network's transport capacity due to the varying slope distribution within the network. The River Carron, with slopes ranging from 0.0004 to 0.4 m/m, exemplifies this variability (Figure 5.1). Consequently, both supply-limited and transport-limited reaches coexist within the network, preventing complete alluviation despite high overall sediment supply. This result suggests limitations in the system's capacity to distribute sediment effectively and indicates that river channels can maintain a mixed bedrock-alluvial state over long periods. The persistence of bedrock exposure despite high sediment supply rates challenges assumptions of complete alluviation, necessitating models to capture such non-linear dynamics at the network scale.

5.6.2 Connectivity and fragmentation of alluvial cover

Our simulations indicate that channel slope significantly influences alluvial cover connectivity, particularly under supply-limited conditions. The distribution of slopes within the network controls the fragmentation of alluvial reaches. Clusters of gentler slopes support more continuous cover, whereas networks with interspersed steep and gentle slopes result in more fragmented alluvial cover (Figures 5.7, 5.8 and 5.12). Among the parameters analysed in this study, we found that sediment supply particularly affects the connectivity of bedrock sections, with long bedrock sections under low sediment supply conditions (Figure 5.10). As sediment supply increased, the fragmentation of alluvial and mixed sections decreased, resulting in longer average covered lengths. Therefore, we observed a transition from slope-controlled to supply-controlled alluvial connectivity as sediment supply increased above the network's transport capacity. This

finding extends previous research by demonstrating how slope and sediment supply varies across a river network. While studies such as Massong & Montgomery (2000) and Whitbread et al. (2015) also identified slope as an important factor in alluvial distribution through field data analyses, our simulations verify the effect of hydraulic and sediment supply dynamics in alluvial cover connectivity under various conditions. However, channel width and lithology, not included in our model, could also influence alluvial cover patterns. While wider channels often support more extensive alluvial cover (Massong & Montgomery, 2000; Whitbread, 2015), some studies did not find this relation (Buckley et al., 2024; Montgomery & Gran, 2001). Lithology can also affect channel geometry and sediment availability (Buckley et al., 2024; Massong & Montgomery, 2000), potentially modifying the distribution and connectivity of alluvial sections across the network.

Longitudinal profile analysis (Figure 5.11) demonstrated that the direction of alluvial cover expansion is controlled by local slope patterns. Alluvial patches initially form in low slope sections and tend to expand in the direction of increasing bed gradient. This results in downstream expansion in convex sections and upstream expansion in concave sections as sediment supply and grain size increase or discharge decreases. This slope dependence could be used to predict the location of expansion or reduction of alluvial cover, depending on the variation of channel parameters. Therefore, slope is important for identifying hotspots of potential alluvial cover change. Identifying such hotspots based on slope aligns with the approach used by Czuba & Foufoula-Georgiou (2015), who mapped geomorphic change hotspots based on where sediment accumulates and persists over time. Our study suggests that these areas of accumulation can be predicted by slope patterns in the network.

Persistent and elongated alluvial sections have important implications for habitat conservation and landscape evolution dynamics. Continuous alluvial sections act as storage zones, temporarily retaining sediment and delaying its downstream transfer. This sediment delay affects the connectivity and timing of sediment fluxes through the network, potentially decoupling upstream sediment sources from downstream transport and deposition patterns. In contrast, extensive bedrock sections promote rapid sediment flux, enhancing downstream connectivity and being more susceptible to active incision,

thus controlling landscape evolution. Stable alluvial patches have significant ecological implications, as they create diverse habitats by varying substrate composition, supporting a wide range of species (Buffington et al., 2004; Steiger et al., 2005; Wohl, 2015b). In contrast, bedrock patches limit habitat diversity and are often unsuitable for spawning habitats of certain species, such as salmonids, due to high transport capacity and low sediment availability (Buffington et al., 2004). Therefore, understanding the distribution of bedrock and alluvial patches is crucial for predicting habitat availability and quality within river networks.

The transition probability matrix (Table 5.2) revealed a high likelihood of reaches maintaining their cover type (bedrock, mixed, or alluvial) over consecutive 100-meter segments under default conditions. To the best of our knowledge, this method provides a novel approach for quantifying and comparing the spatial dynamics of alluvial cover across different mixed bedrock-alluvial river networks. Transition probability matrices have been used to explore the spatiotemporal evolution of land use and cover (Keshtkar & Voigt, 2016; Nath et al., 2020), soil cover (Liu et al., 2016), and urban areas (Silver & Silva, 2021). Further applications of this approach in mixed bedrock-alluvial rivers would require constructing transition matrices for different river networks to evaluate if these probabilities are specific for each site or share common patterns across different environments. Constructing similar matrices for other river networks could reveal common patterns in cover dynamics linked to factors, such as regional climate, tectonic regimes, or lithological characteristics. If consistent patterns emerge, transition probabilities from studied networks could potentially be applied to similar river systems; if not, site-specific matrices would need to be developed. While the transition probability matrix could serve as input for predictive modelling of alluvial cover evolution, it does not represent physical processes and may not account for fundamental changes under different conditions. In contrast, using slope patterns to predict alluvial cover evolution considers fundamental physical dynamics but might oversimplify by not considering other influencing factors captured by the transition matrix. Combining both approaches could be most effective in predicting alluvial cover dynamics: using slope patterns as the primary predictor and refining the predictions with the transition probability matrix.

5.6.3 Modelling alluvial cover dynamics: Reach and network scales

The modelling approach employed in this study demonstrated strengths and limitations in capturing patterns of alluvial cover in mixed bedrock-alluvial river systems depending on the scale analysed. The model satisfactorily simulated broad patterns of sediment connectivity and alluvial distribution at the network scale, revealing how changes in upstream sediment supply or flow regimes can propagate through the network and affect downstream sediment dynamics. However, although the overall model accuracy was high, the modelled sediment cover fraction at any discrete location showed substantial variance compared to the field data (Figures 5.2d and 5.2e). This indicates that the model's accuracy at discrete locations was limited. Importantly, the model results presented fluctuating alluvial cover in approximately 30% of the reaches even under steady state conditions. These fluctuations, however, did not impact overall accuracy metrics, as they mostly occurred within reaches that remained consistently alluvial, reflecting variations in sediment depth rather than transitions between bedrock and alluvial states. Fluctuation timescales varied: 43% of reaches exhibited medium-period fluctuations (10–50 timesteps), while 28% and 29% showed shorter (<10 timesteps) or longer (>50 timesteps) periodic behavior, respectively. The magnitude of these fluctuations was substantial and variable, with sediment cover typically varying by a factor of 3 during steady state, and up to a factor of 57 in the most variable reaches. The fluctuations may indicate reaches with observed inconsistent cover over time in the River Carron. Consequently, point-by-point comparisons between model results and field data should be interpreted with caution, considering the potential for temporal variability in cover in real river systems.

Simplifying assumptions in the simulation's setup may have limited its capacity to represent alluvial cover distribution at the reach scale. A simplification was not representing temporal fluctuations in discharge, thus simplifying local sediment transport and deposition patterns. Incorporating realistic flow variability would influence the predicted alluvial cover patterns, depending on the timing and magnitude of high-flow events (DeLisle & Yanites, 2023; Lague et al., 2005; Turowski et al., 2013). The steady-state conditions observed in our simulations might not be achieved under variable flow

conditions. Comparing our high and low flow simulations demonstrate this: the low flow simulation resulted in longer alluvial cover (53% network covered) and steeper alluvial reaches (average covered slope 0.0045 m/m) compared to the high flow simulation (29% network covered, average covered slope 0.00015 m/m) (Figures 5.4 and 5.7). In addition, the system took longer to achieve steady state under low flow conditions. These observations indicate that alluvial cover would oscillate under variable flow conditions, with intermediate slopes being particularly sensitive to flow changes. Moreover, it is uncertain whether high flow conditions would persist long enough in the field for the network sediment cover to fully adjust, potentially leading to transient rather than steady-state conditions.

Another simplification was estimating channel width based on catchment area, which does not account for potential narrowing in bedrock sections and changes in local hydraulics and transport capacity. This could result in an underestimation of shear stress and hence overestimation of sediment deposition in bedrock reaches, particularly under low flow conditions. Additionally, our model assumes a uniform bed elevation within each reach, not accounting for macroroughness or sub-grid variations in bed topography that can influence local sediment deposition patterns (Inoue et al., 2014; Zhang et al., 2015). Furthermore, using a uniform critical shear stress regardless of the amount of alluvial cover simplified the model. In reality, bedrock reaches with smoother surfaces have lower critical shear stresses compared to alluvial surfaces (Ferguson et al., 2017a; Hodge et al., 2011). Our simulations neglected the effect of sand fraction on reference shear stress, although this may be justified for the Carron network where sand content is low (Appendix A2). Models that account for different critical shear stress depending on cover found "runaway alluviation", a rapid transition from bedrock to alluvial conditions when sediment supply exceeds transport capacity (Chatanantavet & Parker, 2008; Cho & Nelson, 2024b). Including these local variations in sediment entrainment would modify the relation between sediment supply and alluvial cover found in our study, possibly inhibiting the formation of alluvial cover in bedrock reaches under low flow conditions or resulting in more sediment cover development on steeper slopes under high sediment supply. Variations in flow, width, sediment supply, sediment entrainment and grain size distribution were not included in our simulations due to the increased complexity for our

network-scale modelling, but they are important areas for future model development to improve reach-scale predictions of this network model.

Additional limitations of our model approach include the extensive computational time required to achieve complete steady state conditions across the entire network (up to two weeks of CPU time) and the simplified representation of sediment supply locations. The complex interaction of sediment routing, storage and channel slope adjustment in the network can lead to long transient states with apparently stable conditions, making it computationally challenging to reach a fully stabilised network. Our model introduced sediments only at headwater reaches, which does not represent lateral sediment input from hillslope to rivers throughout the network. This approach may have led to an overestimation of transport capacity relative to sediment supply in downstream reaches, potentially decreasing alluvial cover with distance downstream. These factors can influence the spatial distribution of alluvial cover, particularly by creating more supply-limited conditions in downstream areas. Future applications of this model could benefit from incorporating distributed sediment inputs along the network to better represent hillslope contributions and improve the representation of sediment dynamics in downstream reaches. Further exploration of these aspects, including a comparison between our results and a simplified zero-order model based on transport capacity, is provided in Appendix A5. This comparison showed that the zero-order model predicted more alluvial reaches than our simulations, particularly under high sediment supply conditions, demonstrating the complex sediment routing, storage dynamics and temporal evolution represented by the NetworkSedimentTransporter model.

Despite the simplifications, our model provides insights that could enhance landscape evolution models (LEMs). Traditional LEMs represent the fundamental processes of fluvial incision into bedrock and sediment transport that shape landscapes over geological timescales (Howard, 1994; Whipple, 2002). However, these models often simplify or ignore the fine-scale dynamics of sediment cover distribution and the transitions between bedrock and alluvial states within river networks. Our results show that bedrock sections persist even under high sediment supply conditions and that the formation of alluvial reaches can decouple sediment connectivity along the network. These results demonstrate the complexity of transitioning between bedrock and alluvial

channel states, and that stable bedrock reaches can persist and erode for a long time despite variations in sediment supply. Detachment-limited LEMs assume an erosion framework, where sediment is readily evacuated from the system (e.g., Howard, 1994). These LEMs may not capture the decoupled sediment dynamics and the coexistence of bedrock and alluvial sections under different sediment regimes. Even transport-limited LEMs, which account for simple sediment transport dynamics (e.g., Willgoose et al., 1991), may fail to recreate the observed coexistence of bedrock and alluvial sections under different sediment regimes, as they often assume more uniform sediment cover conditions. Some recent LEMs, such as SPACE (Shobe et al., 2017), are capable of modelling cover dynamics and the coexistence of bedrock and alluvial reaches. However, our network-scale approach using NetworkSedimentTransporter offers additional insights. For example, our model can incorporate grain size variability, which is not present in SPACE, and focuses on network-scale connectivity and spatial distribution of alluvial cover. These features could provide a more detailed understanding of how sediment routing affects landscape volution.

The alluvial cover model on a network scale used in this study could be integrated into LEMs to enhance their capabilities, such as the persistence and erosion of bedrock sections. An approach is to develop a bed cover evolution sub-model for LEMs that incorporates detailed alluvial cover spatial distribution and connectivity dynamics, building upon existing models such as SPACE (Shobe et al., 2017). This sub-model would use inputs from LEMs, such as topography, discharge, and sediment supply, to calculate the spatial patterns of alluvial cover within the river network. The outputs could then be integrated into the LEMs' erosion and sediment transport calculations, allowing them to capture the influence of these finer-scale sediment dynamics on larger-scale landscape evolution processes. This coupling could improve LEMs' predictive capabilities in mixed bedrock-alluvial river systems by accounting for the feedback between alluvial cover dynamics, sediment connectivity, and broader landscape evolution processes.

5.7 Conclusion

This study combined network scale modelling and connectivity analysis to investigate the complex interactions between primary controls on alluvial cover within a mixed bedrock-alluvial river network. Previous research has focused on reach-scale analysis, while network-scale studies have been limited. We assessed the effects of changing sediment supply, flow depth, and grain size on cover transitions, fragmentation, and expansion of alluvial, mixed and bedrock sections on a network scale.

The results of this study have implications for understanding how mixed bedrock-alluvial systems respond to environmental changes. First, the spatial distribution of alluvial cover was strongly controlled by slope, particularly in supply-limited conditions. However, as sediment supply increased and the system shifted to transport-limited conditions, the influence of slope on spatial distribution decreased, while the effects of sediment supply and grain size became more significant. Second, the extent of alluvial cover was more responsive to changes in sediment supply and discharge in supply-limited conditions compared to transport-limited conditions. This indicates that in supply-limited settings, minor variations in sediment input or discharge can lead to substantial changes in the overall alluvial cover extent, while in transport-limited conditions, the system becomes less responsive to these changes. Third, even at sediment supply rates significantly exceeding the network's transport capacity, not all reaches achieved full alluviation. This suggests inherent limitations in the system's ability to distribute and retain sediment uniformly across the network. Finally, channel slope can potentially be used to predict hotspots of alluvial cover change, with alluvial sections expanding in the direction of increasing slope. Determining these hotspots has implications for predicting habitat availability and quality within river networks. It is important to note that our model assumptions, such as uniform grain size and sediment supply only at headwater reaches, may have affected our findings by simplifying the complex sediment dynamics found in natural systems.

Future research could focus on key areas to further improve the understanding of alluvial cover dynamics in mixed bedrock-alluvial river systems. Firstly, incorporating more detailed reach-scale processes into landscape evolution models (LEMs) could improve

the accuracy in representing alluvial cover dynamics. Traditional LEMs often simplify fine-scale sediment cover transitions and could more accurately simulate these processes, such as the persistence of bedrock sections under high sediment supply found in this study. Second, more research is needed on how the spatial extent and dynamics of alluvial cover change during perturbations to river networks, such as extreme storm events or sediment pulses from landsliding. Third, empirical studies of sediment cover variations throughout river networks in different environments are needed to validate and refine modelling approaches. Some challenges include the need for high-resolution data, increased computational demands, and accurately representing localised hydraulic and sediment transport processes within river network models. Despite these challenges, the potential benefits include improving river management, conservation strategies, and the predictive capabilities of landscape evolution models.

5.8 Acknowledgements

5.9 Open Research

The river data used for model input and evaluation are available in Whitbread (2015) and Whitbread et al. (2015). Grain size and sediment cover data collected during this study and used in the model are available in Guirro et al. (2025b). The NetworkSedimentTransporter model used for simulating sediment transport and alluvial

cover in the river network is freely accessible in Python as detailed in Pfeiffer et al. (2020) and developed openly by the Landlab team (https://github.com/landlab/landlab). The LSDTopoTools topographic analysis software used to delineate the river network is freely available at Mudd et al. (2023).

5.10 Author Contributions

Conceptualization: Mel Oliveira Guirro, Rebecca Hodge, Fiona Clubb, Laura Turnbull

Data curation: Mel Oliveira Guirro

Formal analysis: Mel Oliveira Guirro

Funding acquisition: Rebecca Hodge, Fiona Clubb, Laura Turnbull

Methodology: Mel Oliveira Guirro, Rebecca Hodge, Fiona Clubb, Laura Turnbull

Project administration: Rebecca Hodge, Fiona Clubb, Laura Turnbull

Supervision: Rebecca Hodge, Fiona Clubb, Laura Turnbull

Visualization: Mel Oliveira Guirro

Writing – original draft: Mel Oliveira Guirro

6 Alluvial cover interactions with sediment pulses in mixed bedrock-alluvial rivers

6.1 Abstract

Sediment pulses, such as those induced by landslides and dam removals, can significantly alter alluvial cover patterns in mixed bedrock-alluvial rivers, affecting sediment connectivity, channel morphology and ecological habitats. Despite their importance, there is limited research on how sediment pulses interact with varying degrees of pre-existing alluvial cover in these systems. This study investigates how pre-existing alluvial cover conditions and pulse characteristics influence pulse propagation and post-pulse effects on sediment cover patterns. Using the NetworkSedimentTransporter model applied to the River Carron in the Scottish Highlands, we simulate sediment pulses under different network-scale supply conditions, introduction sites, and pulse volumes. Our results demonstrate that pulses introduced at a bedrock site showed enhanced downstream transport leading to pulse translation, while pulses at an alluvial site showed greater local storage and dispersion behaviour. Network-scale alluvial cover conditions affect pulses, particularly when introduced at a bedrock site, with pulses travelling 47% faster in our low-cover channel network compared to the high-cover network. Smaller pulse volumes initially move faster than larger pulses, while larger pulses maintain higher volumes over longer distances, creating more extensive and persistent alluvial cover. Despite overall deposition, 9% of reaches downstream of a pulse input location eroded to lower cover states than pre-pulse conditions, particularly in steeper sections. These findings improve our understanding of sediment connectivity in mixed bedrock-alluvial systems and have implications for river management and habitat conservation.

6.2 Introduction

Sediment connectivity in rivers, i.e., the degree to which sediment can be transferred between different reaches, fundamentally controls channel morphology, ecosystem processes, and landscape evolution (Bracken et al., 2015; Wohl et al., 2019). In mixed bedrock-alluvial rivers, this connectivity is particularly complex due to the interaction between sediment transport and the degree of alluvial cover (Ferguson et al., 2017b; Hodge et al., 2011; Turowski et al., 2008). The presence or absence of alluvial cover creates feedback processes that influence hydraulics, sediment transport and channel morphology, determining whether a reach experiences net erosion or deposition (Hodge & Hoey, 2016; Sklar & Dietrich, 2004; Turowski et al., 2007). In bedrock reaches, steeper channels and smoother surfaces (assuming bedrock roughness is less than alluvial roughness) reduce critical entrainment thresholds, which increase transport capacities and downstream transport (Ferguson et al., 2017b; Hodge et al., 2011). These steep bedrock reaches tend to maintain their exposed state through positive feedback mechanisms that prevent sediment accumulation. In contrast, alluvial reaches promote positive feedback mechanisms where existing sediment patches increase flow resistance and promote additional deposition (Hodge & Hoey, 2016). These contrasting processes reinforce existing alluvial cover patterns that may need significant perturbation events to disrupt established feedback cycles.

Sediment pulses represent such perturbations, defined as sporadic and discrete inputs of sediments that considerably exceed the average sediment input of a channel (Ahammad et al., 2021; East et al., 2018; Madej, 2001; Morgan & Nelson, 2019). These pulses can be triggered by natural events, such as landslides, extreme floods and wildfires, or by anthropogenic activities, including dam removal (which mobilises previously trapped sediment) and gravel augmentation programs (Benda & Dunne, 1997a; Bennett et al., 2025; East et al., 2018; Murphy et al., 2019; Vazquez-Tarrío et al., 2023). The introduction of these sudden sediment inputs creates challenges for river management and habitat protection, as their behaviour can be difficult to predict (Sklar et al., 2009; Vazquez-Tarrío et al., 2023).

An important question regarding sediment pulses is how they move through river systems, as their transport dynamics directly impact downstream patterns of erosion, deposition and habitat availability along the channel network (East et al., 2018; Gran & Czuba, 2017; Sklar et al., 2009). Previous research has identified two primary mechanisms of pulse propagation: translation (downstream movement as a coherent wave) and dispersion (spreading out or dissipating downstream). Dispersion has been found to be the dominant process in many studies (Cui et al., 2005, 2003; Lisle et al., 1997, 2001; Sutherland et al., 2002), though translation can occur under specific conditions, such as when pulse amplitude is low or when flow exhibits low Froude numbers (Sklar et al., 2009). The balance between translation and dispersion mechanisms is affected by several factors, including pulse characteristics (volume, grain size), channel properties (slope, width, bed roughness), and flow conditions (discharge magnitude and variability) (Ahammad et al., 2021; Cui et al., 2003; Lisle et al., 2001; Sklar et al., 2009; Venditti et al., 2010). For instance, pulses composed of sediment finer than the bed material tend to translate more, as finer particles are more easily entrained and transported by the flow (Cui et al., 2003; Sklar et al., 2009). Pulses with mixed grain sizes can present complex behaviours, with intermediate sizes translating quickly and coarser sizes dispersing slowly (Ahammad et al., 2021). In addition, finer pulses have been shown to increase the mobility of coarser bed material, potentially creating cascading effects downstream (Venditti et al., 2010).

Previous studies have examined sediment pulse propagation primarily in gravel-bed rivers (e.g., Ahammad et al., 2021; An et al., 2017; Cui et al., 2003; Lisle et al., 2001; Piantini et al., 2021), with limited attention to the effect of bedrock reaches on pulse propagation. Through field analysis, Nelson & Dubé (2016) identified different responses to sediment pulses across different reach types, finding that bedrock reaches rapidly flushed sediment downstream without considerable morphological change, while alluvial reaches functioned as deposition zones with evident morphological changes. Although this study investigated reach-scale differences, our understanding of the interaction between sediment pulses and varying degrees of alluvial cover remains limited. This knowledge gap is particularly relevant as sediment pulses such as landslides frequently originate in upland landscapes where river channels often present

partial bedrock exposure mixed with alluvial patches (Montgomery & Buffington, 1997). In these mixed systems, the degree of alluvial cover prior to a sediment input likely affects both the pulse's transport dynamics and its downstream impacts. Guirro et al. (2025a) (Chapter 5) demonstrated that the spatial distribution of alluvial cover in an upland system is controlled mainly by slope, particularly under supply-limited conditions, but that sediment supply and grain size become more influential under transport-limited conditions. These findings suggest that the pre-existing distribution of alluvial cover could affect how sediment pulses propagate through river networks.

At the river network scale, additional complexities in pulse propagation may arise that are not captured by reach-scale studies. The structure of the river network, the geometry of tributary inputs and the spatial patterns of transport capacity influence pulse propagation (Benda & Dunne, 1997a; Gran & Czuba, 2017; Schmitt et al., 2016). For example, areas with decreasing transport capacity downstream or reaches with low transport capacity can act as "bottlenecks", causing pulses to disperse instead of translate (Gran & Czuba, 2017). These network-scale interactions demonstrate the importance of considering both local reach conditions and broader network characteristics when studying sediment pulse dynamics.

In this study, we investigate sediment pulse dynamics in mixed bedrock-alluvial rivers, focusing on three aspects. First, the influence of pre-existing alluvial cover on pulse propagation dynamics. While studies have shown that bed roughness and alluvial cover affect sediment transport (Ferguson et al., 2017b; Hodge et al., 2011), the interactions between alluvial cover and sediment pulses have not been investigated in mixed bedrock-alluvial systems. Second, how pulse characteristics (volume and alluvial cover fraction of the introduction site) affect transport dynamics. Third, the feedback between pulse propagation and changes in post-pulse alluvial cover patterns to understand the long-term effects of sediment pulses on river morphology and sediment connectivity. We address these aspects by investigating the following research questions:

1. How does pre-existing alluvial cover (at both network and local scales) affect the transport dynamics and propagation of sediment pulses?

2. How do sediment pulses alter the pre-existing alluvial cover pattern in mixed bedrock-alluvial river networks?

3. How does pulse volume affect pulse propagation dynamics and post-pulse alluvial cover patterns in mixed bedrock-alluvial systems?

To answer these questions, we use the NetworkSedimentTransporter model to simulate pulse dynamics in the River Carron, a mixed bedrock-alluvial river network in the Scottish Highlands. By varying pre-existing alluvial cover conditions, pulse introduction sites and pulse volumes, we analyse how these factors affect pulse propagation and alluvial cover distribution. The findings contribute to our understanding of sediment connectivity in mixed bedrock-alluvial systems and have implications for river management and habitat protection (Steiger et al., 2005; Wohl, 2015b).

6.3 Study Area

The River Carron catchment (Figure 6.1), located in the northwest of the Scottish Highlands, has a mixed bedrock-alluvial river network, providing a suitable area for investigating pulse behaviour in mixed bedrock alluvial systems. This area was previously studied by Guirro et al. (2025a) (Chapter 5) and Whitbread et al. (2015), who identified primary controls on the alluvial cover spatial distributions and correlations between reach type and river morphology.

The catchment covers an area of 300 km^2 with a total river network length of around 138 km. The main River Carron extends 44 km. Major tributaries include Rivers Abhainn, Alladale and Glencalvie. Channel slopes vary greatly throughout the network, ranging from 0.00006 to 0.4 m/m in 100 m long reaches, with steeper reaches generally found in headwaters or waterfalls. Bankfull widths and depths for the main channel vary between 3 to 46 m and 0.6 to 6 m, respectively (Whitbread, 2015). The median grain size (D_{50}) found in the catchment is 0.10 m.

The River Carron network presents mixed bedrock-alluvial characteristics, with bedrock reaches distributed throughout the catchment, particularly in steeper, narrower and deeper channel sections (Whitbread et al., 2015). The landscape was glaciated during

the Last Glacial Period and deglaciated approximately 11,000 years ago (Bennett & Boulton, 1993; Small & Fabel, 2016), with U-shaped valleys and irregular topography created by glacial erosion. Sediment deposits are mainly of glacial origin, including till, glaciofluvial sediments and organic peat material (British Geological Survey, 2008). Current sediment inputs to the river system mainly come from the reworking of these glacial deposits, particularly through erosion of raised alluvial terraces and debris fans associated with tributary streams. The region is not tectonically active and lacks records of recent extreme sediment pulse events. However, paleo-landslides were documented by the British Geological Survey (2024) using data from the BGS National Landslide Database, forming mass movement deposits near channels (Figure 6.1). These varied sediment sources, topography and alluvial cover patterns make the Carron catchment suitable for investigating how sediment pulses interact with the existing patterns of alluvial cover in a post-glacial mixed bedrock-alluvial river network.
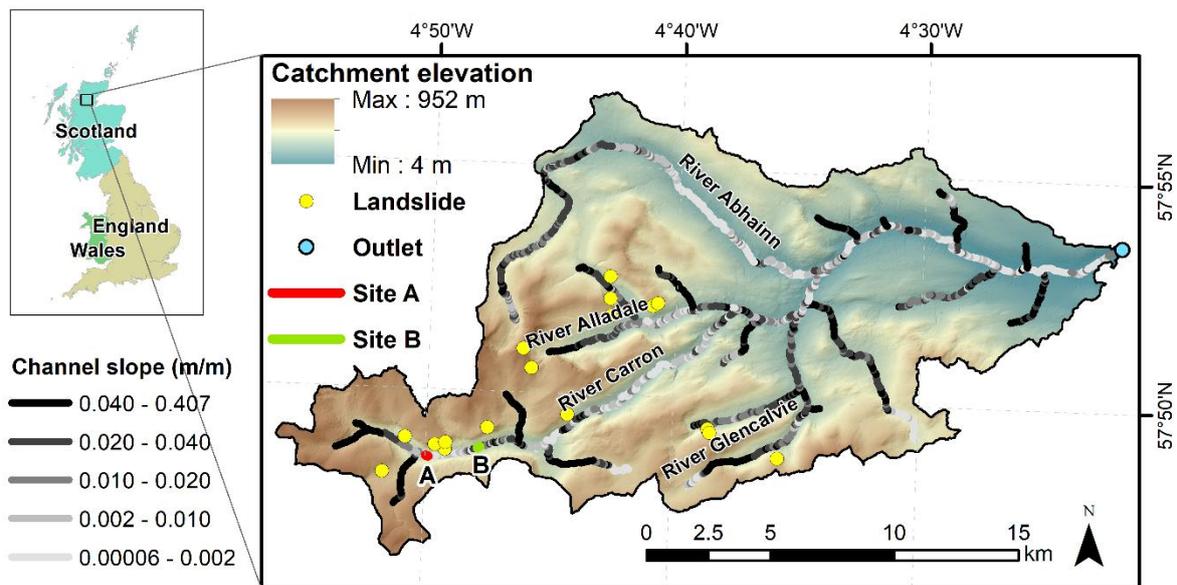
Figure 6.1: Carron catchment showing locations of paleo-landslides (data source: British Geological Survey, 2024). Sites A and B in the upstream area of the main channel indicate the experimental sediment pulse introduction locations used in this study.

6.4 Methods

We investigated how sediment pulses interact with varying degrees of alluvial cover in a mixed bedrock-alluvial river using numerical modelling. We employed the NetworkSedimentTransporter (NST) model (Pfeiffer et al., 2020) to simulate sediment transport and cover evolution across the River Carron network, focusing on how pre-existing alluvial cover conditions affect pulse propagation and post-pulse effects on the sediment cover patterns.

6.4.1 Sediment transport simulations

The NST model simulates bedload sediment transport and riverbed evolution on a river network by tracking individual sediment parcels (representing groups of particles with identical characteristics) and computing changes in their locations, bed elevation and bed slope. We used the modified version of NST described in Chapter 4, which includes advancements for calculating alluvial cover percentage, handling sediment inputs, managing transport capacity in low slope reaches and updating parcel velocities during downstream movement. The model determines the percentage of alluvial cover (p_c) for each river segment using Equation (6.1):

$$p_c = \frac{V_l}{l_l \cdot W_l \cdot D_l \cdot (1-\varphi)} \times 100 \qquad \text{(Equation 6.1)}$$

where p_c is the alluvial cover percentage in link l; V_l is the volume of sediment parcels in link l (m³); l_l is the link length (m); W_l is the link width (m); D_l is the average median grain size of sediment parcels in link l (m); and ϕ is the bed porosity, which was set as 0.3. Alluvial cover values can exceed 100% when sediment volume is sufficient to create multiple bed layers, with values above 100% representing sediment layers rather than additional area covered.

We used the same river network configuration as Guirro et al. (2025a) (Chapter 5), defined with a 5-m resolution Digital Elevation Model (DEM) of the River Carron from OS Terrain 5 (Ordnance Survey, 2022). The network was constructed using LSDTopoTools (Mudd et al., 2023) with a minimum drainage area threshold of 2.5 km² and link lengths of

approximately 100 m. Channel geometry was derived from established hydraulic scaling relationships for the River Carron (Whitbread et al., 2015). The flow depth in the simulations is set to bankfull conditions, with each timestep representing approximately 7 years in the catchment.

Our experiments were structured in two main groups (Table 6.1): (1) experiments examining how pre-existing network-scale alluvial cover affects pulse propagation, and (2) experiments investigating the influence of pulse volume on transport dynamics.

Table 6.1: Summary of sediment pulse experiments. Supply conditions are relative to the average transport capacity of the network (Q_t).

Experiment group	Purpose	Network cover	Introduction site	Pulse volume (m³)
Pre-existing cover effects	Examine how alluvial cover affects pulse propagation	• Low (0.5 Q_t) • Medium (1.0 Q_t) • High (1.5 Q_t)	• Site A (Alluvial) • Site B (Bedrock)	• Medium (10,000)
Pulse volume effects	Examine how pulse volume affects pulse propagation	• Medium (1.0 Q_t)	• Site A (Alluvial)	• Small (1,000) • Medium (10,000) • Large (100,000)

For the first group of experiments ("Pre-existing cover effects", Table 6.1), we defined three baseline network conditions with varying alluvial cover distributions. The low, medium and high cover networks were defined by running the model to steady state with different headwater sediment supply relative to the average transport capacity across all reaches in the network (Q_t):

1. Low-cover network: Using headwater sediment supply of 30 parcels/tributary/timestep (0.5 Q_t).

2. Moderate-cover network: Using headwater sediment supply of 60 parcels/tributary/timestep (1.0 Q_t).

3. High-cover network: Using headwater sediment supply of 90 parcels/tributary/timestep (1.5 Q_t).

These supply rates were selected based on the systematic analysis in Guirro et al. (2025a) (Chapter 5), which tested a range of sediment supply rates relative to transport capacity. The chosen values span from a supply-limited (0.5 Q_t), through balanced (1.0 Q_t) to transport-limited (1.5 Q_t) network conditions. The sediment supply consisted of parcels with a uniform grain size of 0.10 m, equal to the median grain size measured in the field.

Steady state was defined following Guirro et al. (2025a) (Chapter 5): a reach was considered to be in steady state if its alluvial cover varied by less than 10% in 100 timesteps, and the system as a whole was considered at steady state when the number of reaches meeting this criterion remained constant for 100 timesteps. These three baseline simulations were run until steady-state conditions were achieved, creating three distinct initial configurations of alluvial cover distribution across the network. Considering the full network, the low-cover network exhibited 66% average alluvial cover across all reaches, the moderate-cover network 76% average alluvial cover and the high-cover network 78% average alluvial cover.

An identical pulse was added into each steady-state system. The pulse consisted of 10,000 sediment parcels (10,000 m³ total volume) with a uniform grain size equal to the median grain size of the riverbed (D_{50} = 0.10 m). This volume represents a moderate sediment input, characteristic of "medium" landslide classifications (McColl & Cook, 2024), which defines medium landslides as those with volume between 10^3 and 10^6 m³ in their proposed universal size classification system. This volume is similar to documented sediment inputs, such as gravel augmentation projects (Vázquez-Tarrío et al., 2023), small dam removals (Major et al., 2017) and mass movements in Scotland (Bainbridge et al., 2022; Ballantyne, 2004). To isolate the specific influence of different network-scale alluvial cover distributions, we maintained consistent pulse and flow conditions across all scenarios: identical pulse volume, grain size, input location and flow depth.

To examine the influence of local alluvial cover conditions at pulse introduction sites, we conducted separate simulation runs introducing identical pulses at two different locations (Tables 6.2 and 6.3, Figures 6.1 and 6.2): (1) an alluvial reach (Site A) with >100% sediment cover across all three baseline simulations, and (2) a bedrock reach (Site B)

with 0% cover. The alluvial reach (Site A) is situated around 2 km upstream of the bedrock reach (Site B). These two pulse introduction sites were selected because they are situated near documented landslide sites in the catchment and have very similar slopes (0.018 and 0.019 m/m respectively), which isolate the impact of alluvial cover from slope effects. They also are positioned in the upper region of the main channel, allowing sufficient downstream distance to analyse pulse propagation effects. In addition, these locations maintain consistent cover conditions (alluvial or bedrock) across all three baseline simulations. By comparing pulse behaviour between these two introduction scenarios across three different background supply conditions, we conducted six independent runs that isolated the influence of both local and network-scale alluvial cover patterns on pulse propagation.

Table 6.2: Characteristics of pulse introduction sites (sites A and B) prior to pulse introduction. Note that Site B is around 2 km downstream Site A.

Site	Cover type	Cover percentage	Slope (m/m)	Downstream characteristics
A	Alluvial	100%	0.018	Alluvial for 2 km, then predominantly bedrock for 2 km, then variable
B	Bedrock	0%	0.019	Predominantly bedrock for 2 km, then variable
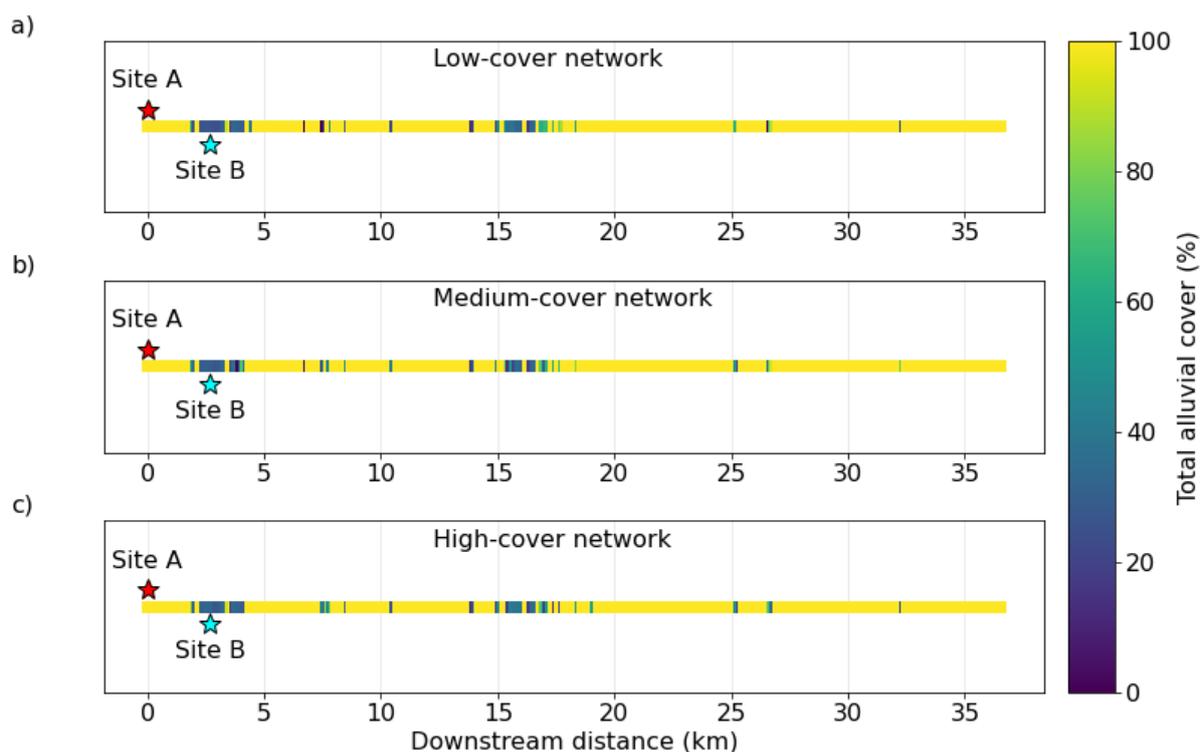
Figure 6.2: Spatial distribution of alluvial cover (ranging from 0% to 100%) along the main channel under different supply conditions at steady state (before pulse introductions): a) Low-cover network, b) Moderate-cover network, and c) High-cover network. Site A (red star) and Site B (blue star) mark locations along the river where pulses are introduced. Site B (Bedrock) is situated approximately 2.6 km downstream from Site A (Alluvial).

Table 6.3: Summary statistics of the downstream path from pulse introduction (Site A) in the baseline river network configurations at steady state prior to pulse introduction.

Parameter	Low-cover network	Moderate-cover network	High-cover network
Partially exposed reaches (< 100% cover)	21%	19%	20%
Fully alluvial reaches (100% cover)	78%	81%	80%
Median channel slope (m/m)	0.010	0.011	0.011
Standard deviation of channel slope (m/m)	0.012	0.013	0.012

For the second group of experiments (Table 6.1), we investigated how pulse volume affects sediment transport dynamics. Using the moderate-cover network condition at steady state, we introduced pulses of three different volumes at the alluvial site (Site A) in a single timestep: a small pulse (1,000 m^3), the standard-medium pulse (10,000 m^3) and a large pulse (100,000 m^3). These volumes correspond to small, medium and large landslides (Bainbridge et al., 2022; McColl & Cook, 2024), while the small pulse could also correspond to small gravel augmentation (Vazquez-Tarrío et al., 2023) and the large pulse to a large-scale dam removal (East et al., 2018). In terms of local sediment transport in our simulations, these volumes represent approximately 13, 132 and 1320 times the transport capacity per timestep of the introduction reach, respectively. All other pulse parameters (grain size, introduction location, flow conditions) remained constant across these simulations to isolate the influence of pulse volume on transport dynamics.

All sediment parcels were tracked with source identifiers that we implemented by adding specific tags to the Landlab DataRecord (which tracks the parcel characteristic): "initial" for parcels present at simulation start, "upstream input" for parcels introduced at tributary headwaters during each timestep, and "pulse" for parcels introduced at the pulse location at a single timestep when the system reached steady state. We tracked the pulse propagation until the system reached a new steady state.

6.4.2 Analysis of pulse dynamics

Several metrics were used to characterise pulse movement, dispersion and impact on channel morphology, in order to quantify how different pulses behaved differently under varying conditions. Three metrics were used to quantify pulse dynamics across all simulations: (1) maximum travel distance, (2) centre of mass movement and (3) pulse dispersion.

Maximum travel distance measures the furthest downstream distance reached by any pulse particle relative to the input location. This metric identifies the maximum extent of pulse influence in the network and investigates how different network conditions affect

the mobility of the fastest parcels from pulses. We identified reaches containing any pulse material and tracked the furthest downstream reach in each timestep.

Centre of mass movement characterises the average downstream movement of the pulse, calculated as Equation 6.2.

$$CoM = \frac{\sum V_i \times d_i}{\sum V_i}$$ (Equation 6.2)

where *CoM* is the distance of the centre of mass relative to the pulse input location (m); V_i is the volume of pulse sediment in reach *i* (m³); and d_i is the downstream distance of reach *i* from the pulse input location (m). This weighted average accounts for the distribution of pulse material throughout the network and provides a measure of overall pulse movement.

Pulse dispersion quantifies how widely the pulse sediment spreads during transport, calculated as Equation 6.3. This metric represents the standard deviation of the pulse volume distribution around the centre of mass. Higher dispersion values indicate greater longitudinal spreading of pulse material.

$$Dispersion = \sqrt{\frac{\sum V_i \times (d_i - CoM)^2}{\sum V_i}}$$ (Equation 6.3)

These three metrics were tracked over time for all pulse experiments, enabling analysis of both spatial and temporal evolution of pulse dynamics under different conditions. In addition, to explore the spatial-temporal dynamics of pulse propagation, the longitudinal distribution of pulse sediment volume at different timesteps was analysed.

To assess how the pulse affected alluvial cover patterns throughout the pulse path, we used three other metrics that characterise different aspects of cover dynamics: (1) pulse-created alluvial cover; (2) pulse contribution to total cover; and (3) change in total alluvial cover.

Pulse-created alluvial cover maps the spatial-temporal distribution of alluvial cover due to pulse sediment. For each reach, we applied Equation 6.1 specifically to pulse sediment volumes (tracked separately through source identifiers) to calculate the percentage of bed area that would be covered by pulse material alone. Where pulse cover exceeded 100%, this indicates that pulse sediment volume is sufficient to create multiple

layers of bed coverage, but we reported this as 100% maximum bed coverage with the understanding that excess material contributes to bed thickness rather than additional area covered.

Pulse contribution to total volume quantifies the relative importance of pulse sediment in the overall sediment volume at each location and timestep (Equation 6.4).

$$V_P = \frac{V_{pulse}}{V_{total}}$$

(Equation 6.4)

where V_P is the pulse contribution ratio (dimensionless), V_{pulse} is the volume of pulse sediment parcels (m³) and V_{total} is the total volume of all sediment parcels (m³). This ratio ranges from 0 to 1, with higher values indicating reaches where pulse material is the majority of sediment volume. This metric identifies where pulse sediment has become a dominant component of the riverbed material volume, regardless of whether total alluvial cover increased.

Change in total alluvial cover measures the difference between post-pulse and pre-pulse alluvial cover conditions at each reach (Equation 6.5).

$$\Delta p_c = p_{c,post} - p_{c,pre}$$

(Equation 6.5)

where Δp_c is the change in alluvial cover percentage (percentage points); $p_{c,post}$ is the post-pulse alluvial cover percentage, and $p_{c,pre}$ is the pre-pulse reference cover percentage. This metric indicates areas of net deposition (positive values) or erosion (negative values) resulting from pulse introduction, regardless of whether this resulting cover consists of pulse material or pre-existing sediment.

To analyse the relationship between post-pulse alluvial cover change and channel characteristics, we conducted a detailed analysis of the moderate volume pulse (V = 10,000 m³) introduced at the alluvial site (Site A) in the moderate-cover network. For this analysis, we applied Equation 6.5 to calculate the change in total alluvial cover (Δp_c) at each downstream reach, then averaged these values over all post-pulse timesteps to characterise the overall response pattern for each reach. We implemented two complementary approaches to find the correlation between reach response and channel characteristics. The first analysis used uncapped alluvial cover values (as in Equation 6.1), allowing calculated cover to exceed 100% when sediment volume is sufficient to

create multiple bed layers. In this uncapped approach, reaches were classified as experiencing deposition (>5% increase in alluvial cover), erosion (>5% decrease) or neutral response (-5% to 5% change), indicating the overall tendency of bedload sediment accumulation or loss in each reach. The second analysis capped alluvial cover values at 100% to focus specifically on morphological transitions between alluvial and bedrock channel states. This approach classified reaches as transitioning toward alluvial conditions (>5% increase), toward bedrock (>5% decrease), or maintaining the same channel type (-5% to 5% change). For both approaches, we quantified how many reaches actually transitioned between channel states (becoming fully alluvial ≥100% or developing some bedrock exposure <100%) by comparing pre-pulse and final alluvial cover values. To test whether channel slope and pre-pulse cover distributions differed between response groups, we applied Kruskal-Wallis tests (Kruskal & Wallis, 1952). The Kruskal-Wallis H statistics measures how much the group distributions differ from each other, with larger H values indicating greater differences between groups. This test is appropriate for comparing distributions across three independent groups without assuming normality. When significant differences were detected ($p < 0.05$), we conducted pairwise Mann-Whitney U tests to determine the differences between specific group pairs. The Mann-Whitney U test assesses whether one group tends to have higher or lower values than another group. For example, it can indicate whether erosional reaches have consistently steeper slopes than depositional reaches.

All analyses were conducted relative to the pulse introduction site, with downstream distances measured from this location. Temporal data in sediment volume and alluvial cover were averaged in 10-timestep windows to reduce short-term fluctuation in the data while preserving the overall patterns.

6.5 Results

6.5.1 Pre-existing alluvial cover effect on pulse transport

The maximum travel distance of any pulse particle (Figures 6.3a and 6.3b) showed similar linear progression patterns over time regardless of network alluvial cover condition (low, moderate or high network cover) or local sediment cover (Site A or B), with rates of approximately 0.09 km/timestep. By the end of the simulation period (350-400 timesteps), pulse particles had travelled a maximum distance of 27-31 km downstream, approaching the catchment outlet.

Pulse centre of mass movement and dispersion (Figure 6.3c and 6.3d) showed more distinct differences between alluvial cover conditions, particularly when the pulse was introduced at the bedrock reach (Site B, Figure 6.3d and 6.3f). In the low-cover network, the pulse centre of mass moved faster, reaching approximately 12.5 km by timestep 350, compared to 10.5 km for the moderate-cover network and 8.5 km for the high-cover network. This represents approximately 47% faster movement in the low-cover compared to the high-cover conditions. Pulse dispersion (Figures 6.3e and 6.3f) showed similar trends to the centre of mass movement. At the bedrock site, pulses dispersed more in the low-cover network and less in the high-cover network (Figure 6.3f). However, for pulses introduced at the alluvial site (Figures 6.3c and 6.3d), both centre of mass movement and dispersion remained similar across all network conditions. These results indicate that pulses introduced at bedrock sites amplified the differences in pulse propagation between network conditions, whereas pulses introduced at alluvial sites showed similar transport dynamics regardless of network-scale alluvial cover.
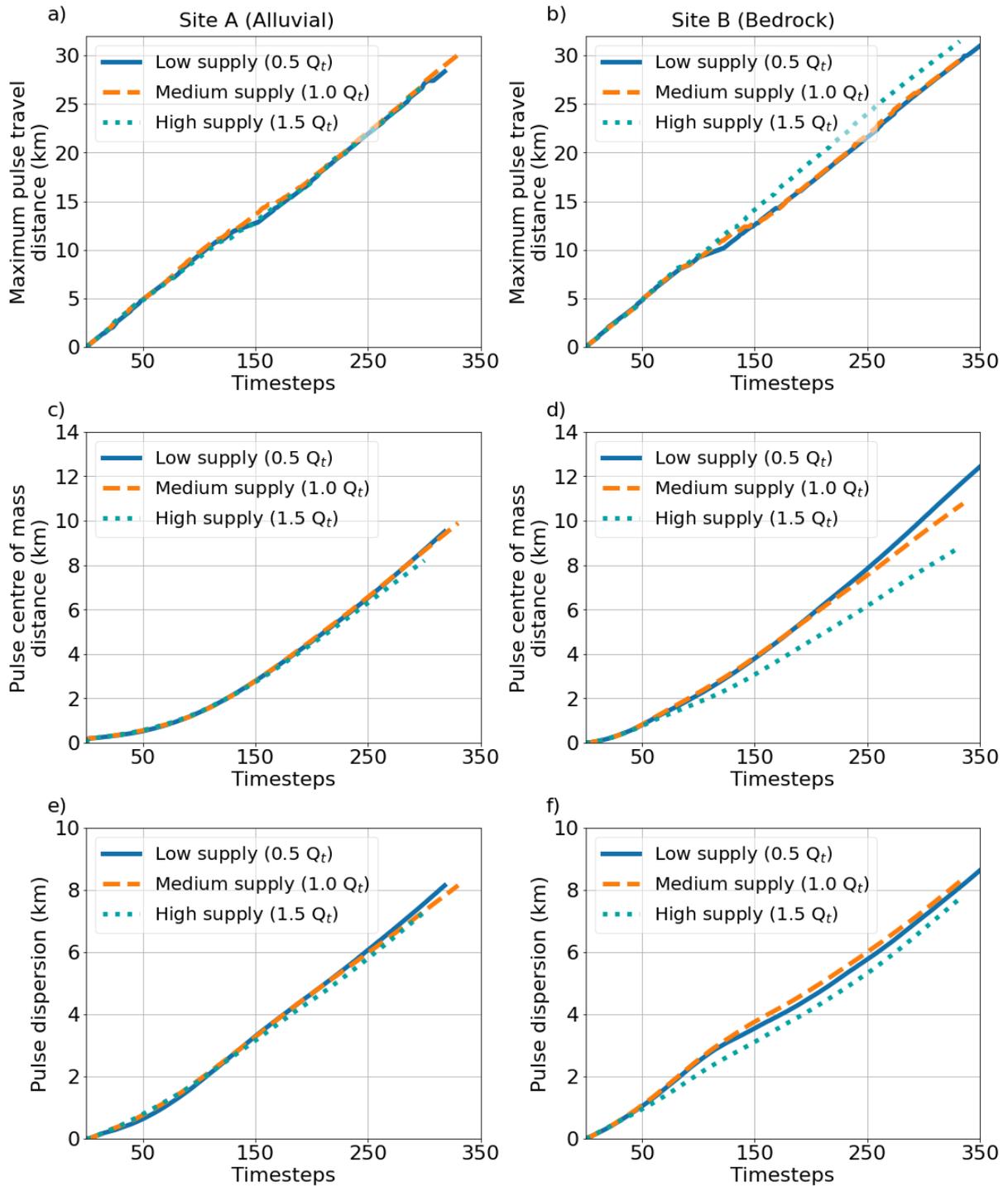
Figure 6.3: Temporal evolution of sediment pulse movement under different pre-existing network alluvial cover conditions (low, moderate and high network cover). Left column (panels a, c and e) shows Site A (Alluvial) and right columns (panels b, d, and f) shows Site B (Bedrock). First row (panels a, b): Maximum travel distance of any pulse particle. Second row (panels c, d): Pulse centre of mass distance. Third row (panels e, f): Pulse dispersion (longitudinal spreading). All time values represent timesteps after pulse introduction.

The longitudinal distribution of pulse sediment volume over time showed different patterns between pulses introduced at the alluvial versus the bedrock site (Figure 6.4). At the alluvial site (Figure 6.4a), pulse sediment moved downstream more gradually, with less material reaching distant downstream locations. By later timesteps (yellow lines, around timestep 330), sediment volumes beyond 20 km downstream the pulse introduction remained below 10 m^3 per aggregated segment. In contrast, the pulse introduced at the bedrock site (Figure 6.4b) travelled downstream faster and maintained higher sediment volumes in the downstream reaches. Both introduction scenarios showed a similar pattern of higher concentration at the input location, with the pulse material gradually dispersing downstream over time. However, the bedrock site scenario demonstrated more effective downstream transport of material, while the alluvial site stored more sediment near the introduction location.
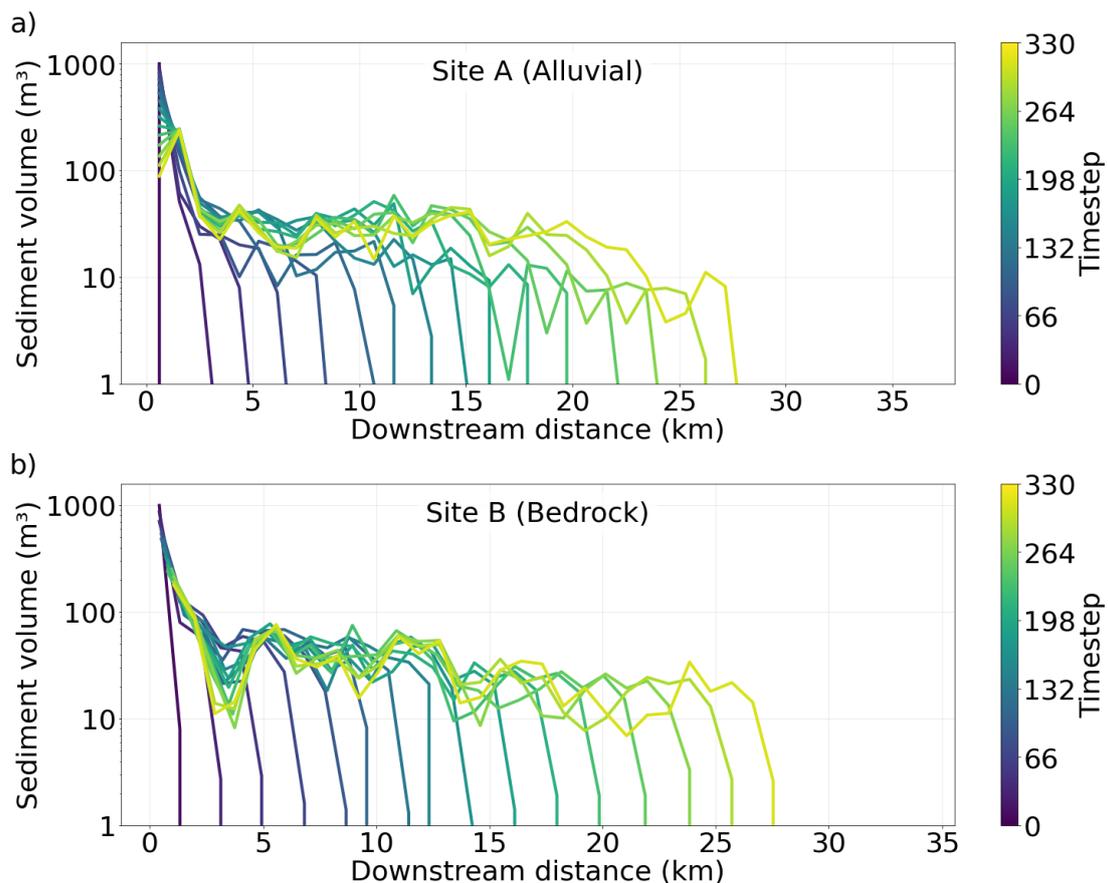
Figure 6.4: Spatial temporal evolution of sediment pulse volumes along the downstream distance for two different pulse introduction locations: a) Site A (Alluvial) and b) Site B (Bedrock) at the medium supply (1.0 Q_t) system. Each line represents the sediment

volume distribution at a specific timestep, with colours indicating the progression of time from early (dark blue, t=0) to late (yellow, t=330) timesteps. Lines are plotted at 20-timestep intervals and data points are aggregated by averaging values over 10 adjacent reach segments to improve visual clarity.

6.5.2 Pulse effects on alluvial cover

The spatial-temporal patterns of alluvial cover created by the pulse varied depending on pulse introduction site and pulse volume (Figures 6.5 and 6.6). The pulse introduced at the alluvial site (Site A) showed slower downstream movement, while the pulse introduced at the bedrock site (Site B) moved more rapidly, extending alluvial cover farther downstream (Figures 6.5a and 6.5b). The contribution of pulse sediment volume to total sediment volume showed different patterns between introduction sites (Figures 6.5c and 6.5d). At the bedrock site (Figure 6.5d), pulse sediment initially dominated the volume composition (ratios > 0.8), indicating that most sediment reaches originated from the pulse, transforming bedrock areas into temporary alluvial reaches. Over time, the pulse volume contribution gradually decreased at the introduction site and nearby downstream reaches, as shown by the transition from yellow (100% pulse contribution) through orange and pulse to white areas (zero contribution with no pulse sediment) by timestep 300 (Figure 6.5d). These white areas, extending from the introduction site to around 1 km downstream at timestep 300, indicate that pulse sediment has been evacuated from these locations, with some reaches potentially reverting back to bedrock exposure. In contrast, at the alluvial site (Figure 6.5c), pulse volume contribution ratios rarely exceeded 0.4, indicating that pulse material mixed with pre-existing sediment rather than dominating the sediment composition. Despite these differences, changes in total alluvial cover following pulse introduction (Figures 6.5e and 6.5f) showed similar patterns at both introduction sites, with predominantly depositional effects and only limited bands of erosion progressing downstream.
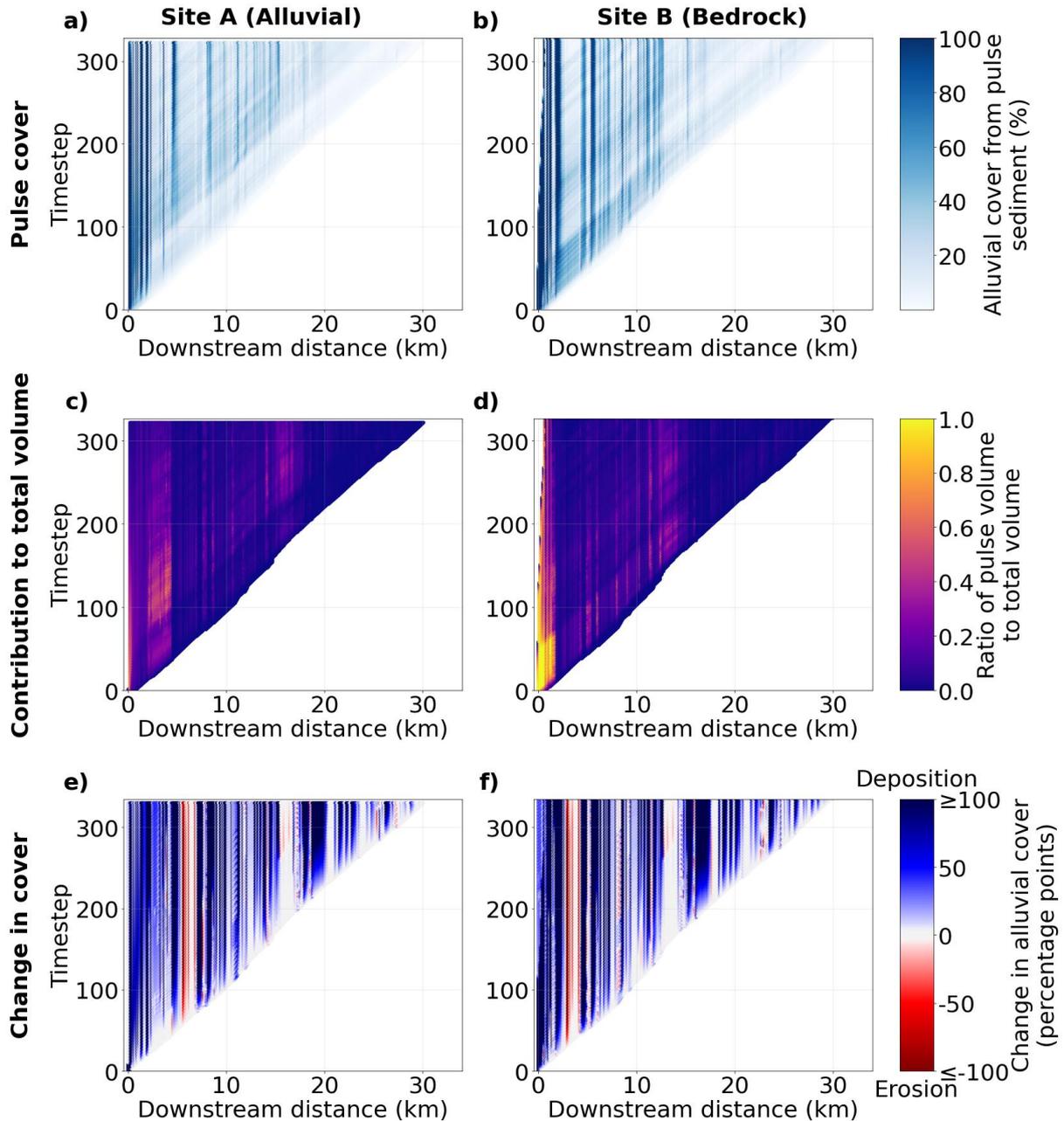
Figure 6.5: Spatial-temporal patterns of pulse effects on alluvial cover for pulses introduced at different locations. Pulses (V = 10,000 m³) were introduced at: a-c-e) Site A (Alluvial) and b-d-f) Site B (Bedrock) in the moderate-cover network. Top row (a-b) shows pulse-created alluvial cover (percentage of bed that can be covered by pulse sediment only). Middle row (c-d) shows the contribution of pulse volume to total volume. Bottom row (e-f) shows the change in total alluvial cover relative to pre-pulse conditions (percentage points, with positive values in blue indicating deposition and negative values in red indicating erosion). White areas indicate location and times where the pulse has not yet reached.

Further analysing the change in alluvial cover from the moderate volume pulse (V = 10,000 m^3) introduced at the alluvial site (Site A), we found that most reaches experienced deposition (n=222, 68%), while fewer showed neutral response (n=77, 23%) and erosion (n=30, 9%) in terms of bedload sediment response (Figures 6.6a and 6.6b). Reaches that experienced erosion had significantly higher slopes (median ≈ 0.025 m/m) than depositional reaches (median ≈ 0.015 m/m), with slope distributions differing significantly between response groups (Kruskal-Wallis H = 100.15, p < 0.001) (Figure 6.6a). Depositional reaches had higher range of pre-pulse cover conditions (median ≈ 600%) than erosional reaches (median ≈ 200%), indicating that reaches with higher initial sediment conditions generally experienced further bedload accumulation (Kruskal-Wallis H = 8.99, p = 0.011) (Figure 6.6b). When analysing morphological transitions between channel types using cover values capped at 100%, the majority of reaches maintained their channel type (n=258, 78%), with more reaches transitioning toward alluvial conditions (n = 51, 16%) than toward bedrock conditions (n = 20, 6%) (Figures 6.6c and 6.6d). Of these transitions toward alluvial conditions, 20 reaches (6%) actually became alluvial (changed from < 100% to ≥ 100% cover), while 7 reaches (2%) changed from fully covered beds to having some bedrock exposure (≥ 100% cover to <100% cover). Reaches transitioning toward bedrock conditions exhibited significantly higher channel slopes (median ≈ 0.035 m/m) than those transitioning toward alluvial conditions (median ≈ 0.020 m/m). In addition, reaches transitioning toward bedrock had high pre-pulse cover (80 - 100%) compared to reaches transitioning toward alluvial conditions (pre-pulse cover near 0%). These findings suggest that despite overall deposition of sediment pulse material in most reaches, steeper channel sections can experience net erosion and transition toward more bedrock-dominated morphology.
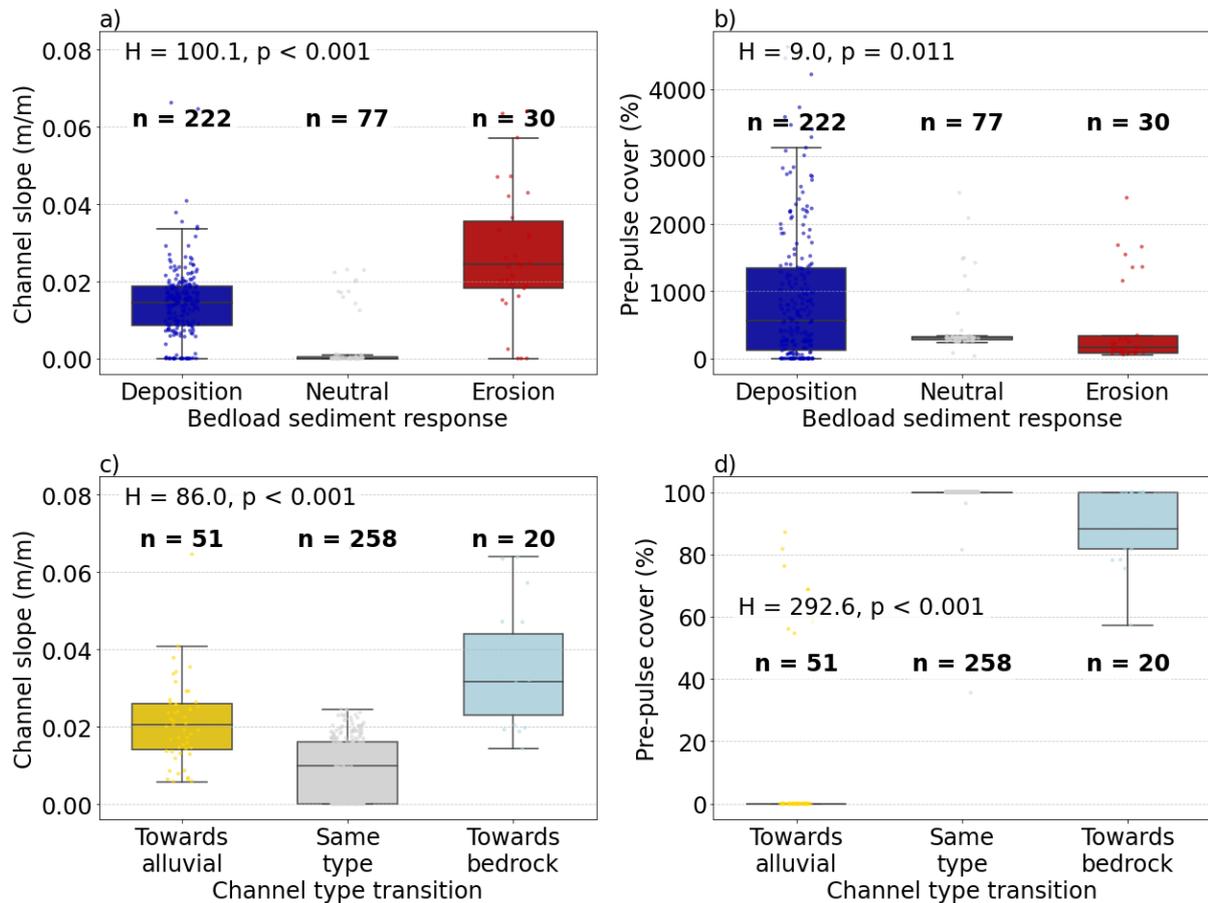
Figure 6.6: Channel characteristics and response type to sediment pulse introduction from the moderate pulse volume (V = 10,000 m³) introduced at Site A (Alluvial) in the moderate-cover network. Box plots showing the relationship between channel slope and pre-pulse alluvial cover (percentage of bed covered by sediment before pulse introduction) with response to sediment pulse. Panels a and b display the bedload sediment response showing overall sediment accumulation or erosion regardless of channel type classification. Panels c and d show channel type transition indicating morphological changes between bedrock and alluvial states. Panels a and c show the distribution of channel slopes for each response type, with Kruskal-Wallis test statistics (H and p) testing whether slope distributions differ significantly between response groups. Panels b and d show pre-pulse cover conditions for each response category. Sample sizes (n) for each category are indicated at the top of each box.

6.5.3 Pulse volume effects on transport dynamics

Sediment transport dynamics were sensitive to pulse volume, with all other variables held constant (Figure 6.7). The maximum travel distance of any pulse particle (Figure 6.7a) showed similar progression patterns across all three pulse volumes (1,000 m³,

10,000 m^3, and 100,000 m^3). The fastest particles of all pulses moved downstream at a consistent rate of approximately 0.09 km/timestep, reaching a maximum distance of around 30 km by timestep 325.

In contrast, the centre of mass movement (Figure 6.7b) varied between different pulse volumes. The small pulse (1,000 m^3) initially showed slightly faster centre of mass transport compared to the standard pulse (10,000 m^3), reaching almost 4 km by timestep 150 compared to about 2.5 km for the standard pulse. However, the standard pulse's movement rate increased in later timesteps and matched the small pulse by around timestep 300, with both reaching approximately 10 km by timestep 275. The large pulse (100,000 m^3) demonstrated much slower centre of mass moment, reaching only 2 km by timestep 300. By timestep 300, the small and standard pulses centre of mass had travelled approximately 4.5 times farther than the large pulse.

Pulse dispersion patterns (Figure 6.7c) showed similar variability. The small pulse (1,000 m^3) dispersed more, with dispersion reaching above 8.0 km by timestep 300. The standard pulse (10,000 m^3) showed intermediate dispersion (around 7.5 km at timestep 300), while the large pulse (100,000 m^3) showed the least dispersion, reaching close to 4.0 km by timestep 300. This difference represents a dispersion rate approximately 2 times greater for the small pulse compared to the large pulse over the first 300 timesteps.
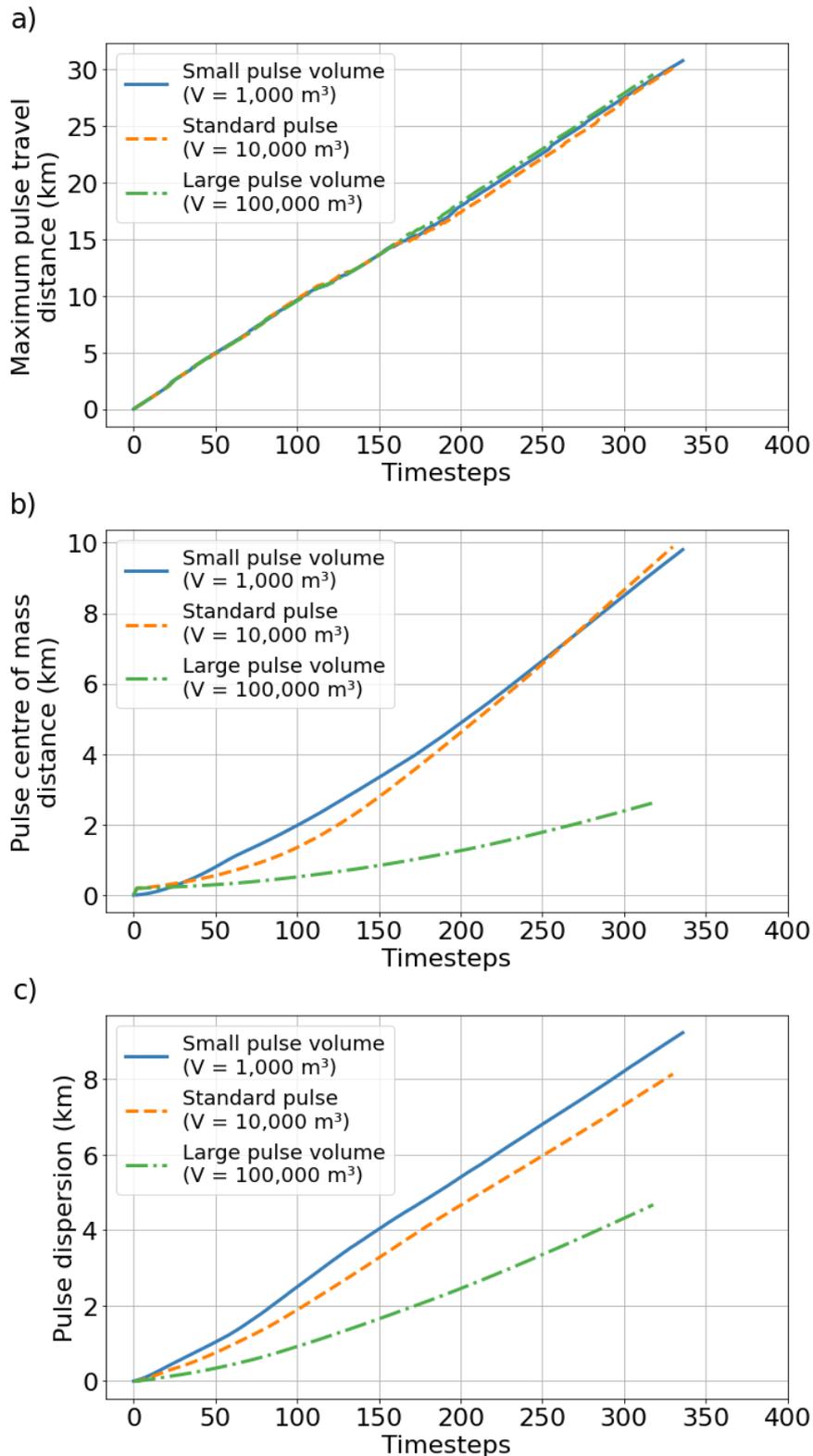
Figure 6.7: Effects of pulse volume on pulse transport dynamics: a) Maximum travelled distance of any pulse particle (m); b) Distance travelled by pulse centre of mass (m); and c) Pulse dispersion (longitudinal spreading). All simulations were conducted under identical flow conditions with pulse volumes of 1,000 m³ (small), 10,000 m³ (standard) and 100,000 m³ (large), introduced at the same alluvial location (Site A).

The longitudinal distribution of sediment volume for pulses of different volumes showed different spatial-temporal patterns (Figure 6.8). All three pulses showed decreasing sediment volumes with increasing distance from the introduction site, but the small pulse (1,000 m^3, Figure 6.8a) rapidly dispersed downstream, forming a fragmented distribution with low volumes (1 to 5 m^3) reaching up to 15 km by timestep 221. The standard pulse (10,000 m^3, Figure 6.8) maintained higher volumes in downstream reaches (20 to 50 m^3), creating a more continuous distribution and achieving a longer distance of approximately 18 km. The large pulse (100,000 m^3, Figure 6.8c) showed even higher volumes in downstream reaches (20 to 80 m^3), reaching approximately 19 km downstream by the final timestep. While the maximum travel distance of the fastest particles was similar across all pulse volumes (Figure 6.7a), larger pulses maintained higher sediment concentrations over longer distances, whereas small pulses dispersed more rapidly with lower downstream volumes.
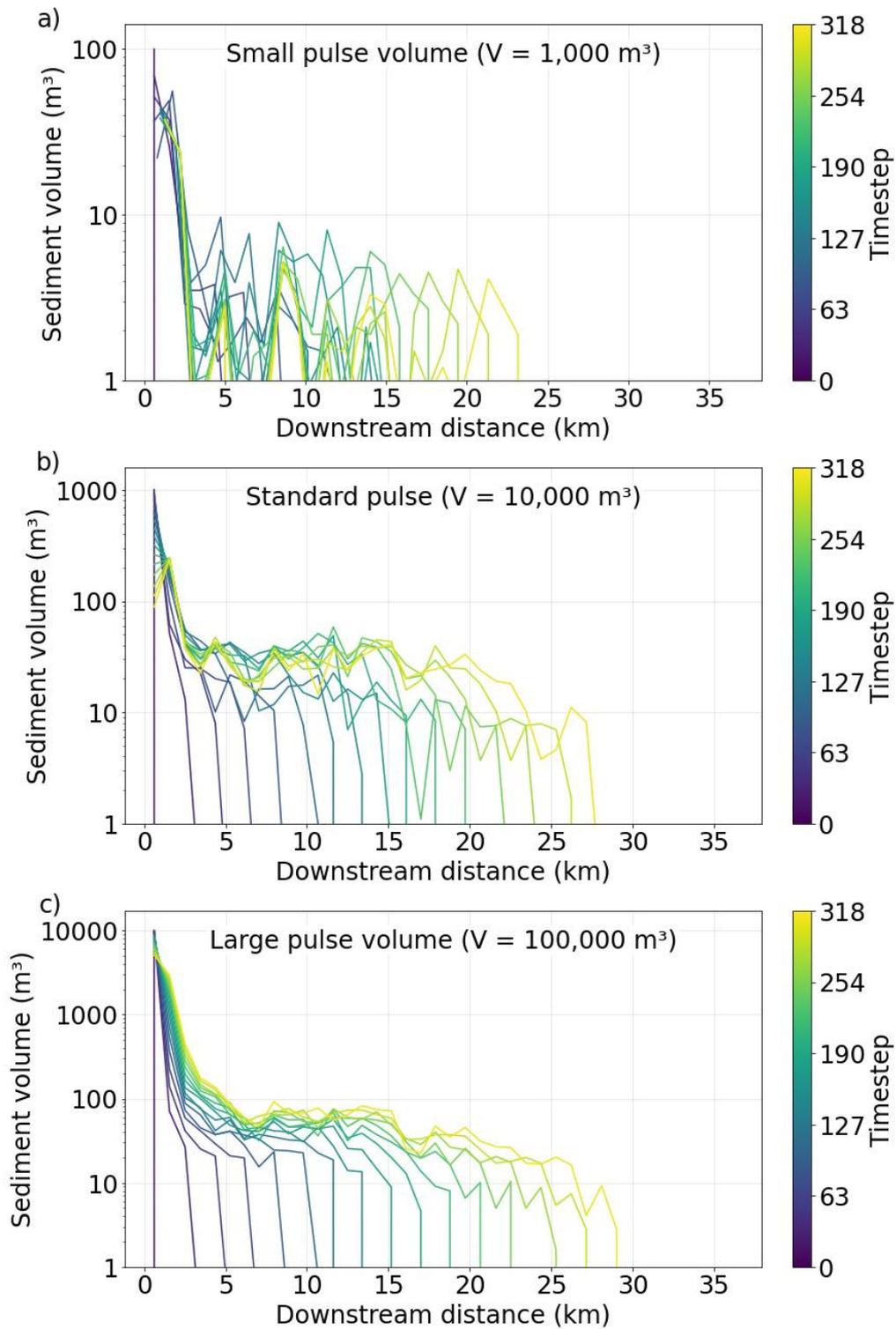
Figure 6.8: Spatial temporal evolution of sediment pulse volumes along the downstream distance for three different initial pulse magnitudes: a) Small pulse (1,000 m³), b) Standard pulse (V = 10,000 m³), and c) Large pulse (V = 100,000 m³) at the Site A (Alluvial). Each line represents the sediment volume distribution at a specific time, with colours indicating the progression of time from early (dark blue, t=0) to late (yellow, t=318) timesteps. Lines are plotted at 20-timestep intervals and data points are aggregated by averaging values over 10 adjacent reach segments to improve visual clarity.

Pulse volume also influenced the spatial-temporal patterns of alluvial cover development (Figure 6.9). The small pulse (Figure 6.9a) created minimal downstream cover, with values exceeding 20% only within 2 km of the introduction site, indicating localised deposition near the input location. However, the small pulse caused a particular temporal pattern in the introduction site: initial alluvial cover increased immediately after pulse introduction, followed by progressive erosion that ultimately resulted in lower alluvial cover than pre-pulse conditions (Figure 6.9e, at distance 0km). In contrast, the large pulse (Figure 6.9d) dominated the total cover composition in the first 5 km downstream throughout the entire simulation period. Both small and large pulses created similar alternating patterns of deposition and erosion (Figures 6.9e and 6.9f), though the large pulse generated more deposition within the 5 km downstream. Neither scenario produced extensive erosion (>50 percentage points decrease), though localised areas of moderate erosion (25-50 percentage points decrease) were observed in both scenarios.
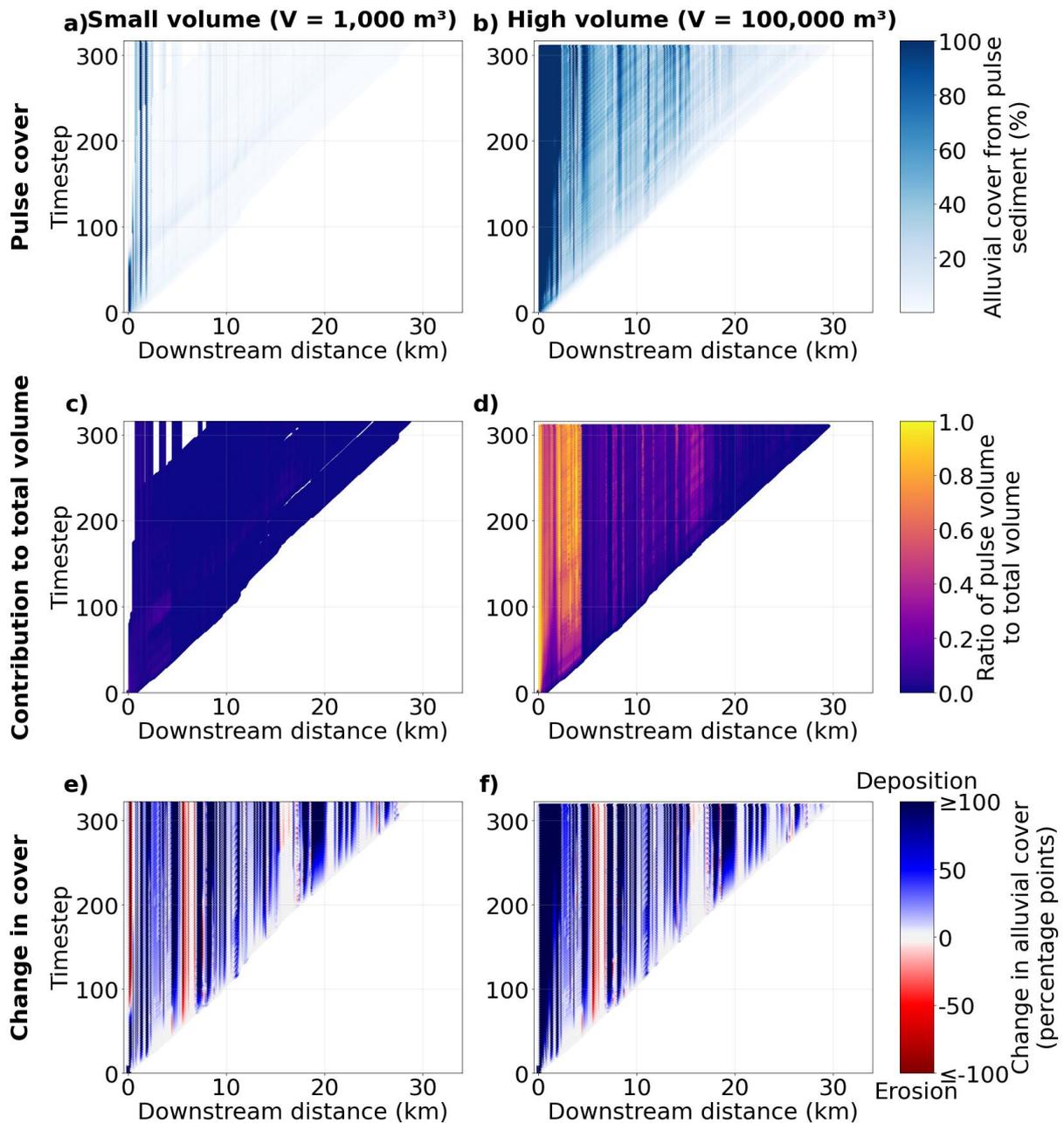
Figure 6.9: Spatial-temporal patterns of pulse effects on alluvial cover for pulses of different volumes. Pulses were introduced at Site A (Alluvial) in the moderate-cover network: a-c-e) Small pulse (1,000 m³) and b-d-f) Large pulse (100,000 m³). Top row (a-b) shows pulse-created alluvial cover (percentage of bed that can be covered by pulse sediment only). Middle row (c-d) shows the contribution of pulse volume to total volume. Bottom row (e-f) shows the change in total alluvial cover relative to pre-pulse conditions (percentage points, with positive values in blue indicating deposition and negative values in red indicating erosion). White areas indicate location and times where the pulse has not yet reached.

6.6 Discussion

6.6.1 Influence of pre-existing alluvial cover on pulse propagation

Results show that local introduction site characteristics influence pulse propagation in mixed bedrock-alluvial rivers. Pulses introduced at bedrock sites promote faster downstream transport of sediments, with pulse centre of mass moving approximately 47% faster in the bedrock introduction scenarios compared to alluvial introduction sites (Figure 6.3). This faster transport at bedrock sites occurs due to higher transport capacity. In our simulations, transport capacity in the bedrock site averaged 306 m^3 compared to 277 m^3 at the alluvial site over the first 10 timesteps after pulse introduction. This transport capacity difference resulted from wider channel geometry (15.9m vs 14.5m) and greater flow depth (1.95m vs 1.85m) at the bedrock site due to its downstream location. In natural systems, bedrock reaches also have more efficient sediment transport due to typical smoother surfaces that reduce flow resistance (Ferguson et al., 2017a) and reduce critical shear stress thresholds for sediment entrainment (Hodge et al., 2011). In contrast, alluvial sites create feedback mechanisms that inhibit downstream transport, with sediment patches increasing flow resistance and promoting additional deposition (Hodge and Hoey, 2016). These feedback processes in natural systems and transport capacity in our modelling implies in greater storage of pulses introduced in alluvial reaches and enhanced downstream propagation in pulses introduced in bedrock reaches.

The contrasting transport mechanisms at different introduction sites influence whether pulses translate and disperse. Pulses introduced at bedrock sites showed enhanced downstream transport, with more sediments travelling longer distances (Figures 6.3f and 6.4b), characteristic of translation-dominant behaviour. In contrast, pulses introduced at alluvial sites showed greater local storage and more gradual downstream movement (Figures 6.3e and 6.4a), indicating dispersion-dominant behaviour. Although most natural sediment pulses tend to disperse rather than translate (Cui et al., 2005, 2003; Lisle et al., 1997, 2001; Sutherland et al., 2002), these studies have predominantly focused on alluvial rivers. Our results suggest that the effect of transport capacity and local bed alluvial cover can affect this tendency in mixed bedrock-alluvial systems. In

addition to previously identified factors that influence pulse behaviour, such as pulse volume and Froude number (Cui et al., 2003; Sklar et al., 2009), our findings indicate that bedrock exposure, particularly at the pulse introduction site, is another factor favouring pulse translation. River networks with greater bedrock exposure transport sediment more efficiently for several reasons. In our simulations, the enhanced transport at bedrock reaches resulted from channel geometry differences and was amplified over time and space. At each timestep, more parcels moved downstream from the bedrock introduction site than from the alluvial site. In addition, the bedrock introduction site was followed by more bedrock reaches downstream that further enhanced transport, whereas the alluvial introduction site was surrounded by alluvial reaches that retained sediments.

Our simulations focused primarily on the influence of sediment quantity on pulse propagation and alluvial development, but grain size also affects these processes. Previous research indicates that finer pulses tend to translate more and disperse less compared to coarser pulses, particularly when travelling over coarse gravel beds (Ahammad et al., 2021; Cui et al., 2003; Sklar et al., 2009). However, our simulations used uniform grain size (D_{50} = 0.10 m) and focus solely on sediment quantity of pulse and riverbed, without capturing grain size effects. Ahammad et al. (2021) used the same NetworkSedimentTransporter model but with mixed grain size distributions to investigate effects on pulse propagation. Their findings demonstrated that intermediate mixed-size pulses (median grain size approximately 0.5 times the bed median) caused the largest downstream accumulation, while finer mixed pulses (~0.15 times bed median) moved through the system more quickly with less aggradation. In addition, mixed-size pulses increasing bed mobility more than uniform pulses as the range of fine sizes helps mobilise larger grains (Ahammad et al., 2021; Venditti et al., 2010). Based on these modelling results with grain size variability, we would expect that finer pulses in mixed bedrock-alluvial rivers would cause more extensive initial alluvial cover development but with shorter duration and potentially more pronounced post-pulse erosion. In contrast, coarser pulses would likely result in more persistent but less extensive alluvial cover changes. Future modelling efforts incorporating grain size distributions would be needed to test these expectations in mixed bedrock-alluvial networks.

This differential pulse response due to introduction sites is clear in our pulse centre of mass movement and dispersion metrics, but not in the maximum travel distance of the fastest particles. Across all simulations, the fastest sediment particles travelled at a consistent rate of approximately 0.09 km/timestep regardless of introduction site or network conditions (Figures 6.3a, 6.3b). In contrast, the pulse centre of mass – representing the average behaviour of pulse particles – varied between introduction sites and was influenced by the distribution of bedrock and alluvial reaches throughout the network. This pattern aligns with flume experiments by Sklar et al. (2009), who found that leading edge celerity remained relatively constant across different pulse characteristics, while trailing edge celerity varied more, contributing to pulse dispersion over time. Our results found a similar characteristic: maximum travel distance (analogous to leading edge behaviour) showed little variation between introduction sites, while centre of mass movement (bulk pulse behaviour) varied more. This suggests that the fastest particles, once entrained, are primarily controlled by local hydraulics conditions, while bulk pulse transport is more sensitive to local storage processes and transport capacity variations throughout the network.

These relationships between alluvial cover and pulse dynamics have implications for sediment connectivity within mixed bedrock-alluvial rivers. As identified by Guirro et al. (2025a) (Chapter 5), channel slope primarily controls alluvial cover distribution under steady-state conditions. Our pulse experiments demonstrate that the distribution of transport capacity, which is correlated to the alluvial cover distribution, influences the efficiency of sediment transport during pulse events. Bedrock reaches function as efficient sediment conduits that enhance connectivity, while alluvial reaches act as buffer zones of reduced transport capacity that can promote disconnectivity (Czuba & Foufoula-Georgiou, 2015; Fryirs, 2013). Therefore, the spatial distribution of bedrock and alluvial reaches controls sediment connectivity during both steady-state and pulse conditions. These findings align with Nelson & Dubé (2016), who identified through field observations different responses to sediment pulses across reach types – bedrock reaches rapidly evacuated sediment downstream with low morphological change, while alluvial reaches functioned as deposition zones with greater morphological changes, particularly by aggrading more. Our modelling results provide the mechanistic basis for

these field observations. The transport capacity differences explain why bedrock reaches evacuate sediment rapidly, with depositional feedback processes in natural systems further enhancing this mechanism (Ferguson et al., 2017b; Hodge et al., 2011; Hodge & Hoey, 2016).

6.6.2 Impact of pulses on alluvial cover patterns

Sediment pulses can considerably change channel cover, with their impact varying based on the pre-existing alluvial cover at the introduction site and pulse volume. In our simulations, analysis of a moderate volume pulse (10,000 m^3) introduced at an alluvial site showed that 68% of downstream reaches experienced deposition and 9% experienced erosion, mainly in steeper reaches (Figure 6.6). In terms of channel type transitions, 6% of reaches converted from having some bedrock exposure to fully alluvial conditions (< 100% to ≥100%) and 2% transitioned from fully alluvial to some bedrock exposure (≥100% to <100% cover) (Figure 6.6). Channel slope was found as a primary factor controlling post-pulse responses, with reaches experiencing erosion having significantly higher slopes (median ≈ 0.025 m/m) than depositional reaches (median ≈ 0.015 m/m) (Figure 6.6).

Studies commonly described general aggradation following pulses, with gradual incision through the new deposits (Baynes et al., 2023; East et al., 2018; Gran & Czuba, 2017; Hoffman & Gabet, 2007; Nelson & Dubé, 2016). This aggradation typically occurs downstream of pulses inputs where transport capacity decreases and in wider channel sections (Ahammad et al., 2021; Cui et al., 2003; Madej, 2001). Some studies identified post-pulse erosion (Ahammad et al., 2021; Baynes et al., 2023; East et al., 2018; Miller & Benda, 2000), with Ahammad et al. (2021) identifying reaches with high to medium slope as more prone to erosion after sediment pulses. In our simulations, erosion occurs because a large sediment input initially perturbs the cover equilibrium and increases channel slope, but as the system adjusts, steeper reaches can erode to a new steady state with less sediment than in the pre-pulse state. This process was particularly evident at the introduction site with small pulse volume (Figure 6.9e), where the pulse

introduction site experienced initial alluvial cover increase followed by erosion, resulting in lower alluvial cover than pre-pulse conditions.

Pulses introduced at bedrock reaches can transform channel cover, particularly near the introduction site, converting bedrock reaches into temporary alluvial sections (Figure 6.5d). This transformation persisted for long periods during our simulations, with pulse-dominated cover (pulse cover contribution ratio > 0.5 in Figure 6.5d) lasting for more than 200 timesteps, which represents approximately 12 centuries in the River Carron, and extending around 2 km downstream from the pulse introduction site. However, our modelling assumes fixed channel width and depth. Field studies have consistently documented channel widening in response to sediment pulses (Bennett et al., 2025; East et al., 2018; Nelson & Dubé, 2016). This widening is often associated with transitions to braided rivers and occurs primarily in reaches with erodible banks, with bedrock banks less likely to widen (Baynes et al., 2020; Hoffman & Gabet, 2007; Nelson & Dubé, 2016).

Pulses affected bedrock and alluvial reaches differently in our simulations. Pulses introduced at bedrock reaches temporarily transformed them into alluvial channels, while pulses introduced at fully alluvial reaches primarily integrated with existing sediment cover (contributions ratios < 0.4 in Figure 6.5c). This suggests that alluvial reaches function as zones where new sediment inputs mix with existing material without causing strong morphological transitions. Field observations support these differential responses. Hoffman & Gabet (2007) observed how debris flow modified channel morphology, leading to aggradation upstream of the pulse introduction site and braiding in downstream reaches. Similarly, East et al. (2018) observed overall downstream aggradation due to a dam removal followed by incision over the pulse deposits. Hoffman & Gabet (2007) noted that width-to-depth ratios in bedrock reaches remained relatively constant following the debris flow, while alluvial reaches upstream and downstream of the pulse introduction site became wider. In contrast, when the pulse was added into an alluvial reach, the introduction site became narrower after incision through the initial pulse deposits. This finding indicates that bedrock and alluvial reaches can present different morphological responses to pulses.

6.6.3 The effect of pulse volume on alluvial cover patterns

Pulse volume is an important factor in determining pulse propagation and post-pulse alluvial patterns. In our simulations, the small pulse exhibited much faster centre of mass movement than the large pulse (about 4.5 times faster in Figure 6.7b) and dispersed two times faster (Figure 6.7c). This inverse relationship between pulse volume and transport rate supports findings from previous studies which found that smaller pulses tend to spread out more quickly relative to their volume, while large pulses are more coherent and tend to translate more (Morgan & Nelson, 2019; Sklar et al., 2009; Venditti et al., 2010). The longitudinal distribution of sediment volume (Figure 6.8) also shows these differences in transport behaviour: the small pulse tended to disperse into fragmented distributions with lower downstream impact (1 to 5 m^3 reaching distances up to 15 km, Figure 6.8a), while the large pulse maintained higher volumes over longer distances (20 to 80 m^3 up to 19 km, Figure 6.8c). Large pulses deliver more sediment to downstream reaches for longer periods, indicating that the pulse volume is a critical factor on how sediment disturbances propagate through river networks and modify alluvial cover patterns.

The volume-dependent behaviours found in this study have implications for alluvial cover development. In our simulations, the small pulse created minimal downstream cover, with values greater than 20% of pulse-created cover only within 2 km of the introduction site and diminishing its impact over time (Figure 6.9). In contrast, the large pulse dominated the total cover composition in the first 5 km downstream throughout the entire simulation period. These results suggest a minimum threshold for effective sediment augmentation in river restoration, as also observed by Sklar et al. (2009), Vazquez-Tarrío et al. (2023) and Venditti et al. (2010), who found that small sediment augmentation volumes have limited downstream reach and persistence. By contrast, large pulses due to major landslides and dam removals can strongly affect alluvial cover patterns across longer portions of a river network. East et al. (2018) and Major et al. (2017) observed that larger sediment inputs from dam removals produced extensive and longer downstream effects. Understanding these volume thresholds and spatial extents of influence is necessary for successful river restoration and improvement of habitats, as

the creation and maintenance of substrate conditions are fundamental to support ecological functions in river systems (Wohl, 2015b).

6.7 Conclusion

This study combined network-scale modelling and pulse propagation analysis to investigate interactions between sediment pulses and alluvial cover in mixed bedrock-alluvial river networks. We assessed how pre-existing alluvial cover conditions affect pulse propagation and how pulses, in turn, modify alluvial cover patterns.

Our main findings indicate that: (1) Local introduction site characteristics influence pulse propagation, with pulses introduced at bedrock reaches exhibiting faster downstream transport with more translation behaviour than pulses introduced at alluvial sites; (2) Network-scale conditions of alluvial cover affect overall pulse transport efficiency, particularly when pulses are introduced at bedrock sites, where pulse centre of mass moves faster in low-cover networks; (3) Pulse volume affects pulse dynamics and alluvial cover development, with smaller pulses initially moving faster but creating a more fragmented distribution and lower cover development than larger pulses; and (4) Channel slope appears to control post-pulse sediment deposition or erosion areas, with some steeper reaches developing bedrock exposure following pulse introduction.

Opportunities for future research remain to improve our understanding of alluvial cover interactions with pulses. Simplifications in our simulations included assuming uniform grain size distributions and constant channel width and depth. Future research should explore the effects of variable grain sizes of pulses on alluvial cover and adjustments in channel width and depth following pulse introduction in mixed bedrock-alluvial reaches. In addition, our study focused on a single pulse event. Future research should investigate how multiple pulses interact and how their cumulative effects differ from single pulse events. Such investigations could provide understanding into the long-term evolution of mixed bedrock-alluvial river networks under different supply regimes and provide understanding for effective management of mixed bedrock alluvial rivers.

7 Research summary, implications and conclusions

7.1 Introduction

This thesis investigated controls on the spatial and temporal variability of alluvial cover in mixed bedrock-alluvial river systems, focusing on the interactions between channel morphology, sediment characteristics and hydrological processes within an upland post-glacial catchment. By combining empirical field research with numerical modelling, this study analysed processes across different spatial and temporal scales, from reach to network scales and from contemporary flow events to decadal evolution of alluvial cover patterns. This chapter summarises the main findings of this thesis by discussing the achievement of research objectives, comparing empirical observations with numerical modelling results, discussing broader implications for different environments and recommending areas for future research.

7.2 Achievement of research objectives and overarching aim

The overarching aim of this thesis was to investigate the mechanisms driving the spatial and temporal variability of alluvial cover in mixed bedrock-alluvial river systems. This aim was addressed through three research objectives, each contributing to understanding alluvial cover dynamics.

Objective 1: Examine how channel and sediment properties correlate with spatial patterns and temporal changes of alluvial cover in an upland post-glacial catchment.

Empirical analysis of field data from the River Carron (Chapters 2 and 3) found that channel slope and bankfull depth were the strongest predictors of alluvial cover spatial distribution, with steeper and deeper channels exhibiting lower sediment cover. The analysis also found high spatial variability of grain size and the occurrence of both

bedrock and alluvial channels throughout the catchment regardless of drainage area. Contemporary flows actively rework grains in most reaches (68%) during moderate floods, but some reaches (12%) are resistant to mobilisation even during extreme floods, indicating persistent influence of glacial history. Temporal analysis over a 12-year period showed a general increase in alluvial cover during a period of relatively stable flow conditions. However, methodological challenges in measuring temporal changes in alluvial cover indicated the need for standardised practices and more frequent monitoring to better understand alluvial cover temporal dynamics.

Objective 2: Identify the main drivers influencing the extent, expansion and spatial distribution of alluvial cover in a river network.

Modelling using the modified NetworkSedimentTransporter model (Chapter 4 and 5) identified that the relative importance of controlling factors varies depending on sediment supply conditions. Under supply-limited conditions, channel slope controls the spatial distribution of alluvial cover, with low-slope reaches developing cover first regardless of their position in the network. Under transport-limited conditions, sediment supply and grain size become more important, while slope effects decrease. In addition, alluvial cover demonstrated high sensitivity to changes in sediment supply and flow depth under supply-limited conditions, but reduced sensitivity under transport-limited conditions. Chapter 5 also discussed how sediment connectivity varies with alluvial cover, with bedrock reaches enhancing sediment transport and alluvial reaches acting as temporary storage zones. The direction of alluvial cover expansion under increasing sediment supply is controlled by local slope patterns, with alluvial patches forming in low-slope sections and expanding in the direction of increasing bed gradient.

Objective 3: Explore how sediment pulses influence the pattern and dynamics of alluvial cover in mixed bedrock-alluvial river networks.

Pulse simulation modelling (Chapter 6) showed that pulse dynamics depends on both pulse characteristics and pre-existing alluvial cover conditions. Pulses introduced at a bedrock site exhibited faster downstream transport with more translational movement, while pulses introduced at an alluvial site showed greater local storage and dispersion-dominant behaviour. Pulse volume also affected dynamics, with smaller pulses moving

faster initially and producing more fragmented volume distributions, while larger pulses moved more coherently and produced more alluvial cover changes. Pulses changed the alluvial cover particularly when introduced at bedrock a reach, where it temporarily transformed channels bedrock into alluvial sections. Post-pulse responses varied spatially, with most reaches (68%) exhibiting deposition but some moderate to high slope reaches (9%) returning to steady state with less cover than before the pulse. This indicates that alluvial cover adjustment processes depend on local channel characteristics, particularly channel slope.

7.3 Linking empirical observations and model results in the River Carron

The combination of empirical and modelling approaches provided a comprehensive understanding of alluvial cover dynamics. The empirical data enabled parameterisation of the numerical model based on a real catchment and provided understanding of how external variables (e.g. climate, glacial history, lithology) control alluvial cover. The modelling, in turn, allowed systematic exploration of controlling variables under different scenarios and time scales that would not be possible to observe in the field, as the simulations represented alluvial cover dynamics in an entire river network over hundreds of years. Therefore, the model provided understanding of network-scale processes, such as connectivity patterns and pulse propagation, that would be difficult to observe directly in the field.

The empirical and modelling approaches converged on the primary role of slope in controlling alluvial cover distribution. Both approaches identified channel slope as the strongest predictor of alluvial cover spatial distribution, with empirical data showing significant negative correlation between slope and alluvial cover percentage, while modelling found that low slope reaches developed alluvial cover first under supply-limited conditions. This agreement between field observations and model simulations strengthens the conclusion that channel slope is a primary control on alluvial cover distribution.

This finding is supported across different environments and methodological approaches. Field studies consistently found that bedrock channels generally have steeper slopes for the same drainage area compared to alluvial channels (Addy et al., 2011; Hodge et al., 2011; Massong & Montgomery, 2000; Montgomery & Gran, 2001; Whitbread et al., 2015). Experimental and numerical modelling studies have provided further understanding of these slope effects (Chatanantavet & Parker, 2008; Cho & Nelson, 2024b; Johnson, 2014). These studies demonstrated that steeper channels have higher transport capacity and therefore require higher sediment supply to exceed this capacity and cause alluviation,, with the critical sediment supply ratio needed to initiate alluviation increasing with increasing slope, similar to the findings from Chapter 5 of this thesis.

Both empirical and modelling results from this thesis showed that local channel characteristics create zones that resist cover change. The empirical analysis found that 12% of reaches had immobile median grain sizes even during extreme events, while modelling showed that some low slope reaches maintained persistent alluvial cover regardless of very high flow conditions and steep channels remained exposed even with high sediment supply. These findings demonstrate how channel slope determines both the transport capacity that controls sediment supply requirements for alluviation and shear stress conditions that determine which grain sizes will be mobilised. This dual control explains why certain reaches maintain persistent characteristics despite varying environmental conditions, creating zones of resistance to morphological change.

This spatial variety in sediment dynamics is particularly evident in studies of post-glacial landscapes, which demonstrate that inherited glacial features create areas of limited fluvial adjustment: paraglacial sediment supply may temporarily increase alluvial cover following deglaciation, but underlying bedrock structure controls where bedrock remained exposed (Jansen et al., 2010); inherited features like lakes and hanging valleys create zones of persistent immobility with very low erosion rates and spatial discontinuities in sediment transport (Brardinoni & Hassan, 2006; Whitbread et al., 2015).

Glacial processes also affect grain size distributions (Towers et al., 2024), creating an important divergence between empirical and modelling results. Empirical observations

found no significant correlation between grain size and alluvial cover, while modelling suggested that larger grains generally increase alluvial cover extent. The empirical finding likely reflects grain size distributions influenced by glacial inheritance and complex sediment sorting processes along mixed bedrock-alluvial systems, where differential transport mechanisms between bedrock and alluvial reaches affect grain size patterns (Ferguson et al., 2017b; Hodge et al., 2011; Hodge & Hoey, 2012). However, the modelling simplified reality by using uniform grain sizes that do not represent the high spatial variability observed in the Carron catchment. This divergence demonstrates challenges in understanding grain size controls across different environments and study approaches.

7.4 Wider implications for different environments

This thesis investigated alluvial cover controls using a post-glacial, tectonically stable mixed bedrock-alluvial river with a temperate oceanic climate and fairly resistant lithology as a reference system. The general findings from this thesis have broad applicability but different environments present particular characteristics that can influence alluvial cover dynamics in specific ways.

7.4.1 Differences between glaciated and non-glaciated landscapes

Non-glaciated landscapes typically exhibit more regular channel profiles with more predictable downstream trends in slope, width and grain size compared to post-glacial landscapes (Ballantyne, 2002; Brardinoni & Hassan, 2006; Towers et al., 2024). As channel slope typically decreases and width increases with drainage area (Leopold & Maddock, 1953; Wohl & David, 2008), the relationship between drainage area and alluvial cover may be stronger in non-glaciated landscapes than observed in this thesis (Chapter 2), with more consistent downstream increases in alluvial cover. In addition, grain sizes in non-glaciated environments typically follow downstream fining patterns (Rice & Church, 1998; Snelder et al., 2011). These typical downstream patterns can create

competing effects on alluvial cover: decreasing slope downstream promotes sediment deposition and increased cover, but decreasing grain size facilitates sediment mobilisation and potentially reduces cover persistence.

As mentioned in section 7.3, this thesis found no significant correlation between grain size and alluvial cover in the Carron catchment (Chapter 2), aligning with Towers et al. (2024) who found no significant relationships between grain size and other topographic, hydrological and climatic variables across several post-glacial catchments in Scotland. Their model for predicting grain size from environmental variables explained only 22% of grain size variance. In contrast, Snelder et al. (2011) found that in France, a largely non-glaciated landscape, environmental variables explained 52% of grain size variance. This suggests stronger correlations between grain size and environmental controls in non-glaciated systems than in post-glacial systems, where glacial inheritance affects typical relationships and influences alluvial cover dynamics.

The Henry Mountains in Utah, United States, provides another comparison as a non-glaciated, tectonically stable setting with mixed bedrock-alluvial rivers. Johnson et al., (2009) found that reaches with abundant coarse sediment (D_{50} = 46 mm, diorite-rich) developed steeper slopes to transport their sediment load, while sediment-poor reaches (98% sand, diorite-poor) maintained gentler slopes. This adjustment of channel morphology to sediment supply indicates a transport-limited equilibrium in the Henry Mountains. In contrast, post-glacial rivers like the Carron show conditions where local sediment supply varies more independently of transport capacity due to inherited glacial topography, as most steep slopes were formed by glacial processes and not yet adjusted to current sediment transport requirements.

These comparisons between post-glacial and non-glaciated landscapes indicate that non-glaciated systems typically present stronger relationships between environmental variables and channel characteristics, more advanced adjustment states where channel morphology has evolved toward equilibrium with contemporary fluvial processes, and potentially more predictable patterns of alluvial cover distribution than post-glacial systems. However, there is a lack of studies exploring alluvial cover distributions in tectonically inactive and non-glaciated regions, limiting our understanding of how

glaciation specifically influences alluvial cover patterns compared to other landscape types.

7.4.3 Tectonically active regions

Tectonically active regions have higher rates of uplift that typically generate steeper channel slopes and bedrock reaches (Whipple, 2004). However, these regions often present higher sediment supplies due to frequent landslides and high erosion rates (Burbank et al., 1996; DiBiase et al., 2010), which can increase alluvial cover. These opposing effects typically create mixed bedrock-alluvial rivers in tectonically active regions.

Comparing findings from the post-glacial Carron with studies from tectonically active regions shows differences in alluvial cover controls. For example, the San Gabriel Mountains, in California, United States, are a rapidly uplifting landscape with erosion rates between 0.1 and 1 mm/year, frequent debris flows into headwater channels, and mixed bedrock-alluvial river systems (DiBiase, 2011). The average alluvial cover found in the San Gabriel Mountains is approximately 96%, with rare bedrock exposure despite bedrock incision (DiBiase, 2011). Even channels experiencing different rates of tectonic forcing showed no observed trend in bedrock exposure with increasing relief or erosion rate in steady-state channels (DiBiase, 2011). This environment contrasts with the River Carron, where the average alluvial cover is lower (around 70%) and with greater spatial variability due to paraglacial processes.

Sediment supply regimes differ between these landscapes. Tectonically active regions like the San Gabriel Mountains have continuous sediment production through active erosion and mass wasting, particularly debris flows that enhance connectivity between hillslopes and the river network (DiBiase et al., 2010; Husic & Michalek, 2022; Lavé & Burbank, 2004; Neely & DiBiase, 2023). Large disturbances such as earthquakes can trigger extensive landsliding that delivers large sediment loads to channels, creating transport-limited conditions where sediment availability exceeds transport capacity (DeLisle et al., 2022; Yanites et al., 2010). This frequent supply maintains higher alluvial

cover even with higher erosion rates. In contrast, post-glacial rivers like the Carron have spatially variable sediment availability, where glacial deposits are often disconnected from the channel network through processes such as paraglacial terrace formation that decouple hillslopes from the channel (Ballantyne, 2002; Brardinoni & Hassan, 2006). This creates a patchy distribution of sediment sources rather than systematic supply limitation or excess found in tectonically active regions.

Another difference between the tectonically active regions and post-glacial landscapes like the River Carron is their adjustment state toward equilibrium. For example, the San Gabriel Mountains show characteristics of a landscape that has adjusted to long-term tectonic forcing, with consistent alluvial cover despite high erosion rates across the range (DiBiase, 2011). This indicates that the system has achieved a balance between sediment supply and transport capacity in most channels (DiBiase et al., 2010). However, exceptions to this balance occur at knickpoints, where sediment cover decreases as valleys narrow and channels steepen in response to tectonic forcing (DiBiase, 2011). The presence of migrating knickpoints indicates ongoing adjustments rather than complete equilibrium. In contrast, post-glacial catchments like the River Carron experience widespread adjustment across the landscape, with the entire network transitioning from glacially inherited conditions toward fluvial equilibrium since deglaciation (Ballantyne, 2002). The post-glacial system has not yet achieved the balance between supply and transport that characterises most tectonically active regions. Adjustment is further limited because fewer extreme events can mobilise all available sediment, as demonstrated by the finding that 12% of reaches remain immobile even during 50-year floods in the Carron (Chapter 2).

7.4.2 Climate and flood regime effects

Climate indirectly influences alluvial cover dynamics through precipitation patterns and flood regimes, which modify both sediment supply and transport processes. Chapter 5 demonstrated that flow depth affects alluvial cover extent, particularly under supply-limited conditions, showing how changes in flow regimes modify alluvial cover patterns. Chapter 6 demonstrated that sediment pulses tend to increase alluvial cover, although

some moderate to high slope reaches return to steady state with less alluvial cover than before the pulse. This occurs because the pulse introduction initially perturbs the equilibrium cover conditions, but as the system adjusts over time, steeper reaches with higher transport capacity can erode the deposited sediment to achieve a new steady state with less sediment retention than their pre-pulse condition.

Research has shown that precipitation events can have complex and contrasting effects: rivers can erode or deposit sediment during high flows depending on sediment supply and local channel characteristics (Cook et al., 2020; DeLisle & Yanites, 2023; Turowski et al., 2013). Cook et al. (2020) demonstrated that a single flood event can lead to both erosion and deposition in different reaches within the same river system, with spatial variations caused by local differences in channel geometry and bedrock roughness. This spatial heterogeneity in flood response is related to the findings from Chapter 6, where sediment pulse simulations showed that most reaches (68%) experienced deposition while some steeper reaches (9%) showed erosion and returned to steady state with reduced alluvial cover. In addition, the effect of precipitation events on alluvial cover depends on stochastic processes that are highly variable in time and space, which creates a complex pattern of disturbance and response that depend on the frequency and magnitude of events (Benda & Dunne, 1997b, 1997a). In this context, the hillslope-river connectivity is particularly important, as it determines how efficiently mass movements triggers by rainfall deliver sediment to river channels (Bracken et al., 2015; Wohl et al., 2019).

Climate change projections indicate a global increase in the frequency of extreme events (Trenberth, 2011), which can increase temporal variability in alluvial cover and modify established patterns. Extreme rainfall events are expected to trigger more mass movements (Gariano & Guzzetti, 2016), potentially leading to larger and more frequent sediment pulses. As demonstrated in Chapter 6, these pulses can transform channel morphology particularly when introduced at bedrock reaches where they can create temporary alluvial sections.

Recent research shows that 20- and 50-year floods have increased in magnitude in temperate zones including the United Kingdom (Chan et al., 2018; Slater et al., 2021). For

post-glacial systems like the Carron, more frequent and intense rainfall could accelerate ongoing paraglacial adjustment processes by mobilising coarse glacial sediments from hillslopes into channels and transporting them downstream. This acceleration could likely result in a more rapid transition from the current state of high spatial variability in alluvial cover toward a more equilibrated system with greater alluvial cover in lower slope reaches and more persistent bedrock exposure in steeper sections. The findings from Chapter 2 that approximately 12% of reaches remained immobile even during extreme events suggest that even with accelerated adjustment, some inherited glacial characteristics would persist.

7.4.4 Lithological controls on alluvial cover

Lithology influences alluvial cover dynamics through its effects on channel geometry, bedrock erodibility, sediment production and grain size characteristics. Channels formed in more resistant lithologies typically develop narrower widths (Massong & Montgomery, 2000; Whitbread et al., 2015), which could potentially promote less alluvial cover due to higher transport capacity per unit width. However, more resistant rocks tend to produce coarser sediment through physical weathering processes (Attal & Lavé, 2009; Sklar et al., 2017), which the modelling from Chapter 5 suggests would increase alluvial cover extent by requiring higher shear stress for mobilisation. In contrast, regions with less resistant lithology typically develop wider channels (Montgomery and Gran, 2001), which would generally promote more alluvial cover. These regions also tend to produce finer sediment (Attal & Lavé, 2009; Roda-Boluda et al., 2018), which is more easily transported and can reduce cover persistence.

The interaction between lithology and sediment supply affects patterns in channel morphology and alluvial cover. Buckley et al. (2024) found that when sediment flux is restricted, bedrock channels may be wider and shallower than alluvial channels with the same lithological characteristics. Johnson et al. (2009) observed this interaction in the Henry Mountains, where diorite-rich and diorite-poor reaches cut through the same sandstone bedrock and developed different morphologies due to variations in sediment supply. These studies demonstrated that lithological controls on alluvial cover are

complex and manifest through the interaction of factors including sediment production rates, grain size characteristics and resulting channel geometry adjustments.

7.5 Practical implications for river management and habitat conservation

The findings of this thesis have several practical implications for river management in mixed bedrock-alluvial rivers, particularly for sediment augmentation programs, habitat conservation and restoration planning. Based on the research results, five management recommendations can be suggested: interventions at specific reaches, long-term monitoring strategies, legacy recognition, network-scale planning and adaptive management approaches.

Interventions at specific reaches takes advantage of the heterogeneous characteristic of mixed bedrock-alluvial systems to select specific reaches for intervention. The finding that slope is a primary control on alluvial cover distribution can inform where sediment management strategies will achieve better results. For example, sediment augmentation programs used to restore habitats (Sklar et al., 2009; Vazquez-Tarrío et al., 2023) should target lower slope reaches that tend to accumulate sediment. Similarly, sediment extraction activities should avoid low slope reaches where alluvial cover is important for habitat, focusing instead on areas where removal will not affect ecological functions (Kondolf, 1997). Another example is related to flow depth. Chapter 5 found that flow depth influences alluvial cover extent particularly under supply-limited conditions, suggesting that dam operators could strategically regulate flows to maintain specific degrees of alluvial cover at specific reaches for ecological purposes (Kondolf et al., 2013), such as preserving salmonid spawning habitat (Buffington et al., 2004).

Long-term monitoring is necessary for understanding long responses to management interventions. The responses observed in pulse experiments (Chapter 6) demonstrate the need for monitoring programs that detect longer-term adjustments that may take years to manifest. The findings suggest that most reaches generally experience rapid aggradation after sediment pulses, followed by gradual incision through the new

deposits, as also observed by East et al. (2018) following dam removals. However, this gradual incision process can lead some reaches to eventually achieve steady-state conditions with lower alluvial cover than their pre-pulse state, indicating the importance of long-term monitoring to observe these delayed responses.

Legacy recognition acknowledges that historical processes continue to influence contemporary river dynamics and must be considered in management planning. In post-glacial systems like the Carron catchment, glacial inheritance creates persistent patterns of alluvial cover that contemporary flows may not yet be able to modify, with some reaches remaining resistant to sediment mobilisation even during extreme events. In addition to natural legacies, Wohl (2015a) discusses legacy effects on sediment dynamics due to human interventions, such as dams or land cover changes, that can persist for decades or centuries. River management strategies should understand existing landscape characteristics and recognise that some features may persist, requiring different management approaches for these resistant reaches.

Network-scale planning considers the upstream-downstream connectivity and broader implications of management interventions. Chapters 5 and 6 showed that bedrock reaches facilitate sediment transport while alluvial reaches act as temporary storage zones. This network perspective is essential for ecological management, as the spatial distribution of different cover types serve for different functions – alluvial segments provide habitats that support diverse species, while bedrock segments control erosion processes within river networks (Steiger et al., 2005; Wohl, 2015b). Local interventions can have effects extending far downstream, affecting sediment connectivity patterns and habitat availability throughout the network.

Adaptive management becomes particularly important as climate change may accelerate the occurrence of extreme events that can exceed historical records (Gariano & Guzzetti, 2016; Trenberth, 2011). The integrated approach adopted by this thesis – combining field observations with network-scale modelling – allows for developing strategies that can respond to varying conditions and extreme events. Effective management of mixed bedrock-alluvial rivers requires developing approaches that can

adapt to changing environmental conditions while considering the high spatial variability of characteristics found in these systems.

7.6 Challenges, opportunities and future research

7.6.1 Data scarcity and challenges in measuring alluvial cover

Research on alluvial cover dynamics in mixed bedrock-alluvial rivers face challenges related to lack of data and difficulties in alluvial cover measurement. The limited availability of long-term datasets in the scientific community restricts our understanding of temporal dynamics and limits model development and validation (Czuba et al., 2017; Murphy et al., 2019). In addition, the field investigations in this thesis faced challenges associated with measuring alluvial cover (Chapter 3). A fundamental limitation is underwater visibility, which affects the accuracy of visual estimates of bed cover, particularly in peat-rich rivers commonly found in post-glacial landscapes. The comparison of surveys from 2010 and 2022 showed difficulties in maintaining consistent methodologies over time, including differences in reach length, sampling strategy and observer bias. These methodological challenges indicate the need for standardised protocols for measuring alluvial cover, allowing for reliable longer monitoring.

Improved practices in methodology include documentation of measurement uncertainty, consistent reach lengths between surveys and supplementary techniques such as probing the riverbed with poles where safe. Advanced technologies such as side-scan sonar, bathymetric LiDAR and drone surveys can improve the measurement accuracy (Buscombe et al., 2016; Dietrich, 2017; Gomez-Heras et al., 2019). However, they still have limitations in terms of cost, accessibility, water visibility and minimum water depth requirements.

Long-term monitoring programs with consistent methodology, particularly around extreme flood events, are essential for improving our understanding of alluvial cover dynamics and validating numerical models. Furthermore, expanding alluvial cover data collection to different environments (e.g. varying climate, tectonic and lithological

conditions) could test the generality of this thesis' findings and improve conceptual models of alluvial cover controls.

7.6.2 Model development and integrating small and large scale processes

Alluvial cover modelling in mixed bedrock-alluvial river network must be advanced to better capture the complexity of these systems. The model development in Chapter 4 provided modifications to the NetworkSedimentTransporter model that enable tracking of alluvial cover in reaches over time across river networks, providing a tool that facilitates more alluvial cover studies at the network scale. Still, the modelling approach adopted in this thesis (Chapters 4, 5 and 6) involved several simplifications that are opportunities for future research. The model assumed uniform grain size throughout the network, although field data showed high spatial variability in grain size. Future simulations should incorporate spatially variable grain size distributions based on field measurements, as demonstrated in the modelling experiments from Ahammad et al. (2021) and Murphy et al. (2019), to better understand how grain size variability affects alluvial cover patterns and sediment transport dynamics.

An additional limitation in this thesis' modelling approach includes channel geometry estimation based on drainage area relationships, which limits understanding of how local geometric variations affect alluvial cover. The model also used uniform critical shear stress regardless of alluvial cover degree, although field studies indicate different entrainment thresholds for bedrock and alluvial surfaces (Ferguson et al., 2017b; Hodge et al., 2011). Furthermore, the model simplified sediment input locations and timings, as well as flow temporal variability, which is necessary for realistic sediment transport and alluvial cover dynamics. Include these variations would require additional field data and computational resources but could improve alluvial cover pattern reproduction and predictions.

The NetworkSedimentTransporter model could be improved by incorporating small-scale processes, particularly grain-to-grain interactions that influence sediment entrainment and deposition at the particle scale (Hodge et al., 2011; Zhang et al., 2015).

Current network-scale models typically aggregate these processes using simplified relationships (Pfeiffer et al., 2020; Shobe et al., 2017; Tangi et al., 2019), but advances in computational capacity could enable the representation of grain-scale physics within network-scale models. Challenges remain in understanding how to couple processes that operate at different spatial and temporal scales (Paola et al., 2009). However, alluvial cover models with this capability could better demonstrate complex non-linear interactions and feedbacks between alluvial cover, hydraulics, and sediment supply, potentially finding emergent behaviours and self-organising properties (Czuba & Foufoula-Georgiou, 2015; Phillips, 2012; Werner, 1999). Recent advances in machine learning offer promising methods for linking these scale gaps (Reichstein et al., 2019), but their application to alluvial cover modelling is unexplored and represents an opportunity for future research.

7.6.3 Connectivity analysis and network-scale understanding

Connectivity analysis of alluvial cover in river networks remains challenging due to the lack of datasets, particularly with temporal data, and limited availability of network-scale models capable of simulating alluvial cover dynamics (Czuba et al., 2017; Turnbull et al., 2018). This thesis provided a model that can generate alluvial cover data for all reaches in a river network over several timesteps, creating opportunities for more advanced connectivity analysis. However, many traditional connectivity metrics from graph theory, such as modularity and clustering coefficient, are not very informative for directed tree-like graphs like the Carron and most river systems (Erős et al., 2012; Heckmann et al., 2015; Zaliapin et al., 2010). Given these limitations of river structure and the inherently dynamic state of river systems, methods that analyse flows and temporal dynamics are valuable, potentially enabling functional connectivity analysis of alluvial cover (Czuba & Foufoula-Georgiou, 2015; Turnbull et al., 2018; Voutsa et al., 2021).

Advanced connectivity analysis methods from other fields such as neuroscience offer promising methods for analysing functional connectivity in mixed bedrock-alluvial rivers (Rinderer et al., 2018). Correlation analyses, such as Pearson Correlation Coefficient and Cross-correlation, are connectivity metrics that can identify river segments with similar

transport behaviours (Rinderer et al., 2018). These connectivity methods allow clustering of functionally connected reaches and indicate how structural network properties such as slope influence functional connectivity. Mutual Information (MI) analysis is a more advanced approach that can promote deeper understanding of functional sediment connectivity in river networks (Kraskov et al., 2004; Rinderer et al., 2018). Unlike simple correlation measures, MI identifies both linear and non-linear relationships between river segments, identifying processes with thresholds that are common in mixed bedrock-alluvial systems. For example, Time Delayed Mutual Information (TDMI) can quantify how sediment pulses propagate through networks, identifying which segments respond similarly to disturbances and determining the time delays between distant segments. These connectivity analyses are relevant to understanding the impact of disturbances on aquatic habitats and for determining flood prevention and river regulation policies (Ascher, 2001).

The application of these connectivity methods to mixed bedrock-alluvial rivers could address important questions about how local processes scale up to network-scale patterns and how different types of reaches (bedrock, mixed, alluvial) contribute to overall network connectivity and resilience (Bracken et al., 2015). However, the application of such advanced connectivity approaches present challenges related to defining adequate spatial and temporal samples to differentiate noises from patterns representing meaningful processes (Rinderer et al., 2018).

7.7 Conclusion

This thesis has made contributions to understanding the mechanisms driving spatial and temporal variability of alluvial cover in mixed bedrock river systems. By combining empirical investigations with network-scale modelling, this research carried out a comprehensive analysis of alluvial cover controls. Channel slope was identified as the primary control on the spatial distribution of alluvial cover, with sediment supply, flow depth and grain size influencing the extent and connectivity of alluvial cover.

Monitoring field data, network-scale modelling and connectivity analysis of alluvial cover is essential to continue improving our understanding of alluvial cover dynamics, particularly temporal dynamics. As climate change and human activities continue to affect river systems worldwide, the understanding of alluvial cover will be increasingly important for climate adaptation strategies, river management and habitat conservation.

Appendices

A1 Model modifications

The NetworkSedimentTransporter (NST) model from Landlab was modified to improve sediment transport modelling and allow specific analyses related to spatial and temporal controls on alluvial cover. Three modifications were implemented:

i.   Function to calculate the percentage of alluvial cover at each link.
ii.   Improved downstream sediment movement algorithm.
iii.   Function to add sediments at any link and timestep.

These modifications are described in Chapter 4 and their codes are shown below. For the original NST code, see Landlab documentation at https://github.com/landlab/landlab.

A1.1 Alluvial cover calculation

A new function was implemented to calculate the percentage of alluvial cover in each reach. The complete code is shown in Listing A1.

```
 1. def calculate_alluvial_cover(nst, timestep, cover_array):
 2.     """
 3.      Calculate the fraction of alluvial cover for each link in the network (both active and
inactive).
 4.
 5.     Parameters
 6.     ----------
 7.     nst: NetworkSedimentTransporter
 8.         Network sediment transport object containing grid, parcels, and parameters
 9.     timestep: int
10.         Current timestep index
11.     cover_array: numpy.ndarray (n_timesteps, n_links)
12.         Array storing alluvial cover history
13.
14.     Returns
15.     -------
16.     numpy.ndarray
17.         Array of alluvial cover evolution where each row represents a timestep and
18.         each column represents a link in the network. Values indicate:
19.         - 0: No sediments deposited (bare bedrock)
20.         - 1: Reach is 100% covered with D50 depth
21.         - >1: Multiple layers of alluvial cover
22.     """
23.     # Calculate mean grain size for each reach
```

```
24.     mean_diameter = calculate_mean_grain_size(nst)
25.
26.     # Initialize array for mean grain size
27.     mean_grain_size = np.full(nst._grid.size("link"), np.nan)
28.     link_ids = mean_diameter.element_id.values.astype(int)
29.     mean_grain_size[link_ids] = mean_diameter.values
30.
31.     # Calculate alluvial cover fraction
32.     cover_fraction = nst._vol_tot / (nst._grid.at_link["channel_width"] *
33.
34.                                     nst._grid.at_link["reach_length"] *
35.                                     mean_grain_size *
36.                                     (1 - nst._bed_porosity))
37.
38.     # Handle reaches with no sediment
39.     cover_fraction = np.nan_to_num(cover_fraction)
40.     print(cover_fraction)
41.
42.     # Store and return results
43.     cover_array[timestep, :] = cover_fraction
44.     nst._grid.at_link["fraction_alluvial_cover"] = cover_fraction
45.
46.     return cover_array
47.
48. def calculate_mean_grain_size(nst):
49.     """Calculate mean grain size for each reach considering all parcels (both active and
inactive)"""
50.     current_parcels = nst._parcels.dataset.isel(time=nst._time_idx)
51.     in_network_parcels = current_parcels.where(
52.         current_parcels.element_id != nst.OUT_OF_NETWORK
53.     )
54.     grouped_parcels = in_network_parcels.groupby("element_id")
55.     mean_diameter = grouped_parcels.mean().D
56.     return mean_diameter
57.
```

Listing A1: Functions to calculate alluvial cover fraction for each link in the river network. The calculate_alluvial_cover function uses the mean grain size to determine the fraction of alluvial cover in each reach, where alluvial cover equal to 0 indicates bare bedrock, 1 indicates complete sediment cove one grain diameter deep, and > 1 indicates multiple layers of sediment cover. The mean grain size (D_{50}) for each reach is calculated using the calculate_mean_grain_size function.

A1.2 Downstream sediment movement

The original NST model's move_parcel_downstream function was modified to improve sediment transport modelling, particularly in steep reaches followed by lower slopes. The modified code updates sediment velocities at each link during transport and transport capacity of links as sediments move downstream. The implementation consists of four connected functions:

1. Main transport function (move_parcel_downstream) (Listing A2)
   - Coordinate sediment movement between links by using the functions below.

2. Velocity update (_calculate_wilcock_crowe_velocity) (Listing A3)

- Implements the Wilcock-Crowe transport equation by calculating updated velocities based on local conditions, i.e., link and sediment characteristics.

3. Transport capacity update (_check_downstream_capacity) (Listing A4)

- Tracks available transport capacity in each link and enforces capacity constraints during transport.

4. Helper functions to define downstream link id (_get_downstream_links, _get_downstream_link_ids) (Listing A5)

- Determines downstream connectivity by assessing downstream link ID.

```python
1. def move_parcel_downstream(nst, dt: float):
2.     """Move and track sediment parcels through the river network.
3.
4.     This is a modified version of the original NST move_parcel_downstream function
5.     by implementing dynamic velocity updating and continuous capacity tracking.
6.
7.     Parameters
8.     ----------
9.     nst: NetworkSedimentTransporter
10.         The NST model instance containing network and parcel information
11.     dt: float
12.         Time step duration in seconds
13.
14.     Notes
15.     -----
16.     The function tracks sediment parcels using:
17.     - Location within each link (0 to 1, representing fractional distance)
18.     - Remaining travel time
19.     - Transport capacity constraints
20.     - Network connectivity
21.     """
22.     # Initialize starting conditions
23.     current_link = nst._parcels.dataset.element_id.values[:, -1].astype(int)
24.     location_in_link = nst._parcels.dataset.location_in_link.values[:, -1]
25.
26.     # Calculate initial travel distances and velocities
27.     distance_to_travel_initially = nst._pvelocity * dt
28.
29.     # Identify active parcels in the network
30.         in_network  =  nst._parcels.dataset.element_id.values[:,  nst._time_idx]  !=
nst.OUT_OF_NETWORK
31.     active = distance_to_travel_initially > 0.0
32.     active_parcel_ids = np.nonzero(in_network * active)[0]
33.
34.     # Initialize tracking variables
35.     moving = np.array(nst._pvelocity, dtype=bool)
36.     time_left_to_travel = np.zeros(np.size(moving))
37.     time_left_to_travel[moving] = nst._time
38.
39.     capacity = (
40.         nst._grid.at_link["channel_width"]
41.         * nst._grid.at_link["reach_length"]
42.         * nst._active_layer_thickness
```

```
43.        )  # in units of m^3
44.
45.       spare_capacity = capacity.copy()  # Track available capacity
46.     actual_distance_traveled = np.zeros_like(distance_to_travel_initially) # Track cumulative
distance for abrasion calculations
47.
48.        link_velocities = np.zeros(nst._grid.number_of_links) # array to store velocities for
each link
49.
50.      while np.any(time_left_to_travel > 0.0):
51.          # Get current link properties
52.          on_network = current_link != nst.OUT_OF_NETWORK
53.          current_link_properties = {
54.              'lengths': nst._grid.at_link["reach_length"][current_link],
55.              'slopes': nst._grid.at_link["channel_slope"][current_link],
56.              'depths': nst._grid.at_link["flow_depth"][current_link],
57.              'active_layer': nst._active_layer_thickness[current_link],
58.              'mean_grain_size': nst._d_mean_active[current_link],
59.              'frac_sand': nst._grid.at_link["sediment__active__sand_fraction"][current_link],
60.              'vol_total': nst._parcels.dataset.volume[:, nst._time_idx].values,
61.              'vol_active': nst._grid.at_link["sediment__active__volume"][current_link]
62.          }
63.
64.          # Calculate velocity for current link conditions
65.          current_grain_size = nst._parcels.dataset.D[:, nst._time_idx].values
66.
67.          current_link_pvelocity = _calculate_wilcock_crowe_velocity_updated(
68.              nst,
69.              current_link_properties,
70.              current_grain_size
71.          )
72.
73.          # Handle zero velocities
74.          current_link_pvelocity = np.maximum(current_link_pvelocity, 1e-10)
75.          print(current_link_pvelocity)
76.
77.          # Store velocities in the corresponding links
78.          # We'll take the maximum velocity for each link if multiple parcels are present
79.          for link_id in np.unique(current_link[current_link != nst.OUT_OF_NETWORK]):
80.              link_mask = current_link == link_id
81.              if np.any(link_mask):
82.                  link_velocities[link_id] = np.max(current_link_pvelocity[link_mask])
83.
84.          # Calculate time to exit current link
85.           time_to_exit = current_link_properties['lengths'] * (1.0 - location_in_link) /
current_link_pvelocity
86.
87.          # Identify parcels that will rest in current link
88.               rest_this_link = (time_left_to_travel < time_to_exit) * on_network *
(time_left_to_travel > 0.0)
89.
90.          if np.any(rest_this_link):
91.              # Store initial position
92.              initial_location = location_in_link[rest_this_link].copy()
93.
94.              # Update locations for parcels staying in current link
95.              location_in_link[rest_this_link] = 1.0 - (
96.                  (current_link_pvelocity[rest_this_link] * time_to_exit[rest_this_link] -
97.                current_link_pvelocity[rest_this_link] * time_left_to_travel[rest_this_link])
98.                  / current_link_properties['lengths'][rest_this_link]
99.              )
100.
101.              # Calculate actual distance traveled based on change in position
102.              actual_distance_traveled[rest_this_link] += (
103.                  current_link_properties['lengths'][rest_this_link] *
104.                  (location_in_link[rest_this_link] - initial_location)
105.              )
106.
107.              time_left_to_travel[rest_this_link] = 0.0
```

```
108.
109.          # Handle downstream movement
110.              moving_downstream = (time_left_to_travel  >=  time_to_exit)  *  on_network  *
(time_left_to_travel > 0.0)
111.
112.          if np.any(moving_downstream):
113.              actual_distance_traveled[moving_downstream] += (
114.                  current_link_properties['lengths'][moving_downstream] *
115.                  (1.0 - location_in_link[moving_downstream])
116.              )
117.
118.              # Reset location for moving parcels
119.              location_in_link[moving_downstream] = 0.0
120.              time_left_to_travel[moving_downstream] -= time_to_exit[moving_downstream]
121.
122.              # Restore capacity in links that parcels are leaving
123.              for link in np.unique(current_link[moving_downstream]):
124.                  if link != nst.OUT_OF_NETWORK:
125.                      leaving_parcels = moving_downstream & (current_link == link)
126.                      spare_capacity[link] += np.sum(
127.                          nst._parcels.dataset.volume.values[leaving_parcels, nst._time_idx]
128.                      )
129.
130.              # Move to downstream link
131.              downstream_link = _get_downstream_link_ids(nst,current_link)
132.              current_link[moving_downstream] = downstream_link[moving_downstream]
133.
134.              # Check capacity constraints in new links
135.              _check_downstream_capacity(
136.                  nst,current_link, time_left_to_travel, spare_capacity
137.              )
138.
139.              # Handle parcels leaving network
140.              moved_oon = (downstream_link[moving_downstream] == nst._grid.BAD_INDEX)
141.              if np.any(moved_oon):
142.                  oon_indices = moving_downstream.nonzero()[0][moved_oon]
143.                  current_link[oon_indices] = nst.OUT_OF_NETWORK
144.                  location_in_link[oon_indices] = np.nan
145.                  time_left_to_travel[oon_indices] = 0.0
146.
147.      # Update parcel properties post-movement
148.
149.      # Calculate abrasion effects
150.      nst._distance_traveled_cumulative += actual_distance_traveled # Update cumulative
distances
151.      vol = _calculate_parcel_volume_post_abrasion(
152.          nst._parcels.dataset.volume[active_parcel_ids, nst._time_idx],
153.          actual_distance_traveled[active_parcel_ids],
154.          nst._parcels.dataset.abrasion_rate[active_parcel_ids]
155.      )
156.
157.      D = _calculate_parcel_grain_diameter_post_abrasion(
158.          nst._parcels.dataset.D[active_parcel_ids, nst._time_idx],
159.          nst._parcels.dataset.volume[active_parcel_ids, nst._time_idx],
160.          vol
161.      )
162.
163.      # Update parcel attributes
164.          nst._parcels.dataset.time_arrival_in_link[active_parcel_ids,  nst._time_idx]  =
nst._time_idx
165.          nst._parcels.dataset.location_in_link[active_parcel_ids,  nst._time_idx]  =
location_in_link[active_parcel_ids]
166.          nst._parcels.dataset.element_id[active_parcel_ids,  nst._time_idx]  =
current_link[active_parcel_ids]
167.      nst._parcels.dataset.D[active_parcel_ids, nst._time_idx] = D
168.      nst._parcels.dataset.volume[active_parcel_ids, nst._time_idx] = vol
169.
170.      return link_velocities  # Return the array of velocities for each link
```

171.

Listing A2: Implementation of the modified sediment transport algorithm. This function manages the downstream movement of sediment parcels, incorporating dynamic velocity calculations and transport capacity tracking. The functions _calculate_wilcock_crowe_velocity_updated, _check_downstream_capacity and _get_downstream_link_ids used in the move_parcel_downstream function are described in Listing A3, A4 and A5. The functions _calculate_parcel_volume_post_abrasion and _calculate_parcel_grain_diameter_post_abrasion are the original described by the Landlab documentation.

```python
1.  def _calculate_wilcock_crowe_velocity_updated(
2.      nst,
3.      link_properties: dict,
4.      grain_size: np.ndarray
5.  ) -> np.ndarray:
6.      """Calculate parcel velocities using the Wilcock-Crowe transport equation.
7.
8.      This function calculates parcel velocities based on current link conditions
9.      and parcel properties. It follows the Wilcock-Crowe (2003) transport
10.     equation.
11.
12.     Parameters
13.     ----------
14.     nst : NetworkSedimentTransporter
15.         The NST model instance
16.     link_properties : dict
17.         Dictionary containing current link properties including:
18.         - slopes: Channel slopes [dimensionless]
19.         - depths: Flow depths [m]
20.         - mean_grain_size: Mean grain size of active layer [m]
21.         - active_layer: Active layer thickness [m]
22.         - frac_sand: Fraction of sand in active layer [dimensionless]
23.         - vol_total: Total sediment volume [m³]
24.         - vol_active: Active sediment volume [m³]
25.     grain_size : np.ndarray
26.         Array of grain sizes for each parcel [m]
27.
28.     Returns
29.     -------
30.     np.ndarray
31.         Array of calculated parcel velocities [m/s]
32.     """
33.     # Physical constants
34.     fluid_density = 1000.0  # kg/m³
35.     sediment_density = 2650.0  # kg/m³
36.     g = 9.81  # m/s²
37.
38.     # Calculate submerged specific gravity
39.     R = (sediment_density - fluid_density) / fluid_density
40.
41.     # Calculate bed shear stress
42.     tau = fluid_density * g * link_properties['slopes'] * link_properties['depths']
43.
44.     # Calculate reference shear stress using sand fraction
45.     tau_ref = (fluid_density * R * g * link_properties['mean_grain_size'] *
46.             (0.021 + 0.015 * np.exp(-20 * link_properties['frac_sand'])))
47.
48.     # Calculate hiding function exponent
49.     b = 0.67 / (1.0 + np.exp(1.5 - (grain_size / link_properties['mean_grain_size'])))
50.
51.     # Calculate reference shear stress for each grain size
52.     tau_r = tau_ref * (grain_size / link_properties['mean_grain_size']) ** b
```

```
53.
54.         # Calculate dimensionless shear stress ratio
55.         tau_tau_r = tau / tau_r
56.
57.         # Convert to complex to handle negative values in power operations
58.         tau_tau_r_complex = tau_tau_r.astype(np.complex128)
59.
60.         # Calculate transport parameter W*
61.         W = np.zeros_like(tau_tau_r_complex, dtype=np.complex128)
62.
63.         # For tau*/tau_r < 1.35
64.         mask_low = tau_tau_r < 1.35
65.         W[mask_low] = 0.002 * np.power(tau_tau_r_complex[mask_low], 7.5)
66.
67.         # For tau*/tau_r >= 1.35
68.         mask_high = tau_tau_r >= 1.35
69.         W[mask_high] = 14 * np.power(
70.             (1 - (0.894 / np.sqrt(tau_tau_r_complex[mask_high]))), 4.5
71.         )
72.
73.         # Calculate volume fraction for each parcel
74.         frac_parcel = np.zeros_like(link_properties['vol_total'], dtype=float)
75.         active_mask = link_properties['vol_active'] != 0.0
76.         frac_parcel[active_mask] = (
77.             link_properties['vol_total'][active_mask] /
78.             link_properties['vol_active'][active_mask]
79.         )
80.
81.         # Initialize velocities array
82.         velocities = np.zeros_like(grain_size, dtype=float)
83.
84.         # Calculate velocities for active parcels
85.     active_parcel_mask = nst._parcels.dataset.active_layer[:, nst._time_idx].values == _ACTIVE
86.
87.         velocities[active_parcel_mask] = (
88.             W.real[active_parcel_mask] *
89.             (tau[active_parcel_mask] ** (3.0/2.0)) *
90.             frac_parcel[active_parcel_mask] /
91.             (fluid_density ** (3.0/2.0)) /
92.             g /
93.             R /
94.             link_properties['active_layer'][active_parcel_mask]
95.         )
96.
97.         # Handle any NaN values
98.         velocities[np.isnan(velocities)] = 0.0
99.
100.        # Warn if velocities exceed 1 m/s (following original implementation)
101.        if np.max(velocities) > 1:
102.            warnings.warn(
103.                f"Maximum parcel virtual velocity exceeds 1 m/s ({np.max(velocities)})",
104.                stacklevel=2
105.            )
106.
107.        return velocities
108.
```

Listing A3: Implementation of the Wilcock-Crowe velocity calculation function. This function calculates parcel velocities using the Wilcock-Crowe (2003) equation, incorporating local hydraulic conditions and sediment properties. This function is called by the main transport algorithm move_parcel_downstream (Listing A2) to update velocities as parcels move through the network.

```python
1. def _check_downstream_capacity(nst, current_link, time_left_to_travel, spare_capacity):
2.     """Check and enforce transport capacity constraints during downstream movement.
3.
4.     Parameters
5.     ----------
6.     nst : NetworkSedimentTransporter
7.         The NST model instance
8.     current_link : np.ndarray
9.         Current link IDs for each parcel
10.     time_left_to_travel : np.ndarray
11.         Remaining travel time for each parcel [s]
12.     spare_capacity : np.ndarray
13.         Array of available transport capacity in each link [m³]
14.     """
15.     for i in range(nst._grid.number_of_links):
16.         # Get parcels in this link
17.         this_links_parcels = np.where(current_link == i)[0]
18.
19.         if this_links_parcels.size == 0:
20.             continue
21.
22.         # Get only parcels that are still moving
23.         active_parcels = this_links_parcels[time_left_to_travel[this_links_parcels] > 0.0]
24.         if active_parcels.size == 0:
25.             continue
26.
27.         # Sort by arrival time (most recent first)
28.         time_arrival_sort = np.flip(np.argsort(
29.             nst._parcels.dataset.time_arrival_in_link.values[active_parcels, -1]
30.         ))
31.         parcel_id_sorted = active_parcels[time_arrival_sort]
32.
33.         # Calculate cumulative volumes
34.         parcel_volumes = nst._parcels.dataset.volume.values[parcel_id_sorted, -1]
35.         cumvol = np.cumsum(parcel_volumes)
36.
37.         # Identify parcels that exceed capacity
38.         exceed_capacity = cumvol > spare_capacity[i]
39.         if np.any(exceed_capacity):
40.             make_inactive = parcel_id_sorted[exceed_capacity]
41.             time_left_to_travel[make_inactive] = 0.0
42.             # Update spare capacity to reflect parcels that were made inactive
43.             spare_capacity[i] -= np.sum(parcel_volumes[~exceed_capacity])
44.
```

Listing A4: Implementation of the transport capacity management function. This function enforces capacity constraints in each reach using a Last-In-First-Out (LIFO) approach, where newer sediments remain mobile while older deposits become immobile when capacity is exceeded. This function is called by the main transport algorithm move_parcel_downstream (Listing A2) to prevent unrealistic sediment movement.

```python
1. def _get_downstream_links(nst) -> np.ndarray:
2.     """Get the downstream link ID for each link in the network.
3.
4.     Parameters
5.     ----------
6.     nst : NetworkSedimentTransporter
7.         The NST model instance
8.
9.     Returns
10.     -------
11.     np.ndarray
12.         Array where index i contains the downstream link ID for link i.
13.         Value is BAD_INDEX (-1) for links that flow to the network outlet.
```

```
14.        """
15.
16.        # Get downstream node for each link
17.        downstream_nodes = nst._fd.downstream_node_at_link()
18.
19.        # Get downstream link for each downstream node
20.        downstream_links = nst._fd.link_to_flow_receiving_node[downstream_nodes]
21.
22.        return downstream_links
23.
24.  def _get_downstream_link_ids(nst, current_links: np.ndarray) -> np.ndarray:
25.        """Get downstream link IDs for a specific set of links.
26.
27.        This is a helper method that uses the pre-calculated downstream links
28.        mapping to quickly get downstream links for a subset of current links.
29.
30.        Parameters
31.        ----------
32.        nst : NetworkSedimentTransporter
33.            The NST model instance
34.        current_links : np.ndarray
35.            Array of link IDs needing downstream connections
36.
37.        Returns
38.        -------
39.        np.ndarray
40.            Array of downstream link IDs corresponding to the input links.
41.        """
42.        # Use pre-calculated downstream links mapping
43.        if not hasattr(nst, '_downstream_links_map'):
44.            _downstream_links_map = _get_downstream_links(nst)
45.
46.        return _downstream_links_map[current_links]
47.
```

Listing A5: These functions map downstream link IDs for each link. The first function (_get_downstream_links) creates a complete network map, while the second (_get_downstream_link_ids) provides a quick lookup of downstream links during sediment transport calculations in the move_parcel_downstream function (Listing A2).

A1.3 Sediment input function

A function was developed to allow sediment inputs at specified locations and times, allowing a flexible sediment input system. The complete code is available in Listing A6. However, the original NST has the SedimentPulserAtLinks class that also adds sediments into the network with greater flexibility.

```
1.    def    add_sediment_parcels(parcels,    receiver_links,    parcels_per_link,    vol_parcel,
median_diameter, density, abrasion_rate, t):
2.        """Add sediment parcels to specified links in the network.
3.
4.        Parameters
5.        ----------
6.        parcels : DataRecord
7.            The parcels dataset
8.        receiver_links : list or array
```

```
 9.          Link IDs where parcels will be added
10.     parcels_per_link : int
11.          Number of parcels to add to each receiver link
12.     vol_parcel : float
13.          Volume of each parcel [m³]
14.     median_diameter : float
15.          Median grain diameter [m]
16.     density : float
17.          Sediment density [kg/m³]
18.     abrasion_rate : float
19.          Mass loss per unit distance [mass/m]
20.     t : float
21.          Current timestep
22.     Returns
23.     -------
24.     None
25.          Parcels are added directly to the DataRecord object
26.     """
27.     # Create element IDs for new parcels
28.     element_ids = np.repeat(receiver_links, parcels_per_link)
29.     element_ids = np.expand_dims(element_ids, axis=1)
30.     starting_link = np.squeeze(element_ids)
31.
32.     # Set random seed for reproducibility
33.     np.random.seed(0)
34.
35.     # Create arrays for parcel properties
36.     n_parcels = np.size(element_ids)
37.
38.     # Initialise basic properties
39.     time_arrival = 0.1 * np.ones(np.shape(element_ids))
40.     volume = vol_parcel * np.ones(np.shape(element_ids)) # (m3)
41.     active_layer = np.ones(np.shape(element_ids)) # 1= active, 0 = inactive
42.     density_array = density * np.ones(n_parcels) # (kg/m3)
43.     location = np.random.rand(n_parcels, 1)
44.     abrasion_array = abrasion_rate * np.ones(np.size(element_ids)) # (mass loss /m)
45.
46.     # Generate lognormal grain size distribution
47.     mu = np.log(median_diameter)
48.     sigma = np.log(2)  # Assumes D84 = 2*D50
49.     grain_diameter = np.random.lognormal(mu, sigma, np.shape(element_ids))
50.
51.     # Define grid elements
52.     grid_elements = np.full(np.shape(element_ids), "link", dtype=object)
53.
54.     # Package data for DataRecord
55.     new_parcels = {
56.         "grid_element": grid_elements,
57.         "element_id": element_ids,
58.     }
59.
60.     new_variables = {
61.         "starting_link": (["item_id"], starting_link),
62.         "abrasion_rate": (["item_id"], abrasion_array),
63.         "density": (["item_id"], density_array),
64.         "time_arrival_in_link": (["item_id", "time"], time_arrival),
65.         "active_layer": (["item_id", "time"], active_layer),
66.         "location_in_link": (["item_id", "time"], location),
67.         "D": (["item_id", "time"], grain_diameter),
68.         "volume": (["item_id", "time"], volume),
69.     }
70.
71.     # Add parcels to DataRecord
72.     parcels.add_item(time=[t], new_item=new_parcels, new_item_spec=new_variables)
```

Listing A6 – Function to add sediment parcels to specified links in the network. The function creates sediment parcels with specific properties (volume, grain size, density) and adds them to chosen links in the network. The grain size follows a lognormal

distribution representing variability in sediment sizes. The initial positions of each within each link are random.

A2 Grain Size Distributions in the Carron Catchment

The grain size data collected in the field were analysed and the Grain Size Distributions for several gravel bars within the Carron Catchment were determined using PebbleCounts (Purinton & Bookhagen, 2019) (Figure A1a and A1b). The grain size survey revealed low sand presence across the catchment. Only around 25% of the gravel bars analysed contained sand, and, in these locations, sand coverage averaged 4% of the surface area. The exception was a flatter alluvial section in the northern tributary (Abhainn), which was predominantly covered by sand but represented only about 5% of the total river network length. The overall median grain size (D_{50}) for the entire catchment was found to be 0.098 m. Analysis of individual tributaries showed differences in grain size distributions. The main channel of the River Carron exhibited a slightly smaller median grain size (D_{50}) of 0.096 m. In contrast, the Glencalvie tributary and other minor tributaries had larger median grain sizes of 0.1135 m and 0.1167 m, respectively. This pattern suggests a general trend of coarser sediment in the tributaries compared to the main channel. The Alladale and Abhainn tributaries had limited data points, with only one sampling location each, which does not represent these tributaries' overall grain size distributions.

Our analysis found significant relationships between grain size (D_{50} and D_{84}) and both channel slope or shear stress (Figures A1c and A1d). The correlations were particularly strong for D_{84}, with p-values of 0.01 for both slope and shear stress relationships. For D, the correlations were also significant, with p-values of 0.05 for slope and 0.03 for shear stress.
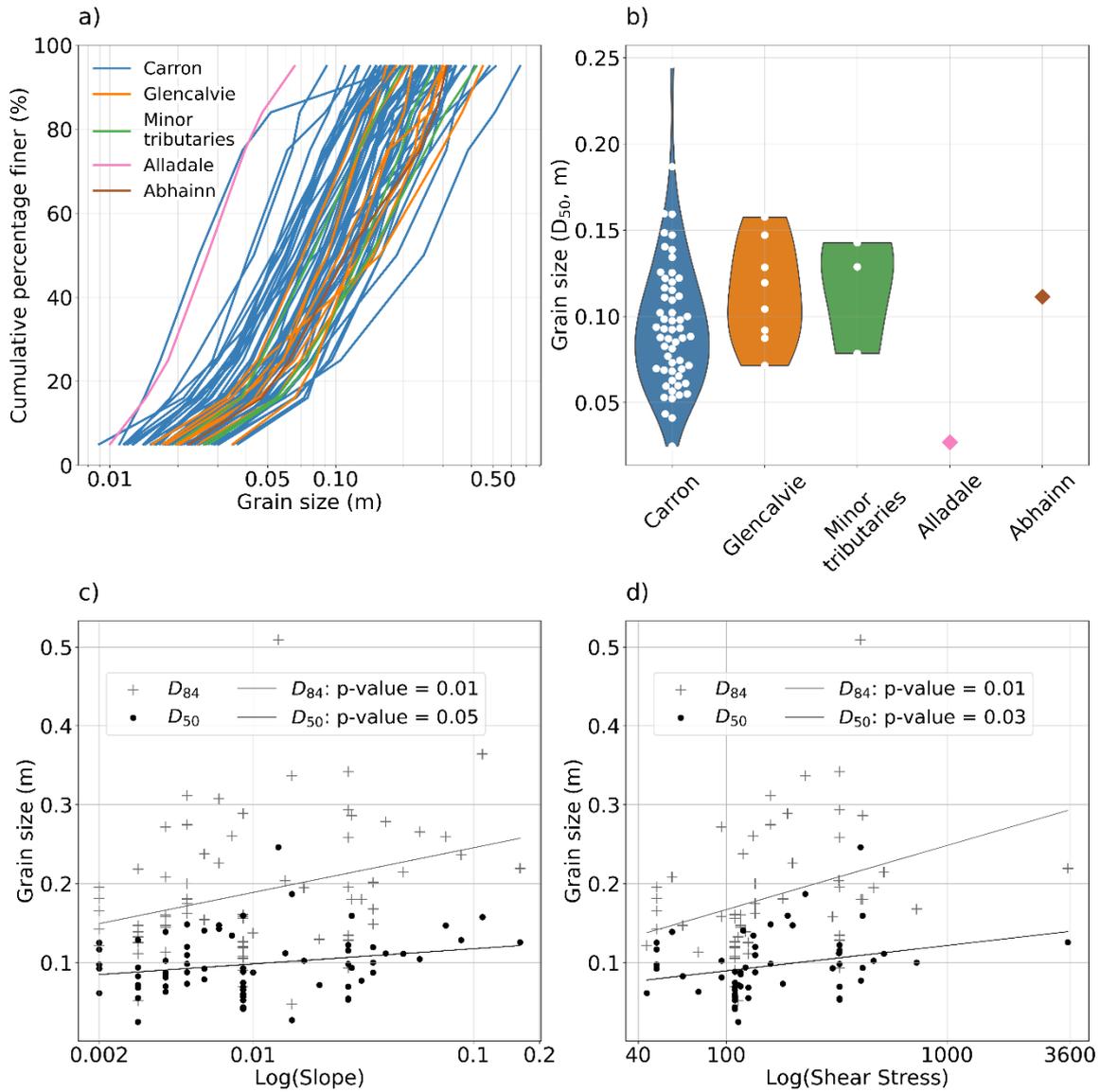
Figure A1: Grain size distributions of gravel bars and relationships in the Carron Catchment. a) Cumulative grain size distributions for different tributaries. b) Violin plots showing the distribution of median grain sizes (D_{50}) across tributaries, with individual data points. Alladale and Abhainn tributaries had data collected from only one gravel bar. c) Relationship between grain size (D_{50} and D_{84}) and channel slope. d) Relationship between grain size (D_{50} and D_{84}) and shear stress. P-values indicate the statistical significance of the relationships and the line shows the linear regression between the variables in c) and d).

A3 Results of the spatial variation of the alluvial cover fraction

The spatial variations of the cover fraction at a steady state for all scenarios are presented in supplementary videos (V1, S2, S3, S4). These videos enhance the visualization of how different parameters affect the alluvial cover. They illustrate the dynamics of alluvial reach expansion and contraction in response to varying initial sediment cover, sediment supply, grain size, and flow depth.

Increasing the initial sediment cover resulted in the expansion of alluvial patches, leading to longer and more continuous alluvial reaches (Video V1). Conversely, increasing flow depth decreased the alluvial cover, demonstrating an inverse relationship between flow depth and sediment deposition (Video V2). Higher sediment supply resulted in an increased number of alluvial patches and longer continuous alluvial reaches, highlighting the critical role of sediment availability in the development of alluvial cover (Video V3). Larger grain sizes led to an expansion of the alluvial cover compared to smaller grain sizes, due to their greater capacity to resist transport and settle in the riverbed (Video V4).

These visual aids enhance the understanding of the network-scale dynamics of alluvial cover in mixed bedrock-alluvial river systems. They provide a comprehensive view of how variations in each parameter influence the spatial distribution and extent of alluvial patches.

Video V1. Spatial variations of the cover fraction for all scenarios of the initial sediment cover simulated. This short video shows how different levels of initial sediment cover influence the extent of alluvial patches at steady state.

Video V2. Spatial variations of the cover fraction for all scenarios of flow depth simulated. This short video demonstrates the impact of varying flow depths on the alluvial cover at steady state.

Video V3. Spatial variations of the cover fraction for all scenarios of sediment supply simulated. This short video illustrates the effect of different sediment supply rates on the development of alluvial patches.

Video V4. Spatial variations of the cover fraction for all scenarios of grain size simulated. This short video highlights how different grain sizes affect the spatial distribution of the alluvial cover.

A4 Connectivity analysis of cover sections comparing field data to model simulations

Figure A2 provides a quantitative comparison of connectivity metrics between observed and modelled cover patterns in the main trunk of River Carron, complementing the network-wide analysis presented in Figure 5.10 in Chapter 5. This analysis shows that the model consistently produced shorter and more numerous sections for all cover types compared to the field data (Figure A2). This difference in connectivity between the model and field observations may be influenced by the difference in the definition of sections. The river sections were defined in the field as a river segment with similar channel characteristics, such as slope, width and alluvial cover. The river sections of the simulations were simply defined according to the alluvial cover percentage. This may have led into consistently shorter sections in the model results.

The comparison between Figure A2 and Figure 5.10 in Chapter 5 provides insights of connectivity trends of the main trunk of River Carron compared to the entire network. Although the general connectivity trends among them were similar, the sediment supply showed a prominent difference in the connectivity of bedrock sections: the length of bedrock sections in the main channel (Figure A2d) was less affected by changes in sediment supply compared to the network-wide analysis (Figure 5.10 in Chapter 5). This difference likely happened because the main channel received sediment input from all tributaries, generating a minimum level of sediment cover even under low supply conditions. Differently, smaller tributaries from the network were more affected by low sediment supply conditions, generating longer bedrock sections.
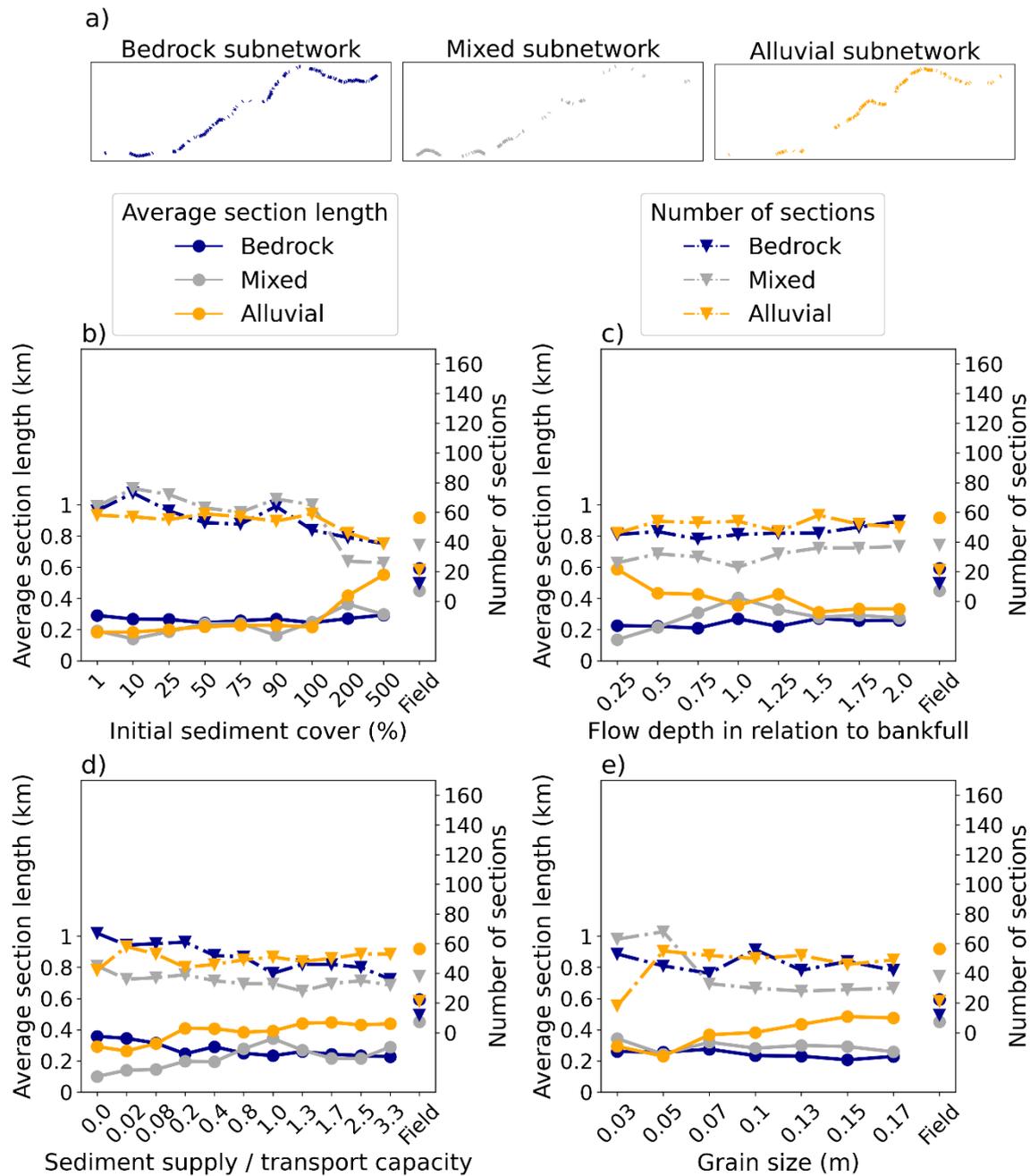
Figure A2: Connectivity analysis of cover sections for the main River Carron, comparing field data to model simulations. a) Examples of subnetworks for each cover category (bedrock, mixed, or alluvial) from the default simulation for the main river. Comparison of average section length and number of sections for each cover category between field data and different simulations varying: b) initial sediment cover; c) flow depth relative to bankfull depth; d) sediment supply relative to transport capacity; and e) grain size.

A5 Comparison of NetworkSedimentTransport (NST) model with a zero-order model based on transport capacity

We conducted further analysis on the NST model results by comparing it with the results of a simplified zero-order model based on transport capacity. This zero-order model assumes full alluviation when a reach's transport capacity exceeds the sediment supply. Therefore, we first calculated the transport capacity for each reach using the initial conditions of the NST model. Then, we compared the transport capacity with the sediment supply at each reach. Finally, we simply classified reaches as "alluvial" if the sediment supply exceeded the transport capacity and "bedrock" otherwise. Key differences between the NST and the zero-order models are:

1. Sediment routing: The NST model represents complex sediment routing and storage dynamics that affect transport capacity, potentially showing bottleneck locations where sediments accumulate for a long time before moving downstream. The zero-order model assumes that all sediments are being transported downstream without accounting for potential bottlenecks and local storage effects.

2. Partial cover: The NST model allows for partial sediment cover, while the zero-order model uses a binary classification (alluvial or bedrock).

3. Temporal dynamics: The NST model represents the temporal evolution of sediment cover, including adjustments in channel slope and transport capacity over time, which the zero-order model does not consider.

The zero-order model resulted in considerably more alluvial reaches compared to the NST model, particularly under high sediment supply conditions (Figures A3 and A4). This indicates that the NST simulations are not completely in steady state, as some bottleneck reaches are partially restricting the transport of sediments downstream, creating more supply-limited conditions in downstream areas. Achieving a complete steady state in NST would require a very long computation time and it was not feasible for our simulations. Our current simulations represent hundreds of years (up to around 3000 years) of river evolution, which was still not sufficient to reach full steady state in all reaches. The NST results are probably a better representation of what might actually be

observed in the field. Real river systems rarely reach a complete steady state due to ongoing environmental changes and the very long time needed to achieve equilibrium. The results found by NST after hundreds of years of simulation provide valuable insights into the system's evolution and relative stability. More realistic simulations could incorporate sediment supply along the network to better represent hillslope conditions and prevent issues with bottlenecks.

In conclusion, the zero-order model provided a useful first approximation of alluvial cover distribution at steady state. However, strengths of using the NST model include deeper understanding of temporal and spatial dynamics of sediment transport, storage and channel slope adjustments. It captures partial cover conditions and allows for analysis of additional parameters such as grain size variability and temporal flows variations.
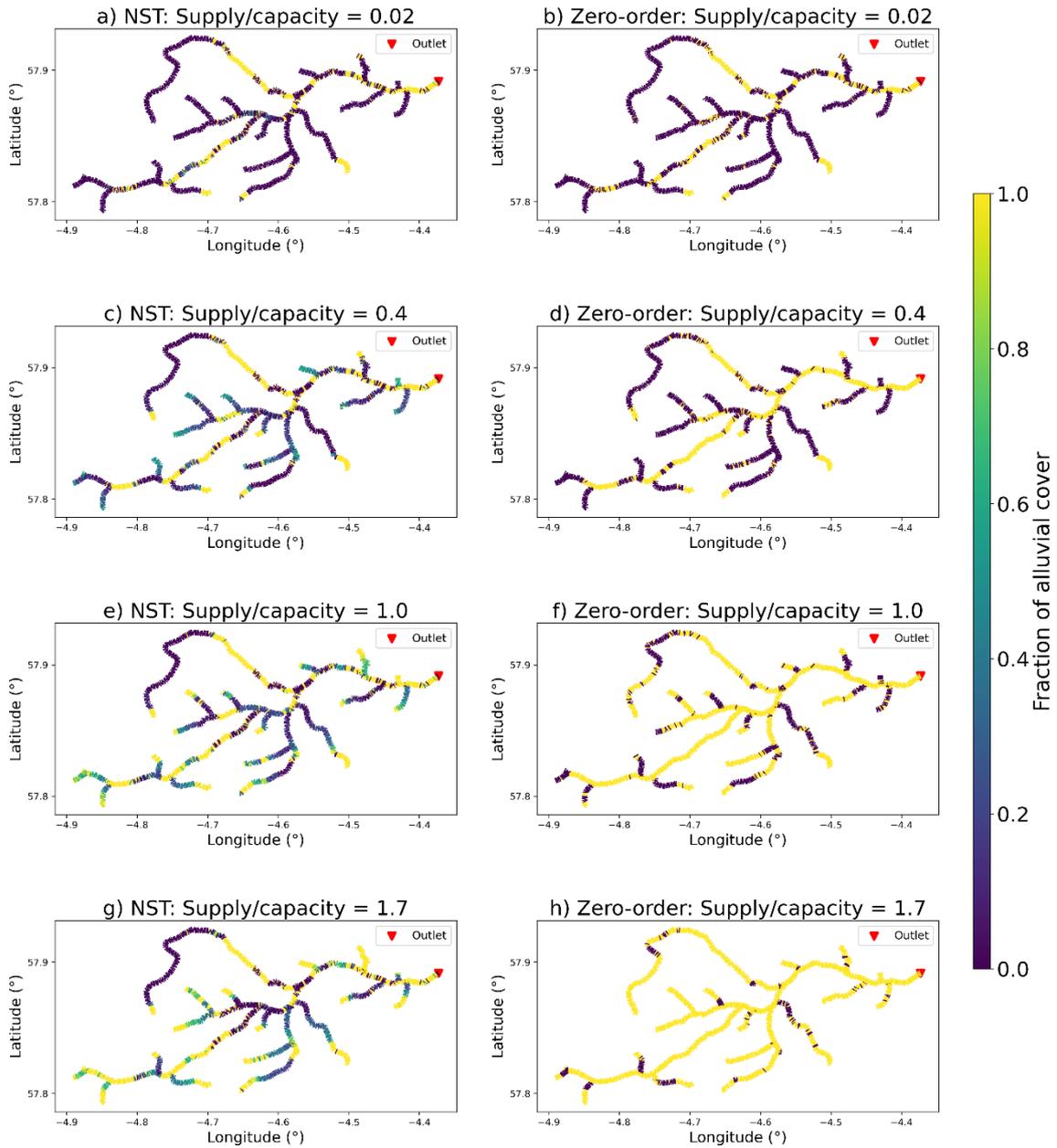
Figure A3: Comparison of alluvial cover distribution between NST model results (left column) and zero-order model results (right column) at varying sediment supply conditions: (a,b) supply/capacity = 0.02; (c,d) supply/capacity = 0.4; (e,f) supply/capacity = 1.0; (g,h) supply/capacity = 1.7.
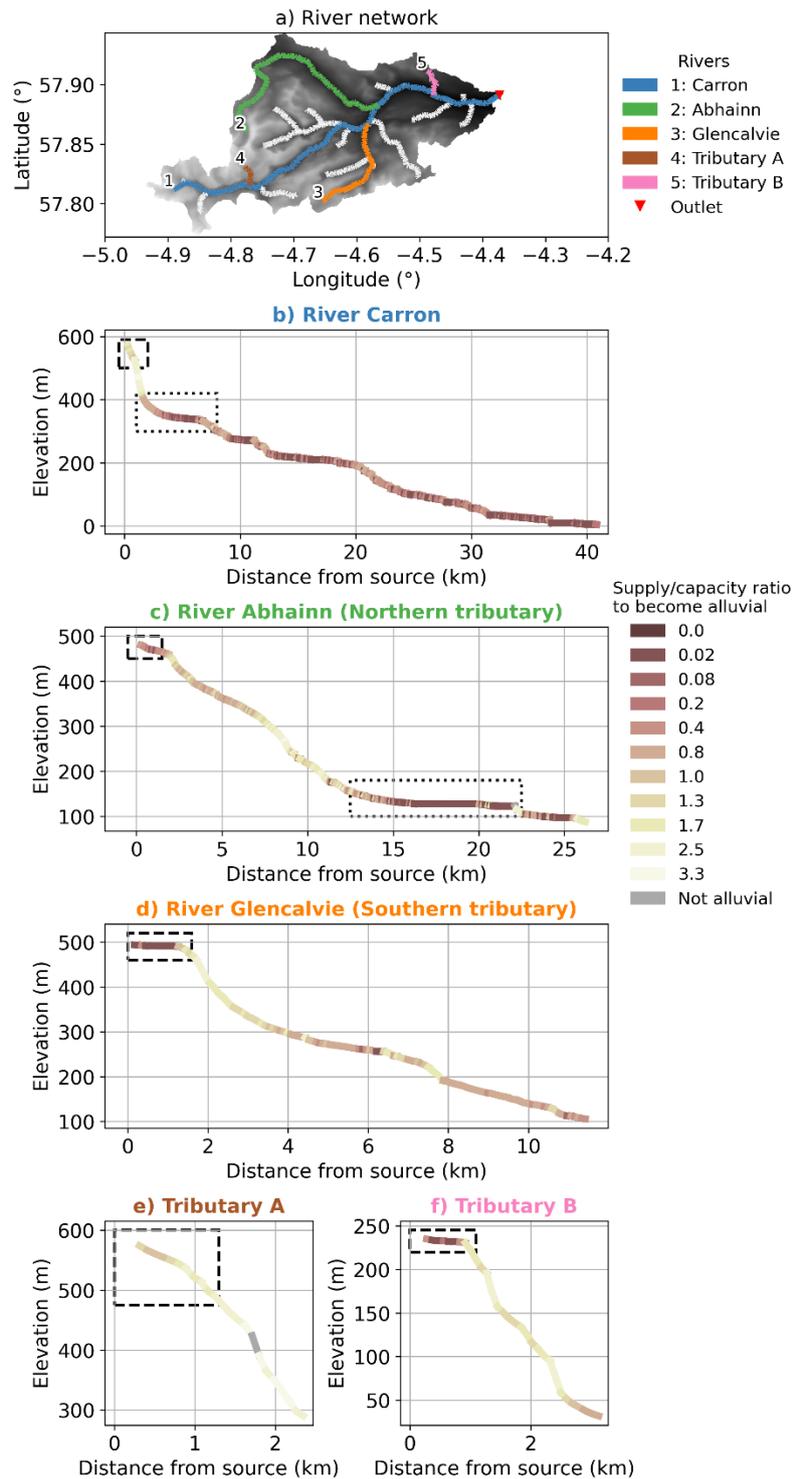
Figure A4: Longitudinal river profiles showing the sediment supply/capacity threshold required for reaches to become alluvial according to the zero-order model. This figure can be compared with Figure 5.11 in Chapter 5, which shows equivalent results from the NST model.

Bibliography

Addy, S., Soulsby, C., Hartley, A. J., & Tetzlaff, D. (2011). Characterisation of channel reach morphology and associated controls in deglaciated montane catchments in the Cairngorms, Scotland. *Geomorphology*, *132*(3–4), 176–186. https://doi.org/10.1016/j.geomorph.2011.05.007

Agostinelli, C. (2002). Robust stepwise regression. *Journal of Applied Statistics*, *29*(6), 825–840. https://doi.org/10.1080/02664760220136168

Ahammad, M., Czuba, J. A., Pfeiffer, A. M., Murphy, B. P., & Belmont, P. (2021). Simulated Dynamics of Mixed Versus Uniform Grain Size Sediment Pulses in a Gravel-Bedded River. *Journal of Geophysical Research: Earth Surface*, *126*(10). https://doi.org/10.1029/2021JF006194

An, C., Cui, Y., Fu, X., & Parker, G. (2017). Gravel-bed river evolution in earthquake-prone regions subject to cycled hydrographs and repeated sediment pulses. *Earth Surface Processes and Landforms*, *42*(14), 2426–2438. https://doi.org/10.1002/esp.4195

Arcement, G. J., & Schneider, V. R. (1989). *Guide for selecting Manning's roughness coefficients for natural channels and flood plains* (Water Supply Paper, p. 38) [USGS Numbered Series]. USGS. https://doi.org/10.3133/wsp2339

Ascher, W. (2001). Coping with Complexity and Organizational Interests in Natural Resource Management. *Ecosystems*, *4*(8), 742–757. https://doi.org/10.1007/s10021-001-0043-y

Attal, M., & Lavé, J. (2009). Pebble abrasion during fluvial transport: Experimental results and implications for the evolution of the sediment load along rivers. *Journal of Geophysical Research: Earth Surface*, *114*(F4), 2009JF001328. https://doi.org/10.1029/2009JF001328

Bainbridge, R., Lim, M., Dunning, S., Winter, M. G., Diaz-Moreno, A., Martin, J., Torun, H., Sparkes, B., Khan, M. W., & Jin, N. (2022). Detection and forecasting of shallow landslides: Lessons from a natural laboratory. *Geomatics, Natural Hazards and Risk*, *13*(1), 686–704. https://doi.org/10.1080/19475705.2022.2041108

Ballantyne, C. K. (2002). Paraglacial geomorphology. *Quaternary Science Reviews*, *21*(18–19), 1935–2017. https://doi.org/10.1016/S0277-3791(02)00005-7

Ballantyne, C. K. (2004). *Geomorphological changes and trends in Scotland: Debris-flows* (Commissioned Report No. 052 (ROAME No. F00AC107A); p. 19). Scottish Natural Heritage. https://www.nature.scot/doc/naturescot-commissioned-report-52-geomorphological-changes-and-trends-scotland-debris-flows

Ballantyne, C. K. (2008). After the Ice: Holocene Geomorphic Activity in the Scottish Highlands. *Scottish Geographical Journal*, *124*(1), 8–52. https://doi.org/10.1080/14702540802300167

Baynes, E. R. C., Kincey, M. E., & Warburton, J. (2023). Extreme Flood Sediment Production and Export Controlled by Reach-Scale Morphology. *Geophysical Research Letters*, *50*(10), e2023GL103042. https://doi.org/10.1029/2023GL103042

Baynes, E. R. C., Lague, D., Steer, P., Bonnet, S., & Illien, L. (2020). Sediment flux-driven channel geometry adjustment of bedrock and mixed gravel–bedrock rivers. *Earth*

Surface Processes and Landforms, *45*(14), 3714–3731. https://doi.org/10.1002/esp.4996

Benda, L., & Dunne, T. (1997a). Stochastic forcing of sediment routing and storage in channel networks. *Water Resources Research*, *33*(12), 2865–2880. https://doi.org/10.1029/97WR02387

Benda, L., & Dunne, T. (1997b). Stochastic forcing of sediment supply to channel networks from landsliding and debris flow. *Water Resources Research*, *33*(12), 2849–2863. https://doi.org/10.1029/97WR02388

Bennett, G. L., Panici, D., Rengers, F. K., Kean, J. W., & Rathburn, S. L. (2025). Landslide-channel feedbacks amplify channel widening during floods. *Npj Natural Hazards*, *2*(1), 7. https://doi.org/10.1038/s44304-025-00059-6

Bennett, M. R., & Boulton, G. S. (1993). Deglaciation of the younger dryas or Loch Lomond Stadial ice-field in the northern Highlands, Scotland. *Journal of Quaternary Science*, *8*(2), 133–145. https://doi.org/10.1002/jqs.3390080206

Bergman, N., Van De Wiel, M. J., & Hicock, S. R. (2022). Sedimentary characteristics and morphologic change of till-bedded semi-alluvial streams: Medway Creek, Southern Ontario, Canada. *Geomorphology*, *399*, 108061. https://doi.org/10.1016/j.geomorph.2021.108061

Bizzi, S., Tangi, M., Schmitt, R. J. P., Pitlick, J., Piégay, H., & Castelletti, A. F. (2021). Sediment transport at the network scale and its link to channel morphology in the braided Vjosa River system. *Earth Surface Processes and Landforms*, *46*(14), 2946–2962. https://doi.org/10.1002/esp.5225

Bracken, L. J., Turnbull, L., Wainwright, J., & Bogaart, P. (2015). Sediment connectivity: A framework for understanding sediment transfer at multiple scales: SEDIMENT

CONNECTIVITY: SEDIMENT TRANSFER AT MULTIPLE SCALES. *Earth Surface Processes and Landforms*, *40*(2), 177–188. https://doi.org/10.1002/esp.3635

Brardinoni, F., & Hassan, M. A. (2006). Glacial erosion, evolution of river long profiles, and the organization of process domains in mountain drainage basins of coastal British Columbia. *Journal of Geophysical Research: Earth Surface*, *111*(F1), 2005JF000358. https://doi.org/10.1029/2005JF000358

Brardinoni, F., & Hassan, M. A. (2007). Glacially induced organization of channel-reach morphology in mountain streams. *Journal of Geophysical Research*, *112*, 18. https://doi.org/10.1029/2006JF000741

British Geological Survey. (2008). BGS Geology 625K. Retrieved from https://www.bgs.ac.uk/datasets/bgs-geology-625k-digmapgb/

British Geological Survey. (2024). National Landslide Database [Data set]. Retrieved from https://www.bgs.ac.uk/datasets/national-landslide-database/

Buckley, J., Hodge, R. A., & Slater, L. J. (2024). Bedrock rivers are steep but not narrow: Hydrological and lithological controls on river geometry across the USA. *Geology*. https://doi.org/10.1130/G51627.1

Buechel, M. E. H., Hodge, R. A., & Kenmare, S. (2022). The influence of bedrock river morphology and alluvial cover on gravel entrainment: Part 1. Pivot angles and surface roughness. *Earth Surface Processes and Landforms*, *47*(14), 3361–3375. https://doi.org/10.1002/esp.5463

Buffington, J. M., Montgomery, D. R., & Greenberg, H. M. (2004). Basin-scale availability of salmonid spawning gravel as influenced by channel type and hydraulic roughness in mountain catchments. *Canadian Journal of Fisheries and Aquatic Sciences*, *61*(11), 2085–2096. https://doi.org/10.1139/f04-141

Burbank, D. W., Leland, J., Fielding, E., Anderson, R. S., Brozovic, N., Reid, M. R., & Duncan, C. (1996). Bedrock incision, rock uplift and threshold hillslopes in the northwestern Himalayas. *Nature*, *379*(6565), 505–510. https://doi.org/10.1038/379505a0

Buscombe, D., Grams, P. E., & Smith, S. M. C. (2016). Automated Riverbed Sediment Classification Using Low-Cost Sidescan Sonar. *Journal of Hydraulic Engineering*, *142*(2), 06015019. https://doi.org/10.1061/(ASCE)HY.1943-7900.0001079

Carretier, S., Martinod, P., Reich, M., & Godderis, Y. (2016). Modelling sediment clasts transport during landscape evolution. *Earth Surface Dynamics*, *4*(1), 237–251. https://doi.org/10.5194/esurf-4-237-2016

Chan, S. C., Kahana, R., Kendon, E. J., & Fowler, H. J. (2018). Projected changes in extreme precipitation over Scotland and Northern England using a high-resolution regional climate model. *Climate Dynamics*, *51*(9–10), 3559–3577. https://doi.org/10.1007/s00382-018-4096-4

Chatanantavet, P., & Parker, G. (2008). Experimental study of bedrock channel alluviation under varied sediment supply and hydraulic conditions: EXPERIMENTS. *Water Resources Research*, *44*(12). https://doi.org/10.1029/2007WR006581

Cho, J., & Nelson, P. A. (2024a). Patterns of Alluviation in Mixed Bedrock-Alluvial Channels: 1. Numerical Model. *Journal of Geophysical Research: Earth Surface*, *129*(1), e2023JF007292. https://doi.org/10.1029/2023JF007292

Cho, J., & Nelson, P. A. (2024b). Patterns of Alluviation in Mixed Bedrock-Alluvial Channels: 2. Controls on the Formation of Alluvial Patches. *Journal of*

Geophysical Research: Earth Surface, *129*(1), e2023JF007293. https://doi.org/10.1029/2023JF007293

Church, M. and Ryder, J.M., 1972. Paraglacial Sedimentation: A Consideration of Fluvial Processes Conditioned by Glaciation. *Geological Society of America Bulletin*, 83(10): 3059-3072.

Clark, P. U., Dyke, A. S., Shakun, J. D., Carlson, A. E., Clark, J., Wohlfarth, B., Mitrovica, J. X., Hostetler, S. W., & McCabe, A. M. (2009). The Last Glacial Maximum. *Science*, *325*(5941), 710–714. https://doi.org/10.1126/science.1172873

Cook, K. L., Turowski, J. M., & Hovius, N. (2020). Width control on event-scale deposition and evacuation of sediment in bedrock-confined channels. *Earth Surface Processes and Landforms*, *45*(14), 3702–3713. https://doi.org/10.1002/esp.4993

Coulthard, T. J., Neal, J. C., Bates, P. D., Ramirez, J., De Almeida, G. A. M., & Hancock, G. R. (2013). Integrating the LISFLOOD-FP 2D hydrodynamic model with the CAESAR model: Implications for modelling landscape evolution: INTEGRATING HYDRODYNAMICS IN LANDSCAPE EVOLUTION MODELS. *Earth Surface Processes and Landforms*, *38*(15), 1897–1906. https://doi.org/10.1002/esp.3478

Croissant, T., Lague, D., Steer, P., & Davy, P. (2017). Rapid post-seismic landslide evacuation boosted by dynamic river width. *Nature Geoscience*, *10*(9), 680–684. https://doi.org/10.1038/ngeo3005

Cui, Y., Asce, M., Parker, G., Asce, M., Engineer, H., Sciences, S., & Ave, T. (2005). Numerical Model of Sediment Pulses and Sediment-Supply Disturbances in Mountain Rivers. *Journal of Hydraulic Engineering,* 131(8), 646–656. https://doi.org/10.1061/(ASCE)0733-9429(2005)131:8(646)

Cui, Y., Parker, G., Lisle, T. E., Gott, J., Hansler-Ball, M. E., Pizzuto, J. E., Allmendinger, N. E., & Reed, J. M. (2003). Sediment pulses in mountain rivers: 1. Experiments. *Water Resources Research*, *39*(9), 2002WR001803. https://doi.org/10.1029/2002WR001803

Czuba, J. A. (2018). A Lagrangian framework for exploring complexities of mixed-size sediment transport in gravel-bedded river networks. *Geomorphology*, *321*, 146–152. https://doi.org/10.1016/j.geomorph.2018.08.031

Czuba, J. A., & Foufoula-Georgiou, E. (2014). A network-based framework for identifying potential synchronizations and amplifications of sediment delivery in river basins. *Water Resources Research*, *50*(5), 3826–3851. https://doi.org/10.1002/2013WR014227

Czuba, J. A., & Foufoula-Georgiou, E. (2015). Dynamic connectivity in a fluvial network for identifying hotspots of geomorphic change. *Water Resources Research*, *51*(3), 1401–1421. https://doi.org/10.1002/2014WR016139

Czuba, J. A., Foufoula-Georgiou, E., Gran, K. B., Belmont, P., & Wilcock, P. R. (2017). Interplay between spatially explicit sediment sourcing, hierarchical river-network structure, and in-channel bed material sediment transport and storage dynamics. *Journal of Geophysical Research: Earth Surface*, *122*(5), 1090–1120. https://doi.org/10.1002/2016JF003965

Davy, P., & Lague, D. (2009). Fluvial erosion/transport equation of landscape evolution models revisited. *Journal of Geophysical Research: Earth Surface*, *114*(F3), 2008JF001146. https://doi.org/10.1029/2008JF001146

DeLisle, C., & Yanites, B. J. (2023). Rethinking Variability in Bedrock Rivers: Sensitivity of Hillslope Sediment Supply to Precipitation Events Modulates Bedrock Incision During Floods. *Journal of Geophysical Research: Earth Surface*, *128*(9), e2023JF007148. https://doi.org/10.1029/2023JF007148

DeLisle, C., Yanites, B. J., Chen, C.-Y., Shyu, J. B. H., & Rittenour, T. M. (2022). Extreme event-driven sediment aggradation and erosional buffering along a tectonic gradient in southern Taiwan. *Geology*, *50*(1), 16–20. https://doi.org/10.1130/G49304.1

DiBiase, R. A. (2011). *Tectonic Geomorphology of the San Gabriel Mountains, CA* [PhD Dissertation]. Arizona State University.

DiBiase, R. A., Whipple, K. X., Heimsath, A. M., & Ouimet, W. B. (2010). Landscape form and millennial erosion rates in the San Gabriel Mountains, CA. *Earth and Planetary Science Letters*, *289*(1–2), 134–144. https://doi.org/10.1016/j.epsl.2009.10.036

Dietrich, J. T. (2017). Bathymetric Structure-from-Motion: Extracting shallow stream bathymetry from multi-view stereo photogrammetry. *Earth Surface Processes and Landforms*, *42*(2), 355–364. https://doi.org/10.1002/esp.4060

East, A. E., Logan, J. B., Mastin, M. C., Ritchie, A. C., Bountry, J. A., Magirl, C. S., & Sankey, J. B. (2018). Geomorphic Evolution of a Gravel-Bed River Under Sediment-Starved Versus Sediment-Rich Conditions: River Response to the World's Largest Dam Removal. *Journal of Geophysical Research*, *123*(12), 3338–3369. https://doi.org/10.1029/2018JF004703

Erős, T., Olden, J. D., Schick, R. S., Schmera, D., & Fortin, M.-J. (2012). Characterizing connectivity relationships in freshwaters using patch-based graphs. *Landscape Ecology*, *27*(2), 303–317. https://doi.org/10.1007/s10980-011-9659-2

Ferguson, R. I., Sharma, B. P., Hardy, R. J., Hodge, R. A., & Warburton, J. (2017a). Flow resistance and hydraulic geometry in contrasting reaches of a bedrock channel: BEDROCK FLOW RESISTANCE. *Water Resources Research*, *53*(3), 2278–2293. https://doi.org/10.1002/2016WR020233

Ferguson, R. I., Sharma, B. P., Hodge, R. A., Hardy, R. J., & Warburton, J. (2017b). Bed load tracer mobility in a mixed bedrock/alluvial channel: Tracer-Pebble Mobility Over Bedrock. *Journal of Geophysical Research: Earth Surface*, *122*(4), 807–822. https://doi.org/10.1002/2016JF003946

Finnegan, N. J., Klier, R. A., Johnstone, S., Pfeiffer, A. M., & Johnson, K. (2017). Field evidence for the control of grain size and sediment supply on steady-state bedrock river channel slopes in a tectonically active setting: Grain size and steady-state bedrock river channel slopes. *Earth Surface Processes and Landforms*, *42*(14), 2338–2349. https://doi.org/10.1002/esp.4187

Finnegan, N. J., Sklar, L. S., & Fuller, T. K. (2007). Interplay of sediment supply, river incision, and channel morphology revealed by the transient evolution of an experimental bedrock channel. *Journal of Geophysical Research: Earth Surface*, *112*(F3), 2006JF000569. https://doi.org/10.1029/2006JF000569

Fryirs, K. (2013). (Dis)Connectivity in catchment sediment cascades: A fresh look at the sediment delivery problem: (DIS)CONNECTIVITY IN CATCHMENT SEDIMENT CASCADES. *Earth Surface Processes and Landforms*, *38*(1), 30–46. https://doi.org/10.1002/esp.3242

Gariano, S. L., & Guzzetti, F. (2016). Landslides in a changing climate. *Earth-Science Reviews*, *162*, 227–252. https://doi.org/10.1016/j.earscirev.2016.08.011

Getmapping. (2023) High Resolution (25cm) Vertical Aerial Imagery [JPG geospatial data], Scale 1:500, Updated: 7 September 2023, Using: EDINA Aerial Digimap Service, <https://digimap.edina.ac.uk>, Downloaded: 2025-04-04.

Gilbert, G. K. (1877). Report on the geology of the Henry Mountains. U.S. Geographical and Geological Survey of the Rocky Mountain Region, Government Printing Office, Washington, D.C.

Gomez-Heras, M., Ortega-Becerril, J. A., Garrote, J., Fort, R., & Lopez-Gonzalez, L. (2019). Morphometric measurements of bedrock rivers at different spatial scales and applications to geomorphological heritage research. *Progress in Earth and Planetary Science*, *6*(1), 29. https://doi.org/10.1186/s40645-019-0275-0

Goode, J. R., & Wohl, E. (2010). Coarse sediment transport in a bedrock channel with complex bed topography. *Water Resources Research*, *46*(11), 2009WR008135. https://doi.org/10.1029/2009WR008135

Gran, K. B., & Czuba, J. A. (2017). Sediment pulse evolution and the role of network structure. *Geomorphology*, *277*, 17–30. https://doi.org/10.1016/j.geomorph.2015.12.015

Guirro, M. O., Hodge, R., Clubb, F., & Turnbull, L. (2025a). Network-Scale Dynamics of Alluvial Cover in a Mixed Bedrock-Alluvial River. *Journal of Geophysical Research: Earth Surface*, *130*(3), e2024JF007968. https://doi.org/10.1029/2024JF007968

Guirro, M. O., Hodge, R., Clubb, F., & Turnbull, L. (2025b). Sediment Cover and Grain Size Data for the River Carron Catchment, Scotland (2022) [Dataset]. Zenodo. https://doi.org/10.5281/zenodo.14826181

Hagberg, A. A, Schult, D. A., Swart, P. J., (2008). Exploring network structure, dynamics, and function using NetworkX, in *Proceedings of the 7th Python in Science Conference (SciPy2008)*, Gäel Varoquaux, Travis Vaught, and Jarrod Millman (Eds), (Pasadena, CA USA), pp. 11–15.

Hauer, F. R., Locke, H., Dreitz, V. J., Hebblewhite, M., Lowe, W. H., Muhlfeld, C. C., Nelson, C. R., Proctor, M. F., & Rood, S. B. (2016). Gravel-bed river floodplains are the ecological nexus of glaciated mountain landscapes. *Science Advances*, *2*(6), e1600026. https://doi.org/10.1126/sciadv.1600026

Heckmann, T., Schwanghart, W., & Phillips, J. D. (2015). Graph theory—Recent developments of its application in geomorphology. *Geomorphology*, *243*, 130–146. https://doi.org/10.1016/j.geomorph.2014.12.024

Heimsath, A., Hudnut, K., Lamb, M., Whipple, K. (2019). Mapping of San Gabriel Mountains, CA 2009 Fire. National Center for Airborne Laser Mapping (NCALM), Distributed by OpenTopography. https://doi.org/10.5069/G94M92N4.. Accessed: 2024-09-03

Hodge, R. A., & Hoey, T. B. (2012). Upscaling from grain-scale processes to alluviation in bedrock channels using a cellular automaton model: CA MODEL OF BEDROCK RIVER SEDIMENT COVER. *Journal of Geophysical Research: Earth Surface*, *117*(F1), n/a-n/a. https://doi.org/10.1029/2011JF002145

Hodge, R. A., & Hoey, T. B. (2016). A Froude-scaled model of a bedrock-alluvial channel reach: 2. Sediment cover: Bedrock-Alluvial Model: Sediment. *Journal of Geophysical Research: Earth Surface*, *121*(9), 1597–1618. https://doi.org/10.1002/2015JF003709

Hodge, R. A., Hoey, T. B., & Sklar, L. S. (2011). Bed load transport in bedrock rivers: The role of sediment cover in grain entrainment, translation, and deposition. *Journal of Geophysical Research*, *116*(F4), F04028. https://doi.org/10.1029/2011JF002032

Hoffman, D. F., & Gabet, E. J. (2007). Effects of sediment pulses on channel morphology in a gravel-bed river. *Geological Society of America Bulletin*, *119*(1–2), 116–125. https://doi.org/10.1130/B25982.1

Howard, A. D. (1994). A detachment-limited model of drainage basin evolution. *Water Resources Research*, *30*(7), 2261–2285. https://doi.org/10.1029/94WR00757

Husic, A., & Michalek, A. (2022). Structural Hillslope Connectivity Is Driven by Tectonics More Than Climate and Modulates Hydrologic Extremes and Benefits. *Geophysical Research Letters*, *49*(15), e2022GL099898. https://doi.org/10.1029/2022GL099898

Inoue, T., Izumi, N., Shimizu, Y., & Parker, G. (2014). Interaction among alluvial cover, bed roughness, and incision rate in purely bedrock and alluvial-bedrock channel. *Journal of Geophysical Research: Earth Surface*, *119*(10), 2123–2146. https://doi.org/10.1002/2014JF003133

Jafarinik, S., & Viparelli, E. (2020). Alluvial Morphodynamics of Low-Slope Bedrock Reaches Transporting Nonuniform Bed Material. *Water Resources Research*, *56*(10), e2020WR027345. https://doi.org/10.1029/2020WR027345

Jansen, J. D., Codilean, A. T., Bishop, P., & Hoey, T. B. (2010). Scale Dependence of Lithological Control on Topography: Bedrock Channel Geometry and Catchment

Morphometry in Western Scotland. *The Journal of Geology*, *118*(3), 223–246. https://doi.org/10.1086/651273

Johnson, J. P. L. (2014). A surface roughness model for predicting alluvial cover and bed load transport rate in bedrock channels: Bedrock roughness alluvial cover model. *Journal of Geophysical Research: Earth Surface*, *119*(10), 2147–2173. https://doi.org/10.1002/2013JF003000

Johnson, J. P. L., & Whipple, K. X. (2010). Evaluating the controls of shear stress, sediment supply, alluvial cover, and channel morphology on experimental bedrock incision rate: STRESS, SEDIMENT SUPPLY, AND ALLUVIATION. *Journal of Geophysical Research: Earth Surface*, *115*(F2). https://doi.org/10.1029/2009JF001335

Johnson, J. P. L., Whipple, K. X., Sklar, L. S., & Hanks, T. C. (2009). Transport slopes, sediment cover, and bedrock channel incision in the Henry Mountains, Utah. *Journal of Geophysical Research*, *114*(F2), F02014. https://doi.org/10.1029/2007JF000862

Keshtkar, H., & Voigt, W. (2016). A spatiotemporal analysis of landscape change using an integrated Markov chain and cellular automata models. *Modeling Earth Systems and Environment*, *2*(1), 10. https://doi.org/10.1007/s40808-015-0068-4

Khan, S., Fryirs, K., & Bizzi, S. (2021). Modelling sediment (dis)connectivity across a river network to understand locational-transmission-filter sensitivity for identifying hotspots of potential geomorphic adjustment. *Earth Surface Processes and Landforms*, *46*(14), 2856–2869. https://doi.org/10.1002/esp.5213

Kondolf, G. M. (1997). PROFILE: Hungry Water: Effects of Dams and Gravel Mining on River Channels. *Environmental Management*, *21*(4), 533–551. https://doi.org/10.1007/s002679900048

Kondolf, G. M., Podolak, K., & Grantham, T. E. (2013). Restoring mediterranean-climate rivers. *Hydrobiologia*, *719*(1), 527–545. https://doi.org/10.1007/s10750-012-1363-y

Kraskov, A., Stögbauer, H., & Grassberger, P. (2004). Estimating mutual information. *Physical Review E*, *69*(6). https://doi.org/10.1103/physreve.69.066138

Kruskal, W. H., & Wallis, W. A. (1952). Use of Ranks in One-Criterion Variance Analysis. *Journal of the American Statistical Association*, *47*(260), 583–621. https://doi.org/10.1080/01621459.1952.10483441

Lague, D. (2010). Reduction of long-term bedrock incision efficiency by short-term alluvial cover intermittency. *Journal of Geophysical Research: Earth Surface*, *115*(F2). https://doi.org/10.1029/2008JF001210

Lague, D., Hovius, N., & Davy, P. (2005). Discharge, discharge variability, and the bedrock channel profile. *Journal of Geophysical Research: Earth Surface*, *110*(F4), 2004JF000259. https://doi.org/10.1029/2004JF000259

Lavé, J., & Burbank, D. (2004). Denudation processes and rates in the Transverse Ranges, southern California: Erosional response of a transitional landscape to external and anthropogenic forcing. *Journal of Geophysical Research: Earth Surface*, *109*(F1), 2003JF000023. https://doi.org/10.1029/2003JF000023

Leopold, L., & Maddock, T. (1953). *The hydraulic geometry of stream channels and some physiographic implications* (Professional Paper 252; Professional Paper). USGS. https://doi.org/10.3133/pp252

Lisle, T. E., Cui, Y., Parker, G., Pizzuto, J. E., & Dodd, A. M. (2001). The dominance of dispersion in the evolution of bed material waves in gravel-bed rivers. *Earth Surface Processes and Landforms*, *26*, 1409–1420. https://doi.org/10.1002/esp.300

Lisle, T. E., Pizzuto, J. E., Ikeda, H., Iseya, F., & Kodama, Y. (1997). Evolution of a sediment wave in an experimental channel. *Water Resources Research*, *33*(8), 1971–1981. https://doi.org/10.1029/97WR01180

Liu, R., Men, C., Wang, X., Xu, F., & Yu, W. (2016). Application of spatial Markov chains to the analysis of the temporal–spatial evolution of soil erosion. *Water Science and Technology*, *74*(5), 1051–1059. https://doi.org/10.2166/wst.2016.283

Madej, M. A. (2001). Development of channel organization and roughness following sediment pulses in single-thread, gravel bed rivers. *Water Resources Research*, *37*(8), 2259–2272. https://doi.org/10.1029/2001WR000229

Major, J. J., East, A. E., O'Connor, J. E., Grant, G. E., Wilcox, A. C., Magirl, C. S., Collins, M. J., & Tullos, D. D. (2017). Geomorphic Responses to Dam Removal in the United States – a Two-Decade Perspective. In D. Tsutsumi & J. B. Laronne (Eds.), *Gravel-Bed Rivers* (1st ed., pp. 355–383). Wiley. https://doi.org/10.1002/9781118971437.ch13

Massong, T. M., & Montgomery, D. R. (2000). Influence of sediment supply, lithology, and wood debris on the distribution of bedrock and alluvial channels. *Geological Society of America Bulletin*.

McColl, S. T., & Cook, S. J. (2024). A universal size classification system for landslides. *Landslides*, *21*(1), 111–120. https://doi.org/10.1007/s10346-023-02131-6

Meshkova, L. V., & Carling, P. A. (2013). Discrimination of alluvial and mixed bedrock-alluvial multichannel river networks: CHANNEL METRICS. *Earth Surface Processes and Landforms*, *38*(11), 1299–1316. https://doi.org/10.1002/esp.3417

Miller, D. J., & Benda, L. E. (2000). Effects of punctuated sediment supply on valley-floor landforms and sediment transport. *Geological Society of America Bulletin*.

Montgomery, D. R., Abbe, T. B., Buffington, J. M., Peterson, N. P., Schmidt, K. M., & Stock, J. D. (1996). Distribution of bedrock and alluvial channels in forested mountain drainage basins. *Nature*, *381*(6583), 587–589. https://doi.org/10.1038/381587a0

Montgomery, D. R., & Buffington, J. M. (1997). Channel-reach morphology in mountain drainage basins. *Geological Society of America Bulletin*, *109*(5), 596–611. https://doi.org/10.1130/0016-7606(1997)109<0596:CRMIMD>2.3.CO;2

Montgomery, D. R., & Gran, K. B. (2001). Downstream variations in the width of bedrock channels. *Water Resources Research*, *37*(6), 1841–1846. https://doi.org/10.1029/2000WR900393

Morgan, J. A., & Nelson, P. A. (2019). Morphodynamic Modeling of Sediment Pulse Dynamics. *Water Resources Research*, *55*(11), 8691–8707. https://doi.org/10.1029/2019WR025407

Mudd, S. M., Clubb, F. J., Grieve, S. W. D., Milodowski, D. T., Gailleton, B., Hurst, M. D., Valters, D. V., Wickert, A. D., & Hutton, E. W. H. (2023). LSDtopotools/LSDTopoTools2: LSDTopoTools2 v0.9 (v0.9). Zenodo. https://doi.org/10.5281/zenodo.8076231

Murphy, B. P., Czuba, J. A., & Belmont, P. (2019). Post-wildfire sediment cascades: A modeling framework linking debris flow generation and network-scale sediment

routing. *Earth Surface Processes and Landforms*, *44*(11), 2126–2140. https://doi.org/10.1002/esp.4635

Nath, B., Wang, Z., Ge, Y., Islam, K., P. Singh, R., & Niu, Z. (2020). Land Use and Land Cover Change Modeling and Future Potential Landscape Risk Assessment Using Markov-CA Model and Analytical Hierarchy Process. *ISPRS International Journal of Geo-Information*, *9*(2), 134. https://doi.org/10.3390/ijgi9020134

Neely, A. B., & DiBiase, R. A. (2023). Sediment controls on the transition from debris flow to fluvial channels in steep mountain ranges. *Earth Surface Processes and Landforms*, *48*(7), 1342–1361. https://doi.org/10.1002/esp.5553

Nelson, A., & Dubé, K. (2016). Channel response to an extreme flood and sediment pulse in a mixed bedrock and gravel-bed river. *Earth Surface Processes and Landforms*, *41*(2), 178–195. https://doi.org/10.1002/esp.3843

Nelson, P. A., & Seminara, G. (2011). Modeling the evolution of bedrock channel shape with erosion from saltating bed load: MODELING BEDROCK CHANNEL SHAPE. *Geophysical Research Letters*, *38*(17), n/a-n/a. https://doi.org/10.1029/2011GL048628

Ordnance Survey. (2022). OS Terrain 5 [ASC geospatial data], Scale 1:10,000, Tiles: nh59se, nh69sw..., Updated: 26 February 2022. Available from EDINA Digimap Ordnance Survey Service. Retrieved from https://digimap.edina.ac.uk.

Paola, C., Straub, K., Mohrig, D., & Reinhardt, L. (2009). The "unreasonable effectiveness" of stratigraphic and geomorphic experiments. *Earth-Science Reviews*, *97*(1–4), 1–43. https://doi.org/10.1016/j.earscirev.2009.05.003

Papangelakis, E., Welber, M., Ashmore, P., & MacVicar, B. (2021). Controls of alluvial cover formation, morphology and bedload transport in a sinuous channel with a

non-alluvial boundary. *Earth Surface Processes and Landforms*, *46*(2), 399–416. https://doi.org/10.1002/esp.5032

Pfeiffer, A., Barnhart, K., Czuba, J., & Hutton, E. (2020). NetworkSedimentTransporter: A Landlab component for bed material transport through river networks. *Journal of Open Source Software*, *5*(53), 2341. https://doi.org/10.21105/joss.02341

Phillips, C. B., Masteller, C. C., Slater, L. J., Dunne, K. B. J., Francalanci, S., Lanzoni, S., Merritts, D. J., Lajeunesse, E., & Jerolmack, D. J. (2022). Threshold constraints on the size, shape and stability of alluvial rivers. *Nature Reviews Earth & Environment*, *3*(6), 406–419. https://doi.org/10.1038/s43017-022-00282-z

Phillips, J. D. (2012). Synchronization and scale in geomorphic systems. *Geomorphology*, *137*(1), 150–158. https://doi.org/10.1016/j.geomorph.2010.09.028

Piantini, M., Gimbert, F., Bellot, H., & Recking, A. (2021). Triggering and propagation of exogenous sediment pulses in mountain channels: Insights from flume experiments with seismic monitoring. *Earth Surface Dynamics*, *9*(6), 1423–1439. https://doi.org/10.5194/esurf-9-1423-2021

Purinton, B., & Bookhagen, B. (2019). *Introducing PebbleCounts: A grain-sizing tool for photo surveys of dynamic gravel-bed rivers* [Preprint]. Physical: Geomorphology (including all aspects of fluvial, coastal, aeolian, hillslope and glacial geomorphology). https://doi.org/10.5194/esurf-2019-20

Reichstein, M., Camps-Valls, G., Stevens, B., Jung, M., Denzler, J., Carvalhais, N., & Prabhat. (2019). Deep learning and process understanding for data-driven Earth system science. *Nature*, *566*(7743), 195–204. https://doi.org/10.1038/s41586-019-0912-1

Reid, D. A., Hassan, M. A., & McCleary, R. (2022). Glacial landscape configuration influences channel response to flooding. *Earth Surface Processes and Landforms*, *47*(1), 209–227. https://doi.org/10.1002/esp.5240

Rennie, C. D., Church, M., & Venditti, J. G. (2018). Rock Control of River Geometry: The Fraser Canyons. *Journal of Geophysical Research: Earth Surface*, *123*(8), 1860–1878. https://doi.org/10.1029/2017JF004458

Rice, S. P., & Church, M. (1998). Grain size along two gravel-bed rivers: Statistical variation, spatial pattern and sedimentary links. *Earth Surface Processes and Landforms*, *23*, 345–363.

Rinderer, M., Ali, G., & Larsen, L. G. (2018). Assessing structural, functional and effective hydrologic connectivity with brain neuroscience methods: State-of-the-art and research directions. *Earth-Science Reviews*, *178*, 29–47. https://doi.org/10.1016/j.earscirev.2018.01.009

Roda-Boluda, D. C., D'Arcy, M., McDonald, J., & Whittaker, A. C. (2018). Lithological controls on hillslope sediment supply: Insights from landslide activity and grain size distributions. *Earth Surface Processes and Landforms*, *43*(5), 956–977. https://doi.org/10.1002/esp.4281

Rodriguez, J. D., Perez, A., & Lozano, J. A. (2010). Sensitivity Analysis of k-Fold Cross Validation in Prediction Error Estimation. *IEEE Transactions on Pattern Analysis and Machine Intelligence*, *32*(3), 569–575. https://doi.org/10.1109/TPAMI.2009.187

Rowland, C.S.; Marston, C.G., & O'Neil, A.W. (2025). *Land Cover Map 2024 (1km summary rasters, GB and N. Ireland*. NERC EDS Environmental Information Data Centre. https://doi.org/10.5285/0ac15fd6-6f3a-4f28-8ed7-34461ca62a6e

Schmitt, R. J. P., Bizzi, S., & Castelletti, A. (2016). Tracking multiple sediment cascades at the river network scale identifies controls and emerging patterns of sediment connectivity: TRACKING MULTIPLE SEDIMENT CASCADES AT RIVER NETWORK SCALE. *Water Resources Research*, *52*(5), 3941–3965. https://doi.org/10.1002/2015WR018097

Schmitt, R. J. P., Bizzi, S., Castelletti, A., & Kondolf, G. M. (2018). Improved trade-offs of hydropower and sand connectivity by strategic dam planning in the Mekong. *Nature Sustainability*, *1*(2), 96–104. https://doi.org/10.1038/s41893-018-0022-3

Shobe, C. M., Tucker, G. E., & Barnhart, K. R. (2017). The SPACE 1.0 model: A Landlab component for 2-D calculation of sediment transport, bedrock erosion, and landscape evolution. *Geoscientific Model Development*, *10*(12), 4577–4604. https://doi.org/10.5194/gmd-10-4577-2017

Silver, D., & Silva, T. H. (2021). A Markov model of urban evolution: Neighbourhood change as a complex process. *PLOS ONE*, *16*(1), e0245357. https://doi.org/10.1371/journal.pone.0245357

Sklar, L., & Dietrich, W. E. (1998). River longitudinal profiles and bedrock incision models: Stream power and the influence of sediment supply. In J. Tinkler & E. Wohl (Eds.), *Geophysical Monograph Series* (Vol. 107, pp. 237–260). American Geophysical Union. https://doi.org/10.1029/GM107p0237

Sklar, L. S., & Dietrich, W. E. (2001). Sediment and rock strength controls on river incision into bedrock. *Geology*, *29*(12), 1087. https://doi.org/10.1130/0091-7613(2001)029<1087:SARSCO>2.0.CO;2

Sklar, L. S., & Dietrich, W. E. (2004). A mechanistic model for river incision into bedrock by saltating bed load. *Water Resources Research*, *40*(6). https://doi.org/10.1029/2003WR002496

Sklar, L. S., Fadde, J., Venditti, J. G., Nelson, P., Wydzga, M. A., Cui, Y., & Dietrich, W. E. (2009). Translation and dispersion of sediment pulses in flume experiments simulating gravel augmentation below dams. *Water Resources Research*, *45*(8), 2008WR007346. https://doi.org/10.1029/2008WR007346

Sklar, L. S., Riebe, C. S., Marshall, J. A., Genetti, J., Leclere, S., Lukens, C. L., & Merces, V. (2017). The problem of predicting the size distribution of sediment supplied by hillslopes to rivers. *Geomorphology*, *277*, 31–49. https://doi.org/10.1016/j.geomorph.2016.05.005

Slater, L., Villarini, G., Archfield, S., Faulkner, D., Lamb, R., Khouakhi, A., & Yin, J. (2021). Global Changes in 20-Year, 50-Year, and 100-Year River Floods. *Geophysical Research Letters*, *48*(6), e2020GL091824. https://doi.org/10.1029/2020GL091824

Small, D., & Fabel, D. (2016). Was Scotland deglaciated during the Younger Dryas? *Quaternary Science Reviews*, *145*, 259–263. https://doi.org/10.1016/j.quascirev.2016.05.031

Snelder, T. H., Lamouroux, N., & Pella, H. (2011). Empirical modelling of large scale patterns in river bed surface grain size. *Geomorphology*, *127*(3–4), 189–197. https://doi.org/10.1016/j.geomorph.2010.12.015

Steiger, J., Tabacchi, E., Dufour, S., Corenblit, D., & Peiry, J. -L. (2005). Hydrogeomorphic processes affecting riparian habitat within alluvial channel–floodplain river

systems: A review for the temperate zone. *River Research and Applications*, *21*(7), 719–737. https://doi.org/10.1002/rra.879

Sutherland, D. G., Hansler Ball, M., Hilton, S. J., & Lisle, T. E. (2002). Evolution of a landslide-induced sediment wave in the Navarro River, California. *Geological Society of America Bulletin*, *114*(8), 1036–1048. https://doi.org/10.1130/0016-7606(2002)114<1036:EOALIS>2.0.CO;2

Tanguy, M.; Dixon, H.; Prosdocimi, I.; Morris, D.G.; Keller, V.D.J. (2021). *Gridded estimates of daily and monthly areal rainfall for the United Kingdom (1890-2019) [CEH-GEAR]*. NERC EDS Environmental Information Data Centre. https://doi.org/10.5285/dbf13dd5-90cd-457a-a986-f2f9dd97e93c

Tangi, M., Schmitt, R., Bizzi, S., & Castelletti, A. (2019). The CASCADE toolbox for analyzing river sediment connectivity and management. *Environmental Modelling & Software*, *119*, 400–406. https://doi.org/10.1016/j.envsoft.2019.07.008

Toone, J., Rice, S. P., & Piégay, H. (2014). Spatial discontinuity and temporal evolution of channel morphology along a mixed bedrock-alluvial river, upper Drôme River, southeast France: Contingent responses to external and internal controls. *Geomorphology*, *205*, 5–16. https://doi.org/10.1016/j.geomorph.2012.05.033

Towers, A. H., Attal, M., Mudd, S. M., & Clubb, F. J. (2024). Controls on fluvial grain sizes in post-glacial landscapes. *EGUsphere* [preprint]. https://doi.org/10.5194/egusphere-2024-3084

Trenberth, K. (2011). Changes in precipitation with climate change. *Climate Research*, *47*(1), 123–138. https://doi.org/10.3354/cr00953

Turnbull, L., Hütt, M.-T., Ioannides, A. A., Kininmonth, S., Poeppl, R., Tockner, K., Bracken, L. J., Keesstra, S., Liu, L., Masselink, R., & Parsons, A. J. (2018).

Connectivity and complex systems: Learning from a multi-disciplinary perspective. *Applied Network Science*, *3*(1), 11. https://doi.org/10.1007/s41109-018-0067-2

Turowski, J. M. (2018). Alluvial cover controlling the width, slope and sinuosity of bedrock channels. *Earth Surface Dynamics*, *6*(1), 29–48. https://doi.org/10.5194/esurf-6-29-2018

Turowski, J. M., Badoux, A., Leuzinger, J., & Hegglin, R. (2013). Large floods, alluvial overprint, and bedrock erosion. *Earth Surface Processes and Landforms*, *38*(9), 947–958. https://doi.org/10.1002/esp.3341

Turowski, J. M., Hovius, N., Wilson, A., & Horng, M.-J. (2008). Hydraulic geometry, river sediment and the definition of bedrock channels. *Geomorphology*, *99*(1–4), 26–38. https://doi.org/10.1016/j.geomorph.2007.10.001

Turowski, J. M., Lague, D., & Hovius, N. (2007). Cover effect in bedrock abrasion: A new derivation and its implications for the modeling of bedrock channel morphology. *Journal of Geophysical Research: Earth Surface*, *112*(F4), 2006JF000697. https://doi.org/10.1029/2006JF000697

UKCEH. (2022). Carron at Sgodachail (3002) - Daily and peak flow data. *National River Flow Archive*. Retrieved in 2024, from https://nrfa.ceh.ac.uk/data/station/meanflow/3002

Vázquez-Tarrío, D., Peeters, A., Cassel, M., & Piégay, H. (2023). Modelling coarse-sediment propagation following gravel augmentation: The case of the Rhône River at Péage-de-Roussillon (France). *Geomorphology*, *428*, 108639. https://doi.org/10.1016/j.geomorph.2023.108639

Venditti, J. G., Dietrich, W. E., Nelson, P. A., Wydzga, M. A., Fadde, J., & Sklar, L. (2010). Effect of sediment pulse grain size on sediment transport rates and bed mobility in gravel bed rivers. *Journal of Geophysical Research: Earth Surface*, 115(F3). https://doi.org/10.1029/2009jf001418

Voutsa, V., Battaglia, D., Bracken, L. J., Brovelli, A., Costescu, J., Díaz Muñoz, M., Fath, B. D., Funk, A., Guirro, M., Hein, T., Kerschner, C., Kimmich, C., Lima, V., Messé, A., Parsons, A. J., Perez, J., Pöppl, R., Prell, C., Recinos, S., … Hütt, M.-T. (2021). Two classes of functional connectivity in dynamical processes in networks. *Journal of The Royal Society Interface*, 18(183), 20210486. https://doi.org/10.1098/rsif.2021.0486

Werner, B. T. (1999). Complexity in Natural Landform Patterns. Science, 284(5411), 102–104. https://doi.org/10.1126/science.284.5411.102

Whipple, K. X. (2002). Implications of sediment-flux-dependent river incision models for landscape evolution. *Journal of Geophysical Research,* 107(B2), 2039. https://doi.org/10.1029/2000JB000044

Whipple, K. X. (2004). BEDROCK RIVERS AND THE GEOMORPHOLOGY OF ACTIVE OROGENS. *Annual Review of Earth and Planetary Sciences*, 32(1), 151–185. https://doi.org/10.1146/annurev.earth.32.101802.120356

Whipple, K. X., DiBiase, R. A., & Crosby, B. T. (2013). *9.28 Bedrock Rivers*. *In Treatise on Geomorphology* (pp. 550–573). Elsevier. https://doi.org/10.1016/B978-0-12-374739-6.00254-2

Whitbread, K. (2015). Channel geometry data set for the northwest Scottish Highlands. *British Geological Survey Open Report*, OR/15/040. 12pp.[Dataset].

Whitbread, K., Jansen, J., Bishop, P., & Attal, M. (2015). Substrate, sediment, and slope controls on bedrock channel geometry in postglacial streams. *Journal of Geophysical Research: Earth Surface,* 120(5), 779–798. https://doi.org/10.1002/2014JF003295

Wilcock, P. R., & Crowe, J. C. (2003). Surface-based Transport Model for Mixed-Size Sediment. *Journal of Hydraulic Engineering,* 129(2), 120–128. https://doi.org/10.1061/(ASCE)0733-9429(2003)129:2(120)

Willgoose, G., Bras, R. L., & Rodriguez-Iturbe, I. (1991). A coupled channel network growth and hillslope evolution model: 1. Theory. *Water Resources Research,* 27(7), 1671–1684. https://doi.org/10.1029/91WR00935

Williams, G. P. (1978). Bank-full discharge of rivers. *Water Resources Research*, 14(6), 1141–1154. https://doi.org/10.1029/WR014i006p01141

Wohl, E. (2015a). Legacy effects on sediments in river corridors. *Earth-Science Reviews,* 147, 30–53. https://doi.org/10.1016/j.earscirev.2015.05.001

Wohl, E. (2015b). Particle dynamics: The continuum of bedrock to alluvial river segments. *Geomorphology*, 241, 192–208. https://doi.org/10.1016/j.geomorph.2015.04.014

Wohl, E. (2017). Connectivity in rivers. *Progress in Physical Geography: Earth and Environment,* 41(3), 345–362. https://doi.org/10.1177/0309133317714972

Wohl, E., Brierley, G., Cadol, D., Coulthard, T. J., Covino, T., Fryirs, K. A., Grant, G., Hilton, R. G., Lane, S. N., Magilligan, F. J., Meitzen, K. M., Passalacqua, P., Poeppl, R. E., Rathburn, S. L., & Sklar, L. S. (2019). Connectivity as an emergent property of geomorphic systems: Geomorphic connectivity. *Earth Surface Processes and Landforms*, 44(1), 4–26. https://doi.org/10.1002/esp.4434

Wohl, E., & David, G. C. L. (2008). Consistency of scaling relations among bedrock and alluvial channels. *Journal of Geophysical Research: Earth Surface*, 113(F4), 2008JF000989. https://doi.org/10.1029/2008JF000989

Wong, M., & Parker, G. (2006). Reanalysis and Correction of Bed-Load Relation of Meyer-Peter and Müller Using Their Own Database. *Journal of Hydraulic Engineering,* 132(11), 1159–1168. https://doi.org/10.1061/(ASCE)0733-9429(2006)132:11(1159)

Wong, M., Parker, G., DeVries, P., Brown, T. M., & Burges, S. J. (2007). Experiments on dispersion of tracer stones under lower-regime plane-bed equilibrium bed load transport: FLUME EXPERIMENTS ON DISPERSION OF TRACER STONES. *Water Resources Research*, 43(3). https://doi.org/10.1029/2006WR005172

Yanites, B. J., Tucker, G. E., Mueller, K. J., & Chen, Y.-G. (2010). How rivers react to large earthquakes: Evidence from central Taiwan. *Geology*, 38(7), 639–642. https://doi.org/10.1130/G30883.1

Yuan, X. P., Braun, J., Guerit, L., Rouby, D., & Cordonnier, G. (2019). A New Efficient Method to Solve the Stream Power Law Model Taking Into Account Sediment Deposition. *Journal of Geophysical Research: Earth Surface,* 124(6), 1346–1365. https://doi.org/10.1029/2018JF004867

Zaliapin, I., Foufoula-Georgiou, E., & Ghil, M. (2010). Transport on river networks: A dynamic tree approach: TRANSPORT ON RIVER NETWORKS. J*ournal of Geophysical Research: Earth Surface*, 115(F2). https://doi.org/10.1029/2009JF001281

Zhang, L., Parker, G., Stark, C. P., Inoue, T., Viparelli, E., Fu, X., & Izumi, N. (2015). Macro-roughness model of bedrock–alluvial river morphodynamics. *Earth Surface Dynamics*, 3(1), 113–138. https://doi.org/10.5194/esurf-3-113-2015